From fronds to forests: Applying dynamic energy budget (DEB) theory to individual-based and whole-forest models of *Laminaria hyperborea*

Alejandra Garcia Cabanillas

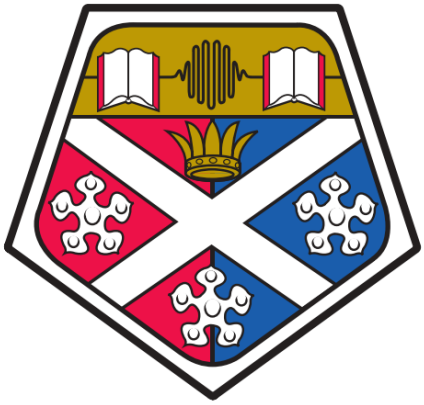

Department of Mathematics and Statistics

University of Strathclyde

Glasgow, Scotland

A thesis submitted for the degree of Doctor of Philosophy

November 2024

Abstract

Kelp forests are dynamic ecosystems that support biodiversity, carbon capture, and primary production while providing critical habitats for marine species. This study uses a Dynamic Energy Budget (DEB) model to simulate the growth of *Laminaria hyperborea* at individual and forest scales. The model tracks the pathways of carbon and nitrogen from environmental uptake to their assimilation into tissue. By integrating physiological processes with environmental factors, it reveals key insights into growth dynamics that are shaped by population structure, such as recruitment, growth and mortality, and intraspecies competition for light.

A significant result is the impact of canopy shading on growth. Cohorts under dense canopies experience constrained growth rates until pivotal events, such as mortality or thinning, allow light to penetrate the canopy, triggering rapid growth acceleration. This dynamic interaction between cohort settlement timing and canopy changes profoundly affects individual growth trajectories and forest biomass. The interplay between shading and canopy structure highlights the importance of population dynamics in kelp forest ecosystems.

The DEB model predicts individual growth curves and seasonal biomass fluctuations with accuracy, showing that shading is a critical factor for younger plants, while mature plants reach stable biomass. Simulations under future environmental scenarios, including the IPCC RCP4.5 and RCP8.5 for 2050 and 2100 periods, predict how changing conditions might alter growth and biomass patterns of *L. hyperborea* in Scottish waters. These findings emphasize the sensitivity of kelp forest ecosystems to environmental changes and the central role of canopy dynamics in mediating these effects.

This study underscores the importance of incorporating canopy dynamics and population structure in modelling kelp forest ecosystems. Unlike traditional approaches that extrapolate individual growth patterns to populations, this model demonstrates how canopy-driven processes influence growth limitations and accelerations. Such insights are essential for understanding the responses of kelp forests to climate change and for guiding conservation and management strategies.

All the data and code used to implement this model and the figures presented here are available at: *https://gitlab.cis.strath.ac.uk/spb19186/laminaria-hyperborea-ibm*

Declaration

This thesis is the result of the author's original research. It has been composed by the author and has not been previously submitted for examination which has led to the award of a degree.

Signed:

Date: 20/11/2024

Acknowledgements

I would like to thank my supervisors, Prof Heath ad Dr Speirs for all the lessons I've learned with them, I would definitely not be where I am today without their efforts.

I could not have done this without the opportunity given by the Saltire scheme to come back to Spain. It is heart-warming that the Scottish government still supports EU collaborations.

Thank to absolutely everyone at IHCantabria, but specially the Ecolit group for making me feel at home and reminding me why I became a scientist. Special thanks to Prof. Araceli Puente Trueba for taking me in. I would not have been able to figure out the environmental data for this project without Dr Camino F. De la Hoz & Dr Elvira Ramos.

Thank you to all the marvellous other PhD student friends I've made along the way, all the support we give each other has been invaluable. Matilda, Fengjia and Bego, Samu, Sara, you're marvellous. Thank you to my favourite postdocs Jack and Emily, you reminded me change can be exciting and things are generally less dire than I think.

I've been supported by so many amazing women along the way that I can't name them all, but thank you Dr Julia Poncela and Dr Jennifer Pestana you've made sure I always have someone on my side. Almudena thank you for your calming influence.

Thank you to my emotional support mathematicians Mikel & Dave for putting up with a biologist learning calculus and stealing your whiteboard during a pandemic.

Climbing and the friends I've made there have been what allowed me to cope with everything and even try to enjoy this last stage. Thank you in so many ways. Sofia, Marta, Andres, Irene, Laura, Cesar, Alfonso, Aritz you've always brought me back up.

Thank you, Miguel, for being my favourite consultant in maths, programming and burocracy, and overall acting psychologist, I could not have done it without all of our coffees.

Ady you have listened to me about so much "numbers stuff" that's not your area that you deserve an honorific scientist tittle. I don't have enough words to thank you.

Thank you to my family, to my dad for showing his thesis with printed code and reminding me to be patient, to my mum for reminding me that some things haven't changed in 30 years but we still have to keep trying, both for always telling me there is always a solution. To my sister for enduring my terrible jokes. To my cousin Ana for always hyping me up.

Gracias por estar. Siempre.

But most importantly thank you to me, for enduring.
Because even when it all seemed unfixable, I didn't give up.

Glossary

1. **Assimilation:** Process of absorbing nutrients to support growth.
2. **Biochemical Processes:** Chemical reactions within organisms that facilitate growth, metabolism, and reproduction.
3. **Bioremediation:** Use of living organisms to remove or neutralize environmental contaminants.
4. **Ecosystem Services:** Benefits derived from ecosystems, including provisioning, regulating, cultural, and supporting services.
5. **Elongation:** Growth in tissue length, relevant in growth models.
6. **Energy Flux:** Rate of energy transfer or transformation in a system, essential for understanding metabolism.
7. **Exudate Material:** Organic compounds released by plants, influencing nutrient dynamics and microbial communities.
8. **Exudation:** Release of organic compounds from organisms into the environment, part of nutrient cycling.
9. **Gametes:** Reproductive cells that unite during fertilization.
10. **Grazing Pressure:** Impact of herbivores on plant populations, influencing density and resilience.
11. **Homeostasis:** Maintenance of stable internal conditions despite external environmental changes.
12. **Maintenance Costs:** Energy and resources required for sustaining an organism's metabolic functions.
13. **Mortality:** Rate of death within a population, crucial for understanding population dynamics.
14. **Parametrization:** Defining model parameters based on empirical data for accurate functioning.
15. **Recruitment:** Addition of new individuals to a population or ecosystem through reproduction or migration.
16. **Saturation Point:** Threshold level where a rate reaches maximum capacity.
17. **Seasonal Fluctuations:** Predictable yearly variations in environmental conditions and biological processes.
18. **Seasonal Phenology:** Timing of biological events in relation to seasonal changes.
19. **Sigmoidal Curve:** S-shaped curve representing growth that accelerates and then slows.
20. **Stoichiometry:** Stoichiometry refers to the balance and proportions of elements in biochemical processes, focusing on how substances combine and react in biological systems. It involves analysing elemental ratios, nutrient utilization, and metabolic pathways to understand nutrient dynamics and their ecological implications.
21. **Turbidity:** Cloudiness of fluid caused by particles, affecting light penetration and photosynthesis.
22. **V1-morph**: An organism with surface area proportional to volume.

Table of Content

List of Figures

List of Tables

1 Introduction

1.1 Review of the biogeography, ecology and ecosystem services of kelp

The aims of this chapter are twofold. The first is to briefly review the biogeography, ecology and ecosystem service value of kelp, to provide context for the thesis and to explain why the development of models of kelp forests are necessary. The second aim, is to review how approaches to process-based kelp modelling methodology, both as individual organisms and as forest populations, have evolved. The main objective is to highlight the formal differences in modelling approaches as well as to identify some knowledge gaps and research opportunities that this thesis aims to fill.

1.1.1 What is a kelp?

The brown algae of the order Laminariales are commonly referred to as kelp; globally this clade of macroalgae are one of the most productive and ecologically relevant (Teagle et al., 2017). Because of these aspects they are sometimes referred to the marine analogue of terrestrial forest trees (Darwin, 1882; Lorentsen et al., 2010).

1.1.2 Where do you find them?

The current distribution of key kelp genera can be seen in Figure 1.1. Their distributions are mostly limited by their temperature tolerances (Smale, 2020), and globally they are found mainly in temperate regions. Kelp species ranges have, however, been shifting due to climate change (Burdett et al., 2019). Specifically, *Laminaria hyperborea* (one of the most prolific kelp species) has a distribution range from 40–60° latitude; the southern limit is set by warmer temperatures, nutrient levels and interspecies competition, while the northern limit is set by light availability (Steneck et al., 2002). The temperature limit is partly due to their gametes not producing an adult plant above 20ºC degrees (Kain, 1969). *L. hyperborea* requires a rocky substrate for holdfast attachment, and their vertical distribution ranges from just below the lowest astronomical tide to 30m depth or more in clear conditions (Kain, 1971a).

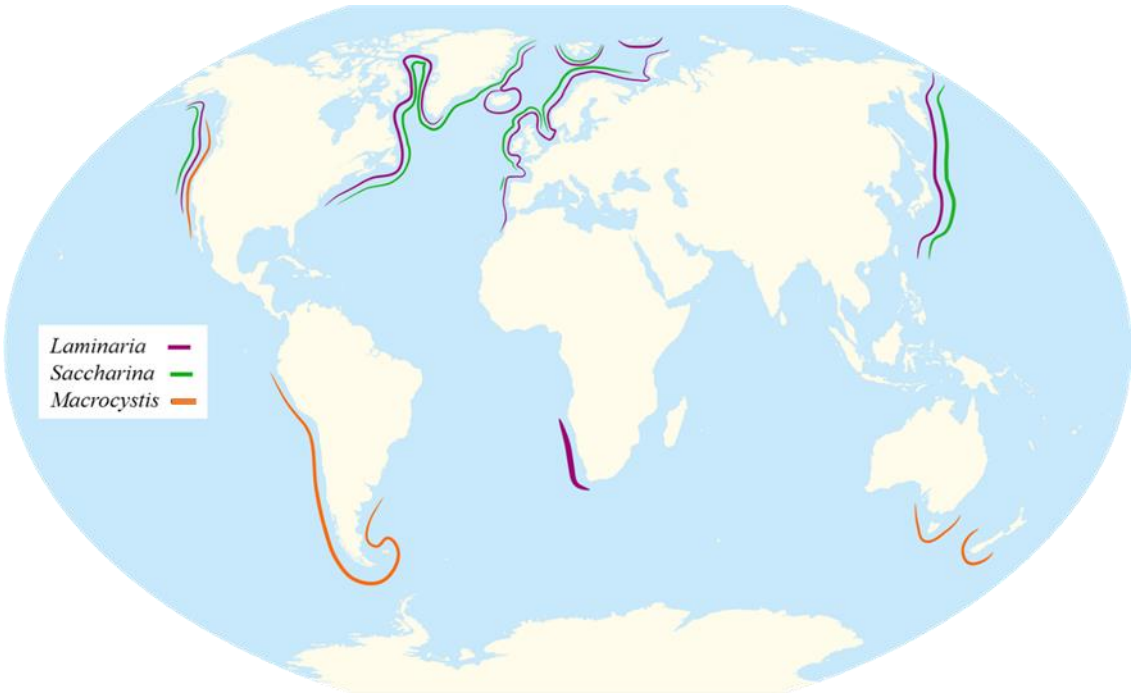

Figure 1.1. Simplified global distribution of various Laminariales genera. Modified and adapted from Smale (2020) and Teagle et al. (2017). The species selected are the ones mentioned in this review.

1.1.3 What is their taxonomy?

Initially grouped together by Lamouroux (1813) under the genus "*Laminaria*," kelps were later separated into distinct genera (Lane et al., 2006). Further research into taxonomical identification based on morphological characteristics, and later confirmed by molecular markers, revealed that relying solely on morphological features was inadequate for determining the phylogeny and taxonomy of these algae (Chi et al., 2014).

1.1.4 What is their phylogeny?

The complex phylogeny of these species contributes to the difficulties behind identification based solely on morphological characteristics. One key morphological feature is the pattern of branching laminar fronds. Branching has evolved independently in several clades over the past 15–20 million years, highlighting morphological convergence. For example, when examining branching morphology evolution across *Saccharina latissima*, *L. hyperborea*, and *Macrocystis pyrifera*, they last shared a common point around 25 million years ago (Starko et al., 2019). Their current characteristics can be seen in Figure 1.2.

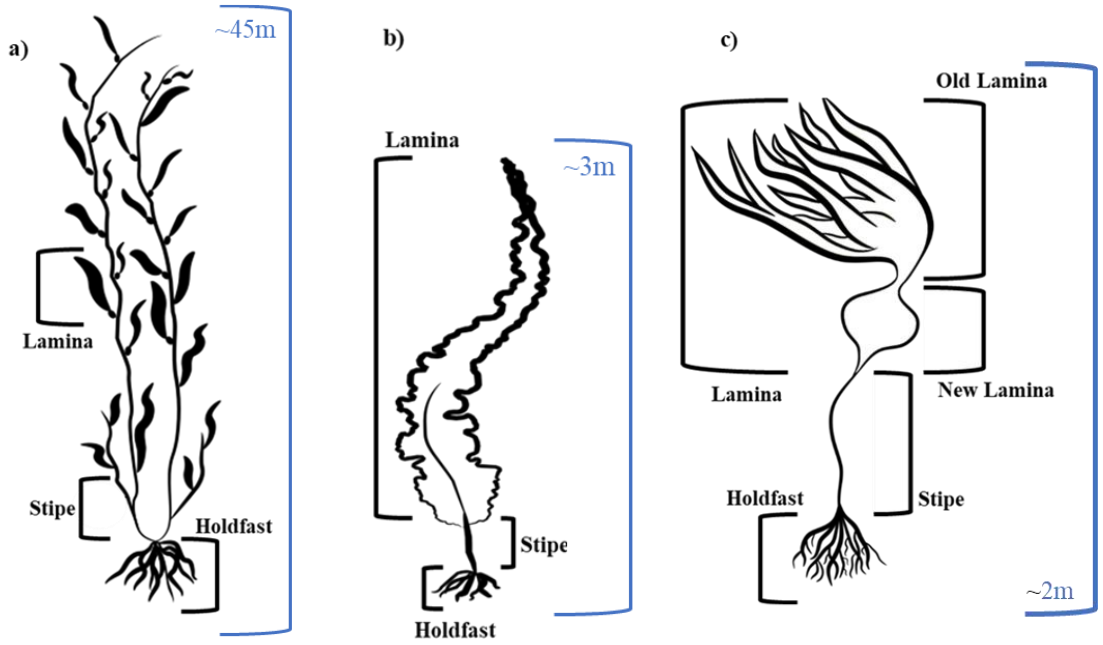

Figure 1.2. Schematic representation of key morphological components of Macrocystis pyrifera (a), Saccharina latissima (b) and Laminaria hyperborea (c). Approximate sizes that can be reached by the individuals of the species indicated in blue.

1.1.5 Life cycle

L. hyperborea has a complex lifecycle, the age at which the adult individual becomes fertile for the first time is dependent on its size, and therefore on the environmental conditions that have influenced its growth (Kain, 1976). In *L. hyperborea* the reproductive cells (spores) develop from specialised structures (sori) in the fronds from September to April (Kain, 1975). This species alternates generations between reproductive phases, with the adult (the diploid sporophyte) producing haploid spores from the sori that can travel ~5km from the parent organism (Kain, 1979; Norton, 1992). Afterwards the spores settle and develop into gametophytes, which become fertile (Fredriksen et al., 1995). Female gametophytes produce pheromones that attract male gametophytes. When the female gametophyte is fertilised it develops into a new sporophyte (Lüning and Müller, 1978). The successful fertilization of female gametophytes depends on a minimum blue light threshold being reached (Lüning, 1980), with an optimal temperature range for survival being between 10-17°C (Kain, 1969). Given the previous information it can be stated that reproduction and recruitment are highly seasonal processes which are limited by temperature and light.

1.1.6 Carbon reserves

One example a high content of carbohydrates, with the specific amounts being dependent on variations on environmental conditions. These carbohydrates accumulate during high irradiance periods, such as summer, followed by a decrease during the darker winter months partially in response to respiration costs likely exceeding the energy produced by photosynthesis at that time (Black, 1950; Kain, 1971a; Schiener et al., 2015). During those winter months the carbohydrates act as reserves for the organism.

1.1.7 Nitrogen reserves

Carbohydrates are not the only reserve material found in *L. hyperborea*, proteins are also present and likewise show a seasonal variation, with their peak being reached around April and their lowest point in August (Kain, 1971a). These proteins serve as a nitrogen storage in the form of inorganic ions, amino acids or other complex functional proteins (Pueschel and Korb, 2001). The required nitrogen for these proteins' formation can be assimilated directly from the surrounding water by all regions of the blade, in the form of nitrate (Davison and Stewart, 1983). For growth to happen, both carbon and nitrogen reserves must be available. Carbohydrates are needed to produce new proteins, and these carbohydrates are made with the help of photosynthetic enzymes, which require nitrogen to function. (Drew, 1983). These conditions create a dynamic balance in the amounts of carbon and nitrogen that can be found in the organism during different periods.

1.1.8 Nutrient assimilation

The assimilation of external nutrients for the formation of carbohydrate and protein reserves, as well as the growth of the individual, is influenced by environmental fluctuations. Consequently, these processes do not occur at constant rates throughout the organism life, as at certain times a limitation of a particular component might occur. When a nutrient is limiting the individual can exudate (release into the environment) the non-limiting nutrient. In kelp this would be the release of dissolved organic carbon (DOC) when nitrogen limitation occurs and there is sufficient light for photosynthesis (Paine et al., 2021). In *L. hyperborea* the DOC exudation rates correlate to the species growing strategy, with more carbon being exuded during slow-growth periods, on average 14-43% of fixed carbon is lost as DOC (Abdullah and Fredriksen, 2004; Sieburth, 1969; Weigel and Pfister, 2021). This changing pattern of nutrient limitation and exudation gives an insight into the internal chemical requirements of the organism for different environmental conditions.

1.1.9 Societal significance

Kelp forests are resilient and stable ecosystems over long periods, providing habitats for a wide range of species (Norderhaug et al., 2012; Teagle et al., 2017). They act as habitat bio-engineers providing three-dimensional spaces and shelter for various organisms, including fish, seabirds, and mammals (Bengtsson et al., 2011; Norderhaug et al., 2012). A study conducted along the Norwegian coast on *L. hyperborea* revealed 7,762 invertebrate organisms on a single individual kelp, with a total of 238 mobile macro-faunal taxa (Christie et al., 2003). These invertebrates serve as crucial food sources for fish species utilizing kelp forests as nursery habitats and shelter from larger predators (Lorentsen et al., 2010). This shows that kelp plays a key stabilising role in a complex ecosystem.

The societal significance of kelp forests becomes clear when looking at the ecosystem services they provide, such as serving as biodiversity hotspots, improving water quality and offering protection to coastlines from wave erosion by wave-dampening, alongside commercial interests (Araújo et al., 2016). The wave-dampening capacity has received particular attention in the light of rising sea-levels and consequent erosion risks. A study looking at *M. pyrifera*, in areas with a density of 8 stipes/m^2, was shown to decrease the wave energy flux between the outside and inside locations of the forest by an average of 7.2 ± 1.2% (Elsmore et al., 2024). A Norwegian study focusing on *L. hyperborea* forests, with a density of 25 large kelp plants per m^2 in a highly exposed site, showed a reduction of wave energy from the outer to inner part of the kelp forest by 70-85% over a distance of 258 meters, with the most significant effects observed during low tide (Mork, 1996), further highlighting the substantial impact of *L. hyperborea* in coastal protection.

An ecosystem service provided by kelp forests that has more recently become apparent is carbon sequestration, this service is often cited in the context of blue carbon. Blue carbon is a concept introduced to define the significant role of coastal vegetated ecosystems in global carbon sequestration (Macreadie et al., 2019). Approximately one-third of the carbon dioxide emitted is absorbed by the ocean (Gattuso et al., 2015). When comparing the specific systems, it has been reported that seagrass beds contribute 48–112 Tg C yr^{-1} to global carbon burial, comparable to terrestrial forests, which sequester 53.0 Tg C yr^{-1} in temperate areas, 78.5 Tg C yr^{-1} in tropical ones, and 49.3 Tg C yr^{-1} in boreal forests (Mcleod et al., 2011). Macroalgae are major players in carbon sequestration, potentially capturing nearly 173 Tg C yr^{-1}, with a range of 61–268 Tg C yr^{-1} (Krause-Jensen and Duarte, 2016). Kelp forests, specifically, have the potential to sequester approximately 4.91 Tg C yr^{-1} from the atmosphere each year, emphasising their role as blue carbon sink for mitigating climate change (Eger et al., 2023).

In terms of the quantifiable economic importance of kelp, an analysis of six major genera (*Ecklonia, Laminaria, Lessonia, Macrocystis, Nereocystis,* and *Saccharina*) revealed that each holds an estimated value ranging from $64,400 to $147,100 per hectare annually (Eger et al., 2023). Globally aquatic plants and algae harvesting increased from 10 Mt of wet biomass in 2000 to over 32 Mt in 2017, with aquaculture accounting for over 97% of

the current volume (Naylor et al., 2021). Common seaweed products include alginates, agar, and carrageen, which uses vary from food production to pharmaceuticals, with the majority of the current production centred in Asia (Bixler and Porse, 2011). Additional proposals have been put forward to refine seaweeds sugars for biofuels production (Wei et al., 2013), which would further increase their economic importance.

Aquaculture can provide a link between direct economic interests and ecosystem services. Kelp aquaculture has emerged as a nature-based approach for coastal protection, suggested for *S. latissima* (Zhu et al., 2020) and *Ecklonia radiata* (Bodycomb et al., 2023). The application of analytical models to current aquaculture practices provides an opportunity to investigate how to increase the ecosystem services they can provide. A practical change, shown by an analytical model, that can improve ecosystem services from a kelp farm is partial and targeted removal of vegetation, rather than complete removal during harvesting. This approach has been shown to increase the coastal protection provided (Bodycomb et al., 2023).

1.2 Comparative analysis of kelp models

The aim of this section is to compare and contrast the past and current approaches to kelp modelling. This review is focused on the methodological components used in process based mathematical models and the biology behind them. The modelling approaches described in the published literature are compared to biological data to assess their realism. The types of models addressed here are defined in Table 1.1.

Table 1.1. Key modelling approaches.

Term	Definition
Statistical distribution model	A model for geographical distribution describes the pattern and likelihood of a species or phenomenon occurring across different locations.
Empirical or statistical based model	Establish relationships between observations, such as environmental factors and growth, based on empirical data (Lobell and Asseng, 2017).
Process based model	Aim to depict the essential mechanisms underlying a phenomenon or system using mathematics (Lobell and Asseng, 2017).
Individual based model	A model focusses on a single individual organism, it can apply the methodology of empirical or process-based models.

Statistical models are not included in this review, as the focus is on the application of mathematics to represent biological processes. Statistical models driven by empirical data have value e.g. for predictive distribution modelling (Bekkby et al., 2009; Franco et al., 2018; Gorman et al., 2013; Jayathilake and Costello, 2020). However, process-based models offer potential advantages over empirical models by extending applicability beyond the spatial and temporal limits of empirical data (Miehle et al., 2009). The focus of this review will be on process-based models for these reasons.

1.2.1 Comparing modelling approaches

Table 1.2 presents an overview and a comparison of process-based models developed for *M. pyrifera, S. latissima* and *L. hyperborea*, which explore growth mechanisms, recruitment strategies, mortality, and the use of reserves, shedding light on different approaches conceptualization and developments for kelp modelling. The models can be split into two main groups, models describing individual growth with a focus on physiological details and those describing the dynamics of a population (a forest or aquaculture patch). Additionally, an increase in biological complexity is seen in successive model generations, one example is the more recent inclusion of biochemical composition (Broch and Slagstad, 2012) compared to only considering external frond elongation (Anderson, 1974). This addition of biochemical components allows for deeper understanding of the internal processes driving individual growth.

1.2.1.1 Recruitment

The distinction between forest population models and individual growth models is clear in the omission of recruitment processes in the latter, as recruitment is only considered by the population forest models (Nisbet and Bence, 1989; Rinde, 2007), which do not explicitly model individuals. Incorporating recruitment into individual growth models is essential for creating a model that is capable of simulating forest growth dynamics with individual level detail. Understanding how many individuals are joining the forest ecosystem is crucial. However, the individual growth models in Table 1.2 don't take into consideration changes in natural populations, as these models are only being applied to describe individual growth to controlled aquaculture environments.

1.2.1.2 Reproduction

There's a noticeable gap in modelling kelp when it comes to representing the reproductive processes of kelps, as it has not been explicitly simulated through process-based models to this date to the best of my knowledge. As highlighted before when explaining its the key processes involved, it's a complex process that heavily relies on both the individual state, such as size, and environmental conditions for success. Therefore, an accurate representation of these processes, their interconnected dynamics with the external environmental conditions and the population dynamics will require a highly detailed model.

1.2.1.3 Mortality

Another key process that would be required to join individual growth models with forest population dynamics models would be mortality. There is, however, no consensus for its representation across the various models addressed in this review, partially due to different species being represented, but also the range of applications for which the models have been developed. Mortality is only explicitly included in the forest population models (Nisbet and Bence, 1989; Rinde, 2007) and in three of the individual growth models (Anderson, 1974; Jackson, 1987; van der Molen et al., 2018). In the individual growth models, it would be more accurate to speak about life expectancy as opposed to a mortality rate.

Table 1.2 Overview of key features of the 10 existing kelp models.

Reference	Species	Model type	Currency	Growth	Recruitment	Reserves	Mortality
Anderson 1974	*Macrocystis pyrifera*	Individual	Frond length	Frond elongation	NA	NA	NA
Jackson 1987	*Macrocystis pyrifera*	Individual	Carbon	Biomass based on frond length.	NA	NA	Set for the frond, when the oldest frond dies or when the net productivity for the oldest frond is 0.
Nisbet and Bence 1989	*Macrocystis pyrifera*	Forest	Adults plant density	NA	Focused on adults with a constant rate of juveniles with an unknown factor effect.	NA	Per capita separate rates for canopy & understory.
Rinde 2007	*Laminaria hyperborea*	Forest	Abundance measured as biomass per area.	NA	Recruitment of canopy and understory individuals based on available space.	NA	Calculated from understory and canopy data.
Broch and Slagstad 2012	*Saccharina latissima*	Individual	Carbon and nitrogen (g)	Frond mass controls structural mass, growth by C and N reserves use. Applies the Droop cell quota model.	NA	N & C present independently. Applying strong homeostasis (Reserves and structure have fixed chemical composition).	NA
Aldridge et al., 2012	*Saccharina latissima*	Individual	Carbon and nitrogen(g)	Frond mass controls structural mass, growth by C and N reserves use.	NA	N & C present independently. Applying strong homeostasis.	NA
Broch et al., 2013	*Saccharina latissima*	Individual	Carbon and nitrogen (g)	Frond mass controls structural mass, growth by C and N reserves use.	NA	N & C present independently. Applying strong homeostasis.	NA
Van der Molen et al., 2018	*Saccharina latissima*	Individual	Biomass density (C, N and P)	Minimal N and P required for growth. Fixed N:P ratio for structure.	NA	C, N and P reserves than are combined to produced structural mass.	Relates apical frond loss exponentially to frond area.
Venolia et al., 2020	*Saccharina latissima*	Individual	Carbon and nitrogen (mol)	Reserves are merged to form C (mol) structure through an enzyme-like synthesis, maintaining a fixed chemical composition ratio.	NA	N & C present independently. Strong homeostasis.	NA
Strong-Wright and Taylor 2022	*Saccharina latissima*	Individual	Carbon and nitrogen	Frond mass controls structural mass, growth by C and N reserves use.	NA	N & C present independently. Applying strong homeostasis.	NA

1.2.1.4 Nutrients

Individual and population growth depend on interactions between internal physiological processes and external driving variables. The principal processes that have been included in existing published models are nutrient uptake, exudation of dissolved organic carbon, maintenance costs, and frond loss due to physical erosion. The principal drivers are temperature, which potentially affects all physiological rates, and external nutrient concentration which determines nutrient uptake rates. The key effects of light are discussed in detail in a later section. These interactions with the environment are mediated through nutrient uptake and metabolic processes, which are described in Table 1.3. A significant portion of the models draw upon or reference methodologies proposed by Broch and Slagstad (2012), indicating a foundational influence and common framework established by these authors. Another similar approach is presented by Venolia et al., (2020), which explicitly uses a Michaelis-Menten relationship to incorporate nitrogen into the reserves. Models included in this review with explicit nutrient uptake present a type II functional response, equivalent to Michaelis-Menten kinetics:

$$V = \frac{V_{max} \cdot S}{K_m + S} \quad , \qquad (1.1)$$

where V represents the rate of the reaction, V_{max} is the maximum rate achievable when the enzyme is fully saturated with a substrate, K_m is the Michaelis constant, indicating the enzyme's affinity for its substrate, and S represents the concentration of the substrate (Michaelis and Menten, 1913, 2013). This representation has been a building block of biochemistry for over a century (Srinivasan, 2022). It shows the effects of the changing concentration of the nutrient availability in the uptake by the organism.

Michaelis-Menten kinetics provide a reference point for understanding, and hence representing, enzyme regulation and the properties of single molecules. It set the basis for the steady state —hypothesis (Briggs and Haldane, 1925) and the subsequent deviation from it such as the feedback inhibition (Umbarger, 1956). The inhibition example can be seen in molluscs, which in the case of heavy metals can inhibit the activity of enzymes, such as carbonic anhydrase, disrupting their ability to regulate their pH and carbonate ion concentrations, both critical for calcification processes (Le Roy et al., 2016). On the other hand, the steady state hypothesis is seen in the nutrient uptake formulations chosen by the models included in this review.

1.2.1.5 Temperature

Table 1.3 highlights that the most frequent approach for incorporating temperature effects is through the direct use of the Arrhenius equation, used by Broch and Slagstad, (2012) and the other publications based on their methods, and by Venolia et al., (2020). The Arrhenius equation considers: the activation energy, a rate constant, a pre exponential factor and the temperature in kelvin to describe how reaction rates increase with temperature due to the increased kinetic energy of molecules (Arrhenius, 1889). As temperature rises, the Arrhenius equation value (k) increases exponentially due to the greater likelihood of reactant molecules possessing the energy required for successful reactions. This functional form is frequently employed to describe the temperature dependence of biological rates, such as metabolic processes and enzyme-catalysed reactions.

The previous described Arrhenius dynamics can be re-expressed as the Q_{10} rate, which describes the rate of change with a ten degree temperature increase (Ito et al., 2015), a more common scenario in biological process. The Arrhenius equation, linked to chemistry, shows that if the temperature increases from 10 degrees to 20 degrees, the proportional change in the rate constant k doubles. This change in the Arrhenius value is proportional to the temperature change, exhibiting the same properties as when defining it using Q_{10}. While it can be written in terms of Arrhenius to relate it to more fundamental physical chemistry constants like the gas constant and activation energy, both forms ultimately represent the same concept. Despite the different expressions, the two rates respond equally to temperature changes (Ito et al., 2015).

Table 1.3. Comparative analysis of process-based models with a focus on growth-influencing processes across different marine macroalgae. Colours indicate the species of the model, blue for M. pyrifera, green for L. hyperborea and orange for S. latissima.

Reference	Nutrient Uptake	Temperature	Maintenance	Exudation	Erosion
Anderson 1974	NA	Effect fitted from data	NA	NA	NA
Jackson 1989	NA	NA	Respiration rates specific for site and blade based on data.	NA	NA
Nisbet and Bence 1989	NA	Acts as proxy measurement for nutrients.	NA	NA	NA
Rinde 2007	NA	NA	NA	NA	NA
Broch and Slagstad 2012	Type II response for external nutrient concentration. Also considers internal nutrient reserves concentrations, water current speed is integrated.	Arrhenius law used for maximum rates for photosynthesis and respiration.	Respiration per frond area rate as a function of temperature.	Only for C. Leaves the organism directly after photosynthesis. It's a monotonical exponential function. Based on two set parameters: rate at which carbohydrates are exuded and minimum carbon reserves.	Apical frond loss increases with increasing area.
Aldridge et al., 2012	Type II response, with maximum uptake rates fixed.	Following Broch and Slagstad 2012.	Respiration at a constant rate but allowed to decrease when C reserves approach their minimum using a Monad saturation function.	Following Broch and Slagstad 2012.	Loss rate increases with frond area. Follows a monad saturation function.
Broch et al., 2013	Following Broch and Slagstad 2012.	Following Broch and Slagstad 2012	Respiration per frond area now basal and active components	Following Broch and Slagstad 2012.	Following Broch and Slagstad 2012.
Van der Molen et al., 2018	Dynamic uptake based on Droop cell quota model. Requires DIC, N, P and light.	Temperature exponential affects C fixation rate. Growth inhibited at 19C.	Following Broch and Slagstad 2012.	Carbon exudation when above minimum carbon from structure mass.	Apical frond loss.
Venolia et al., 2020	By Michaelis Menten relationship with a volume specific maximum for C.	Except for photon binding rates al rates are corrected for temperature using Arrhenius relationships.	Has to be covered from reserves, if not structure can be broken down and consumed.	Excretion mechanism for none limiting reserves when rejected by growth flux when.	NA
Strong-Wright and Taylor 2022	Following Broch and Slagstad 2012.	Following Broch and Slagstad 2012.	Following Broch and Slagstad 2012.	Following Broch and Slagstad 2012.	Following Broch and Slagstad 2012.

1.2.1.6 The influence of light

In Table 1.3 the focus is on processes and their drivers; light has been omitted from it as it is discussed in more detail in Table 1.4. This focus on light stems from the fact that kelp are photosynthetic organisms, making an accurate representation of light-related processes crucial. The first key factor to consider is the light that reaches the organism. Both Jackson, (1987) and Anderson, (1974) included the effects of the angle of solar irradiance on light available to the organism, a methodological aspects that's simplified out of later models in favour of methods more similar to Beer-Lambert law (Beer, 1852). Beer-Lambert law is applied to calculate the attenuation of light with depth, explicitly used by Aldridge et al., (2012).

Originally Broch and Slagstad, (2012) do not explicitly model the effect of light attenuation with depth. In future work the effects of depth are considered through empirical measurements of the attenuated surface irradiance at the depth being modelled (Broch et al., 2013). Nisbet and Bence, (1989) also directly includes the irradiance at the sea-bed to address this. Venolia et al., (2020) does consider the attenuation of light through the effect of depth, by integrating the length of the cultivation ropes being used and a coefficient for extinction of light. In more detail, van der Molen et al., (2018) goes into explicitly modelling the suspended particulate matter and its effects on the light available to the organism. This suspended particulate matter is considered using Beer-Lambert law through the attenuation coefficient. Hence the various different approaches recognised that the irradiance driving data is the first step and needs further processing before the organism being modelled utilises it. Additionally, it highlights the relevance of considering the model purpose when selecting the methodology, only building complexity when its required.

Light attenuation by shading

After the effect of depth in limiting light available to the organism has been taken into account, the effect of shading by other organisms must be considered. For the individual growth models density-dependence is commonly represented by the modelled plant size increasing light attenuation for the organism itself (self-shading) (Broch et al., 2013; Broch and Slagstad, 2012a; Strong-Wright and Taylor, 2022). In forest population models, Rinde, (2007) model has a special focus on the interaction between canopy and understory individuals, as this is the key process that regulates competition for light in the forest. The models presented here move from how individuals process light to how they compete with each other for that resource. Density dependence mediates light competition, as more individuals will mean less light reaching the smaller individuals in response to higher levels of shading by the larger individuals. This separation leads to individual growth models considering the effect of the individual itself (self-shading), while the forest population models consider the effects on the population dynamics. The next modelling step would be the use of the previously described population dynamics with the explicit consideration of individuals' internal biochemical processes, as it is a gap not currently filled for natural populations.

Internal light dependant processes

After the consideration of all the factors influencing the light available to the individual being modelled, the use of it for internal processes is discussed. The use of light is included through the representation of photosynthesis, which can be modelled similarly to other nutrient uptake or by applying rates obtained from statistical relationships from empirical data. Anderson, (1974) obtained the relative rate of photosynthesis by fitting a curve to data of mature kelp fronds, showing a saturating curve of the relative rate of photosynthesis with increasing solar radiation. Jackson, (1987) made photosynthetic rate proportional to the blade area and a function of irradiance, with a saturating rate also present. For representing the use of light in a similar manner to other uptake processes Broch and Slagstad, (2012) photosynthetic rate was written to follows saturating function and was further modified through the presence of a photosynthetic efficiency and photo-inhibition parameters.

In contrast Aldridge et al., (2012) used a linear photosynthesis rate, contrary to the use of a saturating function. Later publications increase the complexity by the explicit consideration of chlorophyll production (van der Molen et al., 2018). Independently, it has also been represented using an enzyme mediated process which explicitly models chloroplasts and the uptake of carbon (Venolia et al., 2020). The use of an enzyme mediated approach followed a Michaelis-Menten relationship as was used for nutrient uptake in multiple models. Regarding the representation of light use by other photosynthetic marine organisms, in microalgae models type I co-limitation was used, which required the presence of both light and CO_2 for carbon assimilation (Lorena et al., 2010), as seen in Venolia et al., (2020). This is in contrast to other individual growth kelp models (Aldridge et al., 2012; Anderson, 1974; Broch and Slagstad, 2012a; Jackson, 1987) which do not consider CO_2 requirements.

Overall kelp models' mathematical representation of the use of light is built upon saturating responses, in a similar approach to nutrient uptake. The methodological decision regarding the level of detail in modelling photosynthesis—whether to include the biochemical processes of carbon uptake and the roles of chlorophyll and chloroplasts, or to focus solely on the influence of light on the carbon available to the organism—depends on the specific objectives and scope of the model being developed. This choice influences the complexity, accuracy, and applicability of the model to different research questions or practical applications in the study of photosynthetic efficiency and plant growth.

Table 1.4. Comparative analysis of process-based models, with an emphasis on features mediating light's influence for various marine macroalgae. Colours indicate the species of the model, blue for M. pyrifera, green for L. hyperborea and orange for S. latissima.

Reference	Photosynthesis	Light Attenuation	Shading	Density Dependence
Anderson 1974	Fitted as a curve to field data.	Daily total radiation was attenuated to depth.	Canopy effect considered.	NA
Jackson 1989	Fitted from data.	Used Anderson light reflectance approach as a function of the surface reflectance.	Probabilistic shading based on frond size and layer. A grid used for shading of surrounding forest individuals, but not explicitly modelled.	Through the surrounding forest grid for calculating shading.
Nisbet and Bence 1989	NA	Shading effects considered.	Constant by adult plants.	Density per unit area of plants.
Rinde 2007	NA	Shading effects considered.	Transition from understory to canopy depends on light available.	Understory to canopy decreases linearly with canopy plants abundance.
Broch and Slagstad 2012	Photoperiod reduction forces changes in growth rate. Photosynthetic efficiency constant.	Background light attenuation.	Attenuation in cultures depending on plant size, vertical rope density and plant density per rope.	Attenuation depending on plant size, vertical rope density and plant density per rope.
Aldridge et al., 2012	Linear photosynthetic rate.	Mean value as a function of latitude, time of the year and cloud cover. With a gaussian diurnal variation. Attenuation at depth using beers law.	NA	Following Broch and Slagstad 2012.
Broch et al., 2013	Following Broch and Slagstad 2012.	Following Broch and Slagstad 2012.	Following Broch and Slagstad 2012.	Following Broch and Slagstad 2012.
Van der Molen et al., 2018	Chlorophyll production modelled. A Chlorophyll to C ratio limits light for C fixation with depth.	Depth incorporated. Turbidity data collected in situ. Chlorophyll from satellite.	Effect by relationship between amount of Chlorophyll in the plant and total carbon content.	Following Broch and Slagstad 2012.
Venolia et al., 2020	Uses enzyme-like synthesis to combine light intensity to photon arrival and bind them before it goes to C assimilation.	Density of macroalga biomass reduces light.	Self-shading defined based on density of macroalgae biomass after a certain threshold.	Density of macroalga biomass reduces light.
Strong-Wright and Taylor 2022	Following Broch and Slagstad 2012.	Following Broch and Slagstad 2012.	NA	Following Broch and Slagstad 2012.

1.2.2 Use of data

Data requirements for a model depend on the model structure and design, with irradiance measures being present in all models with varying levels of detail as driving data. The sources for the driving data can range from in-situ observations (Venolia et al., 2020), to simulated data (Broch and Slagstad, 2012a; van der Molen et al., 2018), and to remote sensed data (Anderson, 1974; Strong-Wright and Taylor, 2022). Table 1.5 provides an overview of practical considerations in the implementation, validation, and intended applications of the reviewed models. Aquaculture growth potential simulations where the most frequent application of the models, with inclusions of kelp impact on bioremediation opportunities (Broch et al., 2013) and surrounding biochemistry and plankton dynamics (van der Molen et al., 2018). A model applied on individuals growing in natural conditions, such as in a forest with a population with a heterogenous age structure, has not been done to include the internal physiological processes. By extension of this, a model applied to understand the effects of harvesting on the internal composition through different ages and simultaneously on population composition in a *L. hyperborea* forest is not currently available.

Model accuracy can be verified with various levels of complexity, a frequent approach carried out is visually comparing the model output to empirical data, either from published work or explicitly collected for that purpose (Aldridge et al., 2012; Broch and Slagstad, 2012a; Rinde, 2007; van der Molen et al., 2018). The data from Sjøtun, (1993) has been used by Aldridge et al., (2012) and Broch and Slagstad,(2012) for this purpose. For visual comparison the authors showed the model output and the empirical data it was being compared to in the same graph. The shape of the growing curves was then compared and showed to be replicated to a realistic (similar magnitude and shape) degree by the models.

A more technical approach for verifying and parametrizing these models would entail a field experiment that allows for the simultaneous data collection of the values of the environmental conditions that are used as driving data, and the individual growth rate during the same time period, as done by Broch et al., (2013) and Venolia et al., (2020). This reduces the variability introduced to the model parametrization caused by variations in environmental drivers, and increases the confidence on the selected parameters that will then define the more abstract internal processes, such as the rate of use of the reserves for maintenance cost and structure growth. The effects of the variations in the parameters can be mathematically quantified by the application of a sensitivity analysis, this explains the influence and degree of each parameter on the model state variables (Broch and Slagstad, 2012a; Jackson, 1987; Strong-Wright and Taylor, 2022; Venolia et al., 2020).

Table 1.5. Comparison of process-based models with respect to data requirements. Colours indicate the species of the model, blue for M. pyrifera, green for L. hyperborea and orange for S. latissima.

Reference	Statistical relationships	Driving Data	Empirical components	Verification	Applications	Limitations
Anderson 1974	Photosynthesis rate. Temperature effect on growth.	Solar radiation data from USA government	Photosynthesis rates manually fitted from data. Temperature effects determined from empirical studies.	Growth curves visually compared to data from another study.	Canopy recovery after harvesting.	No N, metabolism or reserves included.
Jackson 1989	Biomass linked to photosynthetic rates. Respiration rates.	Solar irradiance used as a constant for that latitude.	Light reflectance, as in Anderson.	Compare results of cycles seen to other species.	Harvesting to show response of the model to tissue loss.	No exudation modelled and no nutrients being tracked.
Nisbet and Bence 1989	NA	Surface irradiance, attenuation coefficients and bottom temperature.	Parameters manually fitted to data from the area.	Model mimics observed dynamics.	Research into mechanism regulation giant kelp recruitment.	Temperature is used as a surrogate for nutrient availability.
Rinde 2007	Mortality from Rinde and Sjøtun, (2005). Recruitment rate reduced with decreasing latitude.	NA	Carrying capacity set from data.	Model fit assessed comparing age distribution modelled with data	Determining optimal harvesting strategies.	Authors describes a need for a middle layer to appropriately represents dynamics.
Broch and Slagstad 2012	Weight area relationships for obtaining biomass from published literature. Max growth rate set when reserves are at max s set from literature.	Temperature, Irradiance, water current speed and nutrient concentration	Data used to set parameters, temperature effects, half saturation of N uptake. Parametrised with Sjøtun 1993 data.	Compared to empirical results from published literature.	Aquaculture, bioremediation, depth effects.	No data set with growth, composition alongside the environmental variables was found.
Aldridge et al., 2012	Following Broch and Slagstad 2012.	Temperature, Irradiance, water current speed and nutrient concentration.	Data from Sjøtun 1993 used for parametrisation.	Compared to the range of values reported for other published empirical studies.	Aquaculture potential.	Norwegian individuals used to parametrize Scottish ones, ignoring environmental effects.
Broch et al., 2013	Following Broch and Slagstad 2012.	Following Broch and Slagstad 2012.	Adjusted with data from mesocosm experiment (both growth and environment).	Following Broch and Slagstad 2012	Following Broch and Slagstad 2012.	Hydrodynamics ecological model (SINMOD) applied to estimate cultivation potential.
Van der Molen et al., 2018	Following Broch and Slagstad 2012.	Irradiance, temperature and nutrient concentration.	Following Broch and Slagstad 2012.	Compared to in situ observations for the modelled farms	Potential for aquaculture production.	Coarse representation of coastal geometries.
Venolia et al., 2020	Nitrogen assimilation and photosynthesis rates. For fitting the Arrhenius relationships.	Temperature, irradiance, DIC, nitrate and nitrite.	Calibrated with data from the literature and field data gathered explicitly for this work.	Sensitivity analysis to see the effects of the parameter's changes	Blade length estimates for aquaculture production.	Based on growth is designed for *Ulva lactuca*, a less complex species.
Strong-Wright and Taylor 2022	Following Broch and Slagstad 2012.	Following Broch and Slagstad 2012.	Following Broch and Slagstad 2012.	Repeated Broch and Slagstad 2012 experiments	Feasibility of growth in the open sea. For C removal.	Lacking empirical data for parametrization.

1.2.3 Dynamic Energy Budget (DEB) Theory

The progression from simpler models to those explicitly considering internal biochemical processes highlights the need to accurately represent the balance of these elements within the organism modelled. The first kelp model to consider the internal biochemistry was Broch and Slagstad (2012), before only the elongation of the tissues was included. They make an assumption that the structural mass, the carbon, and nitrogen reserve pools each have a fixed chemical composition, an assumption based in the Dynamic Energy Budget (DEB) theory concept of strong homeostasis (Kooijman, 2000). This implies that, in this case, there are three pools of materials that can vary independently from each other (leading to changes in the overall composition of the organism) while their internal composition remains stable within each pool.

Practical significant of DEB application

DEB theory provides a theoretical context to model metabolism, grounded in shared biological characteristics between species and supported by empirical laws such as von Bertalanffy growth curve (Von Bertalanffy, 1957) and Kleiber's law on metabolic rate (Kleiber, 1932). It applies physical and chemical rules to describe energy uptake and use throughout an organism's life cycle, aiming to capture the quantitative aspects of metabolism. A DEB model essentially tracks energy flow within an organism, from intake, assimilation into reserve to partitioning into structural and reproductive components. It seeks to understand how processes such as feeding, maintenance, growth and reproduction interact, while considering environmental influences like temperature and food availability. Energy serves as a base but it explicitly models the uptake and use of chemical materials (Kooijman, 2000). For a detailed description of this framework, see to Chapter 2.

DEB in the context of kelp

The strong homeostasis principles are applied to maintain the internal stoichiometry of the organism throughout the various processes required to sustain life, where stoichiometry refers to the regulation of the balance and proportions of various substances. Models must account for the variation in the chemical composition of resources assimilated by the organism (Kooijman, 2009). This theory states that while the composition of reserves and structure pools remains constant, it does not imply a fixed chemical composition for the individual, as the amounts of each reserve can vary independent to each other. In the case of autotrophs, the nutrient intakes follow more than one source, for example photosynthesis and nitrogen uptake, hence each potentially limiting resource needs a separate reserve (Ledder, 2014). In their model on *S. latissima*, Broch and Slagstad (2012) include nitrogen and carbon reserves, for structure to increase, and hence growth to occur, both are required in specific amounts (Droop et al., 1982).

In kelp, carbon and nitrogen can take multiple forms inside the organism. Carbohydrates such as laminarin, alginate, cellulose, fucoidan, and the sugar alcohol mannitol (Sharma et al., 2018) constitute the carbon reserve pool. Similarly, nitrogen reserves may include amino acids, minerals, and phenolic compounds (Sharma et al., 2018). These different materials are not modelled individually. The key aspect of all of these components is that their primary element can be defined as carbon or nitrogen, hence assigning them to either reserve pool, illustrating the abstract nature of reserves according to DEB theory. This approach aligns with empirical studies that frequently differentiate carbon and nitrogen content when analysing kelp internal composition (Gevaert et al., 2008; Kregting et al., 2013; Sjøtun et al., 1996). The aggregation of chemical components into generalized pools not only adheres to DEB theory but also reflects the biological reality, as a specific chemical element can be provided through the assimilation of various chemical compounds (Kooijman, 2009), such as nitrogen absorption through nitrate or ammonium.

1.2.4 Connections between the current models

The connections between certain model assumptions, such as the strong homeostasis principle (Kooijman, 2000), used by the different models can be seen in Figure 1.3, where the highly influential effect of Broch and Slagstad, (2012) is apparent. The strong homeostasis ideas applied by Broch and Slagstad, (2012), and the subsequent papers that apply their methodology are also applied in a more strict DEB model by Venolia et al., (2020), highlight the acceptance of the strong homeostasis principle in the current kelp modelling field. This idea is in all of the recent kelp individual growth models. The lack of connections regarding methodological choices between the population dynamics models and the individual based growth models is clear and highlights the next step in the development in the field of kelp process-based modelling being the connection between these two branches of population and individual level models.

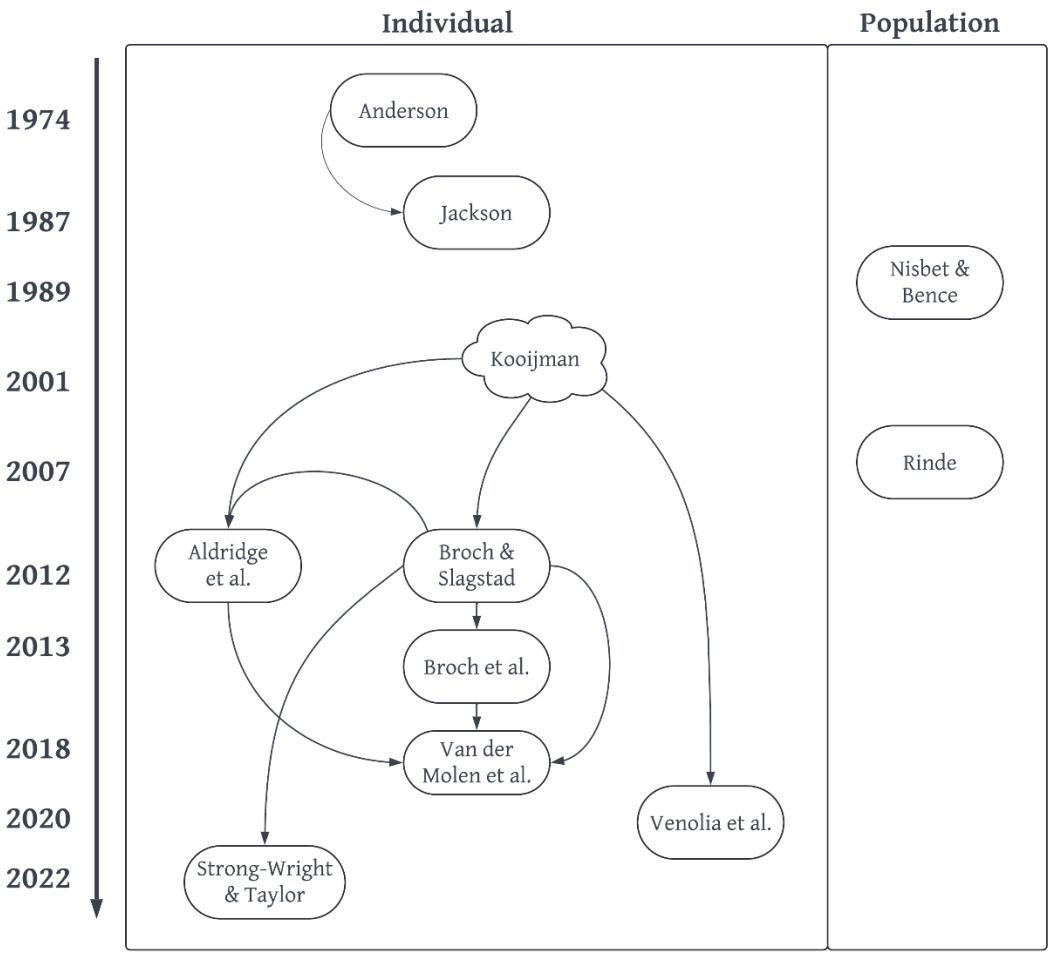

Figure 1.3. A schematic representation illustrating the interconnected methodological choices and concepts among the process-based models for kelp, presented in this thesis at both the individual and population levels. The circles represent kelp models while the cloud shaped represents a specific theoretical framework.

1.3 Desirable features of the next generation of models

This section will first address the current methodological choices in individual growth models, highlighting the frequently used characteristics, as discussed in the previous section, and their biological strengths. Subsequently, the focus will shift into how to integrate these individual growth dynamics into population models, aiming to accurately simulate the dynamics of how a kelp forest grows. As the key gap observed from the previous work is the lack of interconnection between high-level population dynamics and the individuals' internal processes, which drive these population dynamics through their interactions with the environment and each other, competing for available resources and adapting to the highly seasonal nature of said resources in kelp ecosystems.

Previous models represent a kelp forest as a group or collection of groups, not a forest of independently growing individuals, or individuals multiplied to represent an aquaculture setting. An explicit processes-based individual growth model that considers the internal biochemistry of *L. hyperborea* has not been developed. Building on the information from the previous tables, which showed the main components and shortcomings of existing models, the review now looks at how well these findings reflect biological processes, especially focusing on how realistic the modelling decisions are.

1.3.1 Internal biochemistry

Reserves are a key aspect of kelp, specifically in Laminariales, they present a strongly seasonal pattern and are a key adaptation responsible for the species successful occurrence in temperate and polar areas. Here reserves are defined as internal resources of the organism that are used to fuel physiological processes, such as growth and metabolic cost. This definition is based on the dependence of *L. hyperborea* on the internal reserves from their old tissues to sustain the growth of new lamina tissue, during conditions where photosynthesis is not possible, hence showing its reliance on accumulated material (Lüning, 1969a, 1970a).

L. hyperborea and *S. latissima* have different patterns in their use of reserves, which should be taken into account when comparing the representation of reserve in current models (focussed on *S. latissima*) to the developments in the models presented in this thesis. For example, when comparing the carbon content of storage compounds it was shown that *L. digitata* and *L. hyperborea* exhibit notably higher carbon content compared to *S. latissima*, but it's worth noting that the peak still occurs during the autumn season for the three species (Schiener et al., 2015). This difference in how *S. latissima* uses reserves compared to other *Laminaria* species becomes even more pronounced in more northern regions.

The reliance on reserve materials to adapt to harsh winter conditions is evident in *L. solidungula*, an Arctic species that grows during winter under heavy sea-ice cover, using stored carbohydrates from the previous season's blade (Dunton and Schell, 1986) ; a similar pattern is observed in *L. hyperborea* in Helgoland (Lüning, 1969a; Lüning et al., 1973). The opposite behaviour is observed in *S. latissima*, also in the Arctic, with rates for their new growing blade closely tied to active photosynthesis rates (Henley and Dunton, 1995). This example of opposing behaviour highlights the limits for comparisons between models of different species, as a gap for *L. hyperborea* is not necessarily a gap for *S. latissima*. This divergence of behaviour in two closely related species highlights the importance of species-specific modelling choices.

To accurately represent the organism's budget, it is essential to understand the path of the materials entering and leaving the organism, as well as its transformations within the organism. This pathway is clearly stated in DEB models, for example both nitrogen and carbon exudation are consider in explicit DEB models (Venolia et al., 2020) while others (Broch and Slagstad, 2012a) only consider carbon exudation. Empirical research indicates that *L. hyperborea* shows nitrate release during the growth season (Abdullah and Fredriksen, 2014).

Further on maintaining an accurate budget of the internal dynamics, the reserves composition is not made purely of carbon or nitrogen, but of a range of storage compounds. To increase model parsimony each storage compound is not modelled independently, but the total carbon or nitrogen in the aggregate compound is modelled, in other words there is a generalised compound. This is directly a key aspect of DEB strong homeostasis principle, which states that the internal elemental ratio of each generalised compound is fixed, while the total amount of the compound is allowed to fluctuate. Hence, the model response to changes in total nitrogen or carbon reserves at different times of the year can be observed.

1.3.2 Currency

The use of carbon and nitrogen as currencies for modelling these species can be considered appropriate for a species that contains seasonally varying amounts of carbohydrates and proteins (Schiener et al., 2015). In the context of nitrogen, kelp absorbs inorganic nitrogen, including NO_3^- and NH_4^- (Chapman and Craigie, 1977; Chapman and Lindley, 1980), for producing new proteins (Drew, 1983). Hence the use of nitrogen and carbon represents the balance of these elements from the environment through the individual and its subsequent use.

1.3.3 Internal budgeting

Maintenance

To accurately understand the various growth dynamics seen in response to changes in environmental conditions, as those seen through geographic variations, the internal "budget" of the organism must be represented. This is how and in what quantity are the resources that are being taken from the environment used. To accurately represent these behaviours, the model must account for both maintenance and exudation rates. Incorporating maintenance into the model addresses the expenses necessary to sustain the organism's life. This is based on the biochemical process of protein turnover, where cell proteins are constantly broken down and synthesized in eukaryotic cells (Kooijman, 2000). Protein turnover has a cost proportional to the number of cells present, and therefore it is related to the structural volume of an organism (Jusup et al., 2017).

Exudation

A common feature observed in the majority (Table 1.3) of the individual-based kelp growth models presented in this review is use of exudation as a method to maintain the organism's internal biochemical balance. To maintain an internal biochemical balance in the presence of a nutrient limitation, the non-limiting nutrient can be exuded from the organism. In the context of kelp, it would mean that DOC exudation is due to an excess of carbon in relation to the availability of other nutrients, such as nitrogen. Seaweeds preferentially release DOC instead of storing it when there is sufficient light for photosynthesis, but there is limited availability of essential nutrients, such as nitrogen, phosphorus, and iron (Paine et al., 2021).

1.3.4 Light limitation

L. hyperborea grows under light limited conditions for part of the year, with light levels dropping below the saturation point, and frequently falling below the compensation point required for sustaining the individual`s metabolic cost (Kain, 1976, 1971b; Lüning, 1971). The limitations imposed by limited winter light on individual growth rates are further increased by the shading caused by other individuals, adding a light competition element, this is a critical aspect that should be included in individual growth models. This is accurately represented in populations models (Rinde, 2007), but not explicitly included in more recent individual growth models.

1.3.5 Mortality

The modelling methods presented in this review did not reach a consensus regarding mortality. For *L. hyperborea* mortality is linked to drag processes and affected by wave action. Variations in life expectancy are seen in *L. hyperborea*, ranging from 7 years (Kain, 1967, 1963) to 13 years (Jupp, 1972) in the UK, depending on their location. In individual growth models the definition of life expectancy can be set by the run time of the model. For population forest models the issue is more complex, as once the plant reaches sufficient size the probability of death decreases for the individual (Kain, 1963). Later when a larger size is reached, mortality then becomes mediated by wave action through drag (Kain, 1963). Sites with intermediate to high wave exposure tend to contain relatively more young individuals (Kain, 1971a; Pedersen et al., 2012), highlighting the complex interplay between environmental factors and population dynamics. This connectivity leads to the different processes influencing the likelihood of death of the individual are dependent on both its age and size. The effect of individuals life expectancy on populations models will then have an effect in the density-dependent growth dynamics that have been previously highlighted.

Regarding balancing the organism internal composition, both the intake and output of nutrients must be considered for an accurate model. Specifically, methodological choices such as which uptake functions most accurately represent how the process occurs in nature, such as the effects of temperature or when saturation points are reached. The organism is subjected to environmental conditions that then influence that uptake. If the organism grows alongside others in a natural environment rather than a controlled laboratory setting, competition for light will occur and must be accurately represented. Similarly, the "outflow" of nutrients taken in must be considered. No organism can indefinitely accumulate materials, so it is crucial to explicitly account for each nutrient's entry and exit, rather than assuming that this process will not occur.

1.3.6 DEB Summary

Other energy budget models have been developed independently from Kooijman, (2000) framework, but with a focus on energy and not in internal biochemistry (Lika and Nisbet, 2000), this focus does not allow for the direct inclusion of nitrogen and carbon dynamic that is required for the species of interest. Variations in internal nitrogen and carbon dynamics are a key aspect of *L. hyperborea* biology and hence must be the focus when selecting an appropriate framework, leading towards the used of DEB theory from Kooijman, (2000) implementation.

Other theories with a focus on metabolism that do consider the biochemical aspects (Brown et al., 2004) are not focussed on the relevance of reserves to the same degree that Kooijman, (2000) DEB theory. As reserves are a key feature of *L. hyperborea*, this weighs heavily towards selecting DEB theory. Another aspect for the use of Kooijman, (2000) DEB theory over Brown et al., (2004) metabolic theory is the current wide implementation of concepts from DEB (strong homeostasis and the reserve dynamics) for

more than the past decade (Broch and Slagstad, 2012a) for kelp modelling. It should be highlighted that the focus on interactions between temperature and the organism, such as the application of the Arrhenius equation, and the interaction of the organism size with the environmental conditions are present in both approaches. A number of key laws in biology, such as Huxley allometric growth and Kleiber law are presented in both theories to support their specific approaches (Brown et al., 2004; Kooijman, 2020), this highlights that the correct modelling method is highly debatable and multiple ways of expressing the same processes are possible.

1.4 Conclusion

In summary, an ideal physiologically explicit model of a kelp must consider the internal reserves for at least both carbon and nitrogen, and the variation in the organism composition throughout seasonal cycles (for example high C reserves during summer). The life span of the individual, and the interacting processes regulating this such as age and size, must also be take into account. These internal processes must take into consideration the metabolic cost required to keep everything balanced in a dynamic environment. As a method to addressed these required features DEB theory presents as a building point to develop a model that can include these characteristics. There are no individual growth models for *L. hyperborea* developed to the level of detail that is done for in previous models for S. latissima.

The model developed in this thesis addresses the initial gap concerning species specificity. Previous individual growth models have focused on *S. latissima*, accounting for the biochemical processes throughout its life cycle. This thesis, however, specifically addresses *L. hyperborea* growth and its particular adaptations to a light limited environment.

The explicit modelling of reproductive processes has not been undertaken yet and due to its high complexity and specific data requirements it also will not be addressed in this thesis, but the model formulation based on DEB theory is developed here to be able to add this process to the model formulation presented in later chapters.

Previous models (Broch and Slagstad, 2012; Venolia et al., 2020) have not fully integrated carbon and nitrogen dynamics from uptake to exudation. This model fills that gap using DEB principles to separate reserves and structure, essential to *L. hyperborea* biology(Black, 1950; Kain, 1971a; Schiener et al., 2015; Sjøtun, 1993).

It also bridges individual growth and population forest models, where a literature gap exists. Traditional forest models focus on biomass, recruitment, competition, and mortality but lack detailed internal dynamics. Building on Rinde, (2007) two-layer canopy-recruitment-mortality framework, this model adds light, temperature, and nitrogen effects on individual growth. Simulating *L. hyperborea* forests in Scotland, it refines light attenuation and environmental interaction methods for greater accuracy.

The aim of this thesis is to address the gaps in the current models and develop an individual-based process model for *L. hyperborea* forests that provides valuable insights into how these individuals interact with their environment and respond to future scenarios under climate change conditions. Such a predictive approach using process-based modelling offers further understanding of the population dynamics compared to traditional statistical models, particularly in dynamic and complex marine environments. DEB theory stands out as a promising framework because it can handle species-specific complexities and due to its modular approach to metabolic processes, along with the strong homeostasis assumption, helps capture how the organism physiology interacts with the environment and to address forest mortality.

2 Model development and parametrization for a *Laminaria hyperborea* individual using Dynamic Energy Budget (DEB) theory.

2.1 Introduction

In this chapter an individual based model for a *Laminaria hyperborea* individual is developed. The model simulates the growth of an individual throughout its life. Specifically, it addresses how nutrients from the environment are assimilated and used for its internal physiology. To develop this model, Dynamic Energy Budget (DEB) theory (Kooijman, 2000) is used as a framework, due to its focus on organisms internal compositions and its fluctuations in relationship to a dynamic environment. Individual growth models with explicit consideration of internal biochemical dynamics with DEB principles have been developed for *Saccharina latissima* previously (Aldridge et al., 2012; Broch and Slagstad, 2012; Venolia et al., 2020), but not for *L. hyperborea*.

2.1.1 Context for kelp IBM

Broch and Slagstad (2012) applied DEB theory concepts to predict seasonal growth and composition of *S. latissima*. Other more recent DEB models of macroalgae include *Ulva lactuca* (Lavaud et al., 2020) and *Saccharina latissima* (Venolia et al., 2020). The *U. lactuca* model simulates growth dynamics, incorporating nitrogen and carbon assimilation, reserve dynamics, and self-shading effects. The previously mentioned models consider environmental factors like temperature, light, and nutrient levels, specifically incorporating carbon and nitrogen uptake, processing, and growth. A size-structured population dynamics model for *L. hyperborea* has been developed (Rinde, 2007), accounting for recruitment, growth, mortality, biomass, leaf area, and light availability, with a focus on age distribution for the purpose of representing population demographics, not an individual's internal biochemical processes.

The existing literature lacks a DEB model specifically tailored for *L. hyperborea*. Here, I aim to developed a model to start addressing this gap. By shedding light on the growth dynamics and metabolic processes of this species, my research holds the potential to contribute to both scientific knowledge and practical applications in the context of sustainable resource management and conservation efforts.

The following sections first introduces the key aspects of DEB theory, then describes the methods developed in the context of their DEB framework and the modifications that have been made to this framework in my research. Then I will go into detail of the environmental data used as the driving data of the simulations, before moving on to the biological data used for model parametrization. The results will show the model fit to empirical data and the different key processes that this modelling framework can support. Finally, the discussion of my results will highlight their relevance to further understand a complex species and the model applications.

2.1.2 DEB

2.1.2.1 General aspects

DEB theory (Kooijman, 2000) is a valuable framework for understanding organisms' energetics and metabolic organization. It provides a comprehensive description of energy and mass fluxes between the environment and the organism as well as within the organism itself, offering a general approach. DEB theory enables the transformation of substrates assimilated from the environment into materials used by the organism while maintaining the chemical balance of each group of substances, such as the reserve compounds. This modular representation focuses on: assimilation, metabolic cost, growth, maturation/reproduction and aging (van der Meer, 2006), their interaction are shown in Figure 2.1. Maturation and reproduction go to the same pool as the energy spent in reproduction before the individual is mature is considered to be spent in maturation. Aging is included through the rate of changes in the processes being modelled over time.

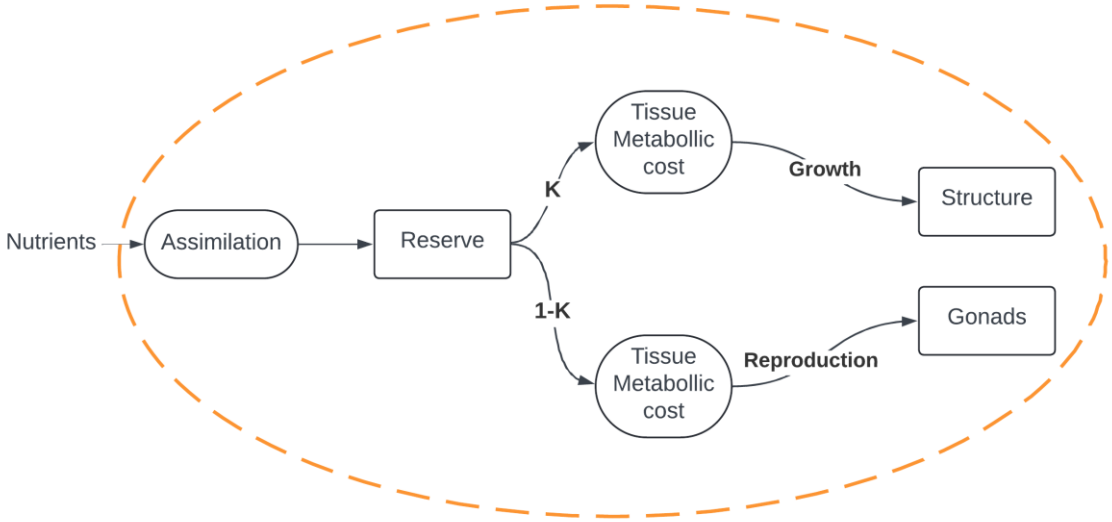

Figure 2.1. Simplified example of DEB model flow of energy. The processes within the dashed orange line are occurring inside the organism. The nutrients are assimilated into the organism from the external environment. The energy acquired is then moved towards the reserves. From the available reserves the parameter κ defines the proportion of energy allocated to either growth or reproduction (Kooijman, 2000). Exudation is not shown as its representation varies highly across the different DEB implementations and this is a general example.

DEB theory is presented as being generally applicable for all species as it is based on fundamental physiological principles of growth and metabolism. The main challenge is to develop taxon specific parameterisations to represent species specific features (Kooijman, 2001; Sousa et al., 2010). Support for this is based on the ubiquitous nature of the laws of thermodynamics (Kooijman, 2001; Sousa et al., 2010), for example, body-size scaling relationships (Nisbet et al., 2000), and generalised relationships such as Von

Bertalanffy growth, which applies only two parameters to describe the growth of a wide range of species (Von Bertalanffy, 1957).

DEB models rely on the application of differential equation to describe the rates of key processes within the organism. These rates are dependent on the state of the individual, for example growth rates seen in a starving individual will be different to those of a healthy one even under the same environmental conditions at that time step (Nisbet et al., 2000). This is due to variations in the size and density of the reserves (Kooijman, 2000; Sousa et al., 2008). The standard DEB model proposed by Kooijman, (2000) uses state variables that do not have a direct biological equivalent. By using abstract concepts to generalise across species it results on DEB models having state variables that cannot be directly measured, although the products of the internal fluxes can be combined into values that are directly observable (Kooijman, 2000; Nisbet et al., 2012).

The internal fluxes in DEB models represent how the energy flows that has entered from the environment into the organism are used, during this process of entering the organism it has to transfer across surfaces (cell membranes as one example), and as a results of this DEB theory can use area and volume to express physiological rates (Nisbet et al., 2000). Those physiological rates are then used to obtain the key components of the organism composition: structure, reserve and reproductive organs, which are the key state variables. Each of the state variables is considered a generalized compound - a combination of a number of chemical compounds which together make up the organism biomass . The partition allows fluctuations in the quantities of internal elements while maintaining a stable internal ratio of those elements (their stoichiometric relationship) required for metabolic functioning.

DEB theory focuses on two main components of organismal mass, structure and reserves. Structure refers to material that needs energy to be maintained - the metabolic cost required to maintain homeostasis. Reserve do not carry a metabolic maintenance cost (Kooijman, 2000). The argument behind reserves not paying maintenance cost relies on their non-permanent nature, i.e. they are constantly being used and replaced (Sousa et al., 2008). The chemical composition of each of the compartments is fixed, and this is termed strong homeostasis. This means that the quantity of structure and reserves can vary independently from each other, while maintaining their stoichiometric balance, it is important that a reserve is present for each pathway of nutrient uptake, for example carbon and nitrogen in autotrophs as opposed to a single reserve in terrestrial heterotrophs.

Energy is essential for growth, and it’s preserved in the new biomass and lost during the creation and maintenance of tissue. These rates are integral components of the modelling process. However, modelling energy itself presents challenges when validating the model against empirical data. To address this, the concept of homeostasis is integrated, where the free energy per mole of structural biomass and reserves remains constant, independent of absolute quantities, this has been an important aspect for cellular function (Kooijman, 2000).

The units chosen are dependent on the specific requirements of the model at hand. Generally, these units can be categorized into flows of substances, quantified in moles of the substance, or into energy, quantified in joules. Moreover, it is possible to define units inside the model by integrating fluxes with physical measurements. A practical case is to look at biomass, in which the molar masses of the structural and reserve components, are combined with their corresponding chemical potentials, measured in joules per mole (J C-mol^{-1}), resulting in ratios that then characterize the relationship between mass and energy. (Jusup et al., 2017).

2.1.2.2 Assimilation

The uptake of energy from the environment into the organism is termed assimilation (Kooijman, 2000). It takes into account the processes required to absorb energy into the reserves for its later use (Sousa et al., 2008). The reason that this process can be seen across different organisms relies on the fact that the molecular process involved all depend on mass transport that occurs through surfaces. As a result, the surface area of an organism is a critical factor in mediating absorption processes, making it a key element in representing assimilation.

2.1.2.3 Reserves

The term reserves is an abstract concept that refers to biological compounds that are used to sustain the organism, they are one of the state variables (Kooijman, 2000, 1986; Sousa et al., 2010). Multiple reserves can be implemented when required, such as the case for autotrophs. These reserves pools ensure that essential compounds are continuously available and the organism growth is not limited by the immediate nutrients availability in its environment (Kooijman, 2000). Under changing environmental conditions the amounts of reserves are able to fluctuate independently to the amount of the structural compound, leading to variation in the overall chemical composition of the organism (Kooijman, 2000).

To account for the effects of nutrient limitation, or simply fluctuating resource availability, the density of the reserves (amount of reserve material per unit volume) is considered, as opposed to just the total amount stored. This is a key aspect given that the body composition of a well fed organism is fundamentally different than one from a resource poor environment (Kooijman, 2000).

2.1.2.4 Maintenance

In simple terms maintenance refers to the cost that needs to be paid to maintain the organism alive. In DEB theory this is termed somatic maintenance (Kooijman, 2000; Sousa et al., 2008). The basis for this process relies on thermodynamics, specifically that the complexity of the organism would decrease in the absence of energy spent on its upkeep (Sousa et al., 2010). Reserves do not pay a maintenance cost due to their transitory nature; reserve compounds are assumed to be in constant use for metabolic process, hence

having a limited lifetime. Structure is assumed to be composed of permanent compounds that require maintenance to remain functional (Kooijman, 2000). The molecular basis that underpins this is the biochemical process of protein turnover, which refers to eukaryotic cell's proteins being constantly degraded and synthesised. This has a cost, which is proportional to the number of cells, and therefore related to the structural volume of an organism (Jusup et al., 2017). Empirical evidence has been used to support this choice, the main example is that freshly produced eggs (which can be assumed to be made almost exclusively of reserve material produced by the parent) do not show a significant oxygen consumption (Sousa et al., 2010, 2008).

A key aspect of somatic maintenance is its priority over growth when energy is being allocated. This means that it increases proportionally to size, enforcing a maximum size for the organisms through maintenance costs (Kooijman, 2000; Sousa et al., 2008). Given the ubiquitous nature of the previously mentioned processes the next step is to state that all the physiological rates are affected by temperature, typically according to a Q_{10} relationship. This relationship defines the proportional change in a physiological rate given a 10°C change in temperature (Kooijman, 2001).

The Q_{10} represent the effects of a 10ºC temperature increase according to the behaviours described by the Arrhenius equation within the DEB framework (Arrhenius, 1889; Kooijman, 2000). Here the Q_{10} rate is chosen as opposed to the basal form of the Arrhenius equation as done in the standard DEB model to focus the temperature increase effects in a biological framework that the model will be acting on. The Q_{10} value for metabolic costs is assumed to be higher compared to that for uptake rates, due to the cost of metabolic maintenance being applied for a volume larger than the surface area through which uptake processes occur.

2.1.2.5 Individual stoichiometry

The balance of the organism's internal composition, or stoichiometry, is maintained through homeostasis, referring to the internal chemical compound composition within an organism (Kooijman, 2000). Control over the internal chemical composition increases an organism's resilience to environmental fluctuation, by acting as a buffer. The chemical composition of the organism varies according to its state, such that well fed and a poorly fed individuals will have different compositions. It is assumed that in an environment with a stable nutrient availability, the organism will reach a stable chemical composition (Kooijman, 2000; Sousa et al., 2008).

When dealing with stoichiometric constrains it is important to consider that when several substrates are required in fixed proportions, then the lack of one of them will limit that uptake (or use) of the other (Kooijman, 2000). This is supported by empirical evidence that demonstrates that the uptake of the most abundant compound can be limited by the least abundant one, this is refer to as the minimum rule by von Liebig (von Liebig and Playfair, 1843). This restriction can be further complicated by the presence of the reserve pools, as the restriction of the minimum compound can then be buffered by the

accumulated reserves, hence no growth restriction would be present to the degree that reserves are available (Kooijman, 2000). These reserve pools are present in nature and function as a buffer, as its seen in kelp (Lüning, 1969a).

2.1.2.6 Limitations

Given the abstract nature of the components of DEB theory the main limitation is the inability to directly demonstrate the rates involved through empirical testing. As the core assumptions relate to homeostasis and the energy allocation, data required for confirming the values would require a vast amount of data that present a significant number of combinations of environmental conditions and output variables. Data from varying environments would be key, as the assumptions proved under constant conditions are most likely not applicable to the entire life on an individual in a dynamic environment. (Nisbet et al., 2000).

Bioenergetics models commonly start by describing energy acquisition from feeding and then splitting it up towards various other process, such as growth, reproduction or respiration. They define these processes in ways that can be directly measured and furthermore converted to energy units, allowing the confirmation of the results through experimental work. This strong empirical foundation comes at the cost of a highly data hungry model, with a large number of parameters required (Nisbet et al., 2012). Although with the application of the more traditional approach special attention should be put upon the dimensionality of the model, basically to avoid the number of parameters increasing to a level where obtaining enough data for them is not possible (Jusup et al., 2017).

2.1.2.7 Criticisms

DEB theory has faced criticism regarding several methodological choices, particularly the lack of the possibility of direct measurement of crucial parameters such as the fraction of utilized energy allocated to growth and maintenance. For instance, oxygen consumption is not only due to maintenance costs, but also the costs associated with growth, reproduction, and mobility (van der Meer, 2006). To address this issue, Kooijman and colleagues employed various strategies, including studying the growth and oxygen consumption of embryos in eggs (Zonneveld and Kooijman, 1993), as embryos rely on initial reserves for growth and maintenance, simplifying the dynamics of reserves and reducing variability caused by variable food intake (van der Meer, 2006).

Furthermore, the high level of abstraction of DEB theory poses a significant limitation to its widespread adoption. This abstraction diminishes the connection to the original theories that describe the variations in the physiological rates being modelled, posing challenges in linking available bioenergetic and biomechanics data to DEB models without compromising their precision (Nisbet et al., 2012).The model assumes that only reserve biomass can fuel metabolic activities, disregarding the degradation of structural biomass to support maintenance respiration during periods of starvation. Addressing these limitations is crucial for the development of a more comprehensive and coherent model of biological growth.

2.2 Methods

This section describes the development of the model of an individual *L. hyperborea* plant, with explicit consideration of the internal biochemical dynamics and their interactions with the external environmental conditions. The model builds upon the strong homeostasis hypothesis, a fundamental tenet of the DEB theory (Kooijman, 2000), which asserts that the chemical composition and thermodynamic properties of an organism's structure and reserves remain fixed within each compound. By maintaining a stable internal chemical composition, organisms gain enhanced control over their metabolism, as the rate of chemical reactions is contingent upon the chemical composition of the surrounding environment (Kooijman, 2000; Sousa et al., 2008).

In autotrophs, such as kelp, the assimilation pathways for the nutrients the organism requires operate independently and due to this multiple reserve pools are required. Specifically, the separation of reserves into specific pools for each assimilation pathways is required to sustain the strong homeostasis assumption that they each have a fixed chemical composition. Therefore, I consider multiple reserves —carbon and nitrogen— each with its own assimilation pathway and reserve.

Furthermore, following DEB theory, the organism's biomass is partitioned into structural mass and reserves, with nutrient uptake being proportional to the organism's surface area. My research expands the standard DEB model to account for the unique characteristics of kelp, such as modelling it as a V1-morph (organisms with surface area proportional to volume) and expanding the standard DEB model to have two separate reserve components (Kooijman, 2001). By incorporating these modifications, I aim to comprehensively represent the metabolic dynamics and homeostasis in *L. hyperborea*, particularly the interplay between different reserves and nutrient availability pathways.

2.2.1 Model description

The development of the model will be explained by focusing on the pathways for nitrogen (N) and carbon (C). A simplified diagram of the model's nutrient flows can be found in Figure 2.2. First, nitrogen is absorbed through nitrate uptake, and carbon is assimilated through a representation of photosynthesis. These nutrients are then stored in the reserve pools.

Once the reserves are built, they are combined into a new flux that accounts for the necessary elemental ratio required for growth. Before growth can occur, a maintenance cost is incurred to ensure the stoichiometric balance of nutrients (in other words such that fixed quantities of each component are used). Since the reserves are not always perfectly balanced due to environmental fluctuations, this balance is achieved through the exudation of the non-limiting nutrient.

Finally, the model can be adapted to divide the flux assigned to growth into two parts: one for the structure pool (growth) and another for the creation of gametes (reproduction/maturation). Although gamete production can be included in the model, this process is currently disabled due to a lack of data for proper parameterization. The model equations are listed in Table 2.1, and then described in detail through the following sections.

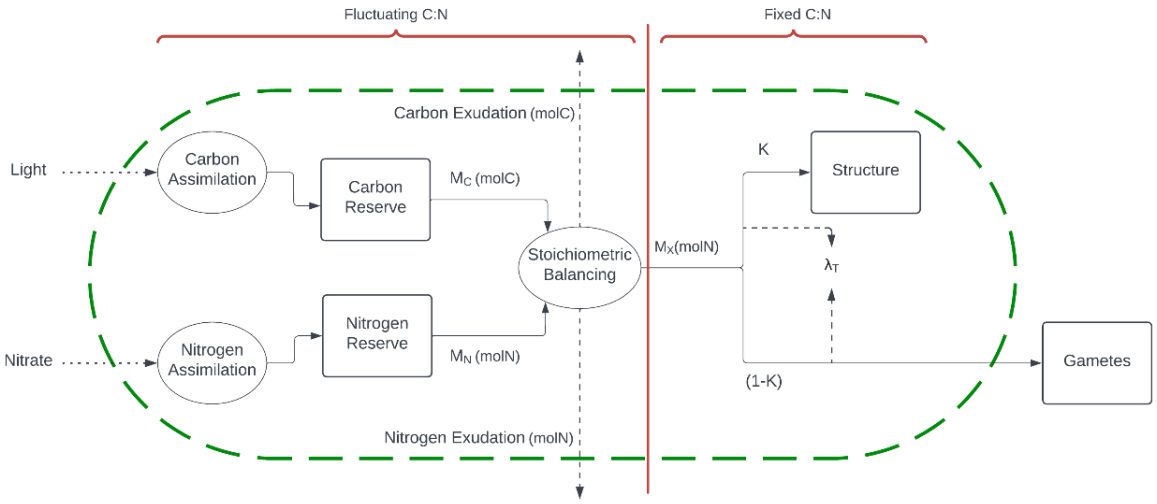

Figure 2.2. Diagram representing the flow of nitrogen and carbon in the model. Dotted lines represent products that either arrive or leave the internal budget. Dashed green line represents the organism internal environment. The red line indicates a change in the behaviour of the C: N composition. The key variables being the reserve and structure pools.

Table 2.1. Model equations and brief descriptions.

Equation	Description	Number
$U_{Nmax_T} = exp\left[\frac{(T_t - T_0)\cdot log(Q_{10U})}{10}\right]\cdot U_{Nmax}\cdot A$	Maximum uptake rate of nitrogen ($moles\ N\ day^{-1}$)	*(2.1)*
$U_{Cmax_T} = exp\left[\frac{(T_t - T_0)\cdot log(Q_{10U})}{10}\right]\cdot U_{Cmax}\cdot A$	Maximum uptake rate of carbon ($moles\ C\ day^{-1}$	*(2.2)*
$U_N = U_{Nmax_T}\cdot\frac{N_t}{N_S + N_t}$	Uptake rate of nitrogen ($moles\ N\ day^{-1}$)	*(2.3)*
$U_C = U_{Cmax_T}\cdot\mu$	Uptake rate of carbon ($moles\ C\ day^{-1}$)	*(2.4)*
$\mu = min\left(1,\frac{L}{L_S}\right)$	Light available for carbon assimilation	*(2.5)*
$\frac{dA}{dt} = \frac{b\cdot A}{S}\cdot\frac{dS}{dt}$	Rate of change in area ($cm^{-2}day^{-1}$)	*(2.6)*
$A = a\cdot S^b$	Area of the plant (cm^2)	*(2.7)*
$\frac{dR_{C_S}}{dt} = \frac{(U_C) - M_C}{S}$	Density of the carbon reserves ($\frac{Reserve\ moles\ C}{Structure\ moles\ N}$)	*(2.8)*
$\frac{dR_{N_S}}{dt} = \frac{(U_N) - M_N}{S}$	Density of nitrogen reserves ($\frac{Reserve\ moles\ N}{Structure\ moles\ N}$)	*(2.9)*
$M_C = \frac{U_{Cmax_T}\cdot R_C}{R_{C_{max}}}$	The mobilisation rate of the carbon reserves ($moles\ C\ day^{-1}$)	*(2.10)*
$M_N = \frac{U_{Nmax_T}\cdot R_N}{R_{N_{max}}}$	The mobilisation rate of nitrogen reserves	*(2.11)*
$p_C = min\left(\frac{\alpha\cdot M_N}{M_C},1\right)$	Usable proportion of available carbon	*(2.12)*
$p_N = min\left(\frac{M_C}{\alpha\cdot M_N},1\right)$	Usable proportion of available nitrogen	*(2.13)*
$M_X = p_N\cdot M_N$	flux of stoichiometrically balanced mobilised nitrogen that can then be used by the organism for structural growth ($moles\ N\ day^{-1}$)	*(2.14)*
$\frac{d^2Ex_C}{dt^2} = \frac{(1-p_C)\cdot U_{C_{max}}}{R_{C_{max}}\cdot\left(A\cdot\frac{dR_C}{dt}\right) + \left(R_C\cdot\frac{dA}{dt}\right)}$	Rate of change of the rate of carbon exudation $moles\ C\ day^2$	*(2.15)*
$\frac{d^2Ex_N}{dt^2} = \frac{(1-p_N)\cdot U_{N_{max}}}{R_{N_{max}}\cdot\left(A\cdot\frac{dR_N}{dt}\right) + \left(R_N\cdot\frac{dA}{dt}\right)}$	Rate of change of the rate of nitrogen exudation $moles\ N\ day^2$	*(2.16)*
$\lambda_T = Q_{10_M}^{T_C}\cdot\lambda$	Temperature dependant maintenance cost	*(2.17)*
$\frac{dS}{dt} = (\kappa\cdot M_x) - \lambda_T\cdot S$	The rate of change in structure nitrogen ($moles\ N\ day^{-1}$)	*(2.18)*
$\frac{dG_M}{dt} = \left((1-\kappa)\cdot M_x\right) - \lambda_T\cdot G_M$	The rate of reproduction ($moles\ N\ day^{-1}$)	*(2.19)*

2.2.2 Assimilation

In this model the organism relies on environmental nitrate to assimilate nitrogen and on light availability to assimilate carbon. Nitrogen availability frequently imposes a limitation on photosynthetic primary productivity in marine waters, as the assimilation cost associated with N is significant (Giordano and Raven, 2014). The extent of competition for it is influenced by factors such as the flexibility of cell stoichiometry (here represented by separate carbon and nitrogen reserves), the availability of the elements in the environment, and the extent to which their acquisition and assimilation can be regulated (Giordano and Raven, 2014). Additionally, reserve nitrogen transport follows similar pathways to reserve carbon (Davison and Stewart, 1983). Carbon assimilation represents the organism's photosynthetic ability, and hence it is completely dependent on light availability. Following these premises, I present the assimilation pathways for nitrogen and carbon in my model, their interaction with other elements is shown in Figure 2.3.

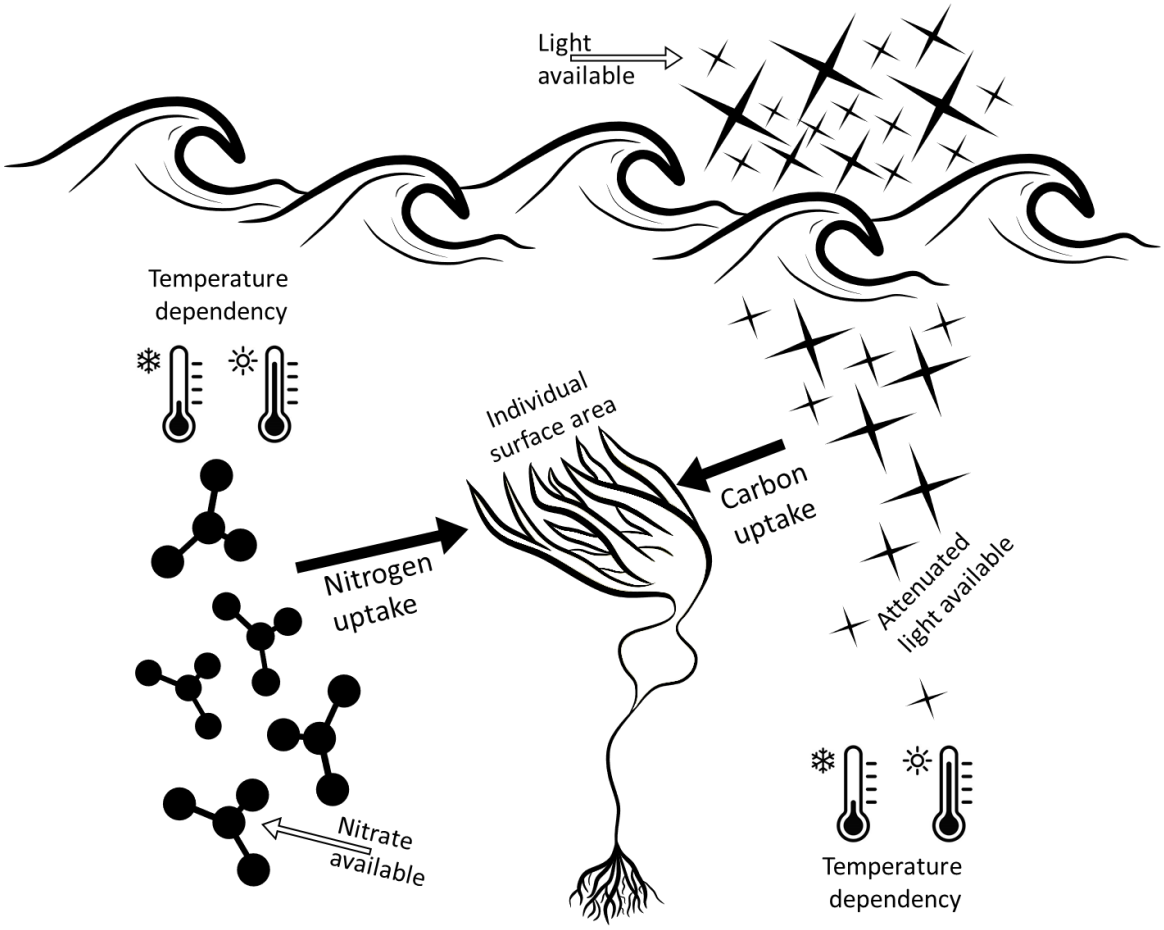

Figure 2.3. Conceptual diagram of the interactions between the different elements of the carbon and nitrogen assimilation processes.

The nitrogen and carbon assimilation processes are modelled based on a combination of environmental factors and biological parameters, following the V-1 morph Dynamic Energy Budget (DEB) framework. The methods used to estimate nitrogen and carbon uptake are outlined below, along with the rationale behind their application.

Nitrogen Assimilation

Nitrogen assimilation is assumed to be proportional to the organism's surface area, in line with the V-1 morph DEB assumptions. Additionally, nitrogen uptake is treated as a temperature-dependent process, meaning that the rate of nitrogen assimilation increases with temperature, up to a certain point.

The temperature effect on maximum uptake rate of nitrogen maximal values ($moles\ N\ day^{-1}$) nitrogen uptake is modelled using the following equation (2.1):

$$U_{Nmax_T} = exp\left[\frac{(T_t - T_0) \cdot log(Q_{10U})}{10}\right] \cdot U_{Nmax} \cdot A \qquad (2.1)$$

Where:

- T_t is the environmental temperature (°C) at the current time step.
- T_0 is the reference temperature (°C), representing the temperature at which the organism's biochemical processes are typically observed.
- Q_{10U} is the temperature sensitivity factor, derived from the Arrhenius relationship (Arrhenius, 1889; Ito et al., 2015), indicating how nitrogen uptake rates change with temperature.
- U_{Nmax} ($moles\ N\ day^{-1}cm^{-2}$) is the maximum nitrogen uptake rate, which is defined during model calibration.
- A is the organism's surface area (cm^2), which affects the extent of nitrogen assimilation.

The equation is based on the Arrhenius relationship, commonly used to describe the effect of temperature on metabolic rates. By incorporating the temperature sensitivity factor (Q_{10U}), the model accounts for variations in nitrogen uptake in response to temperature changes.

Carbon Assimilation

Carbon assimilation is also modelled using a temperature-dependent relationship, analogous to nitrogen assimilation. The maximum carbon uptake rate ($moles\ C\ day^{-1}$) is represented by the following equation:

$$U_{Cmax_T} = exp\left[\frac{(T_t - T_0) \cdot log(Q_{10U})}{10}\right] \cdot U_{Cmax} \cdot A \qquad (2.2)$$

Where:

- U_{Cmax} ($moles\ C\ day^{-1}cm^{-2}$) is the maximum carbon uptake rate.
- The other parameters are defined as in the nitrogen assimilation equation (2.1)

The equation captures the temperature dependence of carbon uptake, with the uptake rate being influenced by the Q_{10U} factor. Just like nitrogen, carbon assimilation is proportional to the organism's surface area, where a larger surface area allows for greater carbon uptake.

Uptake Rate of Nitrogen

Once the maximum uptake rates for nitrogen and carbon are defined, these are incorporated into the actual nutrient uptake rates. The nitrogen uptake rate ($moles\ N\ day^{-1}$) follows a type-II Michaelis-Menten functional response, which represents a saturating process where the uptake increases with availability up to a saturation point. This relationship is modelled by the equation.

$$U_N = U_{Nmax_T} \cdot \frac{N_t}{N_S + N_t} \qquad (2.3)$$

Where:

- N_t is the nitrogen concentration (μ $mole\ N\ l^{-1}$) available in the environment at the current time step.
- N_S is the half-saturation constant for nitrogen uptake, determined empirically from observed nitrogen uptake rates.

The Michaelis-Menten equation models the saturation effect, where the uptake rate increases rapidly at low nitrogen concentrations but levels off as nitrogen approaches its maximum available concentration. This type-II functional response ensures that nitrogen uptake is regulated by the environmental availability of nitrogen, reflecting the limitation in uptake rates as nitrogen becomes scarcer or as the organism's capacity to process nitrogen is exceeded.

The saturation effect of nitrogen uptake is illustrated by the type-II Michaelis-Menten curve, shown in Figure 2.4. This curve demonstrates how the uptake rate increases with nitrogen concentration until it reaches a plateau, representing the maximum assimilation rate. The saturation effect is important in nutrient-limited environments, where organisms compete for limited nitrogen resources.

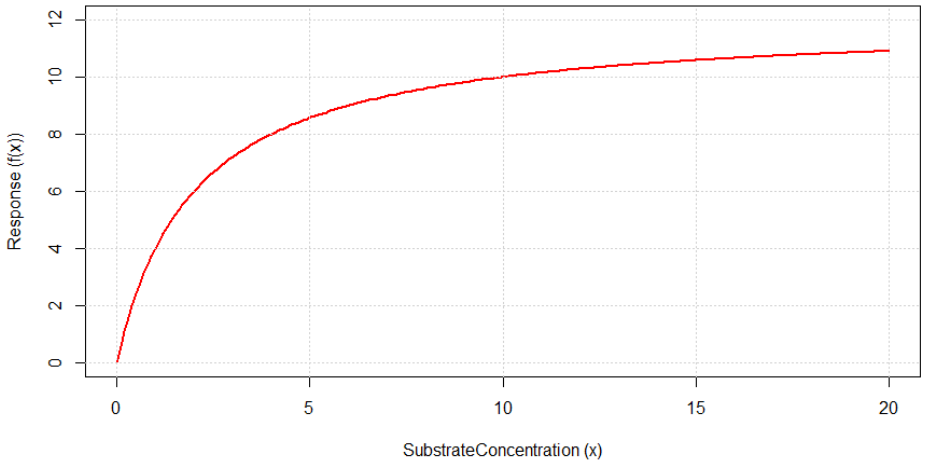

Figure 2.4. Shape of a type - II Michaelis Menten functional response.

By incorporating temperature-dependent uptake rates and a saturating functional response for nitrogen assimilation, the model is able to accurately represent the biological and environmental constraints that govern nutrient acquisition in marine organisms.

Carbon Uptake

The carbon uptake rate ($moles\ C\ day^{-1}$) process is modelled by considering the maximum uptake rate, which is influenced by light availability. The actual carbon assimilation rate is determined by a light-dependent factor, which adjusts the maximum carbon uptake rate according to the light conditions. This is expressed in the following equation.

$$U_C = U_{Cmax_T} \cdot \mu \qquad (2.4)$$

Where:

- U_{Cmax_T} is the maximum carbon uptake rate, which was defined earlier.
- μ is the light dependency function, which limits the uptake based on light availability.

The rate of carbon assimilation depends not only on the organism's maximum uptake capacity but also on the environmental conditions, especially light. This approach allows for realistic modelling of photosynthesis, which cannot occur at its maximum potential unless sufficient light is available.

Carbon Light Dependency

The light dependency of photosynthesis is modelled using a type-I functional response. The function μ (dimensionless) reflects the linear relationship between light availability and the photosynthetic rate up to the point of light saturation. Once the light intensity reaches a certain threshold, the photosynthetic rate cannot increase further. The light dependency is represented by the following equation (2.5):

$$\mu = min\left(1, \frac{L}{L_S}\right) \qquad (2.5)$$

Where:

- L is the environmental light intensity ($Em^{-2}day^{-1}$) at the individual's depth
- L_S is the light saturation point, which is the maximum light intensity the organism can process.

This function indicates that as light availability increases, the photosynthetic rate increases in a linear manner. However, when the light intensity exceeds the saturation point L_S , the rate of photosynthesis levels off, as the organism's capacity to process light becomes fully utilized. The model also incorporates light attenuation through the water column, which is calculated using Beer's Law (Beer, 1852), accounting for the reduction in light intensity with increasing water depth and composition.

The relationship between light availability and photosynthetic response is illustrated in Figure 2.5, which shows the curve of the type-I functional response. This curve demonstrates how the photosynthetic rate increases linearly with light until it reaches a maximum value of 1 at the light saturation point L_S , beyond which the photosynthetic rate becomes constant.

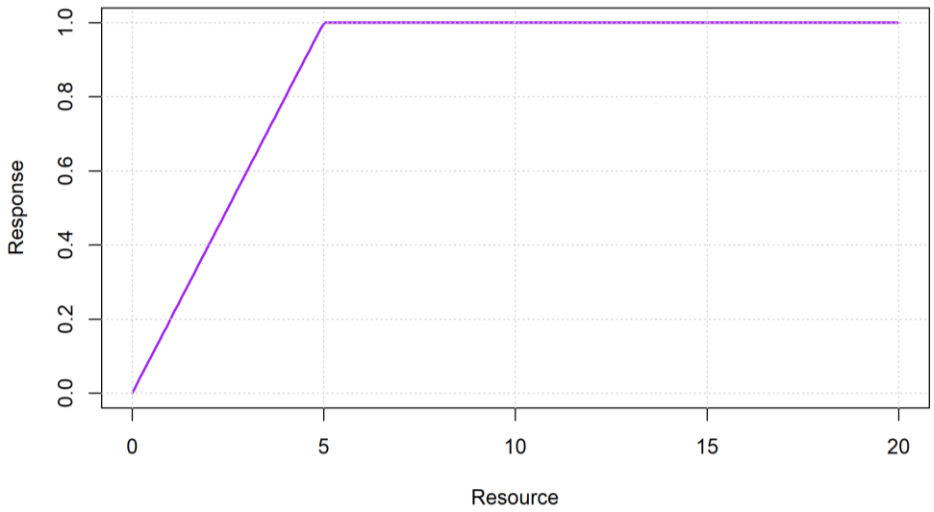

Figure 2.5. The response curve shows how the response changes with increasing resource levels. The response grows until it reaches a maximum value of 1 at the saturation point.

Dependency on Plant Area

The processes of carbon and nitrogen uptake are dependent on the surface area of the plant. A larger individual with a greater surface area will have a higher uptake capacity. As the individual size changes, the surface area adjusts accordingly. The rate of change in surface area ($cm^{-2}day^{-}1$) is given by:

$$\frac{dA}{dt} = \frac{b \cdot A}{S} \cdot \frac{dS}{dt}. \qquad (2.6)$$

Where:

- A is the surface area (cm^{-2}).
- S is the structural nitrogen ($moles\ N$).
- $\frac{dS}{dt}$ is the rate of change in structural nitrogen ($moles\ N\ day^{-1}$).
- b is a scaling coefficient (dimensionless).

This equation reflects the rate at which surface area changes in relation to the plant's structural nitrogen content. The surface area itself is related to the structural nitrogen by the following equation:

$$A = a \cdot S^{b} \qquad (2.7)$$

Where:

- a is a coefficient that defines the relationship between surface area and nitrogen ($cm^{-2}\ moles\ N$).

These relationships follow the principles of von Bertalanffy growth, where the surface area (or size) scales with the available nitrogen in a power-law manner, reflecting typical biological growth patterns. The units are consistent, with $\frac{dA}{dt}$ having units of $cm^{-2}day^{-1}$, and the equation ensuring proper scaling of surface area based on nitrogen availability.

2.2.3 Reserve Dynamics

DEB (Dynamic Energy Budget) models track reserve components, reflecting how well-fed an individual is and indicating which nutrient reserve is limiting growth. Once nutrients are assimilated, they are stored in reserves before contributing to visible growth. These reserve dynamics are expressed in terms of reserve density, rather than absolute material quantities, to provide a clearer representation of the organism's nutritional state and growth potential.

The density of the carbon reserves ($R_{C_S} = \frac{Reserve\ moles\ C}{Structure\ moles\ N}$) depends on the amount of structural nitrogen (S), which represents the size of the organism. The rate of change in carbon reserve density is given by:

$$\frac{dR_{C_S}}{dt} = \frac{(U_C) - M_C}{S} \quad (2.8)$$

Where:

- $\frac{dR_{C_S}}{dt}$ is the rate of change of carbon reserve density (moles of C per mole of structural nitrogen (S) day^{-1}).
- U_C is the carbon uptake rate ($moles\ C\ day^{-1}$).
- M_C is the rate of maintenance cost of carbon ($moles\ C\ day^{-1}$).
- S is the structural nitrogen ($moles\ N$).

The amount of carbon in the organism's structure follows a constant ratio (α) to the structural nitrogen, meaning that the carbon reserve density is directly related to the nitrogen structure of the individual.

Similarly, the nitrogen reserve density $\left(R_{N_S} = \frac{Reserve\ moles\ N}{Structure\ moles\ N}\right)$

per unit structural nitrogen (S)) follows the same type of relationship and is governed by:

$$\frac{dR_{N_S}}{dt} = \frac{(U_N) - M_N}{S}. \quad (2.9)$$

Where:

- $\frac{dR_{N_S}}{dt}$ is the nitrogen reserve density rate of change ($molesN\ day^{-1}$)
- U_N is the nitrogen uptake rate ($moles\ N\ day^{-1}$).

- M_N is the rate of maintenance cost of nitrogen ($moles\ N\ day^{-1}$).

These equations describe the variation in the organism's carbon-to-nitrogen (C:N) composition, as the reserves of each element can fluctuate independently. Additionally, the structure of the organism, influenced by the mobilization of reserves, also plays a role in determining the C:N ratio. As reserves are mobilized, the organism's internal structure is adjusted, further affecting its overall nutrient balance.

2.2.4 Mobilisation

After nutrients are assimilated into the reserves, they must be mobilized to fuel maintenance costs, with the remaining nutrients allocated to growth. The maintenance cost of the structure represents the metabolic cost of the organism. The mobilized reserves rates are denoted as M_C for carbon and M_N for nitrogen.

The mobilization rate of carbon reserves (M_C) ($moles\ C\ day^{-1}$) is given by:

$$M_C = \frac{U_{Cmax_T} \cdot R_C}{R_{C_{max}}}, \qquad (2.10)$$

Where:

- U_{Cmax_T} is the maximum carbon uptake rate ($moles\ C\ day^{-1} cm^{-2}$).
- R_C is the carbon reserves ($moles\ C$).
- $R_{C_{max}}$ is the target ratio of carbon to nitrogen reserves (dimensionless), representing the ideal carbon-to-structural nitrogen ratio under non-limiting conditions.

This target ratio reflects the overall chemical composition of the organism, not just the reserves, and defines the "ideal" C:N ratio during conditions of abundant nutrients and light. The same relationship is used for the mobilization of nitrogen reserves $moles\ N\ day^{-1}$ is shown by:

$$M_N = \frac{U_{Nmax_T} \cdot R_N}{R_{N_{max}}}. \qquad (2.11)$$

Where:

- U_{Nmax_T} is the maximum nitrogen uptake rate ($moles\ N\ day^{-1} cm^{-2}$).
- R_N is the nitrogen reserves ($moles\ N$).

- $R_{N_{max}}$ is the target nitrogen-to-structural nitrogen ratio (dimensionless), similar to the carbon reserve ratio.

For an organism to grow, it must maintain a precise balance between the amount of carbon (C) and nitrogen (N) in its structure, known as stoichiometric balance. This balance is crucial because the organism needs both elements to build new tissues (structure) and carry out metabolic processes. However, when nutrients are mobilized from the reserves to support growth, the challenge is to ensure that the available carbon and nitrogen are in the correct ratio to support this growth.

To maintain this balance, the organism uses a stoichiometric coefficient, α, which represents the ideal carbon-to-nitrogen ratio required for proper growth. This ratio defines how much carbon is needed relative to nitrogen during the formation of new structure. In essence, it dictates the "perfect" balance between carbon and nitrogen for the organism.

Usable Proportions of Carbon and Nitrogen

When the reserves are mobilized (i.e., when nutrients are being taken from storage to be used for growth), not all of the available carbon and nitrogen can be used directly. Some of it may be locked in an imbalance that prevents proper use, so it needs to be determine the proportion of carbon and nitrogen that can be used while maintaining the correct balance.

The proportion of usable carbon is determined by the following equation:

$$p_C = min\left(\frac{\alpha \cdot M_N}{M_C}, 1\right), \qquad (2.12)$$

Where:

- p_C is the proportion of the available carbon that can be used for growth.
- M_N is the rate of nitrogen mobilized from the reserves ($moles\ N\ day^{-1}$).
- M_C is the rate of carbon mobilized from the reserves ($moles\ C\ day^{-1}$).
- α is the stoichiometric carbon-to-nitrogen ratio, assigning the amount of carbon needed for each unit of nitrogen.

The term $\frac{\alpha \cdot M_N}{M_C}$ calculates the proportion of carbon that is available to meet the required C:N ratio. The function min (·,1) ensures that the usable proportion of carbon cannot exceed 100% (i.e., the value stays within a range of 0 to 1).

Similarly, the proportion of usable nitrogen is calculated as:

$$p_N = min\left(\frac{M_C}{\alpha \cdot M_N}, 1\right). \quad (2.13)$$

Where:

- p_N is the fraction (or proportion) of the available nitrogen that can be used for growth.
- M_N is the rate of nitrogen mobilized from the reserves ($moles\ N\ day^{-1}$).
- M_C is the rate of carbon mobilized from the reserves ($moles\ C\ day^{-1}$).
- α remains the stoichiometric C:N ratio.

This equation (2.13) ensures that the nitrogen available for growth is balanced with the carbon that was mobilized, ensuring that the proper C:N ratio is maintained

Calculating the Balanced Flux of Nutrients for Growth

After determining the usable proportions of both carbon and nitrogen, they are combined them to calculate the flux of nitrogen that can be used for structural growth while maintaining the correct stoichiometric balance. The equation for this is:

$$M_X = p_N \cdot M_N \quad (2.14)$$

$$= \frac{M_C}{\alpha M_N} M_N = \frac{1}{\alpha} M_C \quad (2.15)$$

Where:

- M_X is the flux of nitrogen available for structural growth ($moles\ N\ day^{-1}$).
- p_N is the proportion of nitrogen that can be used (from the previous equation).
- M_N is the nitrogen mobilized ($moles\ N\ day^{-1}$).

This M_X value represents the nitrogen that can be used to build new structure, ensuring that the organism's growth is supported by a balanced supply of both carbon and nitrogen.

2.2.5 Exudation

During the mobilization of reserves, not all of the mobilized nutrients (carbon and nitrogen) are used by the organism for growth. Some of the remaining excess nutrients are exuded out to avoid an infinite build-up inside the organism. This process is called exudation, and it ensures that the organism maintains a balance in its internal nutrient levels. The key idea behind exudation is that the excess nutrients that are not needed for growth are released into the surrounding environment. This is important because it helps prevent nutrient overload, which could otherwise disrupt the organism's homeostasis.

In the equations describing exudation, second derivatives are used to represent the rate of change in the rate of exudation over time. The reason for using the second derivative is to capture the dynamic nature of exudation in relation to how the reserves (carbon and nitrogen) change. The second derivative reflects how the rate of exudation is changing at any given moment, giving a more precise understanding of how the process evolves in response to the internal nutrient dynamics. By using the second derivative, the model accounts for both the immediate changes in exudation and how those changes themselves might vary over time, which is important for accurately simulating the organism's nutrient fluxes. The equations for exudation are:

$$\frac{d^2Ex_C}{dt^2} = \frac{(1-p_C)\cdot U_{C_{max}}}{R_{C_{max}}\cdot\left(A\cdot\frac{dR_C}{dt}\right)+\left(R_C\cdot\frac{dA}{dt}\right)} \quad (2.16)$$

$$\frac{d^2Ex_N}{dt^2} = \frac{(1-p_N)\cdot U_{N_{max}}}{R_{N_{max}}\cdot\left(A\cdot\frac{dR_N}{dt}\right)+\left(R_N\cdot\frac{dA}{dt}\right)} \quad (2.17)$$

Where:

- Ex_C ($moles\ C\ day^2$) and Ex_N ($moles\ N\ day^2$) are the amounts of carbon and nitrogen exuded, respectively.
- p_C and $p_N$are the proportions of carbon and nitrogen that are being used (calculated in previous steps).
- $U_{C_{max}}$ ($moles\ C\ day^{-1}cm^{-2}$) and $U_{N_{max}}$ ($moles\ N\ day^{-1}cm^{-2}$) are the maximum uptake rates for carbon and nitrogen.
- $R_{C_{max}}$and $R_{N_{max}}$ represent the "target" ratios of carbon and nitrogen in the organism.
- A (cm^{-2}) is the surface area of the organism, which is critical since exudation happens through the surface.

- $\frac{dR_C}{dt}$ $(moles\ C\ day^{-1})$ and $\frac{dR_N}{dt}$ $(moles\ N\ day^{-1})$ represent the rate of change of the carbon and nitrogen reserves.

- $\frac{dA}{dt}$ is the rate of change in surface area $(molescm^{-2}day^{-1})$, which is affected by the organism's growth.

These equations show that the exudation rates depend on how much of the mobilized carbon or nitrogen is **not** used by the organism (represented by $1 - p_C$ or $1 - p_N$) and are adjusted for how the surface area and reserve sizes change over time.

The area (A) of the plant (cm^{-2}) dependent on the amount of structural nitrogen $(moles\ N)$ present at that time, as exudation is a process that occurs through the surface area of the individual.

As shown in Figure 2.6, exudation represents the process where excess carbon and nitrogen that are mobilized and not used for growth are released into the environment. This helps the organism maintain nutrient balance. The dashed green circle represents the boundary of the organism, and the flow of exudated material depends on how much of the mobilized reserves are being used while maintaining the stoichiometric balance between carbon and nitrogen. The interaction of the processes involved in mobilization and exudation is simplified in this conceptual diagram.

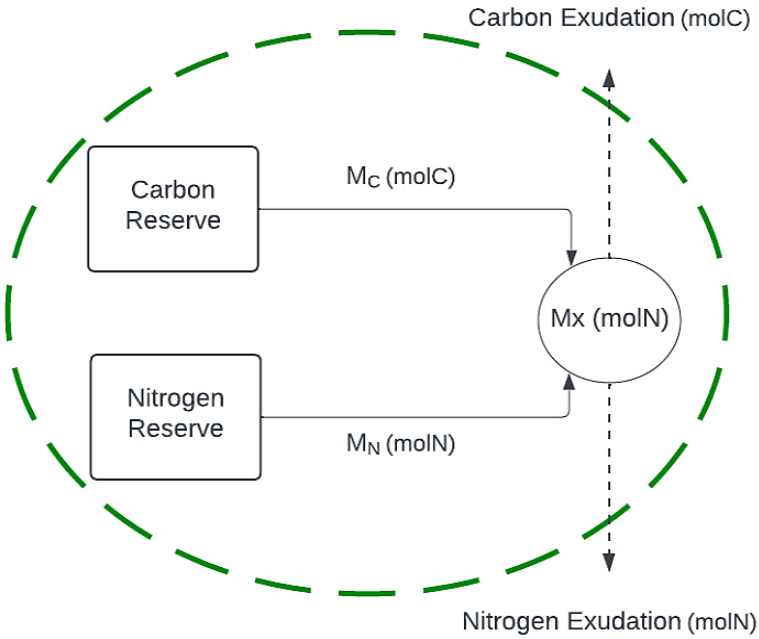

Figure 2.6. Conceptual diagram of the mobilisation and exudation of reserves. The dashed green circle represents the boundary of processes inside the individual. The rate of carbon exudation is determined by the C:N.

2.2.6 Growth

For an organism to grow, it must first meet the metabolic cost associated with its existing tissues. This metabolic cost is necessary to maintain the stability and functioning of the organism's internal environment, and it must be paid before any flux of nutrients can be used for new growth. In this model, the flux of available nutrients, which was previously described as the stoichiometrically balanced flux from the mobilized reserves, is used first to cover the maintenance costs. Once the maintenance needs are met, the remaining flux can be used to expand the organism's structure (i.e., grow).

Maintenance and Temperature Dependence

The maintenance cost is directly influenced by the environmental temperature. To represent how temperature affects this cost, a Q_{10} coefficient is used, similar to how temperature dependence is implemented in the uptake processes. The maintenance cost is thus defined as:

$$\lambda_T = Q_{10_M}^{T_t} \cdot \lambda \qquad (2.18)$$

Where:

- λ_T is the temperature-dependent maintenance cost.
- $Q_{10_M}$is the temperature coefficient for maintenance, showing how much the metabolic rate increases with a 10°C rise in temperature.
- T_t (ºC)is the environmental temperature at the current time step.
- λ is the base maintenance rate, which represents the metabolic cost at a reference temperature.

Growth and Partitioning of Resources

Once the maintenance cost is covered, the remaining flux is available for growth. This flux is partitioned using a factor κ, which determines the portion of the flux that is used for growth. The remaining proportion of the flux (i.e., $1 - \kappa$) is used for reproduction. This partitioning is crucial because it allows the organism to allocate resources efficiently between growth and reproduction based on environmental conditions and energy availability. The key state variable of the model is structure, as it is part of the representation of the biomass of the individual plant, which is the key information that it is used to fit the model to empirical data for *L. hyperborea* growth, together with the amounts of each reserve pool. The rate of change in the structure nitrogen ($moles\ N\ day^{-1}$) is given by the following equation:

$$\frac{dS}{dt} = (\kappa \cdot M_x) - \lambda_T \cdot S \qquad (2.19)$$

Where:

- S is the amount of structural nitrogen ($moles\ N\ day^{-1}$).
- M_x is the flux of stoichiometrically balanced mobilized nitrogen that can be used for growth.
- κ is the proportion of the flux allocated to growth, with the remaining portion allocated to reproduction.
- $\lambda_T \cdot S$ represents the maintenance cost dependant on the structure ($moles\ N$).

This equation describes how the structure of the organism grows over time. The change in structure is determined by the available flux for growth after covering the maintenance cost, with the growth rate being proportional to the flux M_x and the maintenance rate.

Reproduction

In addition to growth, the model also incorporates reproduction. The flux allocated to reproduction is determined by the remaining portion of the flux not used for growth, i.e., $1 - \kappa$. The rate of production of gametes (reproductive tissue) is described by the equation:

$$\frac{dG_M}{dt} = \big((1 - \kappa) \cdot M_x\big) - \lambda_T \cdot G_M \qquad (2.20)$$

Where:

- $\frac{dG_M}{dt}$ represents the reproductive tissue ($moles\ N\ day^{-1}$).
- $1 - \kappa$ is the proportion of the flux allocated to reproduction.
- $\lambda_T \cdot G_M$ represents the maintenance cost of the reproductive tissue ($moles\ N$).

This equation describes how the reproductive tissue (gametes) is produced over time, with the production rate influenced by the available resources and the maintenance cost of maintaining reproductive tissues.

To turn off reproductive output κ is set to 1, leading to all the energy being assigned to structure growth as opposed to partially to reproductive output. This choice has been made due to the lack of data available on reproductive tissue at an individual level with information on internal composition and age. The interaction of the previously described rates can be seen in Figure 2.7.

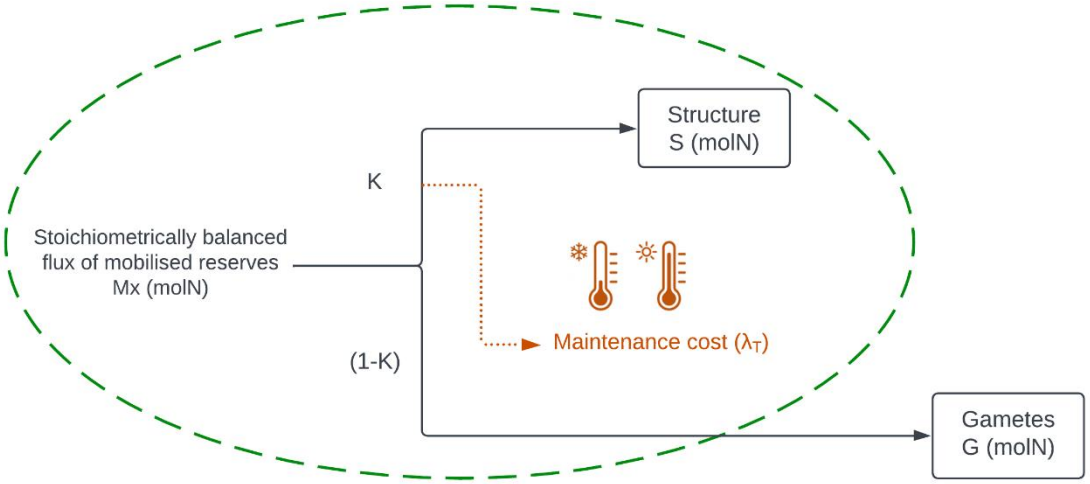

Figure 2.7. Conceptual diagram of the use of the mobilised reserves for growth and reproduction. The dashed green circle represents the boundary of processes inside the individual. The dotted orange line shows the temperature dependent processes, specifically the metabolic cost that must be taken from the flux before it can be assigned to growth.

2.2.7 Biological data for parameterisation

To parametrize the model, biological data specifying the weight and internal chemical composition of the individual at various ages were required. Additionally, the data must be from a single location to remain as close as possible to a growth curve of a single individual, reducing the effect of environmental variations. Data from two contrasting sites were used. First, data from Arisaig, West of Scotland, on *L. hyperborea* which described mean, maximum and minimum weight at various ages and depths were used (Figure 2.8) (Jupp, 1972). The weight of the plants was given by tissue section (i.e., holdfast, stipe and lamina). Secondly, data from Normandy in France provided mean and standard deviations of weights at age by tissue for multiple depths (Sheppard et al., 1978). The Arisaig data were used for model parameterisation, and those from Normandy for validation (Table 2.2). Specific data on carbon and nitrogen content for the two sites were not collected alongside the individual plant measurements. Hence, data from Norway (Sjøtun et al., 1996) and Northern Ireland (Norton et al., 1977), were used as a guidance of the expected values for internal C:N composition during model parametrization (Figure 2.9).

Table 2.2. Site characteristics from the locations of the biological data used, Arisaig (Jupp, 1972) and Normandy, specifically Port Levi (Sheppard et al., 1978).

Characteristic	**Arisaig**	**Normandy**
Latitude/longitude of study site	56º 57'N 05º52'W	49° 41' 11" N. 1° 28' 34" W
Depths at which kelp plants were sampled	3 and 9m	6,9,12 and 15 m
Years in which kelp data were collected	1970	1975-1976
Tidal Streams	Weak tidal streams with eddies	Strong tidal races and currents up to 5 knots for 22 hours per day
Seabed Slope	Gentle westward slope of about 20º	Extremely gradual incline, all depths less than 5º
Substrate	Transition from solid rock to loose stones at 15 m	Predominantly rock, extending to at least 20 m

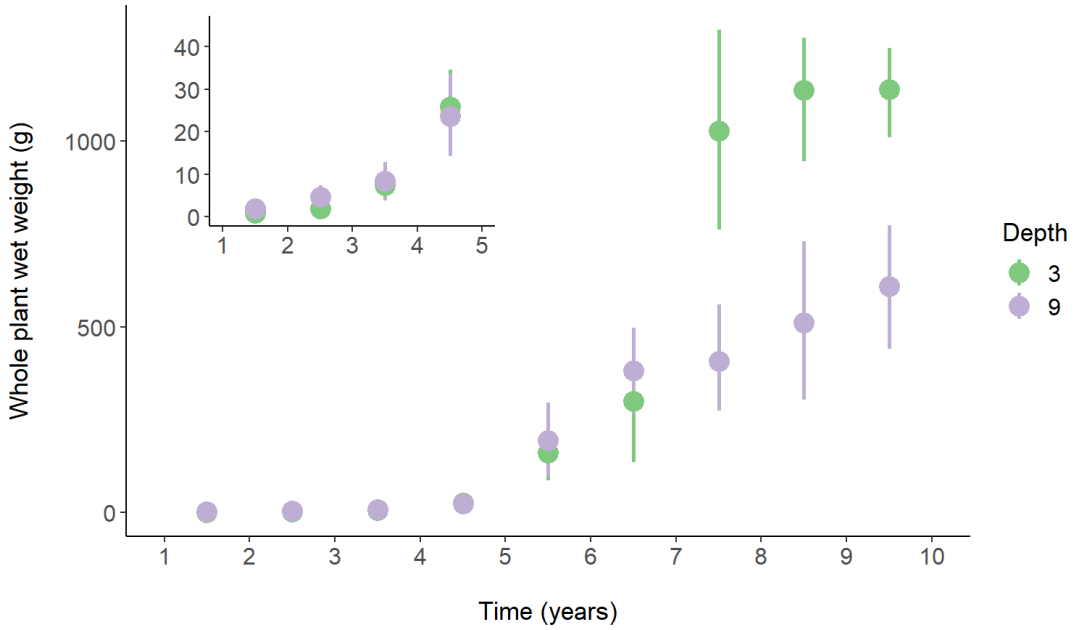

Figure 2.8. Mean whole plant wet weight (g) as points, with minimum and maximum values as lines for the biological data from Arisaig for multiple depths (Jupp, 1972). Subplot shows the first four years in closer detail.

2.2.8 Biological Data Processing

To parametrize the model, the biological data must align with the simulation output, either directly or through conversions, such as converting from moles of carbon and nitrogen to wet weight, using established conversion factors from relevant published literature, described later. The model currency is in moles of nitrogen, with additional information in moles of carbon. To compare this with the empirical data, conversion factors between elemental mass and fresh weight for *L. hyperborea* (Sjøtun et al., (1996)) were used. (Figure 2.9). Given that the organism is composed of more elements than just carbon and nitrogen the following procedure was followed. If its assume that the total wet weight of the plant (W_T) is:

$$W_T = W_C + W_N + W_X, \tag{2.21}$$

where W_C is the total carbon weight, W_N is the total nitrogen weight and W_X is the contribution to the weight of the rest of the components (for example water, phosphorus, iron, etc.). From Sjøtun et al., (1996) the average over year of the dry weight that is not carbon or nitrogen was calculated to be 0.068. A mean value was chosen instead of a seasonal one as the seasonal variations in the content of carbon and nitrogen of the organism will be reflected in the internal composition of the model regardless.

To convert to total wet weight using the known molecular weight of carbon and nitrogen combined with the model output in moles of carbon and nitrogen the following is applied:

$$W_T = \frac{W_C + W_N}{0.068}. \tag{2.22}$$

The molecular weight of a mole of carbon and a mole of nitrogen, together with the amount of each in the model output, given by *S*, are then used in the above equation to obtain the final wet weight. The effects of depth, population structure and location on the environmental condition to which the plant is subjected to did not enable the aggregation multiple sources of empirical data to create a detailed enough data set for a formal fitting process. Parameters were manually tuned to represent model estimates of converted biomass to observations sourced from the literature most complete data set (Jupp, 1972).

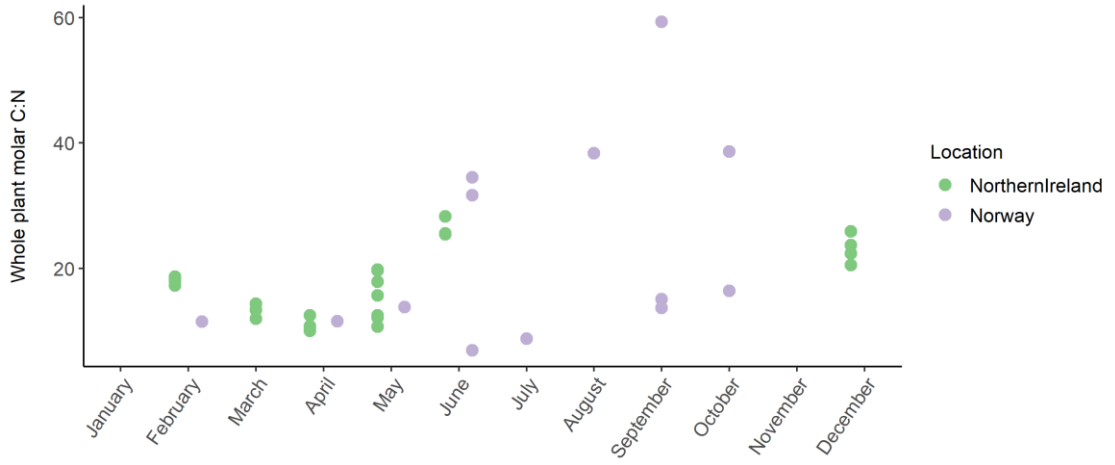

Figure 2.9. Whole plant molar C:N ratio through the year. Data digitised from the literature, combining multiple depths and ages for L. hyperborea *(Northern Ireland - Kregting et al., 2013; Norway - Sjøtun et al., 1996).*

2.2.9 Environmental Data

2.2.9.1 Scotland West Coast

The model parameterization aimed to replicate the biological data from Arisaig, a location chosen due to its comprehensive records of age and weight measurements of individual kelp provided by Jupp (1972). This qualitative, manual fitting process involved aligning the model with these observations to capture kelp growth patterns. The parameterisation process required the model to be driven by a continuous time series of environmental data, nitrate concentrations ($\mu\, mole\, N\, l^{-1}$), light intensity ($Em^{-2}day^{-1}$), and temperature ($°C$), corresponding to the conditions experienced by the sampled plants. However, since Jupp did not record these variables, representative environmental data had to be sourced elsewhere.

The Arisaig study site lies near the MALININ region, used for hydro-chemical monitoring and periodic reporting of environmental conditions (Figure 2.10; e.g. Slesser and Turrell, 2013, 1999). This region is considered hydro-chemically uniform, making it a suitable proxy for missing data. A year-long survey in 1991 (Heath, 1991), conducted close to the MALININ boundary in Loch Linnhe and the Firth of Lorne, provided the necessary environmental data. Measurements of nitrate, sea surface irradiance, light attenuation, and temperature from this survey were compiled into an annual cycle, forming a repeating climatology to drive the kelp model. Figure 2.10 illustrates the location of Arisaig in relation to Loch Linnhe and the Firth of Lorne, highlighting the connectivity of these areas within the MALININ region.

Loch Linnhe, a fjord on Scotland's west coast, is characterized by interconnected basins separated by shallow sills. The Inner Basin, measuring 10 km by 2 km with a maximum depth of 155 m, connects to the larger Outer Basin, which is 30 km by 5 km and 200 m

deep, via the Corran Narrows sill. The area experiences high rainfall (>2000 mm/year), leading to significant thermohaline stratification. The Outer Basin connects to the continental shelf via the Firth of Lorne and the Sound of Mull, areas known for tidal mixing and a dynamic marine environment. This system supports diverse planktonic communities, with turbidity controlling primary production. Plankton species include small calanoids, euphausiids, and larvae, while the area serves as a nursery for juvenile fish such as cod, whiting, and sprat.

The 1991 survey involved 12 sampling campaigns using the vessel *Lough Foyle*. Sampling employed three main methods: the ARIES system for vertically undulating tows, fixed-depth zig-zag tows, and point-station water sampling. These methods captured data on light attenuation, nutrient concentrations, and chlorophyll fluorescence. ARIES collected data at multiple depths using a CTD, rosette sampler, and various sensors, while the fixed-depth zig-zag surveys utilized a continuous nitrate auto-analyser alongside other instruments. Data were aligned with GPS and echo-sounder records to map spatial and temporal variations precisely.

Light attenuation coefficients were derived from vertically undulating surveys, with over 741 measurements recorded during ascents and descents. Daily irradiance values were integrated into a year-long series using PAR data from the Dunstaffnage Marine Laboratory. The zig-zag surveys collected over 3,000 nitrate measurements and 70,000 temperature observations. Environmental data were grouped by month and latitude to estimate depth-specific averages for the Inner Basin, Outer Basin, and Firth of Lorne. These averages provided a robust climatology to drive the kelp model, ensuring a comprehensive representation of environmental conditions. For more detail in the environmental data gathering process see section 7.1 in the supplementary material.

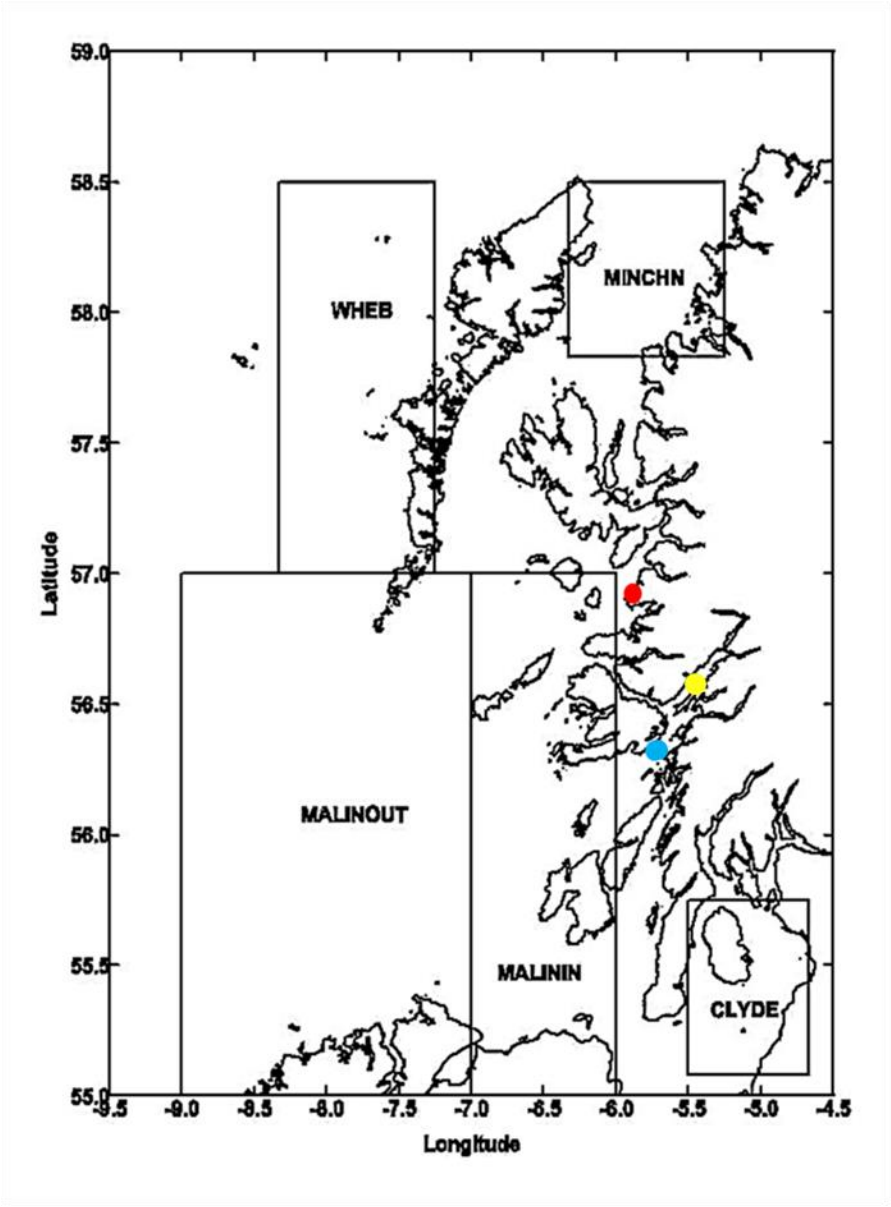

Figure 2.10. Arisaig in red, Loch Linhe in yellow and Firth of Lorne in blue (modified from Slesser and Turrell, 2013, 1999).

2.2.9.2 Normandy

Once the model was parameterized based on the kelp and environmental data from Arisaig, a validation experiment was designed to test the model in a different context, using the Normandy observations. The details of this data can be seen in (Table 2.3).

As for Arisaig, the test for Normandy kelp measurement required environmental driving data corresponding to the conditions experienced by the plants. In this case there were no known intensive survey data, so data were obtained from The Open Access Database on Climate Change Effects on Littoral and Oceanic Ecosystems (OCLE) (de la Hoz et al., 2018). This comprehensive resource provides data on key environmental variables such as temperature, light, light attenuation, salinity, and nutrients, which are vital for studying

marine ecosystems. Focused on seagrasses and macroalgae, the OCLE database consolidates historical data from satellite observations, reanalysis, and in situ measurements. Covering all European seas, OCLE provides data at 0.1° resolution for coastal waters and 0.5° for oceanic waters, represented by 18,200 virtual sensor points.

The dataset utilized includes mean monthly values for each required data component, derived from various resolutions of available data. Due to data availability constraints, the periods vary across different variables, as detailed in Table 2.3. This approach was chosen to provide a comprehensive representation of environmental conditions near Normandy, allowing for the construction of an average annual cycle. By mitigating fluctuations caused by extreme events, this methodology offers a more consistent basis for evaluating the model's performance. The standardized annual cycle derived from this dataset was applied throughout the experiment's duration, repeated annually for each year of the model simulation.

Table 2.3. Summary of information on the data points available from OCLE for each variable, including the number of values, the years covered, and the resolution

Parameter	**Number of values**	**Years**	**Resolution**
Attenuation coefficient (m^{-1})	216	1998-2015	Monthly
Nitrate concentrations (μ $mole\ N\ l^{-1}$)	204	1998- 2014	Monthly
Light intensity ($Em^{-2}day^{-1}$)	135,864	1985 - 2015	Hourly
Temperature ($°C$)	11321	1985 - 2015	Daily

The light data, initially comprising 271,728 points, was reduced to 135,864 points by considering only mean light values during daylight hours. The resolutions were standardized to monthly values, and the mean monthly values for each month of the year were computed. This approach generated a single standardized year of environmental fluctuations, normalized to account for year-to-year variations and focusing on the overall environmental characteristics for the region near Port Levi (Figure 2.11).

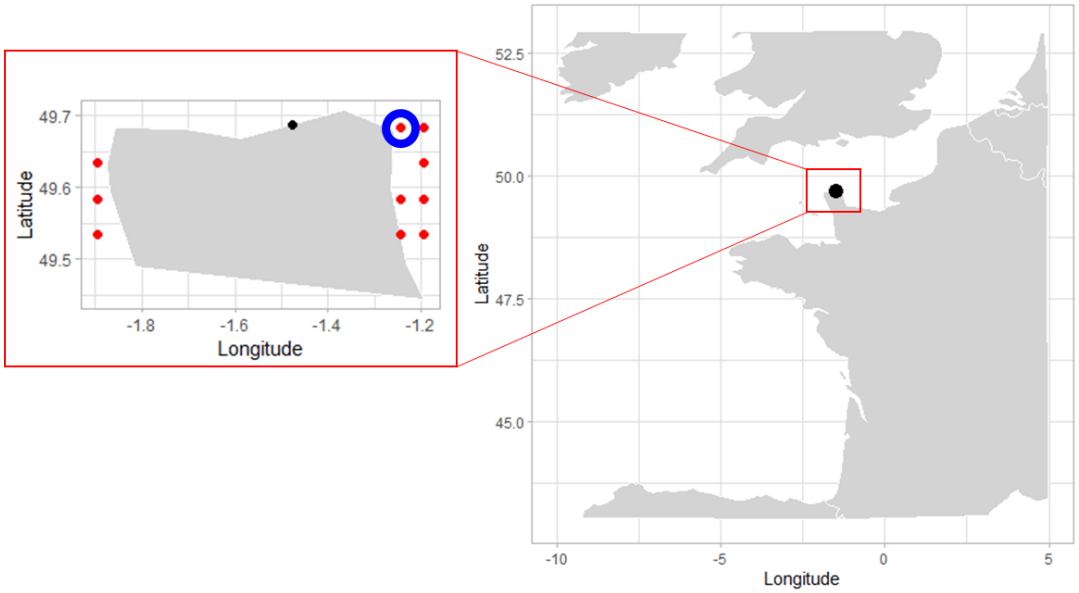

Figure 2.11. Map of the sampling locations. Sheppard et al., (1978)data origin is marked in black, the OCLE points are highlighted in red, and the selected point from which data was extracted is circled in blue, as it was the closest match to the reference location.

2.2.9.3 Final driving data set

This process-based kelp IBM is developed to represent how the internal dynamics of an *L. hyperborea* individual respond to environmental conditions. Since measurements of light intensity are typically taken at the sea surface, while the simulated growth occurs at a particular depth, it is essential to consider the attenuation of light in the driving data. Therefore, an additional category of driving data, namely the attenuation coefficient, needs to be included to account for this factor. To obtain the light intensity at depth (L_d) Beer-Lambert law is used (Beer, 1852) to attenuate the light available at surface level:

$$L_d = L_0 \cdot exp(-k \cdot d), \qquad 2.23$$

where L_0 refers to the light intensity at the surface, d is the depth (m), and k is the attenuation coefficient.

The light data for both locations was attenuated to the respective depth of the individuals from the biological data they were being compared to. The single annual cycle that is repeated in the driving data to be implemented as a repeating annual cycle for the duration of the simulation is seen in Figure 2.12. The irradiance at surface is then subjected to the mean attenuation coefficient of the specific locations being simulated, Normandy (0.323) (de la Hoz et al., 2018) and Scotland (0.212) (Heath, 1995). Similar nitrate values are seen in both locations, this simplifies the data interpretation of the effects of latitudinal variation, as only temperature and irradiance show a drastic difference.

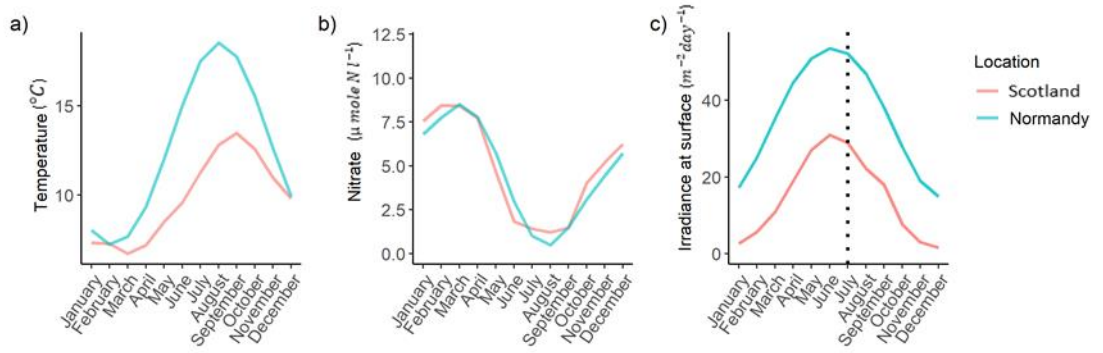

Figure 2.12. Standardised single year cycle of environmental driving data from the west coast of Scotland (Berx et al., 2015; Heath, 1991, 1995a) and for Normandy (de la Hoz et al., 2018). Temperature (a), nitrate(b) and irradiance at surface (c) are shown. The surface irradiance data is then attenuated applying Beers-Lambert law top obtain attenuated irradiance at depth.

2.2.10 Parameters

Following DEB methodology, the initial parameters were split between fixed (Table 2.4) free (Table 2.5) and free ones are those that have to be estimated by optimisation to data since they could not be estimated directly from independent evidence. Fixed parameters are based on independent evidence (Marques et al., 2014). Parameters a and b source data can be seen in the supplementary material (Table 7.1).

Table 2.4. Fixed parameters list and their respective values.

Parameter	Description	Unit	Value	Source	Modification
a	coefficient of area to moles structure relationship	$mol\ N\ cm^{-2}$	15145	(Kain, 1977)	Determined from published digitised data
b	power of area scaling with structure	dimensionless	0.89	(Kain, 1977)	Determined from published digitised data
N_S	nitrogen uptake half saturation	$mM\ m^{-3}$	5	(Gagné et al., 1982)	Used directly from the literature
α	stoichiometrically balanced carbon to nitrogen molar ratio	dimensionless	20.28	(Kregting et al., 2013)	Used directly from the literature
Q_{10_U}	Q_{10} for uptake	dimensionless	1.67	(Aamot, 2011)	Used directly from the literature

Parameter	Description	Unit	Value	Source	Modification
Q_{10_M}	Q_{10} for maintenance	dimensionless	2.1	(Aamot, 2011)	Used directly from the literature
L_S	light saturation intensity	Em^{-2}	10	(Johnston et al., 1977)	Used directly from the literature

2.3 Results

2.3.1 Model fitting

The free parameters (Table 2.5) were hand tuned to fit the growth curve shape of the older plants in the Arisaig data (Jupp, 1972), assuming that these plants reflected the climatological annual cycle of environmental driving data. Additionally, as per the authors description, the younger plants had grown under a heavy canopy with significant light restriction and there was a lack of middle length individuals (Jupp, 1972). For the tuning procedure the parameters where first sorted into three groups: uptake, reserves and metabolism. The initial stages of the values were selected to maintain biological realism in the results, for example the reserves ratio will always have to store a higher amount of carbon than of nitrogen, as per empirical results for this species (Sjøtun et al., 1996). The Q_{10} reference temperature started at 10°C as the Arrhenius dynamics can be re-expressed as the Q_{10} rate, which describes the rate of change with a ten-degree temperature increase (Ito et al., 2015). The uptake rates started with values from 1.5 e^{-4} mol values seen in (Venolia et al., 2020) for volume specific nitrogen assimilation. Reproduction was not included, through $\kappa = 1$, assigning all the mobilised resources to growth,

Table 2.5. Free tuning parameters and their respective values developed to match the Arisaig biological data (Jupp, 1972).

Parameter	Description	Unit	Value
$U_{C_{max}}$	uptake rate of carbon per unit area at the reference temperature	$moles\ C\ day^{-1}cm^{-2}$	2 x 10^{-5}
$U_{N_{max}}$	uptake rate of nitrogen per unit area at the reference temperature	$moles\ N\ day^{-1}cm^{-2}$	2 x 10^{-6}
$R_{C_{max}}$	'target' ratio of reserve moles carbon to structural moles nitrogen	dimensionless	80

Parameter	Description	Unit	Value
$R_{N_{max}}$	'target' ratio of reserve moles nitrogen to structural moles nitrogen	dimensionless	4
κ	proportion of resources allocated to structure	dimensionless	1
λ	maintenance cost at the reference temperature	$mol\ N\ day^{-1}$	0.0181
T_0	Q_{10} reference temperature	$^{\circ}C$	12

2.3.2 Fitting of starting conditions

The starting conditions of the simulation were treated as fitting values and therefore were manually adjusted to fit the growth curve inferred from the empirical data used, as no data was obtained that was compatible with direct input into the model (Table 2.6). These conditions were selected to ensure smooth and biologically plausible initial stages of the model.

Table 2.6. Starting value for the state variables of the model.

State Variable	**Description**	**Unit**	**Value**
Reserve Carbon to Structure Nitrogen	Density	$moles\ C/molesN$	0.005
Reserve Nitrogen to Structure Nitrogen	Density	$molesN/molesN$	0.005
Structure Nitrogen	Mass	$moles\ N$	1×10^{-15}

2.3.3 Case Study: Arisaig

2.3.3.1 Arisaig Growth Dynamics

Before interpreting these results, it is important to consider that the empirical data does not represent a growth curve for an individual. Instead, it reflects weights at various ages from a cross-section of the population, it is a snapshot of individuals from multiple annual cohorts and their respective weights. As a result, younger plants in the population may have experienced different light conditions compared to older ones due to shading effects.

The model that was manually tuned to the Arisaig 3m depth canopy plants was applied to simulate the complete life span of an individual with the west coast of Scotland environmental driving data for 3m and 9m depth (Figure 2.13).

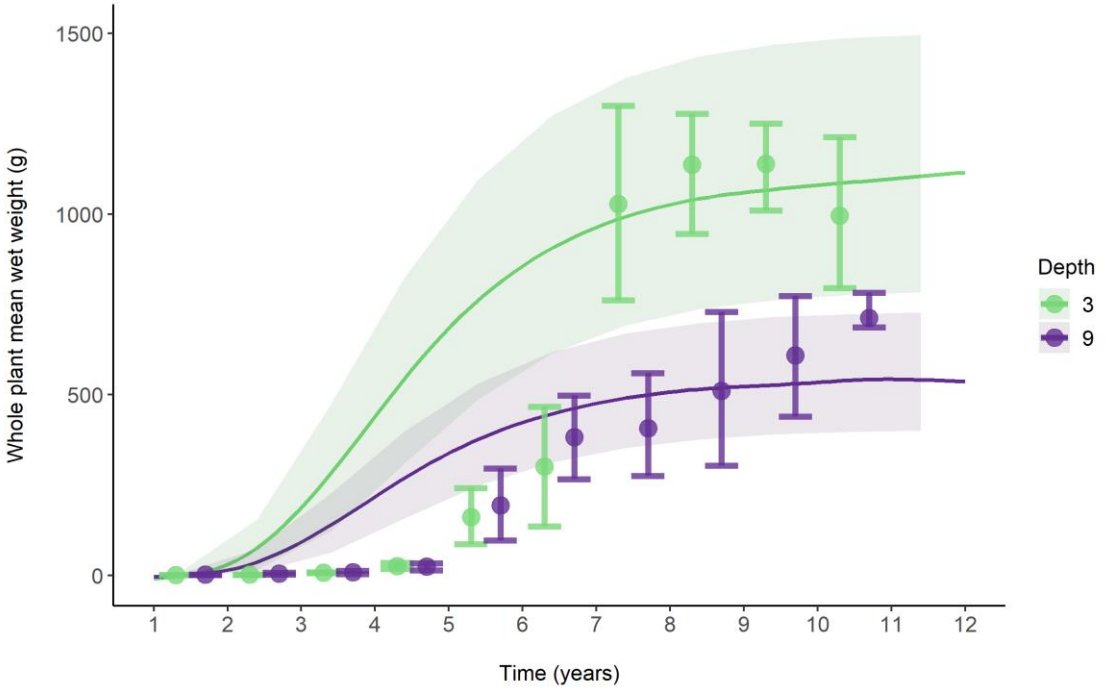

Figure 2.13. Mean model output converted to wet weight shown by the continuous line, the shadings show the variations due to seasonal fluctuation. Data used for model parametrization shown by points, the maximum and minimum values are given by the bars (Jupp, 1972). The model output is a continuous growth curve while the empirical data is a snapshot of the weights and ages of the populations at the time of sampling. The depth at which the data was gathered is shown by the colours, the simulation was run at matching depths. Model output shown for 3m (green) and 9m (purple) depth.

Both the modelled growth curve and the weight-age relationship observed in empirical data (Jupp, 1972) exhibit a sigmoidal curve, albeit with a more pronounced shape in the empirical data. The more pronounced shape in the empirical data was described by the author (Jupp, 1972) as the effect of competition for light under the canopy having a significant effect on the younger individuals (Jupp, 1972). This effect of competition for light is not present in this model, as it represents a single individual and hence no competition is present. To address this divergence caused by the effects of population structure on the reference data, additional experiments were conducted on light attenuations, as detailed in the supplementary material (Figure 7.6,Figure 7.7). These experiments revealed that if the individual was initially subjected to significantly reduced light conditions during its early years, followed by a substantial improvement in conditions (such as those seen if a storm that removed older individuals and increased light availability), the growth curve closely matched the empirical data. This is further developed in later chapters, and served as the initial building aspects of the individual based forest growth model.

Depth plays a crucial role in diminishing the final stable state weight of the individual due to light attenuation, which limits the photosynthetic rates that can be achieved. The variation in the model weight represents the reserves and structure fluctuations (Figure 2.14) in response to the environmental seasonal fluctuations. They compare to the maximum and minimum weight seen in the empirical data (Figure 2.8, Figure 2.13). It should be taken into consideration that the range of values the empirical data also reflects the individual variations.

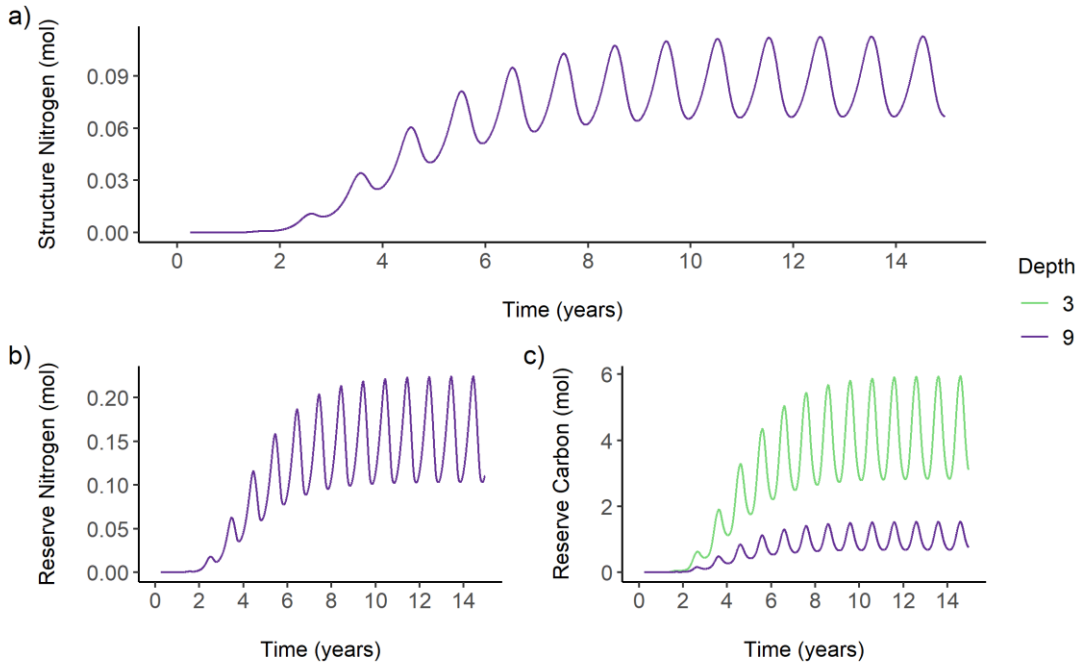

Figure 2.14. Structure nitrogen (a), reserve nitrogen (b) and reserve carbon (c) amount throughout the simulation. Structure carbon is not shown as it follows the same curve as structure nitrogen given their fixed ratio. Model output shown for 3m (green) and 9m (purple) depth. All values shown in moles of their respective element. The presence of a single line indicates a complete overlap for both depths.

Structure nitrogen and structure carbon follow a constant ratio, hence the total structure of the individual will always have the same proportion of carbon to nitrogen. At both depths (3m and 9m), the internal composition of the state variables (structure and reserve) for nitrogen displays similar patterns, as the simulation does not alter the environmental nitrates with depth. However, the carbon reserves show a clear reduction with depth due to the attenuation of light (Figure 2.14, c). In the deeper simulation (9m), individuals do not reach their light saturation point, even during the summer season, this results in a restricted accumulation of carbon reserves. The effect of the previously mentioned light restriction can be clearly observed when comparing the carbon reserves from both sites, specifically as the values for the shallower depth more than double the values for the deeper depth.

The model's yearly fluctuations correspond to seasonal changes. The maximum temperature is seen in September, while the maximum in light availability occurs in June, and for nitrate in February (Figure 2.12). These three factors interact to drive seasonal fluctuations in the individual, which are dampened by the presence and reliance of reserves during the limiting periods. This approach ensures that carbon and nitrogen reserves peak at different times, aiming to maintain a consistent flux of stoichiometrically balanced materials for structural growth. Additionally, these dynamics are further influenced by the effects of temperature on metabolic costs, represented by maintenance cost in DEB theory. The decrease in structure seen is due to the mobilisation of reserves not being sufficient to pay the metabolic cost. The interactions between the state variables and their environment are not linear processes, but complex interdependent dynamics that are explained by further interaction of internal processes.

2.3.3.2 Arisaig Biochemical Fluxes

The model represents reserve carbon and reserve nitrogen as independent pools of substrate following the strong homeostasis assumption (Kooijman, 2000), when they are considered in combination with the structure pools the cyclical fluctuations in the total plant C:N composition throughout its life (Figure 2.15) are obtained. The individual C: N fluctuations during the first year of the simulation, and its divergence from the steady repeating cycle seen later on, responds to the initial conditions of the state variables C:N ratio, the initial peak is due to the selected values at the start of the individual's life and not the steady state of the system. The effect of the reduced carbon reserves due to increasing depth is clearly shown by the less pronounced curve seen at 9m depth.

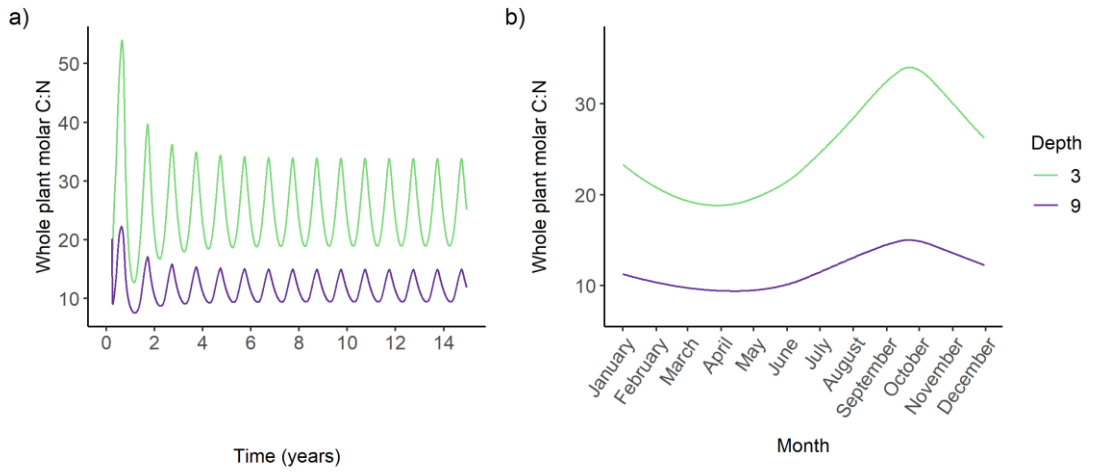

Figure 2.15. Whole plant molar C:N ratio for the entire simulation run time shown on the left (a) and a single year from 6 to 7 years old shown on the right (b). Model output shown for 3m (green) and 9m (purple) depth.

The internal dynamics of carbon and nitrogen within the individual are significantly influenced by external seasonal fluctuations. The model captures this dynamic by simulating the balance between utilization(Figure 2.16, a), uptake (Figure 2.16, b), and exudation fluxes (Figure 2.16, c), which reflect the individual's adaptation to these seasonal variations while maintaining internal homeostasis. The overall increase in maximum uptake rate is due to the increase in the individuals surface area with age. The previously observed decrease in carbon reserves can be attributed to a reduction in carbon uptake, resulting in the following decline of carbon mobilization. The limitation imposed on plant growth becomes evident when considering the absence of carbon exudation at a depth of 9 meters, indicating it becoming a limiting substrate. Moreover, the importance of this light limitation becomes apparent when comparing it to the behaviour of nitrogen fluxes, which exhibit no variation with depth (Figure 2.17).

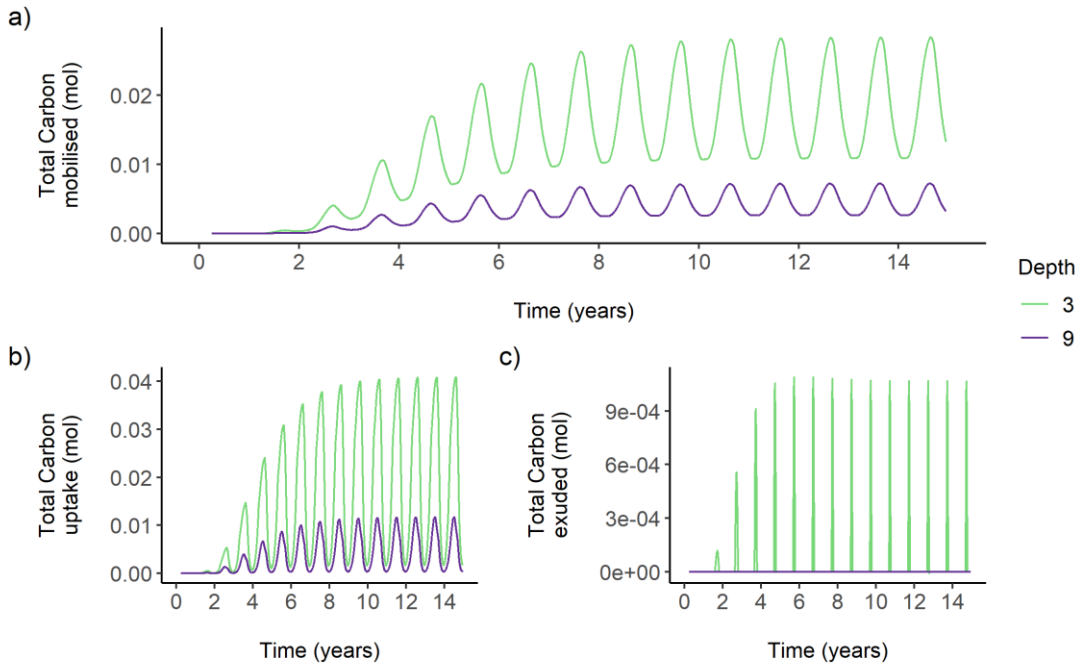

Figure 2.16. Input and output of carbon fluxes throughout the simulation. Carbon mobilised (a) refers to the amount of carbon uptake (b) that was incorporated onto the state variables. Carbon exuded (c) refers to the material that left the organism to maintain internal homeostasis. Model output shown for 3m (green) and 9m (purple) depth.

The model nitrogen fluxes exhibit distinct responses to seasonal changes in nitrate availability (Figure 2.17). Environmental fluctuations cause nitrate levels to remain above the individual half saturation points from November to the end of April, while the remaining months experience lower nitrate concentrations. This, in combination with the increased structural growth during late winter to early spring, results in higher maintenance costs as a results of the greater quantitiy of structure. This timing aligns with the decrease in nitrogen availability and the rise in temperature, leading to even higher metabolic costs in summer. Nitrogen uptake displays a larger peak in early spring and a smaller one in autumn. This flux reflects nitrate availability in relationship to the individual size. However, the pattern observed in mobilized nitrogen does not mirror this behavior. The absence of an exudation flux indicates that there is no nitrogen surplus.

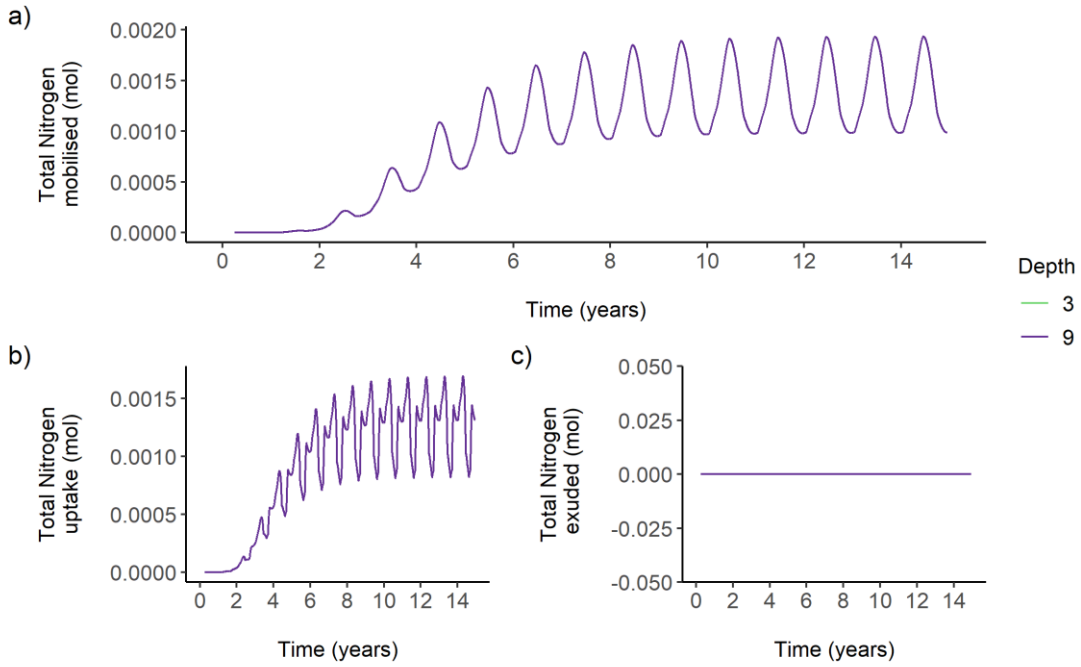

Figure 2.17. Input and output of nitrogen fluxes throughout the simulation. Nitrogen mobilised (a) refers to the amount of nitrogen uptake (b) that was absorbed onto the state variables. Nitrogen uptake is the moles of nitrate that are then absorbed into the organism. Nitrogen exuded refers to the material that left the organism to maintain internal homeostasis (c), the constant value here is in response to a nitrogen limitation in this scenario. Model output shown for 3m (green) and 9m (purple) depth Green is not seen due to the overlap in results for both depths.

2.3.4 Case study: Normandy

The model, parametrised using the west coast of Scotland data, was subjected to the Normandy driving data as a cases study, and the results compared to the Normandy empirical data (Sheppard et al., 1978). This allows us to assess how realistically the model responds to higher temperature and irradiance conditions, with similar nitrate concentrations.

The model weights at age shows an underestimation compared to the Normandy empirical data at all depths, with the exception of the 18m´s depth individuals. The effect of light limitation from 6 to 18 m for the growth rate is clear in the reduction in weight with depth, both in the empirical data (Sheppard et al., 1978) and in the simulation (Figure 2.18).

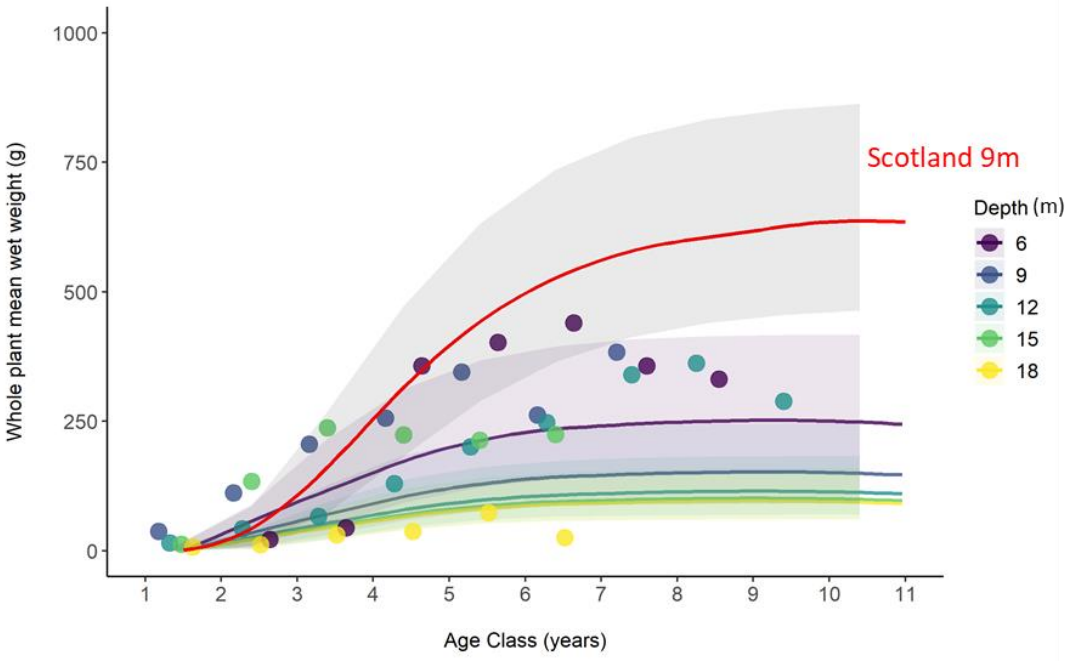

Figure 2.18. Simulations for Normandy. Mean model output converted to wet weight shown by the continuous line, with the variations due to seasonal fluctuation shown by the shading. Mean biomass from the empirical data shown by points (Sheppard et al., 1978). The model output is a continuous growth curve while the empirical data is a snapshot of the weights and ages of the populations at the time of sampling. The depth at which the data was gathered is shown by the colours, the simulations were run at matching depths. Depth of the simulation shown in the legend. The baseline run is represented by the red line, for the original Scotland run at 9m depth with the west coast of Scotland environmental data.

The cycles in the internal fluxes of the organism (Figure 2.19) are in response to seasonal variations in the environmental data. The fluctuation in the internal composition of the individual further reflects the effect of light limitations on growth. Increasing depth has a drastic effect reducing the carbon reserves of the individual. This limitation in the carbon reserves would then have an effect on the amount of carbon available to provide the stoichiometrically balanced flux of nitrogen available for structure growth, in other words not enough carbon is available to sustain the fixed C: N proportion required in the structure pools. The pattern in size reduction among the different depths previously shown is driven mostly through the reduction in carbon reserves, which is even more clear when compared to the baseline carbon reserves values that were observed in Scotland. The overlap in the lines for each depth resulting in the appearance of a single line shows that they have an identical response to the changing depth in their nitrogen dynamics. The limitation on structure responds to the increasing maintenance cost due to a temperature increase seen at the more southern location. The mismatch with the Normandy data could be influenced by factors such as temperature-dependent maintenance costs or the choice of Q_{10} reference temperature. Further data, including energy expenditure and internal composition from individuals of different ages across both locations at different times of the year, may help clarify this.

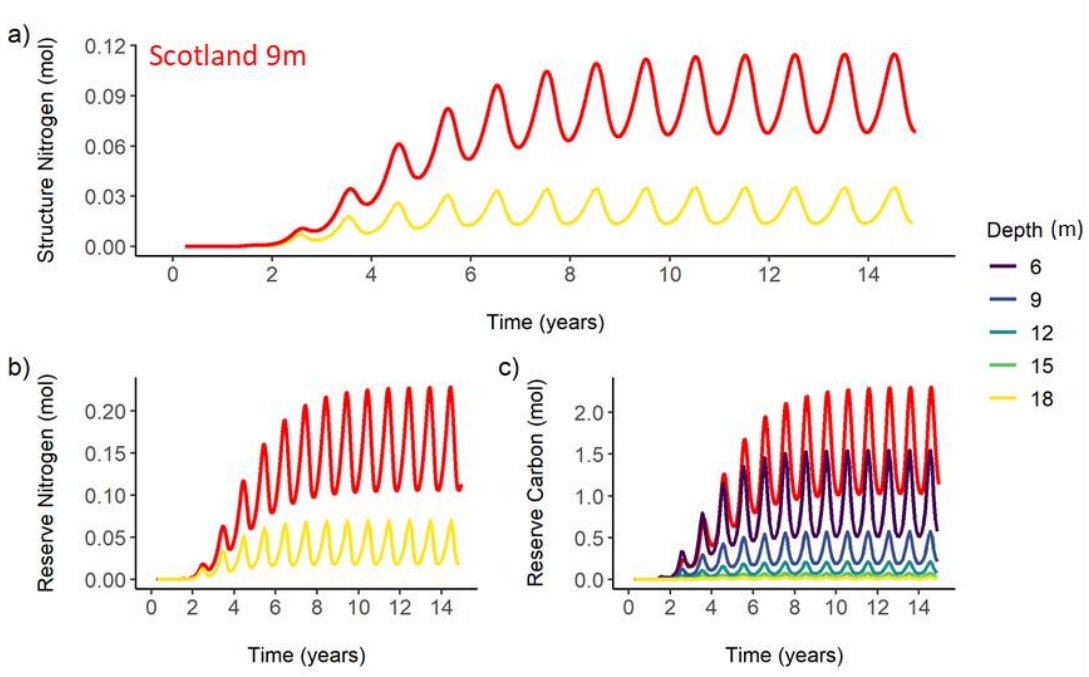

Figure 2.19. Simulation for Normandy. Structure nitrogen (a), reserve nitrogen (b) and reserve carbon (c) amount throughout the simulation. All values shown in moles. The presence of a single line indicates a complete overlap for all depths. Depth of the simulation shown in the legend. The baseline run is represented by the red line, for the original Scotland run at 9m depth with the west coast of Scotland environmental data.

The overall carbon uptake and mobilization is higher in Normandy than in Scotland, as expected in response to the higher light availability seen further south in the environmental driving data. The amount of carbon exuded is also higher, showing that not all of the carbon been mobilized is being used for growth. The effect of higher temperature on increasing maintenance cost that was previously mentioned to be limiting the individual growth would not be reflected in the carbon dynamics, but in the nitrogen ones.

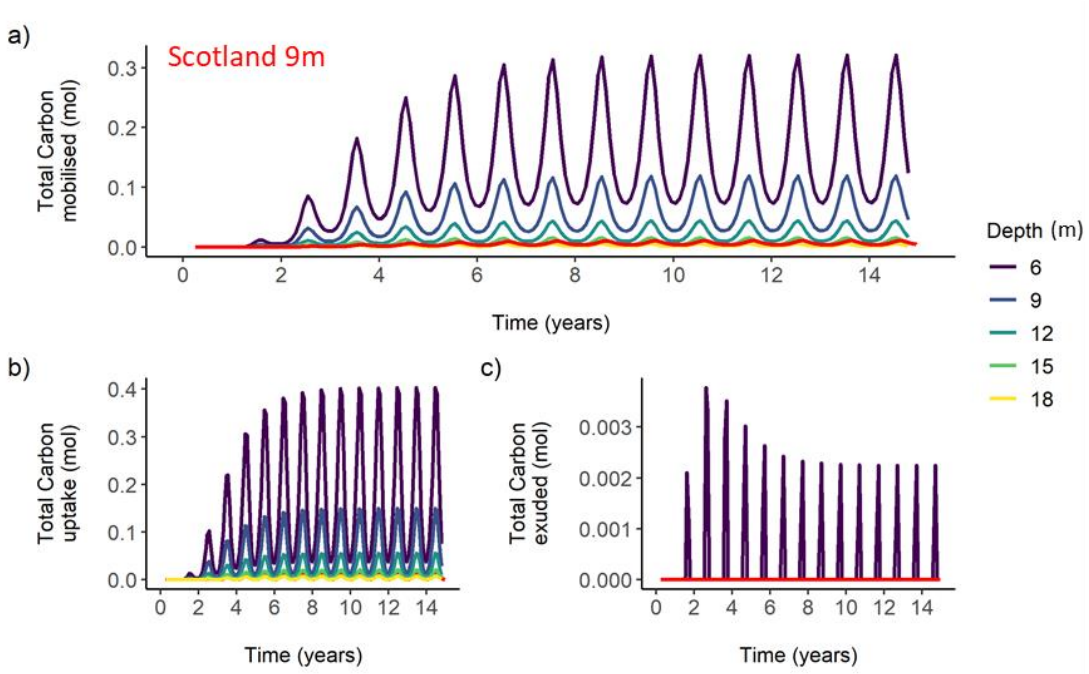

Figure 2.20. Simulation for Normandy. Input and output of carbon fluxes throughout the simulation. Carbon mobilised (a) refers to the amount of carbon uptake (b) that was absorbed onto the state variables. Carbon exuded (c) refers to the material that left the organism to maintain internal homeostasis. Depth of the simulation shown in the legend. The baseline run is represented by the red line, for the original Scotland run at 9m depth with the west coast of Scotland environmental data.

Depth does not impact simulated nitrogen dynamics, but depth-influenced carbon reserves can limit structural nitrogen. No nitrogen exudation occurs in any simulation, indicating no nitrogen surplus. Similar nitrate availability in Normandy and Scotland (Figure 2.12) indicates that simulation differences stem from interactions with other elemental fluxes and variations in temperature and light. Increased carbon and nitrogen uptake in Normandy (Figure 2.19 and Figure 2.20) is due to higher temperatures, which accelerate uptake rates. However, this does not lead to larger size due to higher maintenance costs, which are also temperature-dependent. Maintenance costs are higher in Normandy compared to Scotland because of the warmer temperatures (Figure 2.22).

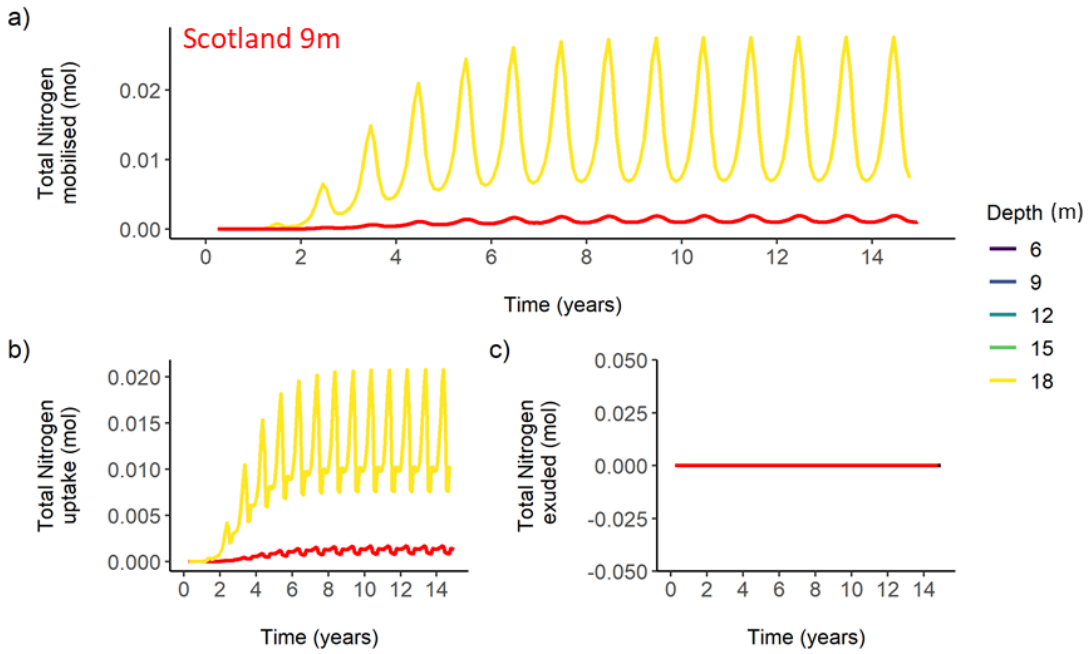

Figure 2.21. Simulation for Normandy. Input and output of nitrogen fluxes throughout the simulation. Nitrogen mobilised (a) refers to the amount nitrogen uptake (b) that was absorbed onto the state variables. Nitrogen uptake is the moles of nitrate that are then absorbed into the organism. Nitrogen exuded refers to the material that left the organism to maintain internal homeostasis (c), the constant value here is in response to a nitrogen limitation in this scenario. Depth of the simulation shown in the legend. The baseline run is represented by the red line, for the original Scotland run at 3m depth with the west coast of Scotland environmental data.

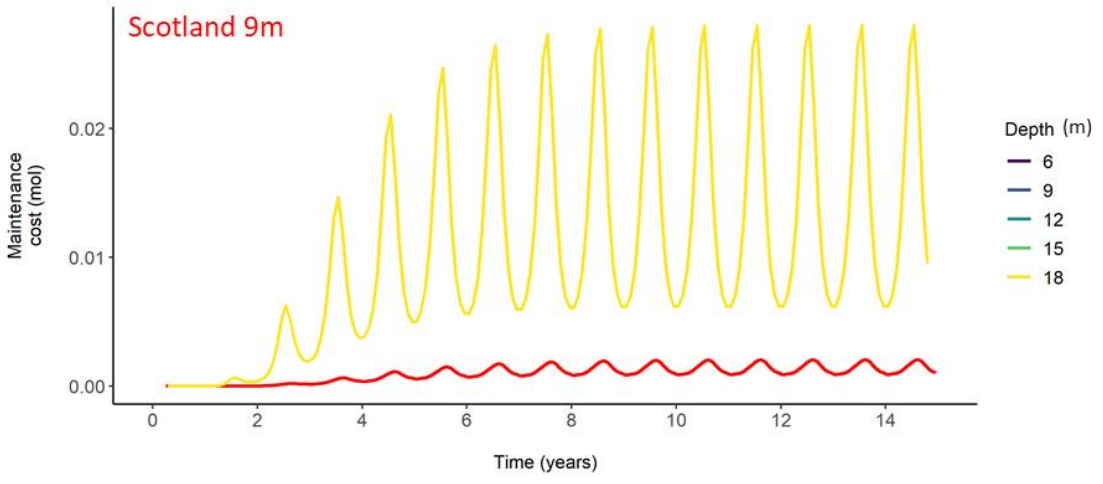

Figure 2.22. Simulation for Normandy. Individual maintenance cost (mol). Depth of the simulation shown in the legend. The baseline run is represented by the red line, for the original Scotland run at 9m depth with the west coast of Scotland environmental data.

A key difference seen in all simulations is the elevated C:N ratio in the first year (Figure 2.23) compared to the stable cycle seen later. The first year C:N ratio is highly dependent

on the starting condition of the simulation. When looking at the stable cycles seen for mature individuals, a decrease in the C:N ratio with increasing depth is present. Significantly, a reduction in the range of the cycle is observed, particularly for individuals at deeper sites, where the difference between their maximum and minimum values shows a notable decrease. The difference caused by the 3m increased depth between the Normandy 6m simulation and the Scotland 3m simulation can be explained by the higher light availability at the surface in Normandy, and the overall differences in reserve and structure proportions.

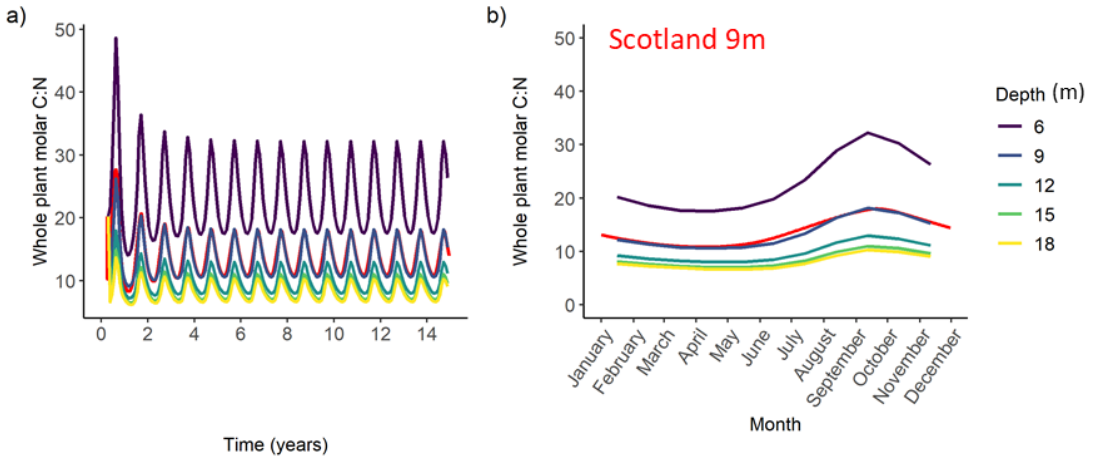

Figure 2.23. Simulations for Normandy. Whole plant molar C:N ratio for the entire simulation run time shown on the left (a) and a single year from years 6 to 7 is shown on the right (b). Depth of the simulation is shown in the legend. The baseline run is represented by the red line, for the original Scotland run at 9m depth with west coast of Scotland environmental data.

2.4 Discussion

This model fills a crucial gap in the existing literature by introducing a novel individual growth model for *L. hyperborea* with an explicit consideration to internal biochemical dynamics and their interaction with external environment variations – up to now there has been no comparable model for this species. This model's significance lies in paving the way for future research endeavours, exploring the potential applications of theoretical experimentation, and deepening our comprehension of kelp forest population dynamics and their underlying mechanistic principles. Specifically, it is the first building block towards filling in the gap towards a complete individual based forest growth model for *L. hyperborea*.

The development of a model, such as the one presented here, offers a tool to understand the processes behind the responses of *L. hyperborea* to a changing climate. Current impacts of climate change have had detrimental impacts on kelp forests, which lead to decreased primary production, biodiversity, and fisheries habitat (Araújo et al., 2016; Smale, 2020). The availability of a process-based model can help us further anticipate any management strategies that might allow for the preservation of this key species in our increasingly changing oceans.

Additionally to the changing climate conditions that this species is facing, the complexities of developing a sustainable harvesting cycle for natural populations has also been highlighted by a comprehensive study on *L. hyperborea* in Norway (Steen et al., 2016) and this was one of the key motivations for the development of this model. As the development of a flexible individual based model can provide information on not only biomass, but also age and internal composition. The presence of detailed information about the internal composition can also provide information on the state of the organisms. In summary, this helps create a clear understanding of how management decisions impact the species, offering a chance to minimize negative effects while still allowing for economic growth. For example, in the implementation of minimum recovery periods between kelp harvests.

2.4.1 Model based interpretation of the field data

For the Scotland simulation, the model output exhibits a deviation from the empirical data from Arisaig during the transition from year 2 to 7. This discrepancy arises due to the population structure present in the empirical data (Jupp, 1972), as the data used does not come from an individual grown in isolation. Unlike the simulated individual, the empirical data originates from multiple individuals constituting a cross-section of the weights at age of multiple annual cohorts that may not have been exposed to the same environmental conditions. In contrast, the simulation assumes no shading from adjacent plants with seasonal limitations as the constraint. Biomass-density effects occur in *Laminaria spp* communities, resulting in skewed size class distributions and reductions in individual weights (Kain, 1976). Competitive suppression can lead to mortality, and self-thinning may occur as a result. These mechanisms have been demonstrated for *L. digitata* (Creed et al., 1998).

When directly measuring the effect of canopy shading on *L. hyperborea* at a depth of 5m, the photosynthetic rate under the canopy was shown to be 13% of that above it, while open water photosynthesis at 20 m was 68% of that at 5 m. Thus, the canopy had a much greater effect than 15m of water (Drew et al., 1976).The irradiance under that canopy can be between 0.004% to 20% of that seen at the canopy top , with those variations resulting from canopy density (Jupp, 1972).

Once the plant has reached a large enough size, mortality rate is low, with removal of the larger plants mostly influenced by wave action (Kain, 1963) being one of the few aspects that might improve the light condition under the canopy. Mortality rate of sub-canopy plants is less affected by wave exposure (Pedersen et al., 2012). However, it's important to note that the light limitation experiment does not precisely represent the empirical data since the recorded weights (Jupp, 1972) pertain to individuals growing simultaneously, and the individual growth curves' light conditions are unknown. Nonetheless, this individual experiment (Figure 7.33) serves as an initial step towards highlighting the need for a comprehensive forest model.

Additionally, when considering the Normandy simulations, specifically the carbon dynamics for 6m depth against the Scotland simulation at 3m depth, the effects of higher irradiance in Normandy counteract the light limitation enforced due to the additional depth. Explaining the lower values for carbon uptake seen in Scotland for a shallower population. The smaller size of these plants is in agreement with the pattern expected from warmer populations (Rinde and Sjøtun, 2005; Smale et al., 2020) due to increased metabolic cost. However, determining the precise extent to which temperature influences metabolism and plant size requires additional data. While both observations and the model indicate smaller plant sizes in the southern range, the magnitude of this reduction remains uncertain. Another potential explanation is that Normandy plants are adapted to warmer conditions, which could be represented by a Q10 parameter adjusted to reflect this temperature adaptation.

The issue of light limitation and the significance of population structure are also emphasized in a population forest model presented by Rinde (2007) for *L. hyperborea* size-structured population dynamics. The author employed a differential equation model with two size-classes, canopy and understory, to illustrate the impact of intra-species competition. While the model's age distribution generally aligns well with observed data, discrepancies exist in certain regions and age categories, further highlighting the importance of intra-species competition and regional variations in environmental conditions.

2.4.2 Model Mechanics

The model is able to show the variations of the individual internal biochemical fluxes in response to environmental fluctuations, leading to an endogenous fluctuation in weight, which is comparable to the behaviour of *L. hyperborea* annual loss of frond tissue (Kain, 1963). The lamina are annual, with the old fronds lost in March, while the stipe and holdfast are perennial (Kain, 1971a), meaning the individual total biomass will not remain stable throughout the year but present cyclical fluctuations. This seasonal aspect of this species biomass is a key part of *L. hyperborea* life cycle and should be an emergent feature of any model – as they are in the model presented here. It should be noted that the annual components of the plant are not separately represented as structure in the model, and the perennial parts are not represented as reserves. In other words, the decrease in reserves and structure does not directly compared to the annual loss of the fronds, but represent the interaction of various processes. It is important to consider that the reserve and structure compartments in DEB theory are not biologically equivalent to a particular tissue of the organism being modelled, but indeed a tool to understand the overall maintenance of internal chemical composition. Hence the reserves model output cannot be directly compared to the annual parts and the structure to be considered as perennial, the model presented here does not differentiate by tissue type.

The model output in the form of converted model total weight shows that the increase in structure starts in January reaching peak in June. Comparing the model results to the total biomass of the empirical data from Jupp (1972) shows that it reaches the peaks faster than what is seen in the empirical data. Further work will be required to tune the individual year phenology, as the main objective of this model was to simulate the growth curve for the entire lifespan. The fine tuning required for fitting the parameters to detailed data on C: N composition that were available for multiple ages throughout the year for multiple individuals was not possible due to the lack of data. Laboratory work focusing on *L. digitata, L. hyperborea and S. latissima* photosynthetic performance showed a spring peak of photosynthetic capacity for all three species (Drew, 1983), which is similar to the model timing for most of the increase in structure.

The pattern seen in response to the environmental fluctuations are also seen in in studies by Kain (1976, 1971) and Lüning, (1971) were underwater irradiance measurements reveal that *L. hyperborea* faces challenging conditions during winter. These conditions were characterized by inadequate light levels, with all developmental stages experiencing levels below saturation and often below compensation in shallow water areas near the Isle of Man and off the coast of Heligoland. Providing further support for the relevance of accurately representing the light limiting processes and the effect of depth, both through how light is attenuated by depth and by how the individual responds to it. The use of a biochemically explicit models allows for deeper understanding of how the light limitation is restricting the growth rate.

The presence of exudate material in the model resembles the stoichiometric overflow hypothesis, which states that dissolved organic carbon (DOC) exudation is due to an excess of carbon in relation to the availability of other nutrients such as nitrogen (Fogg, 1983). Seaweeds preferentially release DOC instead of storing it when there is sufficient light for photosynthesis but limited availability of essential nutrients such as nitrogen (Paine et al., 2021). In the model, carbon exudation arises when the mobilised carbon reserves cannot be fully used for growth due to insufficient mobilizable nitrogen. Mobilisation in the model depends on the state of the reserves (their density instead of their absolute amounts), inspired by modelling of compensatory growth following starvation in fish (Broekhuizen et al., 1994). The results showed that when light limited, carbon exudation did not occur. Empirical research shows that exudation of DOC is not seasonally limited (Abdullah and Fredriksen, 2004). In kelp on average 14-43% of fixed carbon is lost as DOC (Abdullah and Fredriksen, 2004; Sieburth, 1969; Weigel and Pfister, 2021). Showing that it is a relevant process that must be accurately represented in models.

The translocation of reserve material to fuel growth during the limiting season is a key aspect of *L. hyperborea*, as it exhibits new lamina growth during mid-winter to spring, a period with low ambient irradiance (Kain, 1963). The required organic materials for this growth are supplied by resorption from the previous years' lamina (Lüning, 1971). The presence of the old lamina is crucial for the normal growth of the new lamina in winter and darkness, as demonstrated by amputation experiments (Lüning, 1969a, 1970a). Also shown by new lamina encountering difficulties in avoiding a negative carbon balance during midwinter and early spring, until carbon supply by the older blade was made available (Kremer, 1984). Removing old lamina at the beginning of the growing season diminishes the following new lamina area at the end of the season (Jupp, 1972). This supports that new lamina is dependent on reserves translocated from the old lamina until the new lamina photosynthesis can provide enough energy, hence highlighting the need for the reserve component in the model.

The C: N ratios in the simulations approximately double between March and September at 3m depth, which is comparable with *S. latissima* C: N ratio values observed in the eastern English Channel (Gevaert et al., 2001;. C: N = 7 during the beginning of spring and approximately 12 during the summer). This coincides with the seasonal cycle of photosynthetic and growth rates, which take place at the cost of depleting the internally stored nitrogen (Gevaert et al., 2001).

2.4.3 Comparison with other Models

Broch and Slagstad (2012) developed a model that simulates the seasonal growth and composition dynamics of *S. latissima,* while investigating the influence of environmental factors. Their model also utilized a process-based approach, focusing on the kelp frond and incorporating essential physiological processes such as photosynthesis, respiration, and nutrient uptake. I follow a similar approach, but with a stricter use of DEB methodology. Broch and Slagstad only model the kelp frond, but this is also divided into independent carbon and nitrogen reserves and structure components. Their daily carbon budget simulation was conducted for a duration of 385 days (Broch and Slagstad, 2012), in contrast to my model, which integrated the entire lifespan of an individual. Their model also resolved seasonal variations and highlighted the need to include carbon exudation to balance the carbon budget. The aim of Broch and Slagstad (2012) model was to inform aquaculture, hence the choice of only simulating a single year of growth was not a limitation in the context of their model application.

Venolia et al.,(2020) developed a mechanistic model of *S latissima* based on the DEB model proposed by Lavaud et al., (2020) for *U. lactuca*. The transfer of the *U. lactuca* model to *S. latissima,* a more complex macroalgae species, was facilitated by calibration using field data specific to the species and location of interest (Venolia et al., 2020). Both Lavaud et al., (2020) and Venolia et al.,(2020) models used Synthetizing Units (SUs) to process nutrients from the environment, representing an abstraction of an enzyme mediated process. Carbon and light assimilation were initially treated separately and later integrated into the model. In contrast, my model simplified the process by considering carbon and light assimilation together, for the sake of simplicity. SU's were further used to merge carbon and nitrogen reserves while maintaining stoichiometric balance (Venolia et al., 2020). In my model a flux of stoichiometrically balanced nitrogen is made available for growth.

2.4.4 Limitations

The primary limitation lies in the scarcity of biological data and accompanying environmental driving data of sufficient detail for comprehensive parametrization of the model. Unfortunately, the ideal scenario of having multiple individuals with repeated measurements every month over their entire lifespan, especially when it comes to their internal chemical composition, is unattainable due to the limitations imposed by the plants' lifespans and sizes. Furthermore, the light limitation imposed by the canopy significantly confounds the growth of understory individuals, making the parameterization of a model individual not in competition for light inappropriate when applied to those experiencing such competition. Moreover, the need to measure all these factors concurrently with environmental variables and the individual's biomass presents a challenge. This issue of finding simultaneous measurement of growth data and environmental variables was also encountered by Broch and Slagstad, (2012) and addressed by specific field experiments in later research (Broch et al., 2013).

Moreover, the issue of data availability is further complicated by the inability to collate data from multiple sources. Regional differences, such as variations in temperature, wave patterns, light availability, population structure, herbivore levels, depth, substrate composition, storm frequency, and light attenuation due to plankton or suspended particles from river sediment, all contribute to differences in the growth of individual plants. As a result, collating all available data cannot be done to provide a sufficient foundation for a formal fitting process. A controlled laboratory experiment would be required, this imposes other practical considerations due to the large size and long lifespan of this species.

2.4.5 Future Research

Reproduction was not included due to a time limitation in this project, it is a complex subject that to this date has also not been addressed by any other individual growth model for European kelp. In *L. hyperborea* the onset of maturity is weight dependant and follows a strict seasonality, with sorus production also having an effect on blade weight (Kain, 1975). The effect of depth on seasonality was also not shown by the model output. Lamina area at 3m reach maximum expansion in May, while those at 9m reach it in June (Jupp, 1972). Similar results have been showed in other sites (Lüning, 1970a). Future work can address including this process, as the current DEB methodology introduced here can be easily adapted to include the effects energy partitioning between growth and reproduction.

The impact of current and waves was not included, although *L. hyperborea* populations show greater stipe length, blade length, and total biomass under more exposed conditions (Smale et al., 2016). The larger size of these *L. hyperborea* plants in wave-exposed regions may confer a competitive advantage within dense canopies (Smale et al., 2016). The alginate content has been shown to vary between habitats, plants growing in more turbulent water has a higher content than those in more sheltered locations (McHugh, 2003). Indicating that perhaps this is another process that could be of interest to be included in this type of simulation in future work.

The Normandy case study, allows for the study of *L. hyperborea* populations in their southern ranges, as influenced by a warmer climate. The case study on a southern population provides an opportunity to compare the responses to a warmer using available empirical data instead of simulated data, as it will be used in climate change projections. Conducting simulations to examine the impacts of climate change is a crucial area of research. In addition to these, practical applications of the model can be explored within the context of aquaculture. This is particularly relevant since most kelp production models have been employed in this domain. Furthermore, the model holds potential for developing a sustainable harvesting regime strategy. Since the model functions as an individual based growth model, the next crucial step involves its incorporation into a forest population model involving competition between individuals. This integration will enable the testing of more intricate interactions, providing a deeper comprehension of the underlying processes driving kelp forest population dynamics.

2.5 Conclusion

The key aspect highlighted by the development of this individual based growth model is the essential influence of light availability, as shown by empirical research. It is important to recognize that the overall picture cannot be solely explained by alterations in irradiance levels. One must consider that these individuals do not grow in isolation but rather compete with neighbouring individuals for light. This underscores the importance of considering population structure when representing the growth of understory individual plants. The model's ability to replicate growth highlights its effectiveness, while comparisons with other models demonstrate the transferability of DEB principles when modelling macroalgae. However, limitations exist, and future work will address these to enhance the model's applicability and explore further applications. Developing reliable process-based models is crucial for understanding the causes of changes in kelp population dynamics and developing management strategies to preserve them in our changing oceans. By understanding the complexities of light availability and population structure, comprehensive models can be developed, enabling robust conservation strategies to safeguard *L. hyperborea* populations.

3 DEB forest IBM development for *Laminaria hyperborea* in Scotland.

3.1 Introduction

Just as in a terrestrial forest, a kelp forest can be considered in two parts – the canopy and the understory. The understory is a layer consisting of juvenile plants and other species beneath and shaded by the forest canopy. The canopy is formed of the fronds of the larger plants supported by their stipes and holdfasts. Irradiance levels in the understory can be between 0.004% to 20% of that seen at the top of the canopy, depending on canopy density (Jupp, 1972). Kitching, (1941) reported an attenuation of irradiance as low as 1% under a canopy of *Laminaria hyperborea* off western Scotland, preliminary measurements by Kain, (1971a) showed a reduction of approximately 25%, with Norton et al., (1977) documenting a range spanning from 3 to 11%.

Shading of the understory by the canopy has the potential to be a key density dependent regulating factor in the dynamics of the forest as a whole. In a study on *L. hyperborea* in harvested areas, a negative relationship was found between kelp canopy density and understory kelp recruit density, likely due to shading effects from the canopy, hindering the growth conditions for smaller plants in the bottom layers (Steen et al., 2016). This has also been shown by clearing experiments where colonising plants in cleared areas had faster growth rates than those from undisturbed forests (Kain, 1971b; Lüning, 1970a). Hence, shading by larger plants limits the growth for juveniles, until the loss of mature plants allows rapid growth of the understory (Kain, 1963).

In response to the previously described processes, it can be understood that available light controls the initial conditions of each forest cohort. An individual does not grow in isolation, it is surrounded by other individuals of different age and size with which it has to compete. Resource competition revolves around the competition for light in these forests, as the species with maximum final lengths often tend to dominate the community (Bartsch et al., 2008).

Previous models have dealt with the issue of light competition in various way. Some models of individual plants have included a term for self-shading to represent their existence within a forest (Broch and Slagstad, 2012; Jackson, 1987; Lavaud et al., 2020). It should be noted that the focus of such models was an aquaculture context, hence the complex dynamics from competition within multi-cohort size structured populations was not relevant – most aquaculture forests are essentially single cohort populations of plants. Additionally, none of these models were developed for *L. hyperborea*. Only Rinde, (2007) specifically considered interactions between the canopy and understory in a *L. hyperborea* forest, but the internal composition of the organisms within the forest was not in the scope of her model. This chapter will address this gap and extend the individual growth model introduced in Chapter 2 to be the basis of an individual-based forest population dynamics model, where the canopy plays a central role in light shading of the understory.

The intricate interactions among individuals within a forest highlight the potential of applying an individual based model (IBM) for growth as a foundation for a forest model. Building on the previous chapter, the biochemically explicit individual growth model, developed using DEB theory for *L. hyperborea*, represents a high level of detail in how the individuals are responding to these dynamic light conditions created by a complex population structure. The model also has the added advantage of providing an understanding of the internal conditions, such as nutrient limitations, that different sizes and ages of individuals in the population might be experiencing. This understanding is of paramount importance, as the ability of kelp to function both as a primary producer and a habitat is contingent upon these physiologically mediated interactions. These interactions involve recruitment, growth, and mortality, and collectively, they shape the population's dynamics. Hence, for an accurate simulation and comprehension of the mechanisms governing the growth of *L. hyperborea* in natural settings, it is essential not to model an individual in isolation. In this context, I introduce a DEB IBM forest model to address this issue.

3.2 Methods

3.2.1 Model Description

The forest model is structured as a dynamic, multi-cohort system where each cohort represents a group of plants with identical characteristics, all of which are recruited simultaneously and grow under the same light conditions. The individual behaviour is described by the methods in chapter 2. Instead of spatially explicit cells, the forest is organized by time steps and cohorts. Each cohort is treated as a "super-individual," consisting of plants that share the same recruitment time and initial characteristics. All the cohorts occupy the same fixed homogenous area, hence increasing numbers of surviving individuals in the cohorts implies an increase plant density.

Recruitment of new cohorts occurs at regular intervals, and the number of new recruits depends on the overall density of the forest, ensuring that the recruitment process reflects the changing population dynamics. As cohorts grow, their size and biomass are updated over time, and they experience varying light availability, influenced by the density and canopy coverage of all existing cohorts.

Shading effects in the forest are determined by the relative rank of each cohort in terms of biomass, with larger cohorts receiving more light and smaller cohorts being increasingly shaded. The rank within the forest, based on plant size, governs the shading each cohort experiences, rather than any spatial location. This process allows the forest to evolve dynamically, with cohorts growing, interacting, and eventually reaching an extinction threshold if their numbers fall too low. Overall, the forest model represents a complex, multi-age population where each cohort is tracked through its life, from recruitment to death, with light availability acting as a key factor influencing growth and survival.

3.2.1.1 Recruitment

Recruitment definition within the life cycle of *L. hyperborea*

The life cycle of *L. hyperborea* involves alternating generations, with the adult (the diploid sporophyte) producing haploid spores that then settle and develop into gametophytes, which become fertile (Fredriksen et al., 1995). This model represents the adult stage. The absolute size of the individuals at the start of the simulation is part of the model parametrization. Hence, recruitment refers to the point in time in which the individuals start to be tracked by the model. Depending on the intended implementation this can be timed with the specific seasonal period of reproduction of the population being simulated or empirical data on specific times of the year that a sporophyte of a particular size was initially measured.

Cohort Recruitment

At the time of recruitment more than one individual is added to the model. The individuals added in the same recruitment step are part of the same cohort. The number of individuals inside each recruited cohort is defined by the forest density at that time step. A denser forest will result in a smaller number of individuals recruited for the cohort settling under that canopy. The basis for this decision relies on empirical research showing that a canopy cover has a negative effect on recruitment (Steen et al., 2016).

Mathematical description

An exponential relationship describing how as the forest gets denser less recruitment takes place is used. Recruitment is then defined by the relationship between the number of new individuals that settle for that cohort (n_R) and the density of plants already present in the forest (D_C), the maximum number of new plants arriving (n_{max}), recruitment density dependence (F_{max}), and the regulating parameter (χ), (which allows the fine tuning of the model behaviour) is:

$$n_R = n_{max} \cdot exp\left(-\frac{D_C}{\frac{F_{max}}{\chi}}\right). \quad (3.1)$$

Following that the relationship, the density of plants already present for the forest area being simulated (which depends on the intended implementation) is:

$$D_C = \frac{n_F}{A_F} \quad (3.2)$$

where n_F is the number of individual plants (in the preceding cohorts) already present in the forest at the previous time step and A_F is the forest approximate area. This relationship can be seen in Figure 3.1.

Parameters:

- $n_{\max}$: Maximum number of individuals that settle (number of individuals),
- $F_{\max}$: Carrying capacity or maximum number of plants in the canopy (number of individuals per m²),
- χ: Regulatory parameter that determines the strength of the density effect (dimensionless),
- A_F: Forest area (m²).

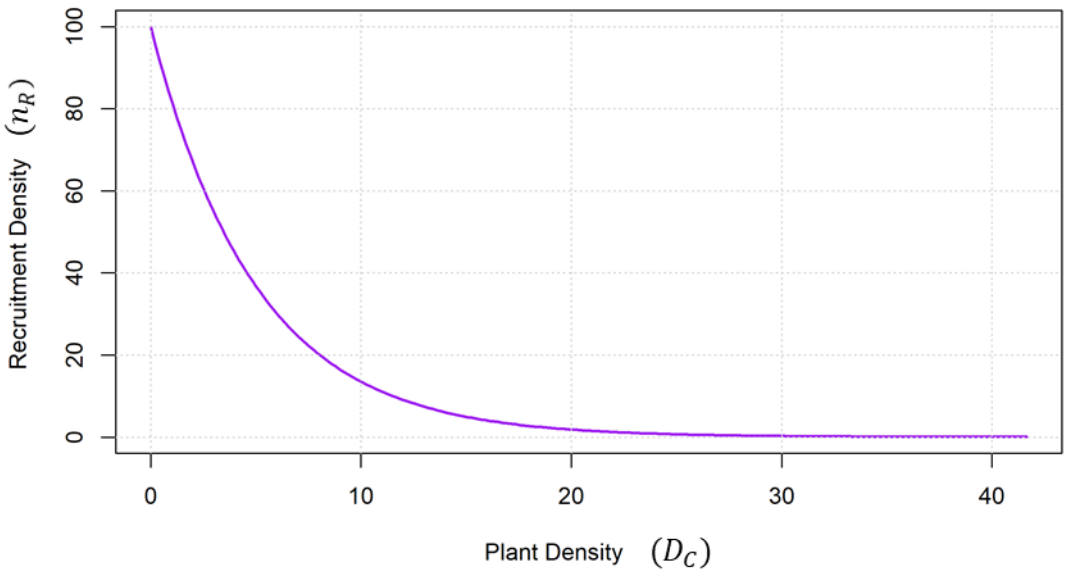

Figure 3.1. Recruitment rate (n_R) as a function of plant density (D_C) in a forest, showing the exponential decrease in recruitment as density increases. The density is calculated based on the number of plants already present in the forest and the forest area.

Several key parameters are defined as follows: n_{max} represents the maximum number of individuals that can settle into the cohort, this value can be adjust for specific applications. F_{max} is a regulating parameter which represents the characteristic value for the decline in recruitment with density, in other words, the strength of the effect of density on recruitment. The regulating parameter χ determines the rate at which the settling number of plants (n_R) decreases from the maximum number of new plants possible (n_{max}) as the density of plants already present (D_C) increases. A higher value of (χ) will result in a more rapid decrease in settling plants, making recruitment more sensitive to forest density, while a lower value of (χ) will result in a slower decrease, a more resilient response to forest density fluctuations. The combined use of both of these parameters allows the model flexibility to be applied to different forest types.

3.2.1.2 Attenuation of light through the canopy

Forest light regime

The light that reaches each individual significantly influences its growth rate, hence it is of utmost importance to consider all the factors that might limit it. An obvious light limitation is enforced by depth, as the water column on top of the plant will attenuate the downwelling light. This is addressed in the previous chapter by describing the application of Beer-lambert law to attenuate the driving data from surface irradiance to irradiance at the depth where the individual is growing. This depth can be considered to be the top of the canopy. The key aspect of modelling a forest instead of a single individual is how the interactions between individuals affects the available light in the understory. This interaction is interpreted as competition for light and results in some individuals being subjected to a poorer light regime.

Mathematical description of light scaling

For each individual, shading by other plants affects its carbon uptake rate:

$$\mu = min\left(\frac{L \cdot \mu_{att}}{L_S}, 1\right), \qquad (3.3)$$

where μ is the light dependent scaling of carbon uptake (the effect of light availability on photosynthesis) and μ_{att} is the shading attenuation coefficient. L is the light at the top of the canopy calculated from sea surface daily integrated irradiance ($Em^{-2}day^{-1}$), and L_S is the light saturation intensity for carbon uptake (relationship seen in Figure 3.2). The minimum rule approach ensures that the light scaling is always a reduction of the light available. The interaction of these three components defines the light available for individual growth on each time step.

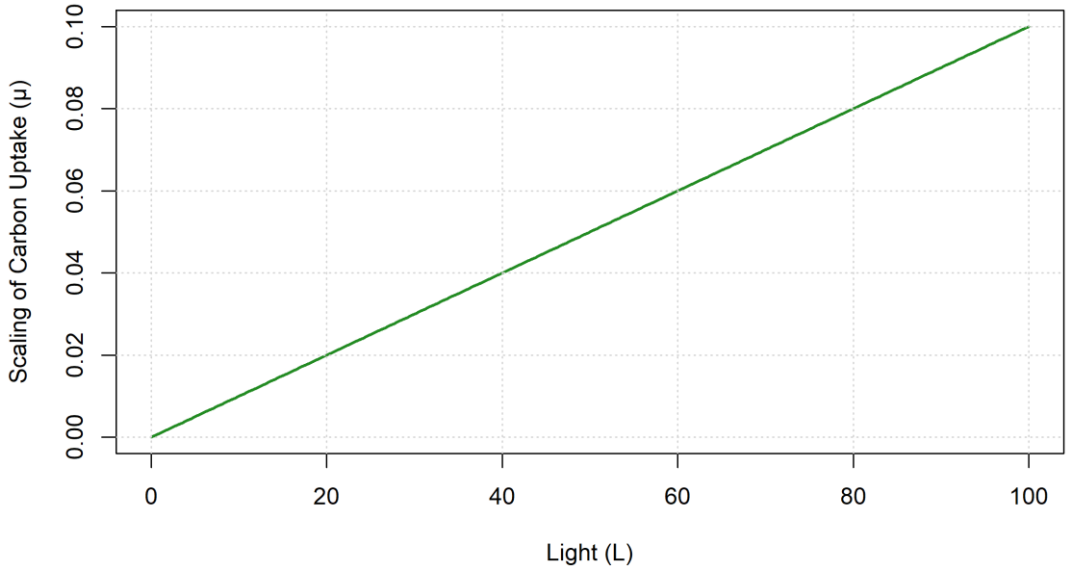

Figure 3.2. Light-dependent scaling of carbon uptake, showing how shading affects photosynthesis based on light intensity, the shading coefficient, and the light saturation point Light distribution inside the forest

Shading attenuation (μ_{att}) for any super-individual plant is dependent on its weight relative to the weights of the surrounding plants in the forest. Super-individual weight is the product of individual wet weight from the model and the numbers of individuals alive in the cohort. The model output in moles of carbon and nitrogen is converted to wet weight using the same process described in the previous chapter. That weight of a single individual is then multiplied by the number of individuals in the cohort, to obtain the total wet weight of the cohort.

After the weight of each cohort is derived, this information is used to rank all the cohorts in the forest. A minimum shading effect value is assigned to the highest-ranking cohort, i.e., the individual at the top of the canopy, the specific number depends on the forest being modelled. Subsequently the shading effect is increased in set steps, which act as another fitting parameter to simulate a particular light regime, with shading increasing as the rank decreases. The smallest individuals will then be subjected to the strongest shading effect. The light limitation in each cohort is seen in Figure 3.3.

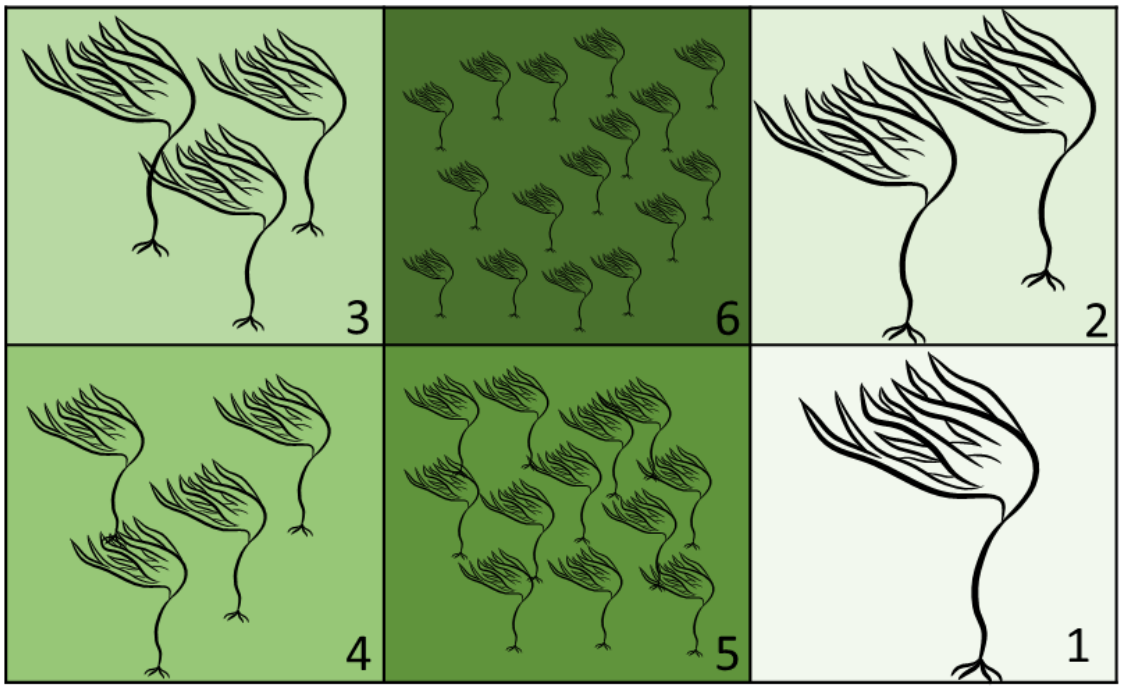

Figure 3.3. A visual schematic diagram illustrates the distribution of available light across the grid cells in the model. Each number in the bottom right of the squares corresponds to the rank by the weight of the super-individual, while the gradual darkening of colour represents the diminishing light availability as the rank order position decreases.

3.2.1.3 Model Area

Abstraction of the shading area

The forest model done here is not spatially explicit, it considers an area over which the individuals compete for space and light, but the location of the individuals in the area is not considered. Hence to designate this area within a realistic dimension, guided by empirical data, is instead conceptualized based on the maximum height of a canopy individual. This approach assumes that the tallest individual casts a shadow whose direction and extent are variable due to changes in the sun's angle and position and the effect of the currents and waves in the individual. This framework simplifies the complexities of shadow dynamics, and inherently abstracts from specific spatial and temporal variabilities.

It’s assumed that the maximum-height individual is positioned at the centre of the defined area, hence it allows the affected region to be approximated as a circle. To address the previously described abstractions, 95% of the area of the circle is used to mitigate potential inaccuracies at the edges, reflecting an effort to capture the core influence of the shadow.

The framework for defining the area based on the tallest individual’s height as a proxy for the radius of the circle is an adaptable method. By focusing on the maximum height of a canopy individual, the approach provides a clear and scalable parameter that can be empirically adjusted to reflect the specific characteristics of different forest types. This flexibility ensures that the model is not overly constrained by one set of conditions and can be recalibrated to account for variations in forest structure.

Furthermore, the reliance on the maximum height observed in a specific empirical dataset, such as Jupp's work in Scotland, strengthens the model by grounding it in observed data. While this specific height is employed in the thesis, the method's adaptability allows for alternative heights to be substituted as new data becomes available for different forest types. This capability to modify the input height ensures the model remains relevant and accurate across diverse ecosystems, enhancing its utility and applicability.

Mathematical approximation for the shaded area

The following description assumes that the sun is vertically overhead; the effects of light angle are not considered. The shaded area is calculated using the maximum height of the tallest plant as the potential shading radius. This maximum height is dependent on the particular forest being modelled (Figure 3.4).

Figure 3.4. Abstract representation of the shaded area of a single individual, illustrating the extent of the area with a 95% probability of being shadowed. The figure shows variability in shading to reflect differences in kelp sizes, as each cell contains a plant of varying dimensions, representing the different cohorts. The top view perspective highlights how the shading effect varies, considering the size and presence of surrounding kelp, representing the effects of being positioned differently in the canopy within the same space (AI generated with DALL E 3).

The calculation of the radius at which 95% shading occurs is based on a model that assumes the shading probability follows a normal distribution. This assumption is in response to the normal distribution being commonly used to describe processes that are symmetrically distributed around a central point, such as shading from a canopy. The shading intensity at any given point is expected to gradually decrease as the distance from the canopy centre increases, which is characteristic of a normal distribution. This approach provides a smooth and simplified representation of how shading changes across the area. The graphical representation of these ideas can be seen in Figure 3.5.

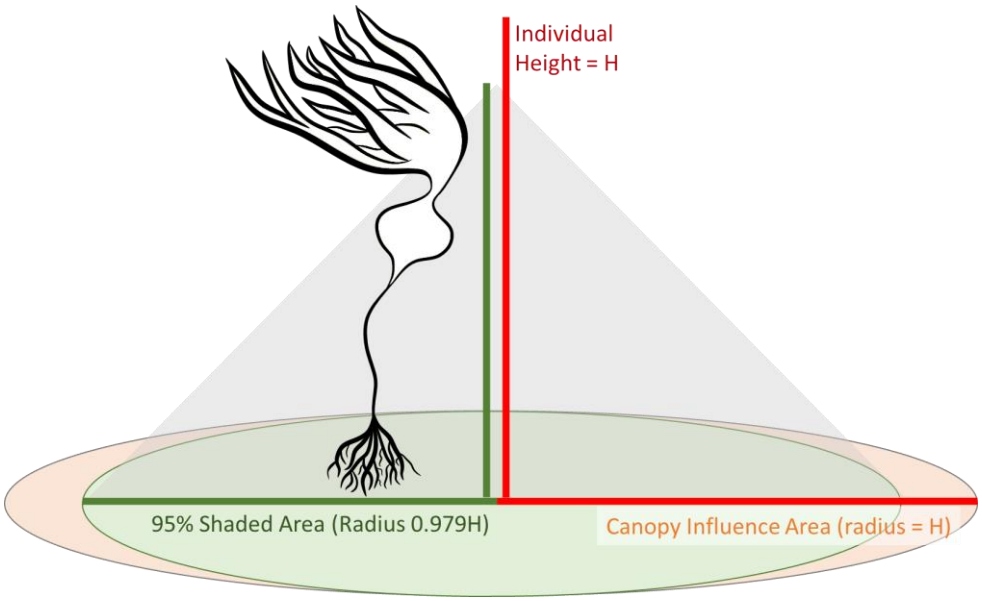

Figure 3.5. Diagram representing how the height of the plant (H) affects the shading radius, with the 95% shading area being approximately 0.979 times the height of the tallest plant. The shading effect is modelled using a normal distribution, where the shading probability decreases from the centre of the plant outward. The standard deviation of this distribution is calculated using the plant height and the z-score corresponding to the 95th percentile.

Step 1: Establishing the Relationship Between Shading and Radius

The shading probability is modelled as a function of the radial distance *r* from the centre of the area. At the centre of the area (r=0), the shading probability is 100% (P_{shade} = 100), and at the edge of the circle (*r* = *H*, where *H* is the maximum canopy height), the shading probability is 0%. This relationship represents that shading probability decreases as the distance from the centre increases. By using a normal distribution to model this process, the shading probability at any radius *r* can be expressed as:

$$P_{shade}(r) = CDF\left(\frac{r - H}{\sigma}\right) \quad (3.4)$$

Step 2: Estimating the Standard Deviation

The standard deviation (σ) represents the spread of shading probability around the centre. It is estimated based on the assumption that at r=H/2, the shading probability is approximately 50% (P_{shade}=0.5). This is the point where the shading is halfway between full and no shading, the half is used to represent one side or another of the circle being shaded here with a particular radius. Using the properties of the normal distribution, the standard deviation σ can be calculated as:

$$\frac{H/2 - H}{\sigma} = 0 \quad \Longrightarrow \sigma = \frac{H/2}{1.96} \tag{3.5}$$

Here, 1.96 is a **z-score** corresponding to the 97.5th percentile of the standard normal distribution. This value is widely used in statistical modelling because it marks the point where 95% of the distribution lies within ±1.96 standard deviations from the mean.

Step 3: Finding the Radius for 95% Shading

To find the radius x where 95% shading occurs, the inverse cumulative distribution function (CDF) is applied. The goal is to find the radius xxx such that the shading probability is 95% (P_{shade}= 0.95). This is expressed as:

$$P_{shade}(x) = 0.95 \Longrightarrow \text{CDF}\left(\frac{x - H}{\sigma}\right) = 0.95. \tag{3.6}$$

Solving for x, this becomes:

$$\frac{x - H}{\sigma} = inverseCDF(0.95) \tag{3.7}$$

The value of inverseCDF (0.95) corresponds to a z-score of 1.645, which is the point that corresponds to 95% of the distribution. Substituting this into the equation gives:

$$x - H = \sigma \cdot 1.645 \Longrightarrow x = H - \sigma \cdot 1.645 \tag{3.8}$$

Step 4: Substituting σ and Simplifying

Substituting the expression for σ from Step 2 into the equation for x:

$$x = H - \left(\frac{H/2}{1.96}\right) \cdot 1.645 \tag{3.9}$$

Simplifying the terms:

$$x = H - H \cdot \frac{1}{2} \cdot \frac{1.645}{1.96} \tag{3.10}$$

The ratio 1.645/1.96 is approximately 0.840, so the equation becomes:

$$x = H \cdot (1 - 0.5 \cdot 0.84) \quad (3.11)$$

This simplifies to:

$$x = H \cdot (1 - 0.42) \Longrightarrow x = H \cdot 0.979. \quad (3.12)$$

The radius x at which 95% shading occurs is approximately 0.979 H, where H is the maximum canopy height. From here this is $r_S = 0.979$. This means the shaded area forms a circle with a radius of approximately 97.9% of the height of the tallest individual in the canopy. The model is flexible, allowing for adjustments based on empirical data specific to different forest types. The standard deviation σ and the maximum height H can be calibrated to reflect the structure of the forest being studied, making the model applicable to a wide range of canopy heights.

3.2.1.4 Mortality

Mortality is included in the model by reducing the number of individuals within each cohort on every time step at a specific rate. This rate will depend on population dynamics of the forest being simulated. All individuals born at the same time are exposed to identical environmental conditions, leading them to exhibit identical growth patterns in response to those conditions. As a result, each cohort is represented as a "super individual" composed of a group of individuals. Mortality occurs at a constant rate, gradually reducing the number of individuals within the "super individual." In the forest simulation cohorts with n < 1 are considered to have died.

3.2.2 Implementation for Scotland West Coast

The forest model was implemented to represent a forest in the west coast of Scotland, due to the biological data available from Jupp (1972). This dataset is crucial as it provides comprehensive information on the age composition of the forest (Figure 3.6), as well as the weights and ages of individuals. The environmental driving data used is described in the previous chapter in detail. The development of the model into a forest model with population dynamics parameters (recruitment and mortality) together with the integration of shading into the model required a revision of the parameters for the individual plant model due to the added complexity of incorporating population structure. To accurately tune the behaviour of this new model more information than just the individual's weight at different ages had to be considered. Taking into account the distribution of the individuals across various age classes was also required. Unlike the previous model, which considered only a single individual without shading effects, this revised model needed to be parameterized to accurately represent these new factors.

The introduction of shading required the parameters of the individual plant model (Chapter 2) to be revised by manual tuning to Juppe data (Table 3.1). This thorough parameterization ensures that the model accurately represents the population structure over time, specifically tuning the interactions between the mortality and recruitment rates. The increase in the forest rates can be interpreted as the individuals under limiting conditions having evolved to thrive under the higher light limitation, as opposed to the individual model organism that grows without competition. The population structure derived from the guidance data is illustrated in Figure 3.6 and the values for the parameters used are shown in Table 3.2.

Table 3.1. Changes in individual growth model tunning parameters.

Parameter	Description	Unit	Forest Model	Individual Model
$U_{C_{max}}$	uptake rate of carbon per unit area at the reference temperature	$moles\ C\ day^{-1}cm^{-2}$	4 x 10^{-5}	2 x 10^{-5}
$U_{N_{max}}$	uptake rate of nitrogen per unit area at the reference temperature	$moles\ N\ day^{-1}cm^{-2}$	4 x 10^{-6}	2 x 10^{-6}
λ	maintenance cost	day^{-1}	0.03232	0.0181

3.2.2.1 Population Structure

The previous model (Ch2) growth curves were unable to simulate the weights at age classes 3-7 years. This mid-range ages can be considered to be the understory of the canopy, as they are bigger than the starting weights but have not reached the final maximum weights seen in the older individuals. Since the individual model (Chapter 2) does not consider the effects of shading, it could not account for shading by larger plants which limited their growth (Jupp, 1972; Kain, 1963; Lüning, 1970b; Steen et al., 2016). The forest model enables this to be taken into account.

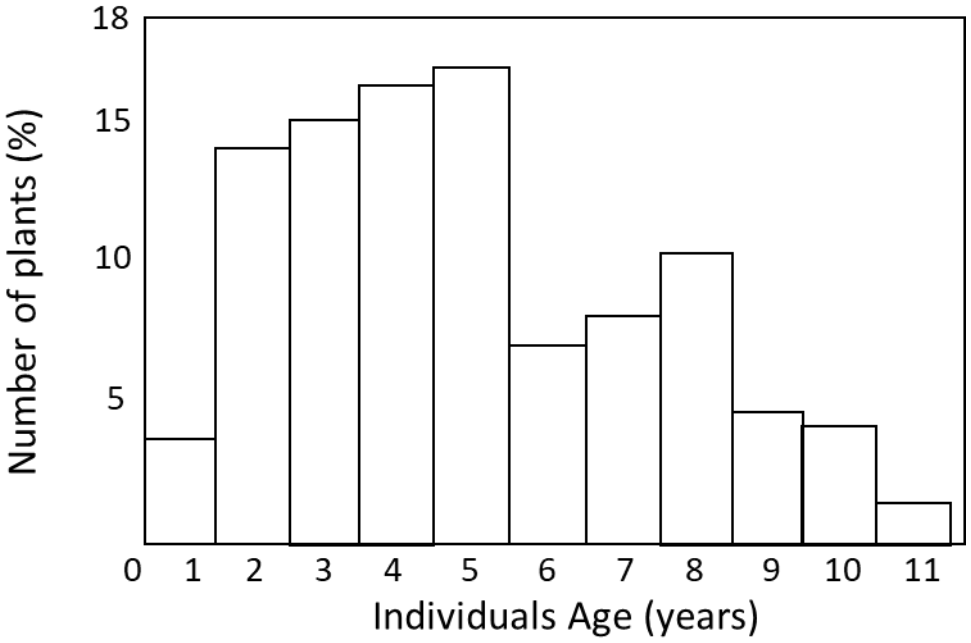

Figure 3.6. Frequency distribution of L. hyperborea individuals age within the population at 3m depth in Arisaig (modified from Jupp, 1972).

Table 3.2. Population structure tuning parameters.

Parameter	Description	Value	Units
A_F	Forest area, based on circle with a radius equal to the maximum canopy height * the radius at which 95% of the shading probability (r_s)	12	m^2
χ	regulatory parameter of the strength of the density effect	4.5	Dimensionless
$F_{\max}$	carrying capacity/max number of plants in canopy as used to define the density of the forest	10	Number of individuals m^2
$n_{\max}$	Maximum number of individuals that settle	100	Number of individuals
r_s	Scaling for the radius at which 95% of the shading probability occurs	0.979	dimensionless
m	Mortality rate	0.0012	day $^{-1}$

The effects of different mortality rates can be seen in Figure 3.7, where the mortality rates selected for this model is shown in red. The example shows how an initial cohort of 100 individuals would be down to a few individuals after 10 years, therefore, approximating the life-span seen in Scottish populations for an *L. hyperborea* individual, the guidance data from Arisaig, Scotland, showed a 13 years life expectancy maximums (Jupp, 1972).

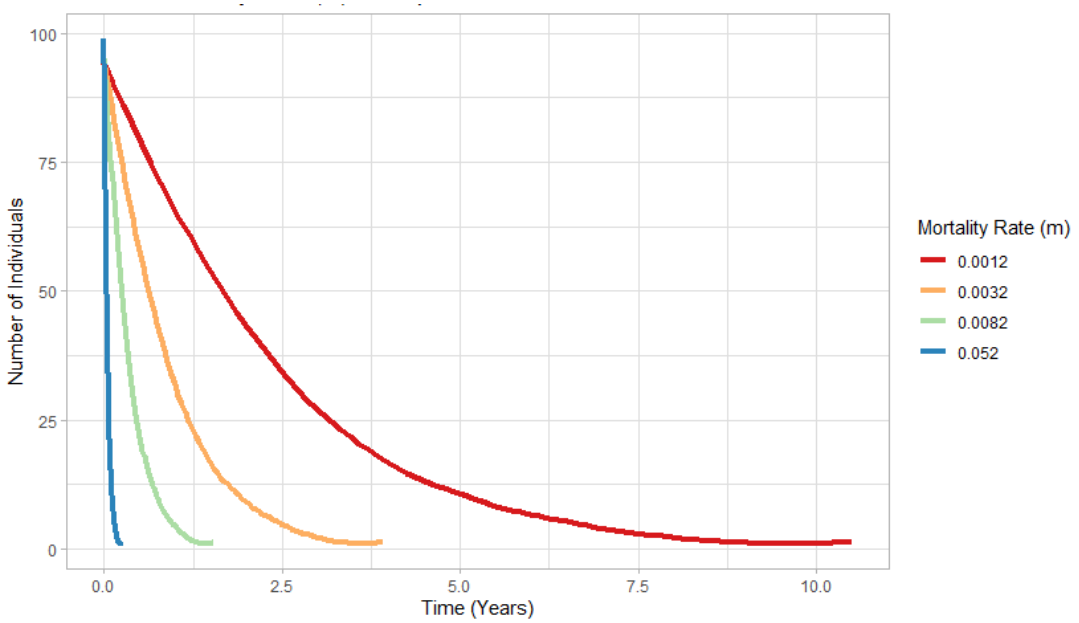

Figure 3.7. Example of different mortality rates on a set population over time. Values for 0 are not shown as the cohort is considered extinct.

3.2.3 Experimental strategy

This study seeks to develop and understand the processes involved in a DEB theory-based model that simulates *L. hyperborea* forest dynamics and individual growth under varying light conditions. There is a specific challenge when comparing empirical data on individual *L. hyperborea* growth to the output of the forest model, as it captures the weights of various individuals of different ages at a single point in time, hence it is a snapshot of weights of the individuals that make up that population, rather than tracking the weight of a single individual over time. To align the model output with this snapshot format, a similar approach is used, by taking a snapshot of the forest model's output at a specific time. This virtual sampling is defined as the weight of all individuals and their age (with their internal conditions given by the model) being extracted for a single day in the simulation. Applying this method represents the processed of sampling the weights of the individuals in the population that is seen in empirical research.

To achieve a close alignment between the model output and the empirical data the sampling time selected must be at a moment in which the forest structure of the model output is similar to the population structure observed in the data. Hence, highlighting the significant impact of the sampling time on individual weight and providing insights into how internal processes of individuals vary under changing population structure. The values for the state variables of the model are processed to get the wet weight in the methods described in the individual model chapter.

3.2.3.1 Forest Simulation

Initial Conditions: The simulation begins with an empty forest, leading to maximum initial recruitment and rapid growth of the first cohort without light competition. This setup allows the study of how a forest colonize a cleared space, providing a baseline for understanding population structure and growth dynamics.

Sampling Strategy: To ensure that the model's output can be meaningfully compared with empirical data, snapshots of the forest are taken at specific time points. These snapshots represent different stages of forest development and mimic the structure of real-world empirical data.

3.2.3.2 Virtual Sampling Points:

Early Growth Stage (a): The first sampling point captures the forest in its early growth phase, where initial conditions lead to peak biomass and minimal recruitment due to dense canopy formation. This helps assess the model's ability to replicate rapid growth and the effects of competition.

Transition Phase (a, b): Subsequent sampling focuses on periods following the decline of the initial cohort, providing insight into how the forest structure shifts and how younger cohorts adapt to changing light conditions.

Mature Forest Stage (c, d): Later sampling points examine the forest as it approaches a stable state, allowing for an evaluation of the model’s accuracy in simulating long-term dynamics and individual growth patterns under established canopy conditions.

3.3 Results

3.3.1 Early Growth Stage

To understand how individuals' growth is affected under different types of population structure, the forest simulation starts in an empty state. In this condition, the first cohort achieves maximum recruitment and grows without competition for light, leading to the maximum annual mean forest biomass when their weights plateau into a stable cycle. This peak in biomass results from the maximum number of individuals growing without light limitations caused by canopy cover, as all the individuals would be part of the canopy.

The long-term dynamics of the forest simulation are observed through the interactions between total forest biomass and recruitment (Figure 3.8). The initial large spike in biomass reflects the first cohort settling with no competition, akin to a post-clearing settlement. The subsequent drop in biomass, due to mortality within this cohort, results in reduced recruitment because the heavy canopy created limits light availability. This process leads to a quasi-limit cycle approximately every 26 years, characterized by peaks and troughs in biomass and recruitment, with recruitment peaking during periods of low biomass. This cycle is in response to the time it takes for two generations to have passed. The selected sampling points represent different states of the forest population structure (Figure 3.8), providing snapshots from the same simulation at various times. This approach replicates repeated monitoring of the same population, capturing the effects of these long-term dynamics.

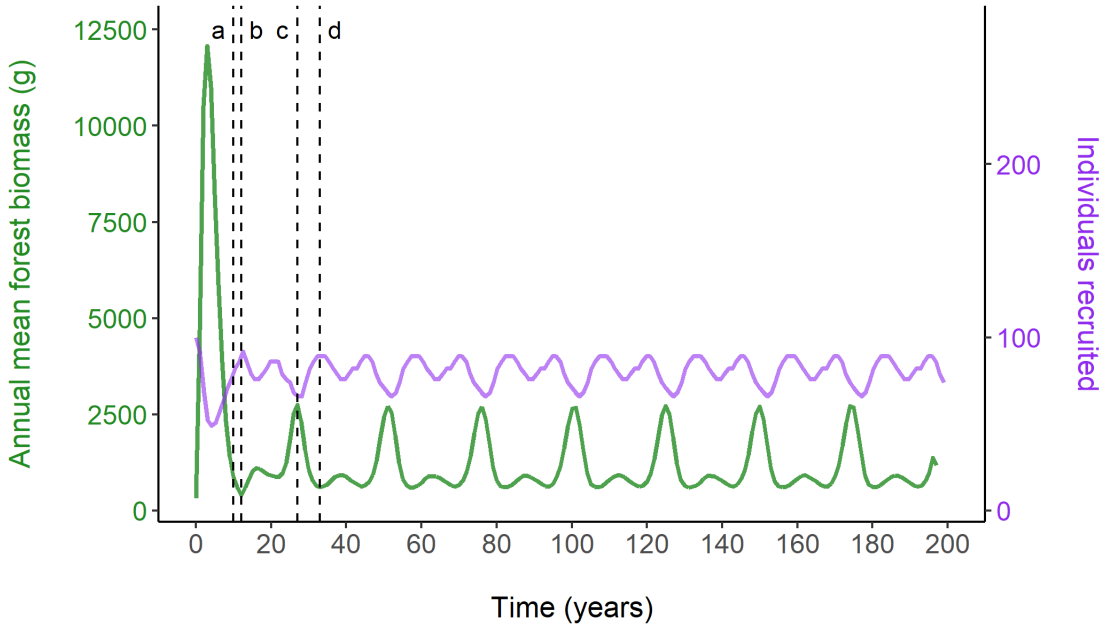

Figure 3.8. Annual mean forest biomass (g) shown in green, individuals recruited every year shown in purple, throughout the 200 years of the simulation. Where a (year 10), b (year 12), c (year 27), d (year 33) represents the timing of forest sampling points.

Higher annual mean forest biomass lead to lower recruitment, this relationship can be seen from a stock-assessment perspective by comparing the individuals recruited against the forest biomass (Figure 3.9) and the number of canopy plants at the time (Figure 3.10). The previously described relationship is distinctly shown in the earlier years of the simulation and it is seen to progress to a less pronounced curve in the later years as the forest settles into its quasi-limit cycle state. The last point with an increase in recruitment (Figure 3.9) is related to the large size of the canopy plants present in small numbers at the beginning of the simulation growing under the special conditions of a clearing state with no competition for light for that cohort (Figure 3.10), leading to a large biomass in the forest but a low density.

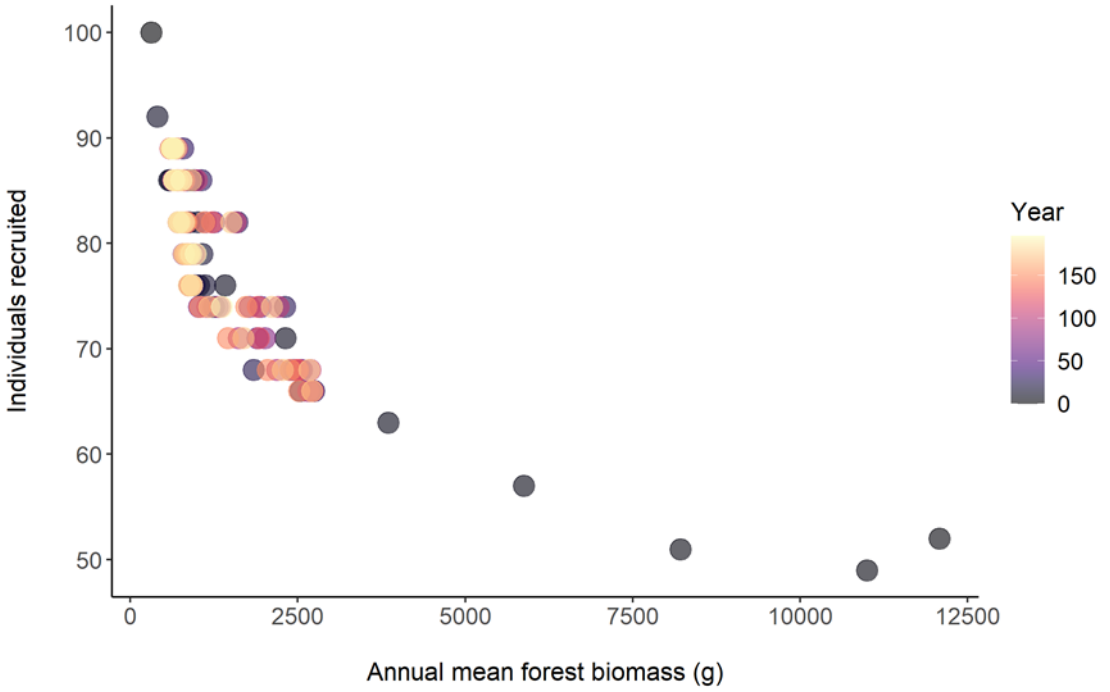

Figure 3.9. Number of individiuals recruited annualy against the annual mean forest biomass (g). The colour of the points refers to the year of the simulation, with early cohorts shown in black and later in yellow.

Canopy plants are defined as the number of individuals in a cohort falling within the 60th percentile of non-zero wet weight values. This threshold was chosen to best represent size distributions observed in the Jupp data (Figure 3.6), following tests of various percentiles ranging from the 50th to the 90th, with the 60th providing the closest fit.

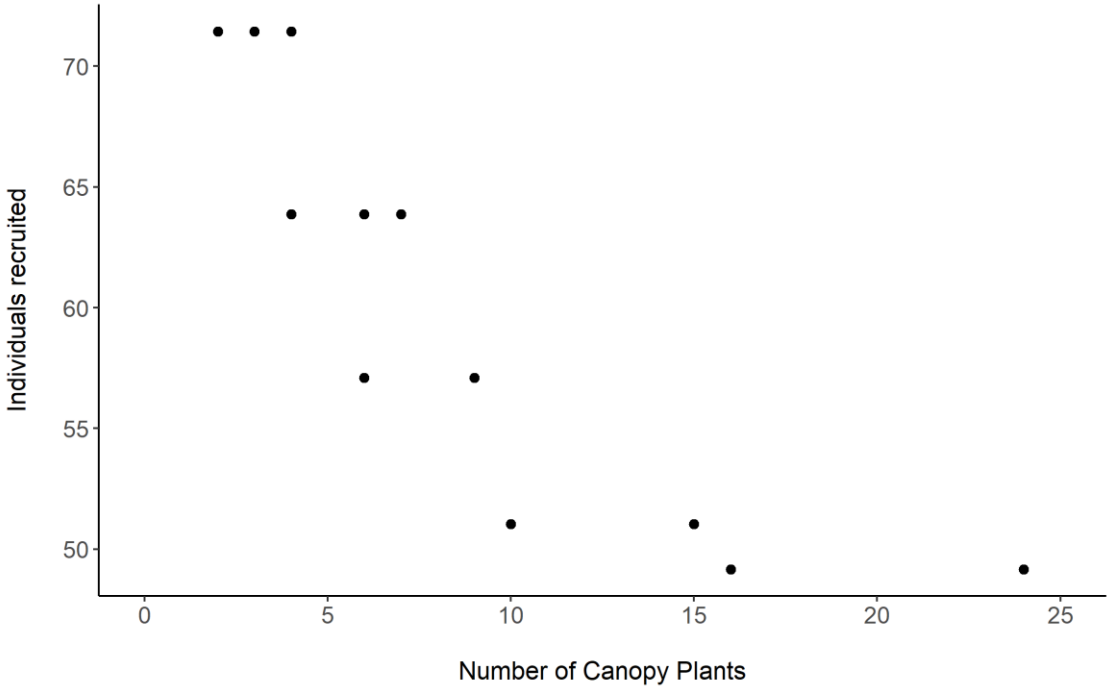

Figure 3.10. Number of individuals recruited on a yearly basis against the number of canopy plants present in the forest at the same time point. The canopy plants are defined as the number of individuals in a cohort that are in the 60th percentile of non-zero values of wet weight at that time step.

3.3.2 Transition Phase (Snapshots)

To understand how the forest dynamics affects the population structure it can be approach from two perspectives: the weight distribution across different age groups and the number of individuals within specific weight categories, both as a snapshot in time (Figure 3.11). This two-fold approach helps assess how well the model represents empirical data and provides an initial idea of the model performance. The forest structure at the time of settling for the guidance data (Jupp, 1972) is unknown. By comparing the simulation results for different snapshots to it an interesting qualitative assessment can be made about the growing conditions that the reference forest may have gone through.

The first sampling point (Figure 3.8, point a) selected shows a subsample of the forest when the individuals from the initial cohort which colonised the empty (cleared) model have achieved their maximum weights, but their numbers are low, hence it represents a heavy canopy of a few large individuals with a dense subcanopy of distinctly smaller individuals. The distribution of weight at age of the individuals in this snapshot close matches what is seen in the empirical data (Figure 3.11, a). At this specific juncture, the original cohort remain, contributing to the heavier weight category. However, the lighter weight class accommodates approximately 200 individuals.

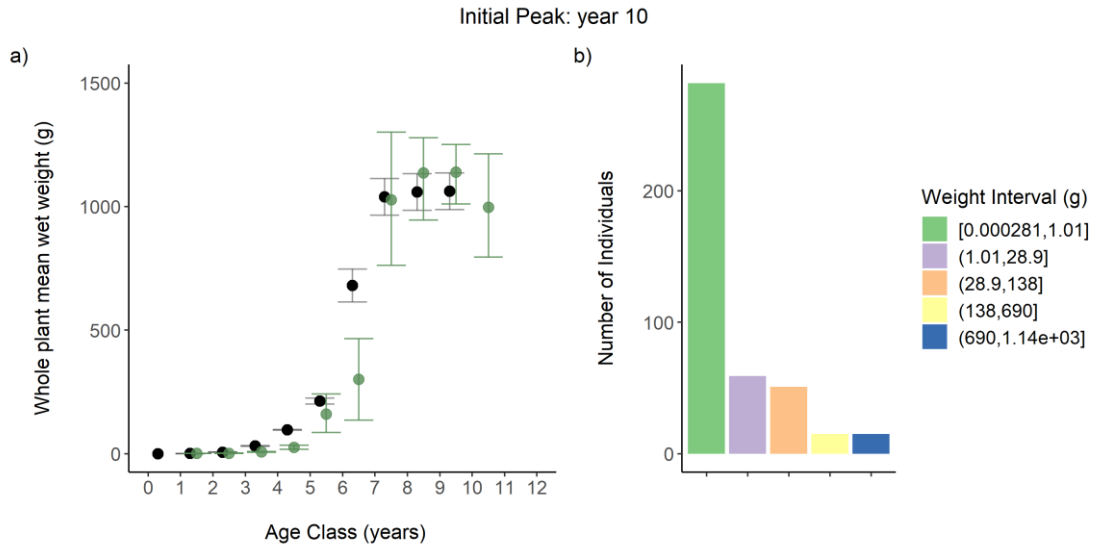

Figure 3.11. The left panel points show the mean model output converted to wet weight for the last month of year 10 of the simulation, with the standard deviation shown by the bars. Mean data used for model fitting shown by the green points, with the maximum and minimum values given by the bars (Jupp, 1972), with the black points being the tuned model output. The right panel shows the model output the number of individuals in each weight category, with the weight intervals of each category given by the colours and described in the legend. Point a in Figure 3.8. The shift in the points is for visual purposes. The lack of a point implies there were no individuals of that age alive.

There is an effect after the first drop in biomass (Figure 3.8, point a) from the original cohort and it is seen in the subsequent recruitment rates (Figure 3.12). Examining the distribution of individuals across weight categories reveals a noteworthy pattern: the lighter weight category has experienced a substantial increase, rising from 300 to nearly 400 individuals. In contrast, the number of individuals in the heavier category has markedly decreased.

The effects of decline in the original cohort are then observed, to understand how the forest begins to approach a steadier state. The selection of year 12 (Figure 3.8, point b) for the analysis aligns with a period following to the initial cohort's dominance, characterized by relatively low competition for available light resources. During this time frame, individuals previously categorized within the 7-year group have advanced and now constitute the forest canopy, benefiting from a more favourable light environment. While the overall weight distribution curve persists, the absence of older individuals does not allow for a clear perspective on weight stabilization of the canopy individuals.

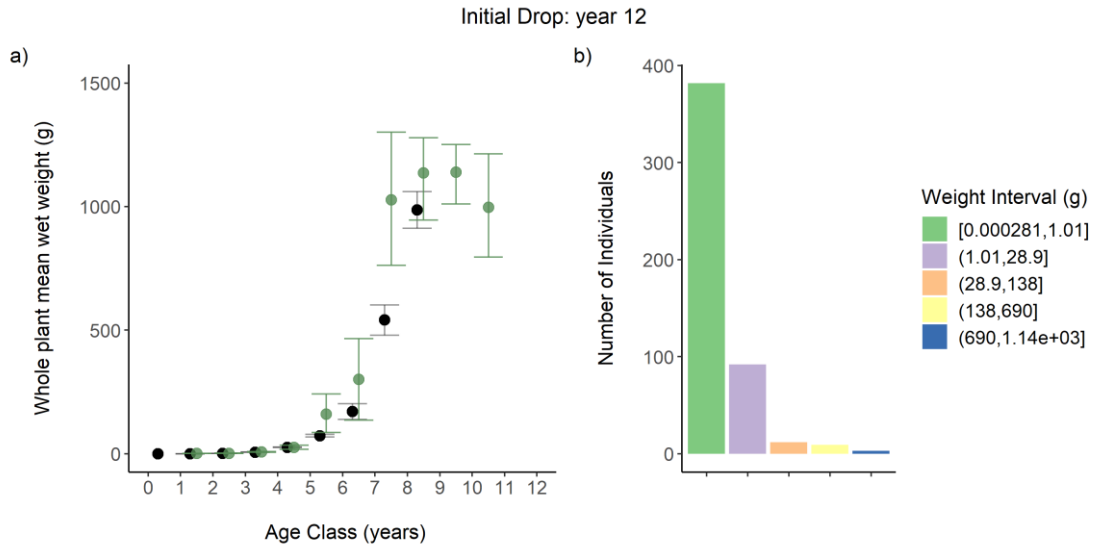

Figure 3.12. The left panel points show the mean model output converted to wet weight for the last month of year 12 of the simulation, with the standard deviation shown by the bars. Mean empirical data used for model parametrization shown by the green points, with the maximum and minimum values given by the bars (Jupp, 1972). The right panel shows the number of individuals in each weight category, with the weight intervals of each category given by the colours and described in the legend. Point b in Figure 3.8. The shift in the points is for visual purposes. The lack of a point implies there were no individuals of that age alive.

Moving on to observe the internal composition of the individuals in the cohorts that lead to the previously described distributions. It is clear that the individuals in the cohorts that settled later have a different growth pattern than those that settled into the cleared space (Figure 3.13). The later individuals are smaller and their weight takes a longer time period to reach the quasi-stable state repeating pattern that indicates their stable period, as the fluctuations seen are responding predominantly to seasonal fluctuations.

This trend is particularly noticeable in cohorts 5 and 6 (Figure 3.13). Several years pass with these cohorts being significantly smaller than previous and latter ones for the same ages, before the first cohort's decline at year 12 (Figure 3.8, point b, dotted line). At this point, it's clear that shading has played a role in this growth limitation, as evidenced by later faster weight increases among individuals growing under a lighter canopy.

Moreover, cohorts recruited around year 12 showed less distinct differences in weight. These individuals grow beneath a younger and less dense canopy, reducing competition for light and promoting a higher growth rate. This pattern is observed to be repeated across all state variables, with reserve carbon exhibiting the most notable recovery after year 12 canopy opening event, consistent with its greater dependence on light availability.

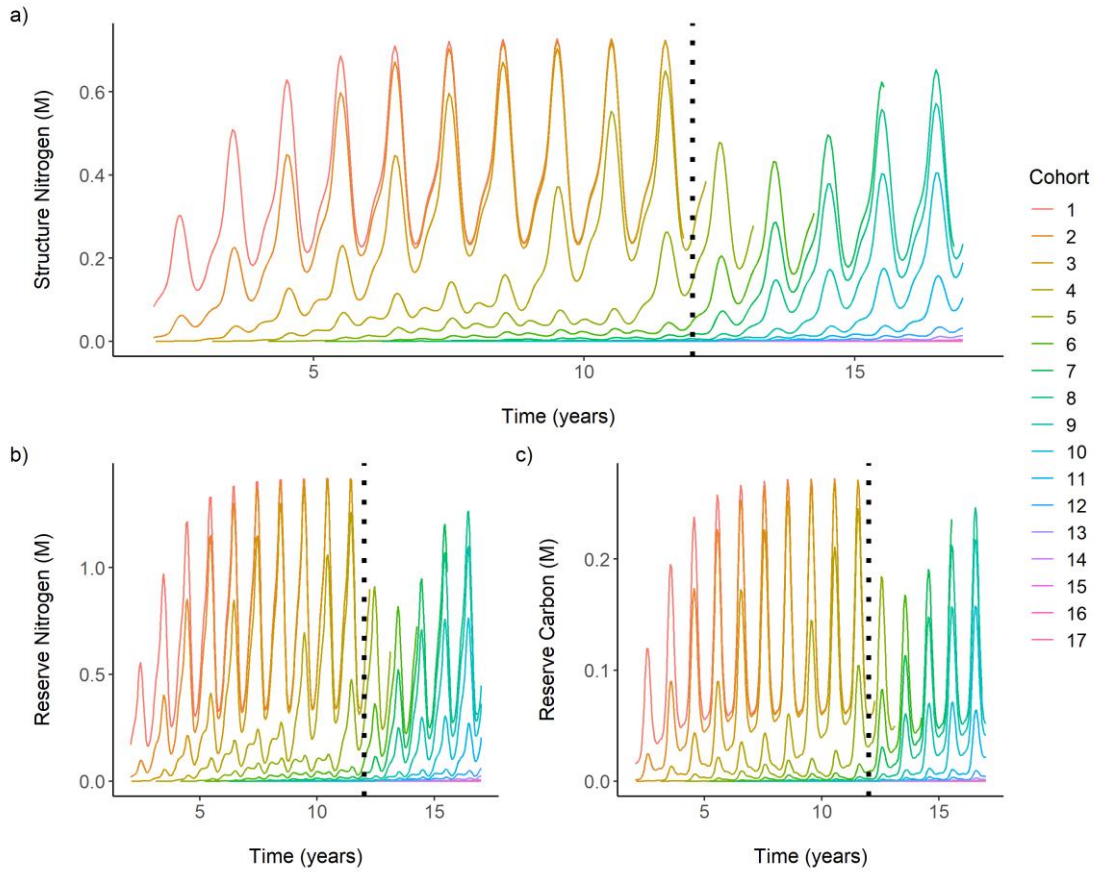

Figure 3.13. Structure nitrogen (a), reserve nitrogen (b) and reserve carbon (c) amount throughout the first 20 years of the simulation. Each cohort is shown in a different colour. The dotted line denotes the point where the initial drop in total forest biomass is observed at year 12.

Regarding the interactions between the different internal elements of the individuals, it is seen that the whole plant molar ratio indicates a response to seasonal fluctuation effects (Figure 3.14). This ratio is inherently governed by the internal reserves of the individuals, and as such, it is intricately linked to the prevailing growth-limiting factors. The timing of the C: N peak is notably delayed in subsequent cohorts, resulting in a reduced period during which their reserves remain at the optimal threshold.

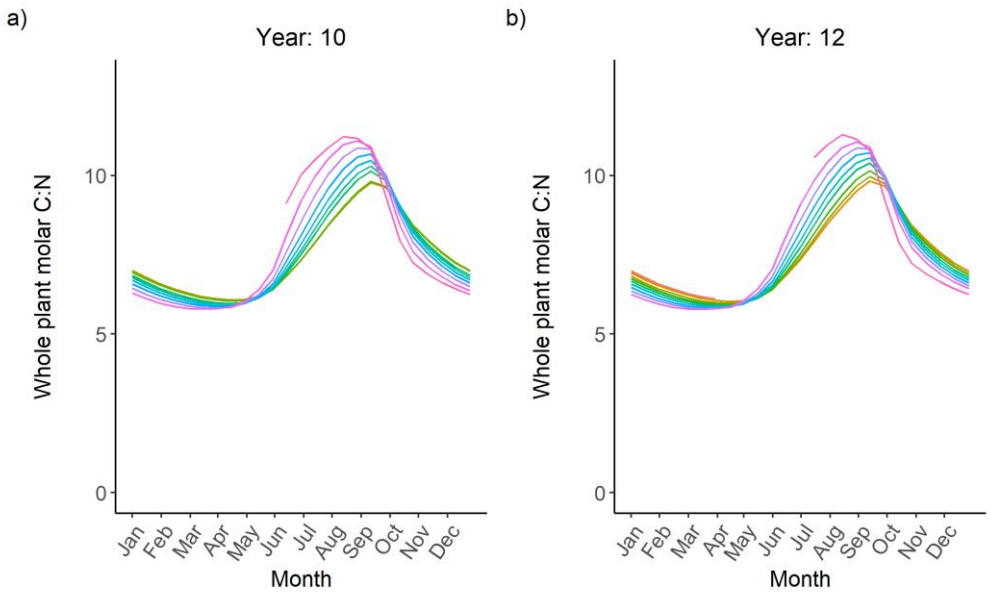

Figure 3.14. Whole plant molar C:N ratio for year 10 and year 12. The individual cohorts are shown by the different colours.

The nutrient limitations imposed by the changes in the environmental conditions can be clearly seen by examining the exudation of carbon and nitrogen. At cohort level, fluctuations in nitrogen exudation are present, whereas no carbon exudation is evident, suggesting a pronounced light limitation (Figure 3.15). The nitrogen exudation observed indicates a light limitation, as it is occurring to maintain stoichiometric balance in the production of structural tissue. These fluctuations in exudation align with the variations in individual weight mentioned earlier, as all processes scale with an individual's weight or size.

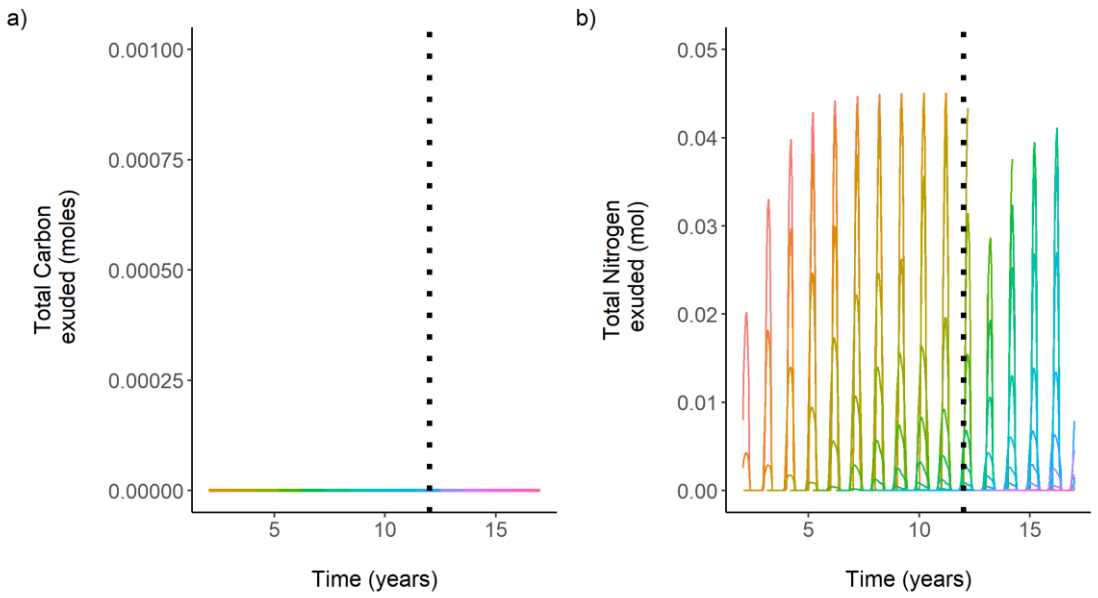

Figure 3.15. Exudation of carbon (a) and nitrogen (b) for the first 20 years of the simulation, this refers to the material that left the organism to maintain internal homeostasis. The dotted line denotes the point where the initial drop in total forest biomass is observed at year 12. Each cohort is shown in a different colour.

The effects of fluctuations in population structure have an effect on maintenance costs, as it scales proportionally with the plant's weight, mirroring the earlier-discussed fluctuations associated with light limitation restricting the growth rate (Figure 3.16). Maintenance costs remain unaffected by light limitation as it is primarily influenced by temperature and individual size, with no other external factors exerting significant impacts aside from the consistent seasonal fluctuations observed in an annual pattern.

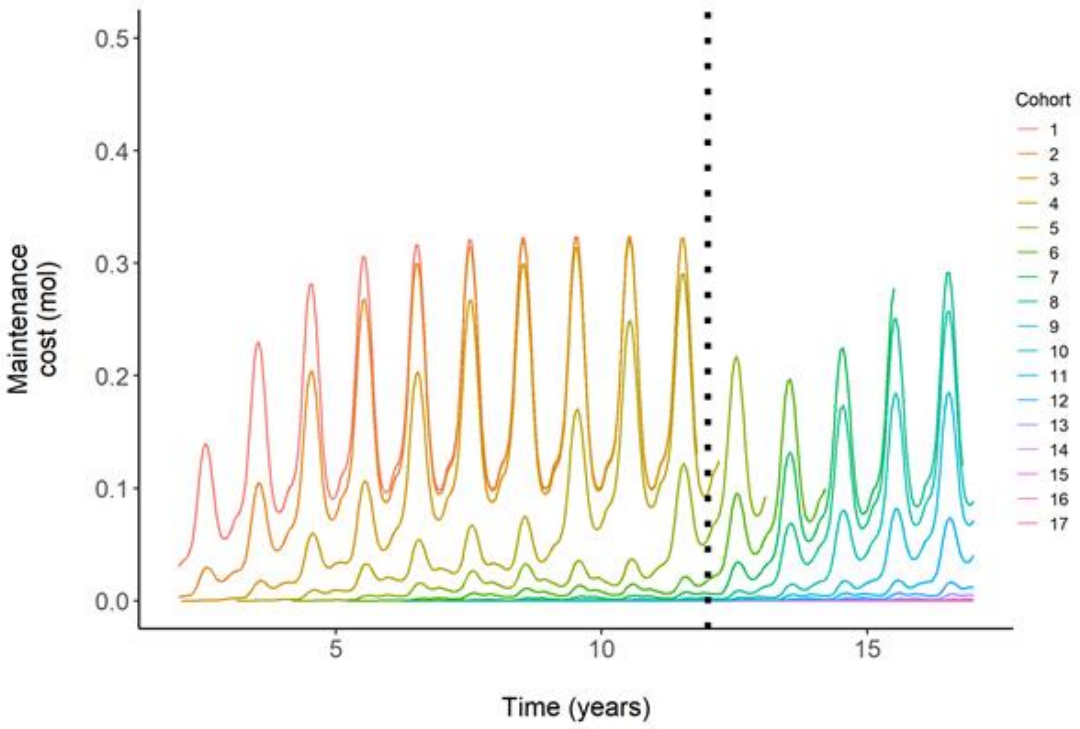

Figure 3.16. Individual maintenance cost (mol) in each cohort for the first 20 years of the simulation. The dotted line denotes the point where the initial drop in total forest biomass is observed at year 12. Each cohort is shown in a different colour.

3.3.3 Mature Forest Stage

After studying the development of the forest population structure and its individual's growth under ideal post-clearing growth conditions, the composition of a more mature forest is observed by selecting a later date in the simulation. The initial difference between earlier sampling points (Figure 3.8, point a and b) with later ones (Figure 3.8, point c and d), following immediate post-clearing growth, is that the plants failed to reach their potential maximum weight within their lifetime. In this context, the weight increase among individuals in each age class shows a continuous linear progression once individuals reach age class 7 (Figure 3.17). This trend is partly reflected in the distribution of individuals across weight categories, which exhibits a reduced degree of skewness compared to the previously observed pattern in the younger forest.

At year 27 (Figure 3.8, point c), the forest experiences a peak in biomass accompanied by an expected decline in recruitment in response. This signifies that the forest has attained its maximum annual mean biomass. Consequently, the smaller individuals, comprising the 60th percentile and below in terms of weight within the forest, become subjected to intense shading.

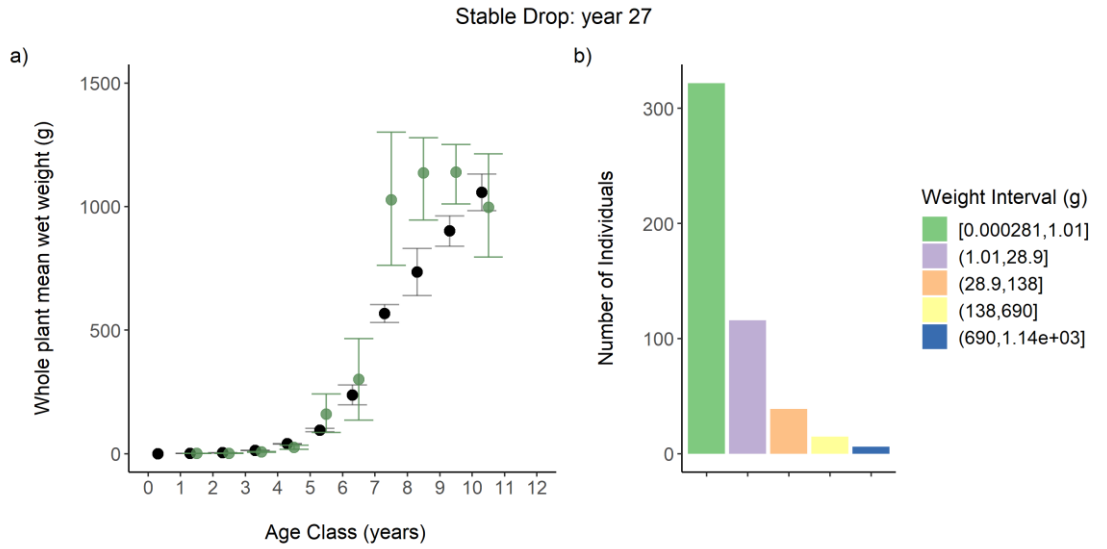

Figure 3.17. The left panel points show the mean model output converted to wet weight for the last month of year 27 of the simulation, with the standard deviation shown by the bars. Mean data used for model parametrization shown by the green points, with the maximum and minimum values given by the bars (Jupp, 1972). The right panel shows the number of individuals in each weight category, with the weight intervals of each category given by the colours and described in the legend. Point c in Figure 3.8. The shift in the points is for visual purposes. The lack of a point implies there were no individuals of that age alive.

In the year 33 of the simulation the forest reaches its stable lowest mean annual biomass, the second lowest point after the first cohort removal and the lowest point to be consistently repeated throughout the simulation (Figure 3.8, point d). The low forest biomass seen suggests that individuals have not yet attained their maximum weights, which becomes particularly evident when examining the cohorts from years 8 and 9 that undergone growth under the dense canopy. These cohorts growing under severely light limiting conditions have been unable to recover within their lifespan after the canopy opened and conditions improved (cohorts aged 8 and 9) (Figure 3.18, a). This is due to their critical early growth phases occurring during unfavourable light conditions, which stunted their potential for later recovery. Conversely, cohorts aged 4 to 7 (Figure 3.18), which grew under a thinner canopy, have achieved weights exceeding those observed in the empirical data for individuals of similar ages.

This contrast becomes more evident when looking at the population distribution within the heavier weight categories, the number of individuals in the maximum weight category is extremely low, especially when compared to the composition of the younger forest at time points a and b. Upon closer inspection of individual numbers across various weight categories, it is shown that the highest number of individuals is within the middle-weight categories, while the first weight category exhibits a low number of individuals.

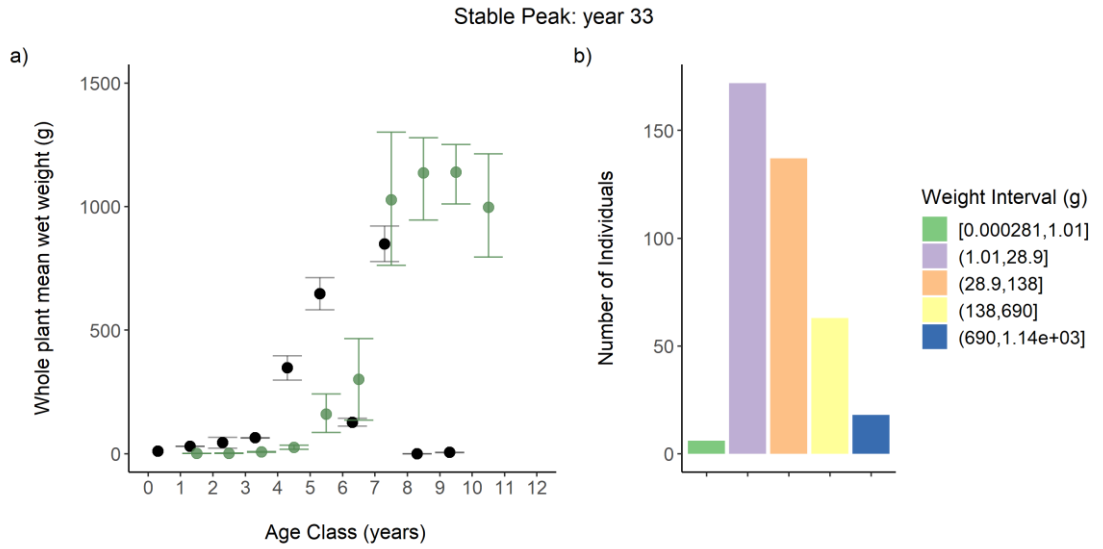

Figure 3.18. The left panel points show the mean model output converted to wet weight for the last month of year 33 of the simulation, with the standard deviation shown by the bars. Mean data used for model parametrization shown by the green points, with the maximum and minimum values given by the bars (Jupp, 1972). The right panel shows the number of individuals in each weight category, with the weight intervals of each category given by the colours and described in the legend. Point d in Figure 3.8. The shift in the points is for visual purposes. The lack of a point implies there were no individuals of that age alive.

When looking at the internal composition of individuals within the cohorts responsible for generating the previously discussed distribution (Figure 3.19), it becomes apparent that later-settling cohorts exhibit distinctly different growth trajectories from the earlier settling cohorts, echoing the trends in Figure 3.13. These individuals, distinct from their earlier-settling counterparts, display a smaller size and a more prolonged period is required to stabilize their weight fluctuations. This extended phase culminates in a distinct recurring pattern, signaling their transition to a the quasi limit cycle state that then fluctuate in response to seasonal enviromental fluctuations.

A consistent pattern emerges within cohorts growing under a denser canopy, with the light limitations imposed by it, before year 27 (Figure 3.19, shown by the shaded green bar). These cohorts exhibit constrained growth rates, mirroring the dynamics of cohorts in similar conditions seen in the forest earlier in the simulation. This pattern persists until the canopy experiences mortality events, after which an acceleration in growth rates as the canopy opens up is observed. Hence, it is vital to note that this restricted growth due to a light limitation pattern persists until the canopy experiences changes, such as mortality events or canopy thinning, marking pivotal moments in the growth dynamics of these cohorts.

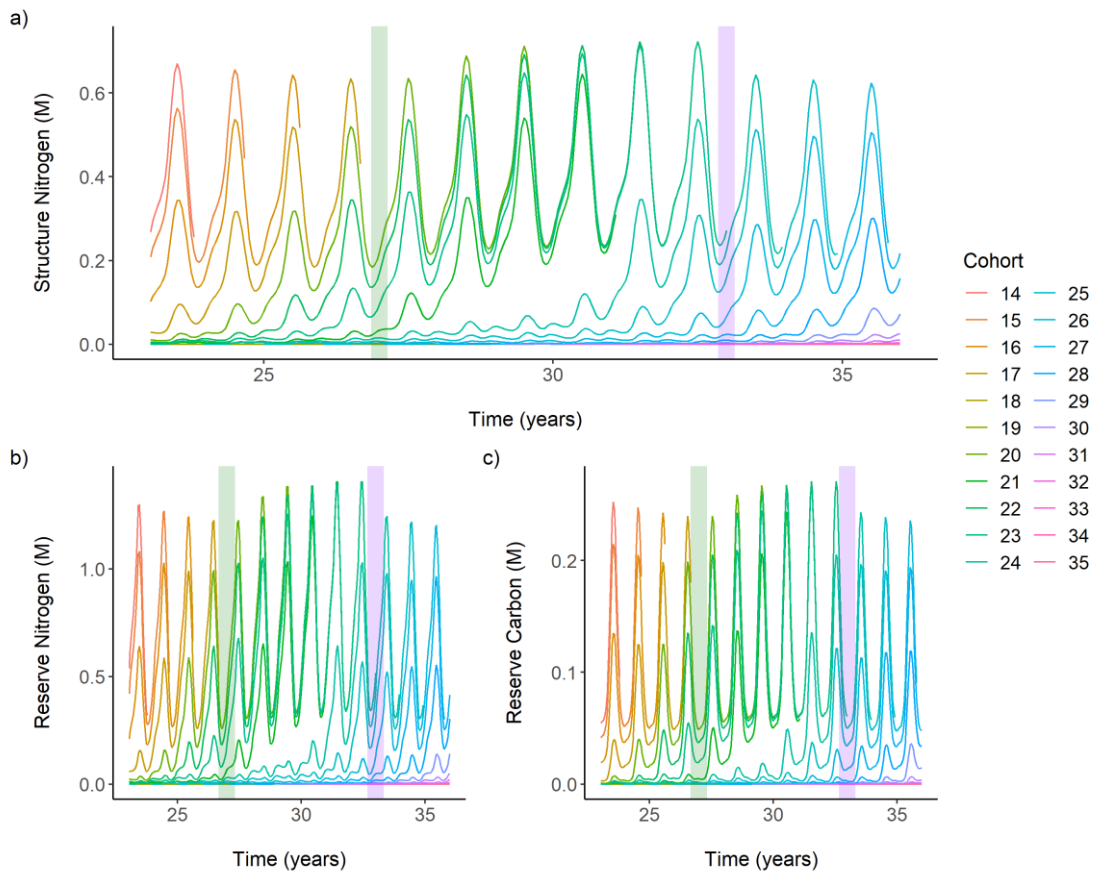

Figure 3.19. Structure nitrogen (a), reserve nitrogen (b) and reserve carbon (c) amount. The shaded green area denotes the drop seen in individuals recruited that coincides with a peak in mean annual forest biomass. The shaded purple area denotes the peak in recruitment seen after the drop-in mean annual forest biomass. The simulation results are shown in the 5 years previous to the first shaded line and in the 10 years that follow. Each cohort is shown in a different colour.

Regarding the internal dynamics of the individuals such as the C:N ratio (Figure 3.20), exudation rate (Figure 3.21) and maintenance cost (Figure 3.22), the same patterns seen above are repeated here. Over time, individuals transition from lower to higher weight categories, with the degree of the shift influenced by a balance between maintenance costs and uptake rates. Later-settling cohorts exhibit unique growth trajectories, characterized by smaller sizes and turning points in weight fluctuations, eventually transitioning into a quasi-limit cycle state that is then influenced by seasonal fluctuations and not intra-species light competition. Furthermore, cohorts under denser canopies consistently show constrained growth rates until pivotal canopy events, such as mortality or thinning, trigger an acceleration in growth rates. These patterns collectively underscore the dynamic interplay between cohort settlement timing, canopy dynamics, and their profound impacts on growth patterns within forest ecosystems, providing valuable insights into the dynamics of these complex ecological systems.

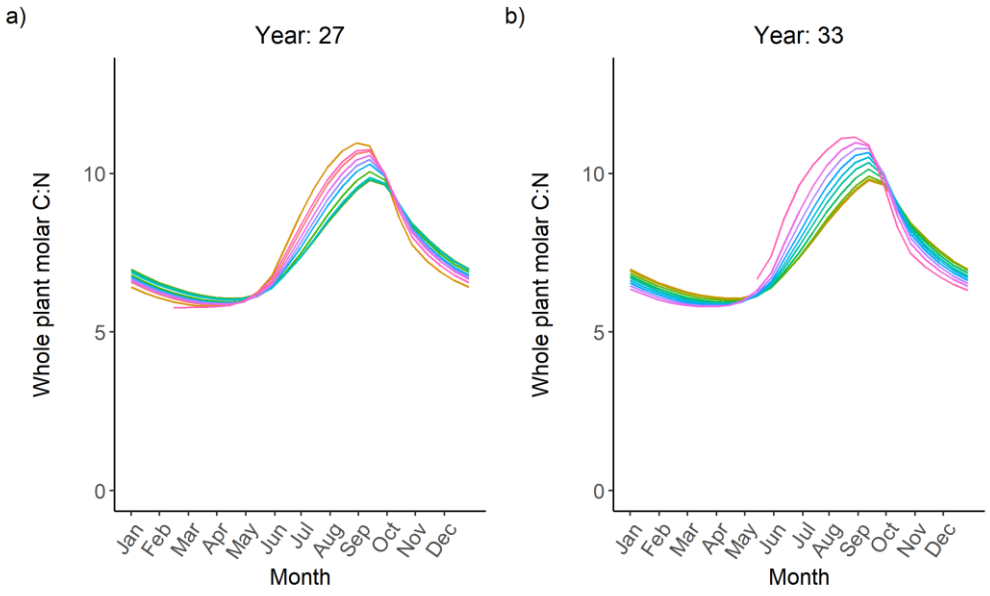

Figure 3.20. Whole plant molar C:N ratio for year 27 and year 33. The individual cohorts are shown by the different colours.

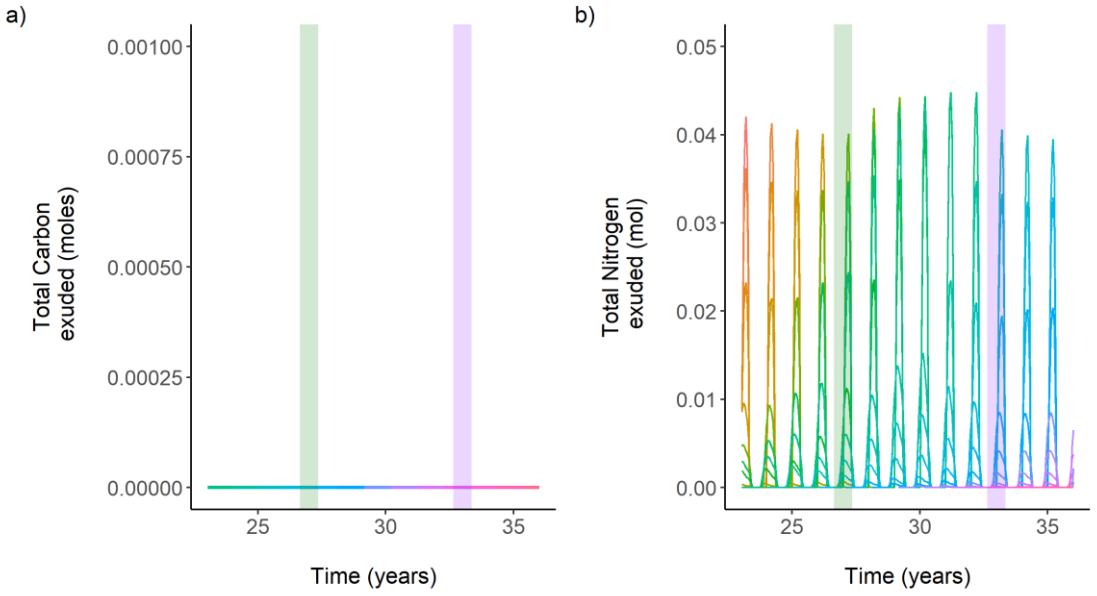

Figure 3.21. Exudation of carbon (a) and nitrogen (b) for the first 20 years of the simulation, this refers to the material that left the organism to maintain internal homeostasis. The shaded green area denotes the drop seen in individuals recruited that coincides with the peak in mean annual forest biomass. The shaded purple area denotes the peak in recruitment seen after the drop-in mean annual forest biomass. The simulation results are shown in the 5 years previous to the first shaded line and in the 10 years that follow. Each cohort is shown in a different colour.

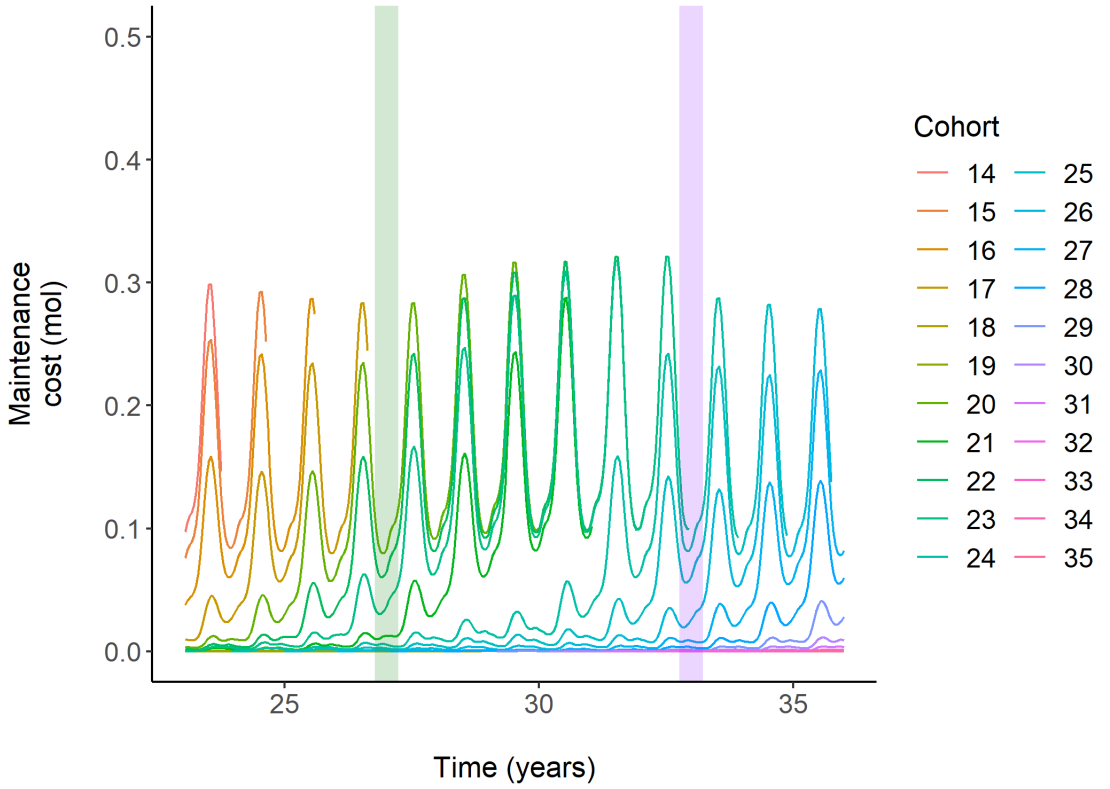

Figure 3.22. Individual maintenance cost (mol) for each cohort. The shaded green area denotes the drop seen in individuals recruited that coincides with the peak in mean annual forest biomass. The shaded purple area denotes the peak in recruitment seen after the drop-in mean annual forest biomass. The simulation results are shown in the 5 years previous to the first shaded line and in the 10 years that follow. Each cohort is shown in a different colour.

3.4 Discussion

The results show a distinct effect from the population structure on the growth rates of the individuals, the effects are mediated through the degree of light limitation enforced by the canopy. The light limitation effects have knock on effect on the internal biochemical dynamics of the individuals. The key point to highlight is that the history of the forest is vital for understanding the final weights that can be achieved by the individuals. Field samples that represent a snapshot in time cannot easily be interpreted without knowing the history.

The model results yield three additional key findings.

1. Over time, individuals shift gradually from lower to higher weight categories as they age, with the rate of growth being dependant on the current forest population and the final stable weights driven by a delicate equilibrium between size dependant maintenance costs and uptake rates.
2. Cohorts settling under an existing mature canopy exhibit distinctively different growth trajectories from the established individuals, characterized by smaller sizes and larger weight fluctuations, culminating in a transition to a quasi-limit cycle state, that then is driven on a yearly basis by annual environmental fluctuations.
3. Cohorts growing under denser canopies consistently display restricted growth rates until pivotal canopy events, such as mortality or thinning, trigger accelerated growth. This is due to shading by larger plants limiting the growth for juveniles, until the loss of mature plants allows rapid growth of the understory, this behaviour is also seen in empirical studies (Kain, 1963).

In summary, the previously described interactions are mediated through light competition, mortality, and recruitment rates. This highlights the importance of considering the population structure's effect on individual internal processes. By explicitly visualizing individual internal composition at different time points and their responses to changing light conditions—such as post-clearing growth versus individuals under a heavy canopy that die before experiencing optimal light conditions, and scenarios in between—the use of an individual-based forest model offers the flexibility to understand these various scenarios. It also allows for a detailed examination of factors like how time of settlement and population structure at settlement time affect C: N composition of individuals.

The values obtained from the model for individual weights fall within the range of the empirical data used for qualitative fitting (Jupp, 1972) and align with other studies (Kain, 1977; Rinde and Sjøtun, 2005; Sjøtun, 1993; Smale et al., 2016). The ages of the canopy also mirror the mean canopy age distribution seen in more recent studies (Smale et al., 2016; Smith et al., 2022). A specific challenge arose when comparing empirical data on individual *L. hyperborea* growth to the forest model results, as the empirical data provide weight measurements of individuals at various ages at a specific time, requiring the alignment of the model by sampling its output to match these time snapshots. Information on the state of the forest at the time that each individual settles is unavailable for the empirical data used in model parameterization, although the issue of lack of information on the initial growth conditions of a kelp forest is not a new one (Kain, 1976).

The effects of light limitation restricting the growth of the modelled individuals, aligns with the effects described in the literature regarding challenging conditions due to light limitations enforced on individuals that settle under a mature canopy (Creed et al., 1998; Sjøtun et al., 2006; Steen et al., 2016). The process behind this restriction can be shown by the lower photosynthesis rates seen when comparing individuals in open deeper water to those growing in shallower but denser conditions (Drew et al., 1976) and by the rapid recovery of biomass seen after canopy removal (Steen et al., 2016). The growth rates are hence constrained by density and irradiance (Kain, 1971b), and the model presented here can replicated these behaviours. Shifts in the timing and duration of C: N peaks in cohorts later in the simulation in the results can be attributed to light shading conditions. This is further supported by the absence of carbon exudation in the results. It also highlights the need for more complex structured models to understand the effects of seasonality on individuals' internal biochemical processes.

As previously mentioned, the empirical data represents a snapshot in time of the weights on individuals, and the model output is presented in a way to emulate this. The choice of the sampling time relative to the endogenous fluctuations in the demography of plants is crucial as it directly impacts the forest's population structure and conditions under which individuals have grown. To ensure robust alignment between the model output and empirical data, the selected sampling time must coincide with a moment when the simulated forest structure closely matches the population structure observed in the data, of which only the data at the time of sampling is known is most cases. The variations observed among different sampling times tested through the simulation highlight the substantial impact of sampling time on individual weight data, offering insights into how internal processes respond to external fluctuations in population structure, driven by changes in recruitment and mortality rates as the forest reaches its long-term state. It also further limits the amount of data that can be pooled together for a formal parametrization of theoretical process-based models.

The simulations illustrates how recruitment decreases as forest biomass increases, which aligns with other studies that report a negative relationship between canopy density and understory kelp recruitment (Sjøtun et al., 2006; Steen et al., 2016). The highest numbers of small kelp individuals are observed around year 12, following the die-off of the initial cohort. This finding is consistent with existing literature, which also reports peak small kelp density during periods of low canopy density or after canopy removal (Sjøtun et al., 2006). The model purpose, and value, is to explore how being able to represent the role of canopy shading affects the population dynamics and the internal energy budget of the individuals.

The predicted regular fluctuations in biomass observed over time are an emergent property of the density dependant processes present in the model. The cycle is dependent on the mortality rate, and its balance with the recruitment rate. The behaviour currently observed responds to the presence of a long-lived senescence species, as for recruitment to increase the older individuals must first die to open the space. This patter follows the

relaxation cycles observed in other open marine population models with space limited recruitment for sessile organisms (Roughgarden et al., 1985), where if the growth rate outpaces the rate of space renewal due to mortality, a critical settling rate determines system dynamics. Below this rate, the population stabilizes with a steady age distribution and free space, while exceeding it causes oscillations in free space and instability in age distribution. The fluctuations seen in my model, hence respond in a similar way, the oscillations and instability are caused by a lack of free space.

The 26-year cycle observed in the model results suggests a pattern of stable dynamics in *L. hyperborea* populations, where the turnover of canopy generations appears to be governed by density-dependent processes. The first generation within the cycle produces a large biomass peak as canopy plants establish and dominate the available space. During this time, recruitment is heavily suppressed due to shading effects, leaving only a limited number of understory individuals capable of growing into the canopy once space becomes available. When the first-generation canopy senesces and dies, it leaves behind a finite amount of open space.

This newly available space allows the recruitment of understory plants into the canopy, forming the second generation. However, because the recruitment during the first-generation peak was limited by shading, the second generation produces a smaller biomass peak. This smaller cohort of canopy plants, in turn, suppresses recruitment for the next cycle, perpetuating the oscillatory pattern. The space left empty by the senescence of the previous, smaller cohort is insufficient to support a large peak in the subsequent generation, maintaining the stable, repeating cycle observed in the model. This dynamic provides insights into how shading, recruitment, and space availability may interact to regulate population turnover and biomass stability over time. In the case of space opening due to trawling or storm events the new space would be colonised by new recruits, but the improved light conditions would benefit all the individuals in the forest.

Regarding the long-term population dynamics, the modelled stability and repeating cycles in canopy dynamics provide valuable insights into kelp forest behaviour. Other modelling studies suggest that canopy suppression of understory growth can have a stabilizing effect on long-term population dynamics (Rinde, 2007). These models predict that demographic differences, such as those caused by latitudinal effects (Rinde and Sjøtun, 2005), are unlikely to alter this stable equilibrium. Given the complex and long-term dynamics observed in these forests, this model offers a valuable opportunity for conducting immediate, low-cost experiments to assess the effects of various disturbances on forest ecosystems.

The results from this chapter forest model when being compared to the empirical data also provides insight into the empirical data used. It suggests that the empirical data (Jupp, 1972) used to parameterize the model came from a forest that had previously undergone a significant clearing event before the oldest plants in the population recruited. This conclusion is based on the match between the population structure, age, and weight distribution of the empirical data and modelled data with known initial conditions. This insight offers a level of detail rarely possible in field studies, unless it is a site that has been consistently monitored for decades. In light of my model results and previous research, it is essential to consider the time it takes for complex habitats like kelp forests to respond and recover from disturbance events. While kelp forests are generally stable across years and seasons, short-term studies should be interpreted cautiously, taking into account the historical forest conditions. Long-term studies, such as those involving artificial reef deployment, suggest that more than 10 years are required for *Laminaria* species to become established (Tsiamis et al., 2020). Harvesting studies in Norway also indicate that achieving full restoration of kelp canopy size and age distribution necessitates a harvesting cycle exceeding the legally mandated 5 years (Steen et al., 2016).

3.5 Conclusion

This chapter offers valuable insights into the growth dynamics of *L. hyperborea* forests. I addressed the challenge of aligning empirical data on individual kelp growth with the forest model by carefully selecting sampling times, emphasizing its critical influence on population structure and individual growth. The model revealed key patterns, including shifts in weight distribution following biomass declines, distinctive growth trajectories in later-settling cohorts, and the influence of canopy shading on growth rates. These findings are aligned with existing research, supporting the importance of canopy dynamics, light competition, recruitment and mortality events in shaping kelp forest ecosystems. Additionally, my results emphasize the need for long-term studies to better understand the complex responses of these habitats to disturbance events, contributing to more effective conservation and management strategies for kelp forests in various environmental conditions and depths. Future research directions should explore the effects of depth, local environmental factors, waves, storms, turbidity, and grazing to enhance our understanding of kelp forest dynamics comprehensively.

3.5.1 Future Research

The analysis presented here pertains to a forest growing at a 3-meter depth, following the irradiance conditions representative for part of Scotland. As previously emphasized in the preceding chapters, the influence of depth and local environmental factors is substantial. Consequently, further experimentation with this model across various depths and locations would provide valuable insights. Additionally, it's crucial to consider the impact of waves and storms, which has been underscored in the literature (Kain, 1971a, 1963; Kregting et al., 2013; Pedersen et al., 2012). These considerations would lead to a more accurate representation of the mortality processes observed in natural forests.

Furthermore, the effects of changes in water turbidity, should get detailed examination (Smale et al., 2016). The influence of waves on plant morphology should also be taken into account, as variations in morphology can affect the drag properties of individual plants, subsequently impacting mortality rates. Moreover, these differences in morphology can manifest in variations in weight and tissue composition, with sturdier plants being more prevalent in rougher waters (Larkum, 1972; Pedersen et al., 2012; Sjøtun et al., 1998; Sjøtun and Fredriksen, 1995; Smale et al., 2016).

The effects of population structure on reproduction, particularly the amount of spores produced by an individual, can be incorporated into the forest model. Adding gametophyte production would bridge the gap between the current open forest model, which assumes unlimited settlement, and a closed forest model, where population tipping points and the impact of limited recruitment on recovery can be observed. This is in response to the minimum age for sporing in *L. hyperborea* was shown at 15 months with minimum fresh weight for an individual to start developing sorus between 30-80 g (Kain, 1975). Although, this is dependent on the environment, as individuals that were growing in an undisturbed forest were seen to take up to 5 years to full maturation, in comparison to those plants from cleared areas that grew much faster (Kain, 1975). This indicates that it is a size dependant process, not only a function of age and hence dependant on the effects of population structure previously described in the chapter.

Currently, the forest model uses one grid cell per year to simulate cohorts, but this could be modified to recycle a set number of grid cells, allowing recruitment only once a grid cell becomes vacant. This change would introduce spatial limitations into recruitment, for instance, modelling a forest on a rocky substrate surrounded by non-viable areas like sand.

Lastly, the model currently does not consider the effects of grazing, which can have significant implications for plant density and the forest's resilience to disturbance events. Existing research highlights the importance of grazing in kelp forest dynamics (Harrold and Reed, 1985; Kain, 1971a; Sjøtun et al., 2006). Exploring these factors in future research would provide a more comprehensive understanding of kelp forest ecosystems.

4 *Laminaria hyperborea* under various climate change scenarios for Scotland.

4.1 Introduction

Ocean warming and the associated environmental effects have already triggered shifts in species distributions (Hargrave et al., 2017), alterations in community structures and ecosystems (Wernberg et al., 2019), and modifications in the provision of ecosystem services (Smale et al., 2013). Alongside gradual warming trends, marine ecosystems are experiencing discrete extreme warming events known as "marine heatwaves" or "heat spikes," which result in abnormally high sea temperatures lasting from days to months (Burdett et al., 2019).

Kelps, as foundation species in coastal marine ecosystems, play a pivotal role in local biodiversity, food webs, and carbon cycling (Teagle et al., 2017). They also significantly contribute to global carbon sequestration (Pessarrodona et al., 2018). Both ecophysiology and distribution of kelp species are intricately linked to temperature (Eggert, 2012), and ocean warming trends have led to notable changes in the structure and functioning of kelp populations and associated communities (Wernberg et al., 2019).

Among the various kelp species, *L. hyperborea* is of particular relevance due to its significance in wave-exposed rocky reef habitats along the NE Atlantic coastline (Kain, 1979). Recent warming trends have triggered shifts in the distributions of different kelp species, including warm-affinity and cold-affinity species, influencing local diversity and ecosystem functioning (Raybaud et al., 2013; Smale et al., 2013). These changes are coupled with the effects of temperature on primary productivity, carbon assimilation, and carbon transfer within interconnected habitats (Pessarrodona et al., 2019). However, while there's a consensus that ocean warming will lead to range shifts and alterations in kelp-dominated communities (Harley et al., 2012), the underlying physiological mechanisms and the variability in responses are still not well understood. For *L. hyperborea* contraction at their southern ranges are already being reported, and future climate scenarios suggest expansions to northern territories for *L. hyperborea* but significant habitat loss at low latitude margins, particularly under the highest emission RCP 8.5 scenario (Assis et al., 2016).

Currently, there are no models in the literature that have developed a *L. hyperborea* forest model based on individual growth with detailed descriptions of internal biochemical processes. Individual-based models at this level of detail are available for *Saccharina latissima* (Aldridge et al., 2012; Broch and Slagstad, 2012a; Venolia et al., 2020), but these models are aimed at more aquaculture scenarios. As such, they lack key processes like the effect of canopy shading by older individuals(Drew et al., 1976; Kain, 1963; Rinde, 2007; Steen et al., 2016). In this thesis, an individual model for *L. hyperborea* has been developed, which does not grow under a canopy (Ch2). It follows a similar framework to other aquaculture models, but one key difference is that this model applies to a different species with unique adaptations and seasonality to varying environments. Together with modelling the entire lifespan of the individual and not only the growing seasons.

The forest model builds on the physiological detail of the individual model and incorporates interactions between individuals—interactions that shape the light regime to which each individual is exposed. This high level of individual physiological detail results in a highly dynamic environment designated by the individuals that make it up, providing information about the weights of individuals forming the canopy, as well as their numbers, allowing for precise understanding of specific canopy conditions. For example, experimental conditions with different canopy densities and mortalities can be set up to understand their responses to different climate conditions.

To fully understand the extent of the predicted future impacts on *L. hyperborea*, a model that includes all key processes determining growth and growth limitation is essential. As previously discussed, canopy shading is one of these critical processes.

Here, the effects of different climate change scenarios on *L. hyperborea* are explored using both the individual-level model and the detailed forest-based IBM approach. Applying both models will highlight not only the impacts of climate change but also the importance of key modelling choices in developing accurate predictions. Insights gained from these models could inform management strategies to mitigate the detrimental effects of anthropogenic climate change, which are already evident in shifting species distributions. These insights highlight the increased stress the forest will face under climate change, as reflected in reduced weights. If harvesting quotas are set based on current height and weight standards, there is a risk of overharvesting a smaller, more vulnerable future forest.

This chapter will focus on the application of DEB theory individual and forest *L. hyperborea* models for various climate change scenarios in the west coast of Scotland, specifically the RCP 4.5 and RCP 8.5 projections, both near-term (2040–2069) and long term (2070–2099). The analysis of outcomes obtained from both simulation approaches will also shed light on the practicality of employing more intricate models compared to more parsimonious ones, thereby informing the ongoing debate regarding the role of model complexity role in achieving optimal results. The use of a mechanistic model should help to highlight the processes underlying the organism's responses to these changing conditions.

4.2 Methods

The individual (Chapter 2) and the forest (Chapter 3) models that have been described previously were subjected to environmental driving data corresponding to four different climate change projections. The aims were a) to discover how the models responded to representations of future climate, and b) compare and contrast the results from the individual and forest models.

The individual DEB model (Chapter 2) represented the growth and internal nutrient budgets of a single isolated plant exposed to annual cycles of temperature, light intensity and nitrate availability. The model parameters were manually tuned so that it replicated an average plant growth trajectory derived from field data collected off Arisaig in western Scotland (Jupp, 1972), while being driven by environmental data collected nearby in the Firth of Lorne (Berx et al., 2015; Heath, 1991, 1995).

The forest model (Chapter 3) comprised multiple interacting DEB models of individuals. In this case, the light conditions under which the individual DEBs develop were not completely prescribed from data, but modelled as a function of shading by the population of DEBs comprising the forest. All the DEB models in the forest shared a common set of parameters, but these were different from those of the isolated individual model. The forest DEB parameters were tuned to reflect the variation in growth trajectories and age structure in the forest sampled off Arisaig, rather than an average individual.

4.2.1 Individual model description summary

The individual model in Chapter 2 describes how a single organism assimilates and utilizes nitrogen (N) and carbon (C) for growth and maintenance, with a focus on the stoichiometric balance between these two essential nutrients. It begins by detailing the uptake of nitrogen through nitrate assimilation and carbon via photosynthesis, both of which depend on external environmental factors like nutrient availability, light, and temperature. The uptake rates of both nitrogen and carbon are temperature-dependent, with the maximum uptake rates modelled using a Q_{10} temperature coefficient to reflect the impact of changing environmental conditions.

Nitrogen uptake follows a saturating type-II Michaelis-Menten functional response, meaning the uptake rate increases with available nitrogen but levels off when the organism's capacity is reached. Carbon uptake is regulated by light availability and follows a type-I functional response, which assumes a linear relationship with available light up to a saturation point. The organism's surface area plays a key role in determining its nutrient uptake, with larger surface areas allowing for higher rates of assimilation.

Once nitrogen and carbon are assimilated, they are stored in separate reserve pools, with their densities reflecting how well the organism is fed. These reserves are mobilized to fuel maintenance costs first, and any remaining nutrients are allocated to growth. The mobilization of reserves must maintain a stoichiometric balance between nitrogen and carbon, which is modelled by adjusting the proportion of each reserve that can be used for growth.

The model also accounts for temperature-dependent maintenance costs, which must be met before growth can occur. Growth is driven by the flux of mobilized, stoichiometrically balanced reserves, and the process is regulated by a partitioning factor that determines how much of the available nutrients are allocated to structural growth versus reproductive output. In the model, reproduction can be turned off to direct all resources to growth if necessary.

In summary, the individual model provides a detailed, dynamic representation of how nitrogen and carbon are assimilated, stored, and utilized by an individual organism, emphasizing the importance of stoichiometric balance and environmental influences on growth processes.

4.2.2 Forest model description summary

The forest model is composed of multiple interacting individual DEB models. The individual models are conceptually organized on a grid where each cell contains a "super-individual," representing a cohort of identical plants that recruit simultaneously and experience the same environmental conditions. These cohorts grow, compete for light, and die off over time, with their population gradually declining due to a set mortality rate. The model tracks each cohort's growth, starting from recruitment and continuing until the cohort's population falls below a critical extinction threshold (less than one individual), at which point the grid cell becomes empty.

Recruitment in the forest model refers to the addition of new individuals to a cohort and is influenced by the density of the forest. As the forest becomes denser, fewer individuals are recruited due to increased competition for light under the canopy. This relationship is described using an exponential function that decreases the number of new recruits as forest density increases, with parameters that can be adjusted for different forest conditions.

Light availability is a critical factor in determining the growth of individual plants. The model simulates light competition by ranking cohorts based on their cohort biomass, which is derived from their size and biomass (carbon and nitrogen content). Heavier, heavier-ranking cohorts receive more light, while lower-ranking, smaller cohorts experience reduced light due to shading from the upper layers of the canopy. This shading effect impacts photosynthesis and slows down the growth of plants in the understory. The amount of light available to each cohort is scaled by a shading attenuation coefficient.

The model abstracts the spatial distribution of plants and focuses on the functional dynamics of light competition and mortality in a forest. Shading effects are calculated based on the height of the tallest plants, from the reference empirical data, which are assumed to cast shadows over the understory, affecting the available light for lower-ranking cohorts. The model allows flexibility in simulating different forest structures by adjusting key parameters like recruitment rates, light attenuation, and canopy height.

4.2.3 Model set up

The free parameters of the isolated individual DEB model were tuned to different observational data than the DEBs comprising the forest model. The former was set so that the model replicated the growth trajectory (weight-at-age) of a typical individual from the Arisaig field data (Jupp, 1972). The forest model DEB parameters were set to replicate the variability in weight-at-age data in the Arisaig forest and the population structure. As far as possible, the parameters for the two DEB model instances were held identical, but three required to be varied (Table 4.1).

It could be argued that the different DEB parameterisation of the individual and forest model render comparison of their results under climate change scenarios somewhat difficult to interpret. However, the two models are different representations of how plants respond to environmental conditions – one as an isolated individual, the other as an interacting population of individuals – even though they share a common representation of physiology. The parameters of each were tuned to different aspect of a common dataset, and it is reasonable to expect that some parameter values may differ.

Table 4.1. Parameters and their respective values for each model.

Parameter	Description	Unit	Forest model Value	Individual model Value
$U_{C_{max}}$	uptake rate of carbon per unit area	moles C $day^{-1}cm^{-2}$	4 x 10^{-5}	2 x 10^{-5}
$U_{N_{max}}$	uptake rate of nitrogen per unit area	moles N $day^{-1}cm^{-2}$	4 x 10^{-6}	2 x 10^{-6}
$R_{C_{max}}$	'target' ratio of reserve moles carbon to structural moles nitrogen	dimensionless	80	80
$R_{N_{max}}$	'target' ratio of reserve moles nitrogen to structural moles nitrogen	dimensionless	4	4
κ	proportion of resources allocated to structure	dimensionless	1	1
λ	maintenance cost	day^{-1}	0.03232	0.0181
m	mortality rate	individuals day^{-1}	0.0012	NA
T_0	Q_{10} reference temperature	$^{\circ}C$	12	12

4.2.4 Environmental Data Sources

Assembly of the common baseline (Present Day) environmental driving data for both the individual and forest model is described in Chapter 2. The data comprise monthly resolution annual cycles of nitrate concentrations ($\mu\, mole\, N\, l^{-1}$), light intensity ($E\, m^{-2} day^{-1}$), and temperature ($^{\circ}C$) from the Firth of Lorne, west of Scotland in 1991. The climate change scenarios data set correspond to Representative Concentration Pathways (RCP) climate scenarios 4.5 and 8.5 as described in the 5th Assessment Report of the Intergovernmental panel on Climate Change (IPCC) (IPCC, 2014).

The climate scenarios data was obtained from the OCLE data base (de la Hoz et al., 2018).Future climate projections were based on data from the fifth phase of the Coupled Model Intercomparison Project (CMIP5, Taylor et al., 2012). This project includes coordinated experiments using General Circulation Models (GCMs) for two periods: a near-term (2040–2069) and a long-term (2070–2099), covering various Representative Concentration Pathways (RCPs).

Parameters for these projections were calculated for each GCM, RCP, and time period, then averaged using the ensemble method (Arnell et al., 2016), with sea level projections referenced from IPCC values (Slangen et al., 2014). The analyses utilized tools such as Climate Data Operators (CDO), NetCDF Operators (NCO), Matlab, and ArcGIS.

To create climate change scenarios for the simulations, the Δ methodology was employed, which involves adding an offset to present-day baseline variables to predict future conditions. The Δ parameter was obtained from the OCLE database on climate change impacts (de la Hoz et al., 2018), with Δ values calculated by comparing historical data to CMIP5 projections. This was the applied to the data assembled described for Chapter 2.

Data was assembled for the near-term (2040–2069) and the long term (2070–2099 futures) (Figure 4.1). RCP 4.5 projections consider that maximum emissions will be reached in 2040, with a subsequent decrease. RCP 8.5 is commonly referred to as the "business as usual" scenario where emission increase is on-going (IPCC, 2014).

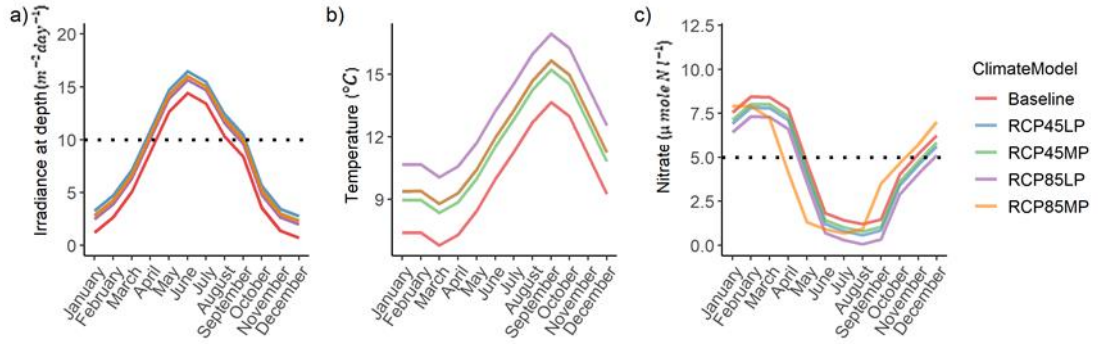

Figure 4.1. Environmental data used in the simulations. Each colour represents the climate scenario simulated. The near-term (2040-2069)(MP) and the long-term (2070-2099) (LP) future scenarios for the Representative Concentration Pathways (RCP) climate scenarios 4.5 and 8.5 as described in the 5th Assessment Report of the Intergovernmental panel on Climate Change (IPCC) are shown (IPCC, 2014). Data shown for irradiance at 3m depth (a), temperature (b) and nitrate (c).

4.3 Results

4.3.1 Individual Model

4.3.1.1 Individual Weight Dynamics

The effects of the four different climate scenarios simulations where compared with empirical data (Jupp, 1972) from the west coast of Scotland. The individual model results show higher weights than the baseline data before the organism reach 7 years of age (Figure 4.2), after this point the effects of climate change are clear in reducing the weight of the canopy individuals. Furthermore, for both RCP 8.5 simulations the model reveals a reduction in the amplitude of seasonal fluctuations, shown by the shading area around the lines, with changing climate condition.

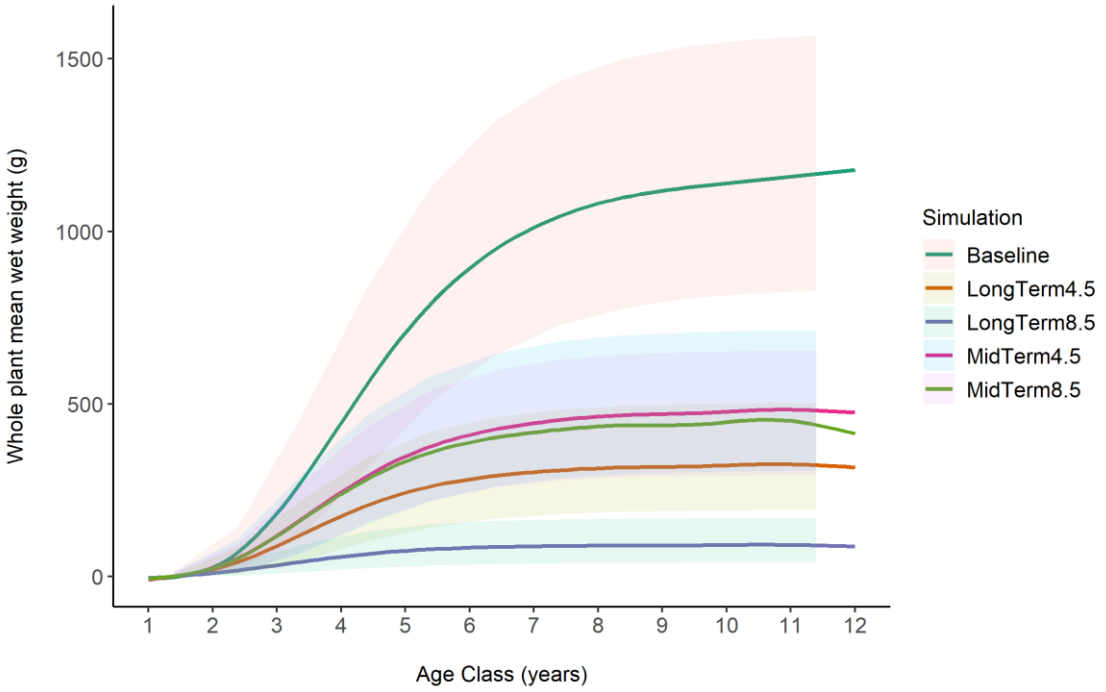

Figure 4.2. Results from the model output under different RCP climate change scenarios (given by the line colour) and the baseline data. Mean wet weight for the individual model age class shown by the continuous line, with the variations due to seasonal fluctuation shown by the shading. Using a depth of 3m across all simulations.

4.3.1.2 Biochemical Fluxes

Structure and Reserve Dynamics

As conditions get warmer, the individuals get smaller. When observing the state variables, structure nitrogen shows the lowest values (Figure 4.3, a), with reserve nitrogen seen in higher quantities (Figure 4.3, b). It is clear that the majority of plant composition is attributed to carbon reserves (Figure 4.3,c), specifically two orders of magnitude more than the nitrogen-based state variables.

A key distinction between the mid-term and long-term scenarios lies in the timing of the peaks of their state variables. In the mid-term RCP 4.5 scenario, this peak occurs further right, indicating a higher and later peak compared to the long-term RCP 8.5 scenario. Additionally, there is a reduction in the amplitude of cycles as conditions diverge further from the baseline, most notably observed in the long-term RCP 8.5 scenario where the maximum values are below the minimum values of any other scenario for structural nitrogen (S_N), carbon reserves (R_C), and are barely reached for nitrogen reserves (R_N).

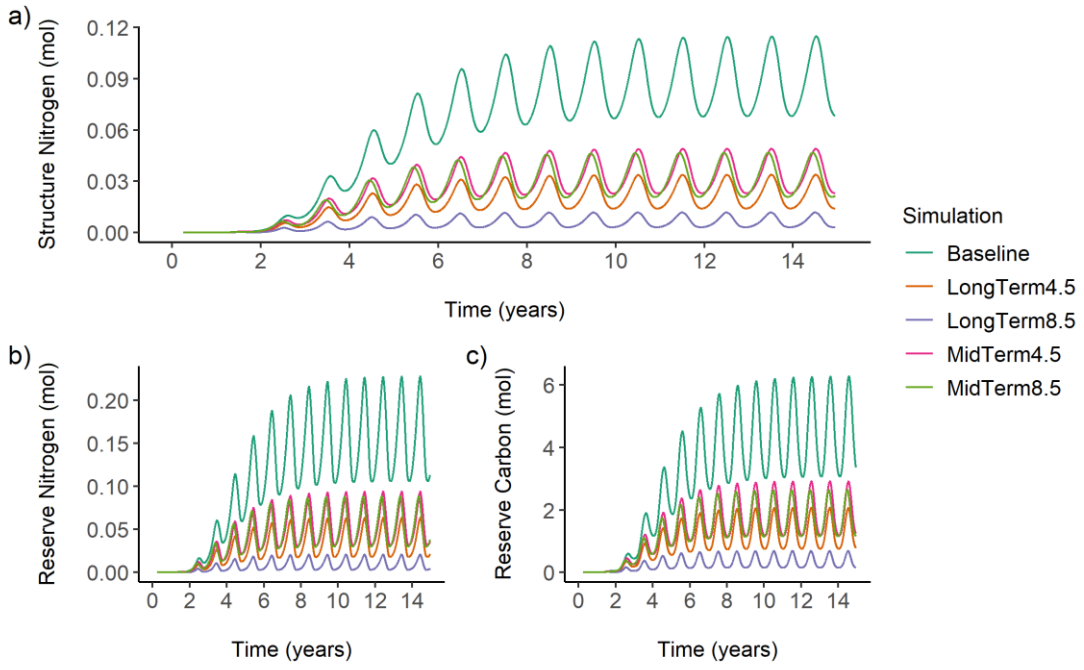

Figure 4.3. Individual model output. Structure nitrogen (a), reserve nitrogen (b) and reserve carbon (c) amount throughout the simulation. All values shown in moles. The climate change simulation used for the environmental driving data is given by the colours on the legend. Using a depth of 3m across all simulations.

Carbon Dynamics

In the mid-term simulations, carbon uptake (~0.02 mol C day^{-2}) shows overlap with the long-term RCP 4.5 scenario, indicating similar carbon dynamics under these conditions (Figure 4.4). As conditions deviate further from baseline, particularly in the RCP 8.5 scenario, carbon uptake decreases, with the long-term models showing a substantial reduction. The maximum mobilisation values in the long-term RCP 8.5 scenario fall below the minimum values seen in other simulations, underscoring how more extreme environmental conditions severely limit carbon availability for growth. This has to be interpreted considering that the weight and hence surface area of the individuals, which mediate the uptake processes is also decreasing in the more severe climate scenarios.

Carbon exudation patterns differ based on the severity of the scenario, with more exudation occurring under less severe conditions, such as in the mid-term RCP 4.5 and RCP 8.5 scenarios. This suggests that in milder scenarios, light and nutrient availability lead to no limitation of carbon. However, as conditions deviate from the baseline, carbon exudation decreases, with the long-term RCP 8.5 scenario showing minimal exudation. In this extreme case, carbon is primarily conserved for structural needs, reflecting the increasing limitations on plant resources as environmental stress intensifies.

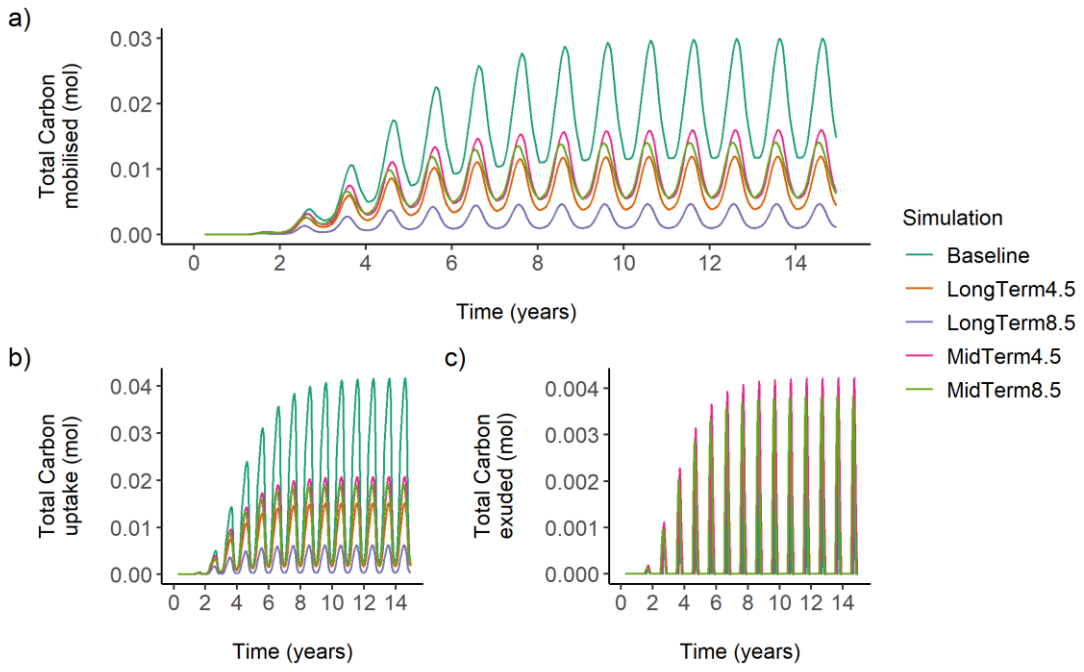

Figure 4.4. Individual model output. Input and output of carbon fluxes throughout the simulation. Carbon mobilised (a) refers to the amount of carbon uptake (b) that was absorbed onto the state variables. Carbon exuded (c) refers to the material that left the organism to maintain internal homeostasis. The environmental driving data is given by the legend. Using a depth of 3m across all simulations.

Nitrogen Dynamics

The nitrogen uptake and mobilisation by the individual show the same pattern of reductions described for the carbon dynamics as conditions deviate further from the baseline (Figure 4.5). A differentiation is made in the timing and shape of nitrogen uptake curves during the yearly cycle. In the individual model, the shift in peak maximum values during mobilization starts as early as year-class 2 for organisms (Figure 4.5,b). The maximum values in long-term RCP 8.5 scenario simulation are lower than or nearly equal to the minimum values in all other simulations, particularly noticeable after year five of the individuals' lives. For younger plants, the environmental limitations have not yet fully impacted growth, and the effect of limitations becomes evident through the plant size and its influence on the maximum uptake rate.

It is important to examine the seasonal patterns in detail (Figure 4.5, d), particularly the effects of the different climate change predictions on the timing of uptake cycles, as these reflect the plant's direct response to the simulated environmental conditions and the interaction between internal processes and the environment. The peak uptake occurs in May, except in the mid-term RCP 8.5 scenario, where it occurs in March. The minimum values exhibit more complex behaviour. As conditions worsen, the cycle range shrinks, reducing the range of values, alongside an overall decrease in uptake in line with the resulting smaller plant sizes.

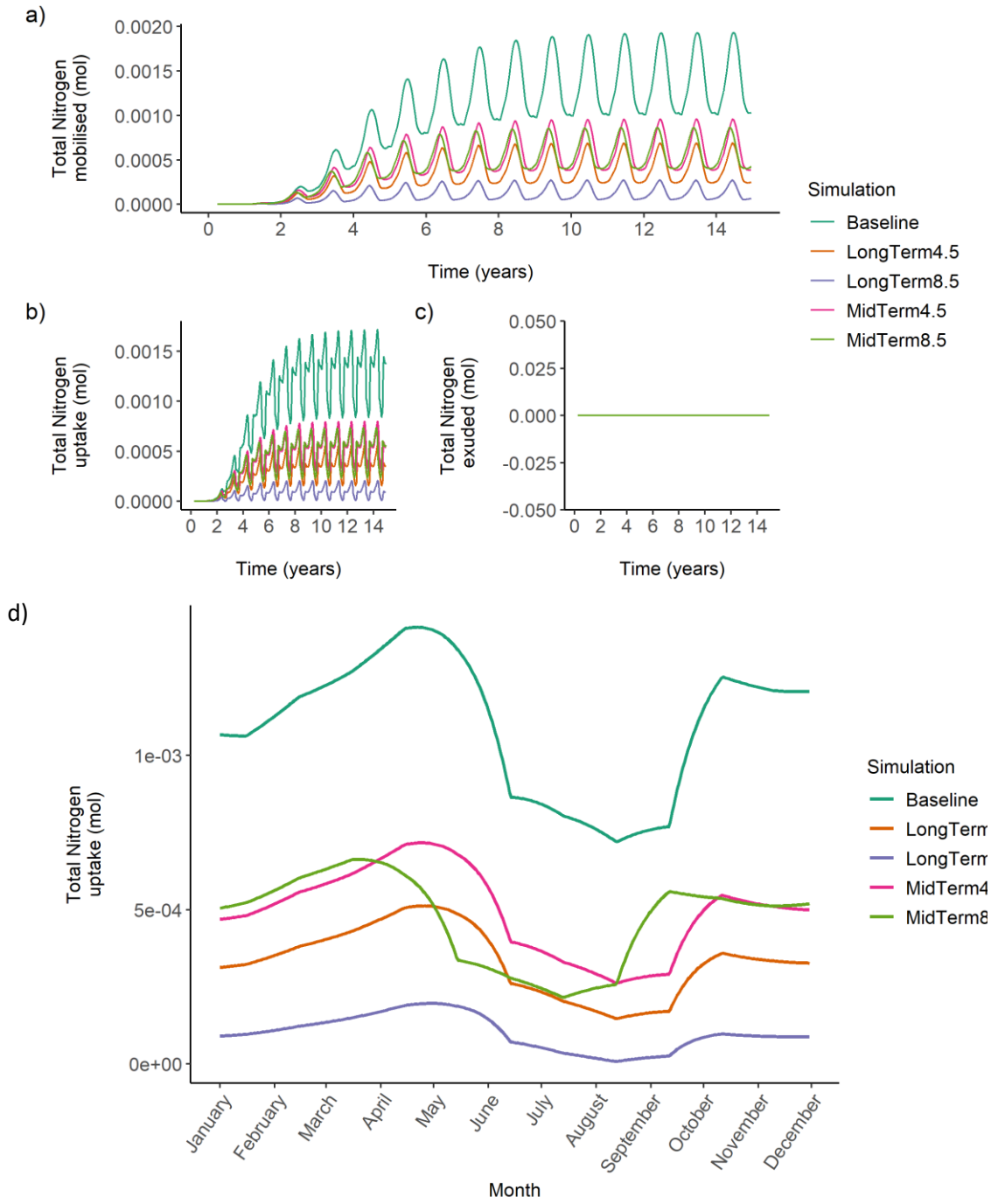

Figure 4.5. Individual model output for nitrogen uptake (a), mobilised (b) and exuded (c) throughout the simulation, with the total nitrogen uptake in a single annual cycle from years 6 to 7 (d) shown in detail. The environmental driving data is given by the legend. Using a depth of 3m across all simulations.

C: N Dynamics

The C: N values of the individual reflect the internal balance between its biochemical processes and its metabolic needs, which are driven by the availability of light and nutrients in its environment. This ratio is influenced by fluctuations in the reserves and structural components of the individual. In the individual model (Figure 4.6, a), the first year of the simulation does not yet exhibit the repeating seasonal cycle that becomes established in subsequent years. This indicates that the plant initially requires time to adjust its internal reserves and structure to align with external environmental conditions. Once this cycle is established, the seasonal pattern (Figure 4.6, b) shows a peak in the C:N ratio occurring in September, coinciding with the lowest environmental nitrogen availability.

These dynamic highlights the importance of the internal reserve and structure balance in responding to seasonal variations. The organisms' metabolic processes adjust throughout the year, storing or using carbon and nitrogen based on what is available in the environment. The high C:N ratio in late summer suggests that, by this time, the plant has maximized its carbon reserves in response to reduced nitrogen and high light availability, reflecting a strategy to manage nutrient scarcity. This internal adjustment process emphasizes the crucial link between external nutrient availability and the internal biochemical balance of the organism.

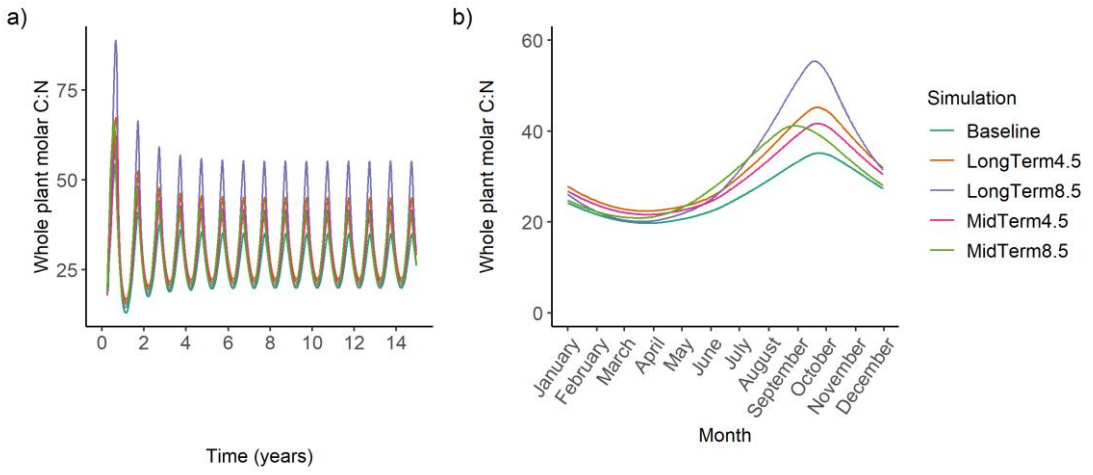

Figure 4.6. Individual model output. Whole plant molar C:N ratio for the entire simulation run time shown on the left (a) and a single year from 6 to 7 years old shown on the right (b). The environmental driving data is given by the legend. Using a depth of 3m across all simulations.

Maintenance Cost

The maintenance cost refers to the metabolic expenses to keep the organism alive. This increases with the organism's size and with the environmental temperature. Hence the highest values been seen for the simulations with the highest temperature, when the effect of individual size is removed (Figure 4.7). The responses to each scenario follow a similar pattern, with all values being lower when compared to baseline conditions. This is partly due to the smaller plant sizes in the simulations compared to the baseline conditions, highlighting the importance of considering size dependencies. As climate conditions deviate further from the current baseline, the maintenance values continue to decrease, due to the decreasing individual size. The effects of changing climate conditions can be better observed at a seasonal level, where a peak in maintenance cost to total nitrogen content between September and October can be seen (Figure 4.7).

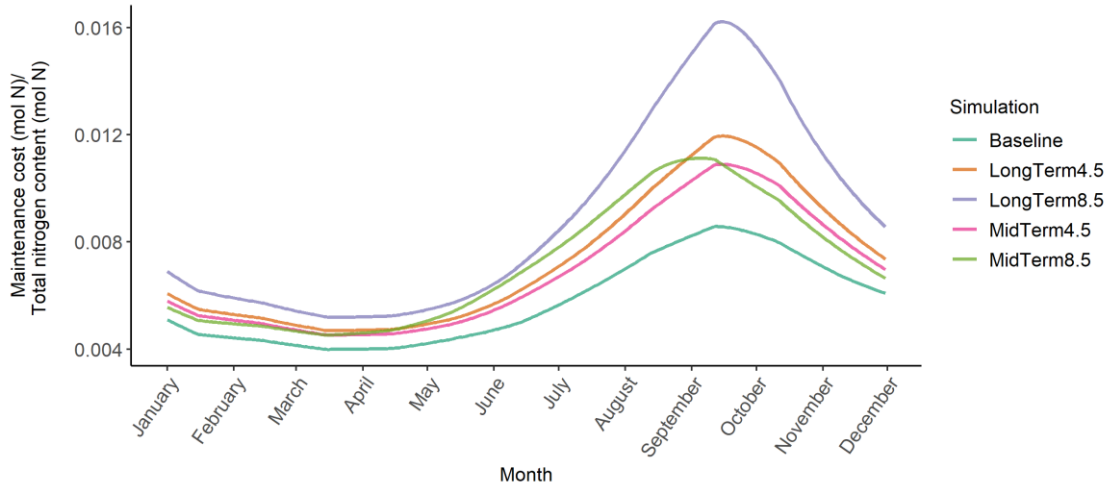

Figure 4.7. Individual model output for a single annual cycle from year 6 to 7 for maintenance cost (mol N) to total nitrogen content (mol N). The environmental driving data used is given by the legend. Using a depth of 3m across all simulations.

4.3.2 Forest Model

4.3.2.1 Population Dynamics

The conditions for each climate simulation are kept in a repeated cycle throughout the simulations. In the forest model, individuals failed to reach the same canopy weights observed after age class 7 in the empirical data (Jupp, 1972), across all simulated climate scenarios (Figure *4.8*). A clear distinction emerges in the intensity of the effects, with the mid-term RCP 4.5 and RCP 8.5 scenarios showing similar maximum weights. However, in the long-term RCP 4.5 scenario, the maximum canopy weights are noticeably lower, with the minimum weights of the mid-term models still being significantly higher than the long-term maximums. The situation is even more concerning for individuals in the forest subjected to the long-term RCP 8.5 scenario, where they perform poorly (showed by their weights) under these extreme conditions. This is evident from the fact that their maximum weights at 9 years old fall within the range of weights for 3- to 4-year-old individuals in the empirical data (Jupp, 1972), highlighting their stunted growth and inability to thrive.

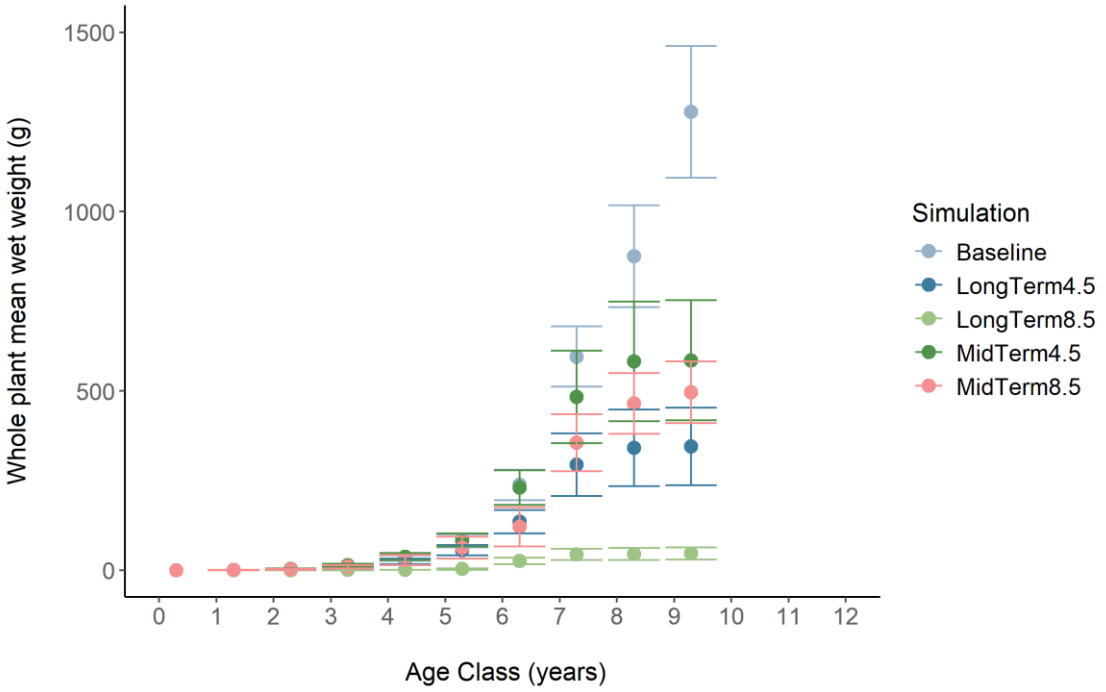

Figure 4.8. Results from the model output under different RCP climate change scenarios (given by the line colour) and the reference data. Forest model output mean wet weight for the last month of year 162 of the simulation shown by the points, with the standard deviation The environmental driving data is given by the legend. Using a depth of 3m across all simulations.

When observing the distribution of the numbers of individuals in each weight category across the different climate change projections (Figure 4.9), the long-term RCP 8.5 simulation has a noticeable absence of individuals in the heaviest weight category (304 – 662g). The smallest weight category (<0.04g) contains nearly 150 individuals, the highest count among all simulations. However, there is a sharp drop to 50 individuals for the weight category following it (<14g), followed by fewer individuals across the 14g to 57g weight range. Comparatively, other simulations display less drastic differences in the distribution of individuals across weight categories. Notably, the mid-term RCP 8.5 simulation also exhibits a significant disparity, with less than a third of individuals falling into the 0.4-14g weight category compared to the <0.4g category (~100 individuals).

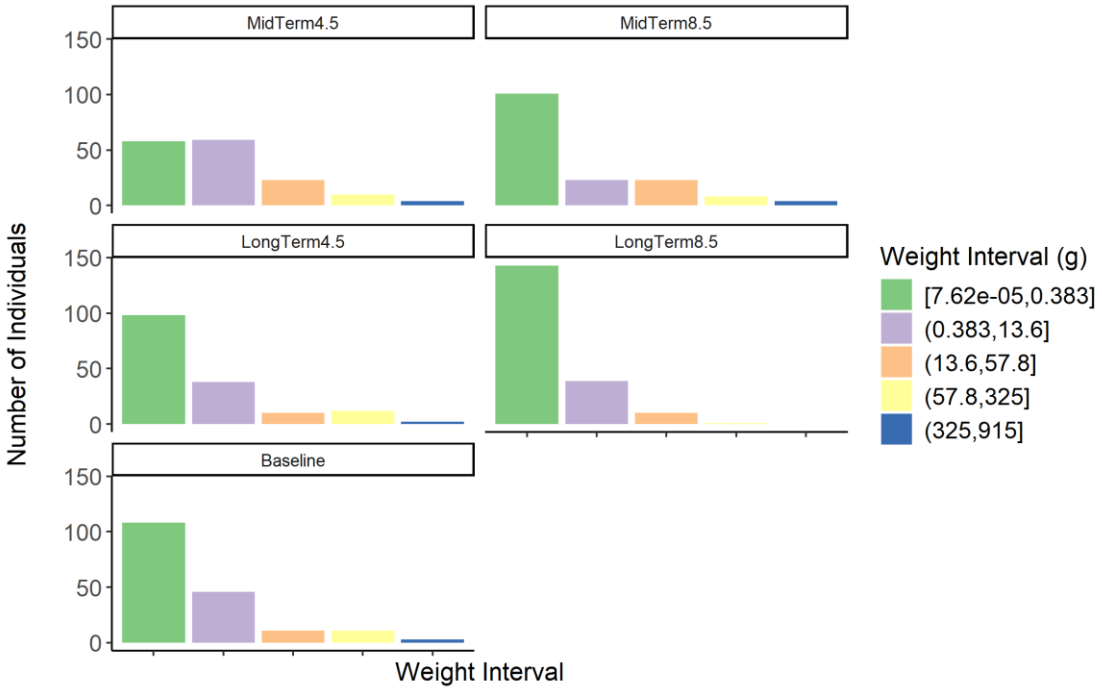

Figure 4.9. Forest model output. Number of individuals in each weight category, with the weight intervals of each category given by the colours and described in the legend. The environmental driving data is given by the facet tittle. Using a depth of 3m across all simulations.

4.3.2.2 Biochemical Fluxes

Structure and Reserve Dynamics

Structural nitrogen values fall within a middle range compared to reserve nitrogen and reserve carbon (Figure 4.10). Reserve nitrogen contributes the most to the organism composition, followed closely by structural nitrogen. The forest model reveals distinct layers within the canopy, shaped by varying light conditions. Canopy individuals achieve maximum weights, determined more by their biomass than their age. In contrast, individuals growing under restricted conditions exhibit slower growth, particularly those first appearing in the graph. The impact of climate change is starkly highlighted in the long-term RCP 8.5 scenario, where the differentiation between canopy and understory individuals diminishes. The overall reduction in plant weight results in a lack of noticeable distinction among these groups, as even the oldest individuals fall within the smallest weight categories.

Growth curves for individual plants consistently show three distinct layers: canopy individuals, very small individuals, and a middle layer that retains higher weights than the smaller plants. A clear reduction in maximum structural nitrogen is observed as climate conditions drift further from baseline levels. In the forest model, most individual plant weight is found in nitrogen reserves, contrasting with the individual model, which emphasizes carbon reserves. This trend is evident across all climate scenarios, underscoring the persistent influence of environmental conditions on resource allocation and growth dynamics.

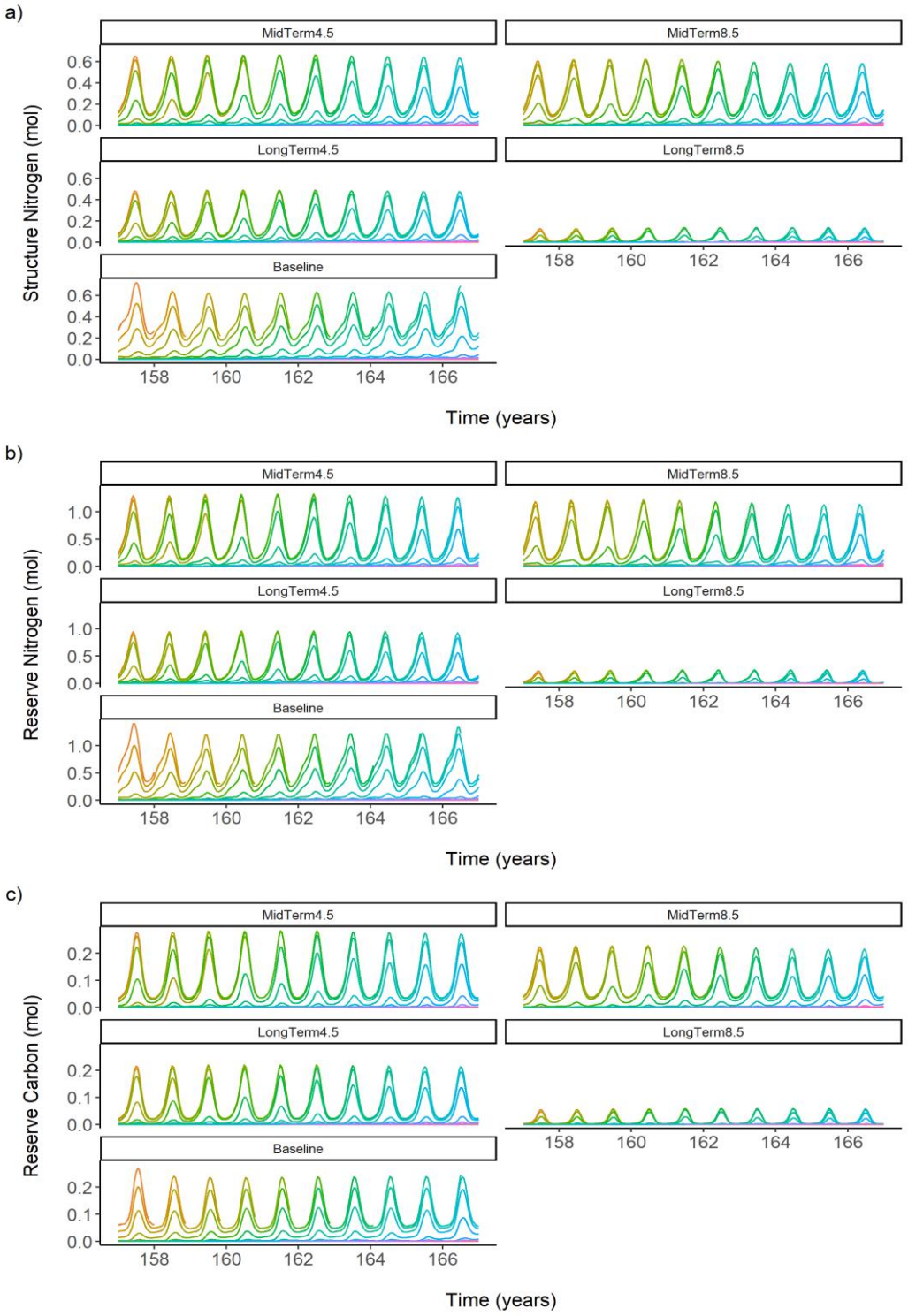

Figure 4.10. Forest model output. Structure nitrogen (a), reserve nitrogen (b), reserve carbon (c) throughout the 10-year interval around the year 162. Each cohort is shown in a different line by and colour, with lines ending when the individual dies. The environmental driving data is given by the facet tittle. Using a depth of 3m across all simulations.

Carbon Dynamics

Regarding the carbon uptake and mobilisation of individuals within the forest being simulated, the canopy effect is clearly observable in the uptake cycles of individuals (Figure 4.11, a), which once again display three distinct growth layers. The levels of carbon mobilized (Figure 4.11, b) in the forest model are less distinctly defined compared to the uptake rates previously discussed. Instead of three clear response layers, there is a higher overlap among multiple layers, with these layers occurring closer to each other. Overall, the maximum amount of carbon mobilized by canopy individuals decreases as climate conditions worsen. Carbon exudation was not seen for any individuals at any time point.

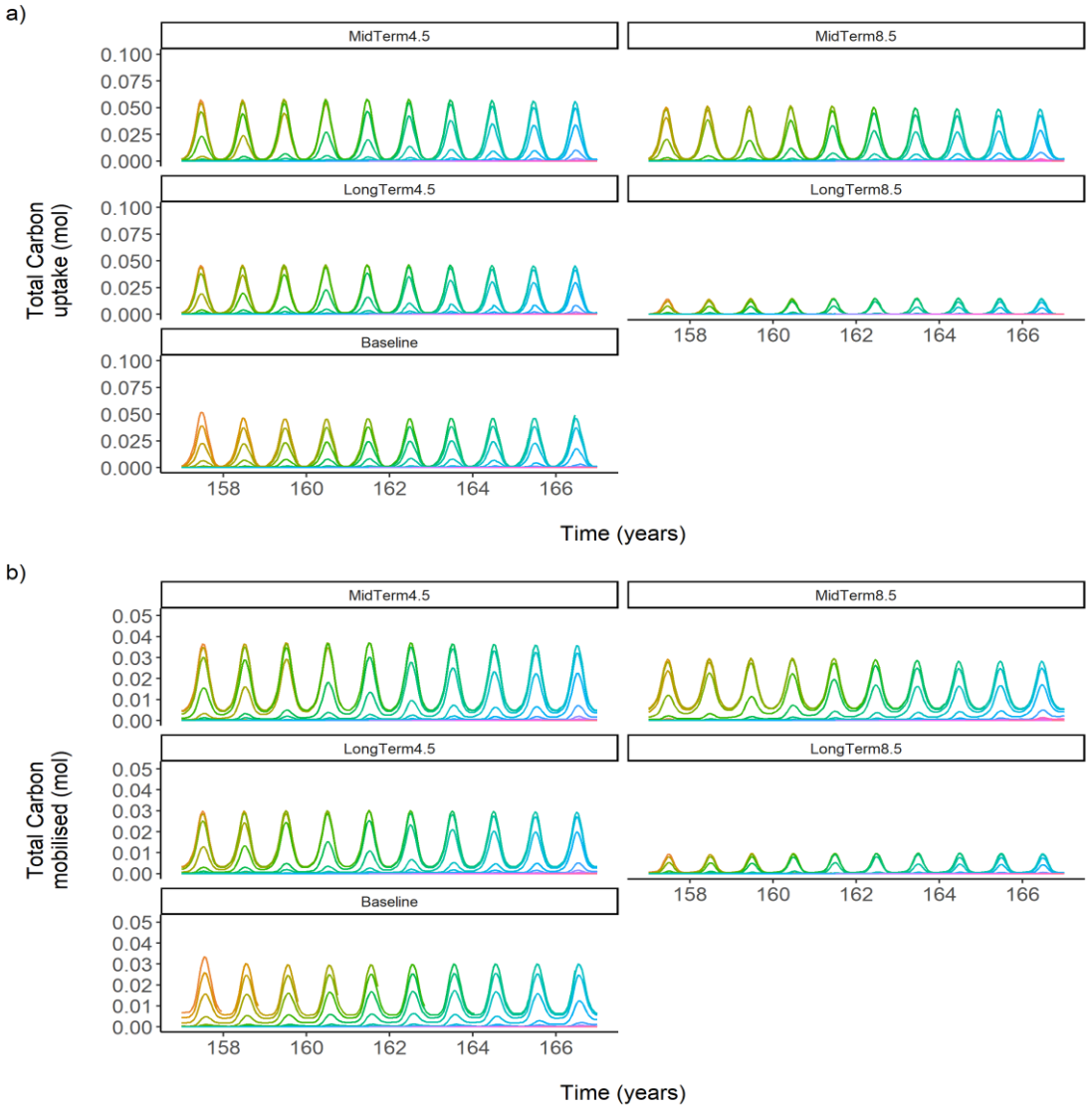

Figure 4.11. Forest model output. for carbon uptake (a) and mobilised (b) throughout the 10-year interval around the year 162. Each cohort is shown in a different line by and colour, with lines ending when the individual dies. The environmental driving data is given by the facet tittle. Using a depth of 3m across all simulations.

Nitrogen Dynamics

The forest model nitrogen uptake (Figure 4.12, a), showed minimum values of the upper group (the canopy individuals) approaching the maximums of the other two forest layers, leading to a noticeable change in the forest dynamics, when these larger canopy individuals die. The mid-term RCP 8.5 scenario also shows a more dome-shaped plateau at its maximum, in contrast to the sharp peak seen in other scenarios. In the long-term RCP 8.5 scenario, the distinction between the forest layers is less clear due to the overall smaller size of all the individuals. For the seasonal uptake of nitrogen, in the long-term RCP 8.5 scenario, this stratification is less distinct due to the overall drastic size reduction of all individuals, with the smallest group (understory) exhibits a much flatter curve compared to the other simulations (Figure 4.12, b).

In the forest model nitrogen uptake yearly cycle dynamics (Figure 4.13, a) is, the peaks occur later in the year as climate change conditions worsen, still falling between December and February, unlike the May peak observed in the individual model. The minimum values for the individuals in the forest model show a two-group response instead of the three seen for maximums. The shape of the curve during the decrease becomes smoother as conditions worsen. In all scenarios except long-term RCP 8.5, there is a slight increase in nitrogen uptake during June and July. This is related to the increase in size seen during this time, as larger plants take up more nitrogen despite the reduced environmental supply.

In the forest model, nitrogen exudation (Figure 4.13, b) is observed in similar amounts across different climate change scenarios. However, as climate conditions deviate from the baseline, the amount of nitrogen exudation decreases. The layers of the canopy are visible, but not very distinct. This trend highlights the impact of increasingly harsh environmental conditions on the forest's ability to exude nitrogen, reflecting the nutrient limitations imposed by more severe conditions.

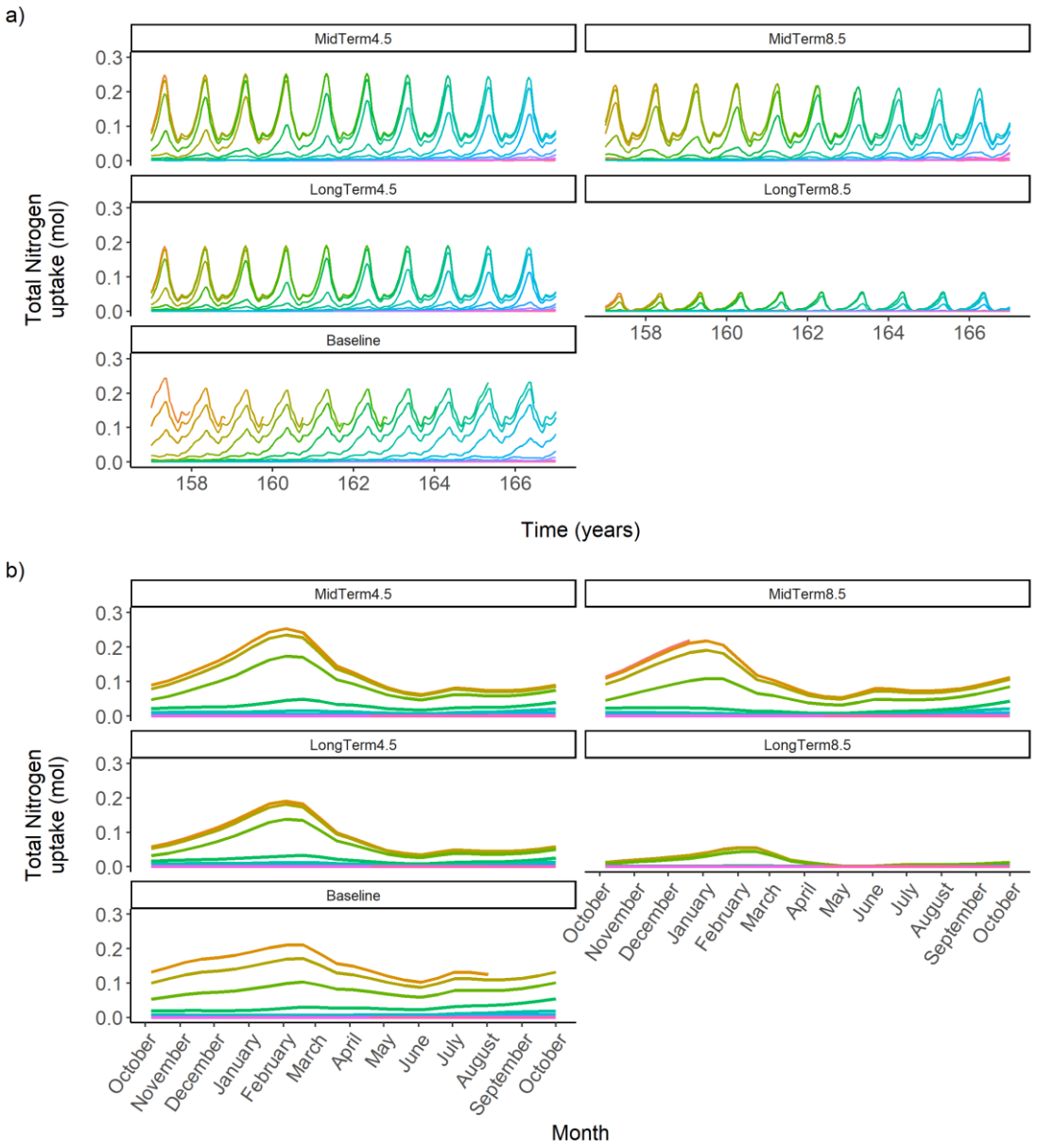

Figure 4.12. Forest model output nitrogen uptake (a) throughout the 10-year interval around the year 162 and in a single annual cycle from years 161 to 162 (b). Each cohort is shown in a different line by and colour, with lines ending when the individual dies. The environmental driving data is given by the facet tittle. Using a depth of 3m across all simulate

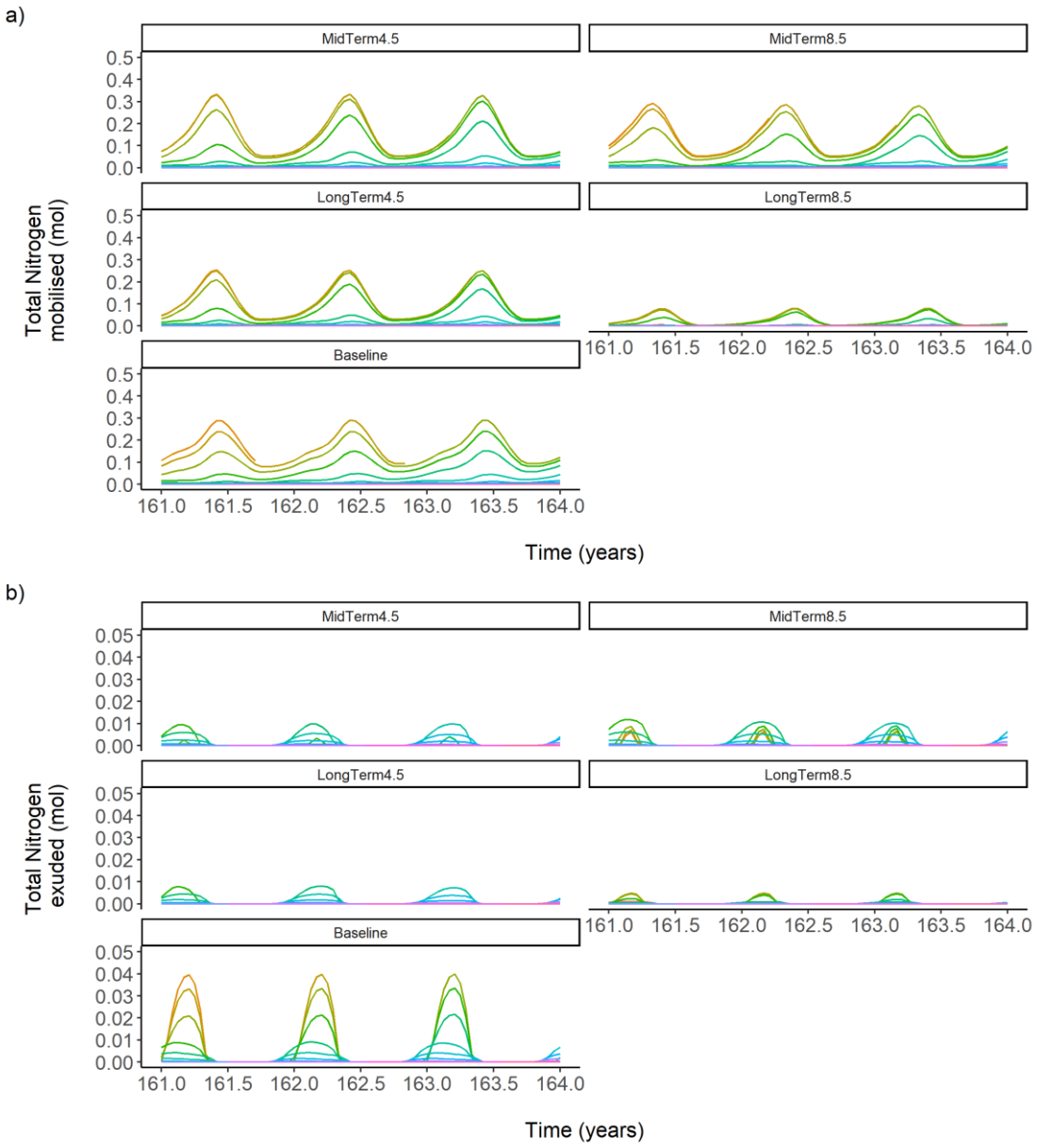

Figure 4.13. Forest model output nitrogen mobilised (a) and exuded (b) from the year 161 to 164. Each cohort is shown in a different line by and colour, with lines ending when the individual dies. The environmental driving data is given by the facet tittle. Using a depth of 3m across all simulations.

C: N Dynamics

For the forest model the newly settled individuals show a lower C:N ratio than the minimum values of the repeating cycle seen for the rest of them (Figure 4.14,a). The September peak in the forest model (Figure 4.14,b), though less pronounced, except for in the mid-term 8.5 RCP scenario. Additionally, canopy individuals exhibit a later peak, while younger individuals have higher and earlier peaks. This is illustrated by the pink line, starting in June and reaching its highest values in August, this would represent a newly recruited individual.

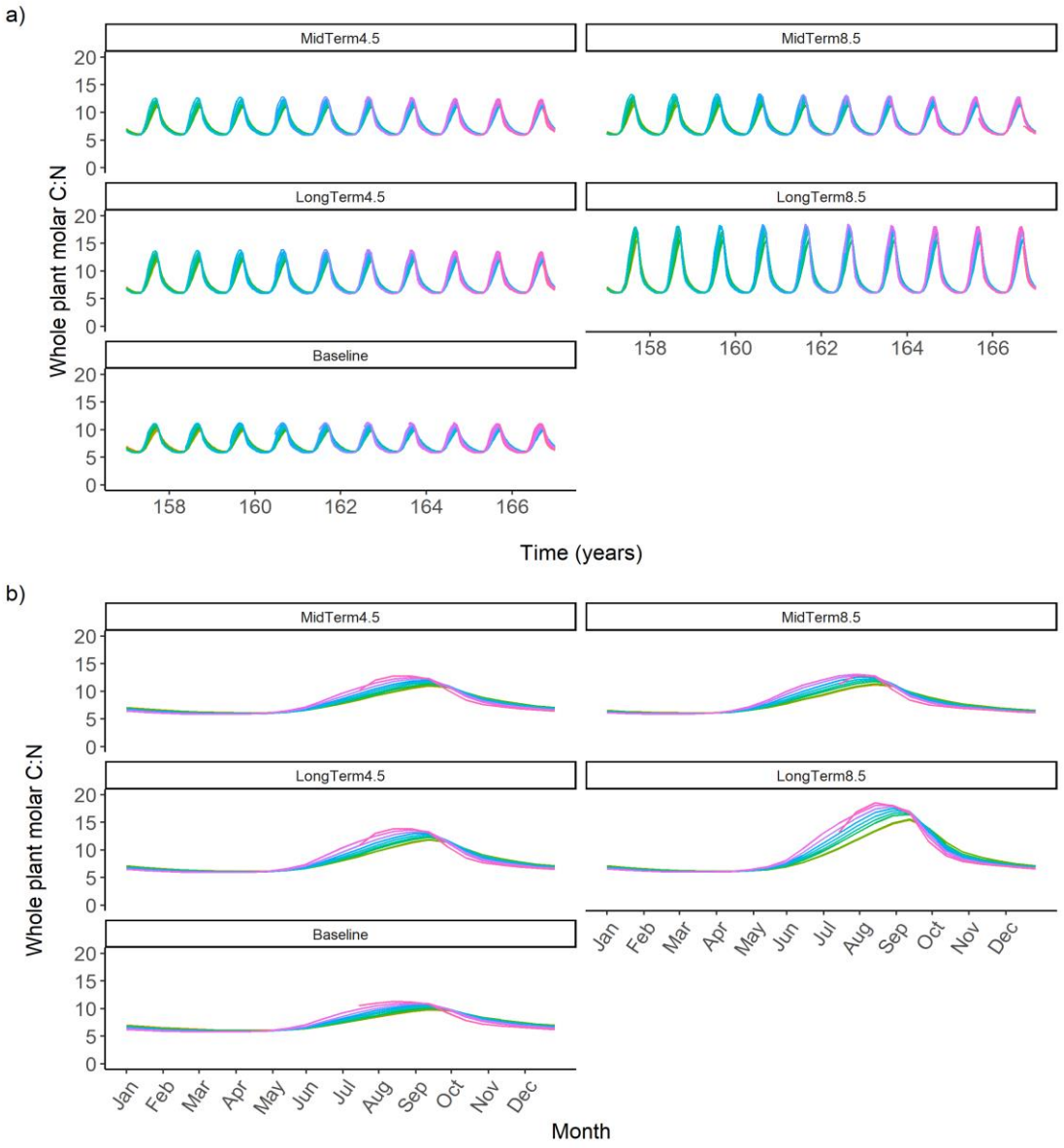

Figure 4.14. Forest model output for whole plant molar C:N ratio (a) throughout the 10-year interval around the year 162 and for a single annual cycle in from years 161 to 162. Each cohort is shown in a different line by and colour, with lines ending when the individual dies. The environmental driving data is given by the facet tittle. Using a depth of 3m across all simulations.

Maintenance Cost

In the forest model (Figure 4.15), a comparison of maintenance carbon to total carbon reveals a seasonal pattern characterized by two distinct peaks: one in September and a smaller one in May or June. The canopy's shading creates a varied light environment for individuals of different sizes within the forest. Newly settled plants exhibit higher maintenance costs compared to the larger, older canopy plants, as indicated by the pink links in each model. These younger individuals benefit from summer growth conditions, which allow them to increase their carbon content due to the higher light availability. As individuals grow larger, the peak costs to carbon content shift later in the year, and the degree of fluctuations diminishes. This trend highlights those younger individuals, with fewer reserves accumulated, are affected to a higher degree by seasonal changes.

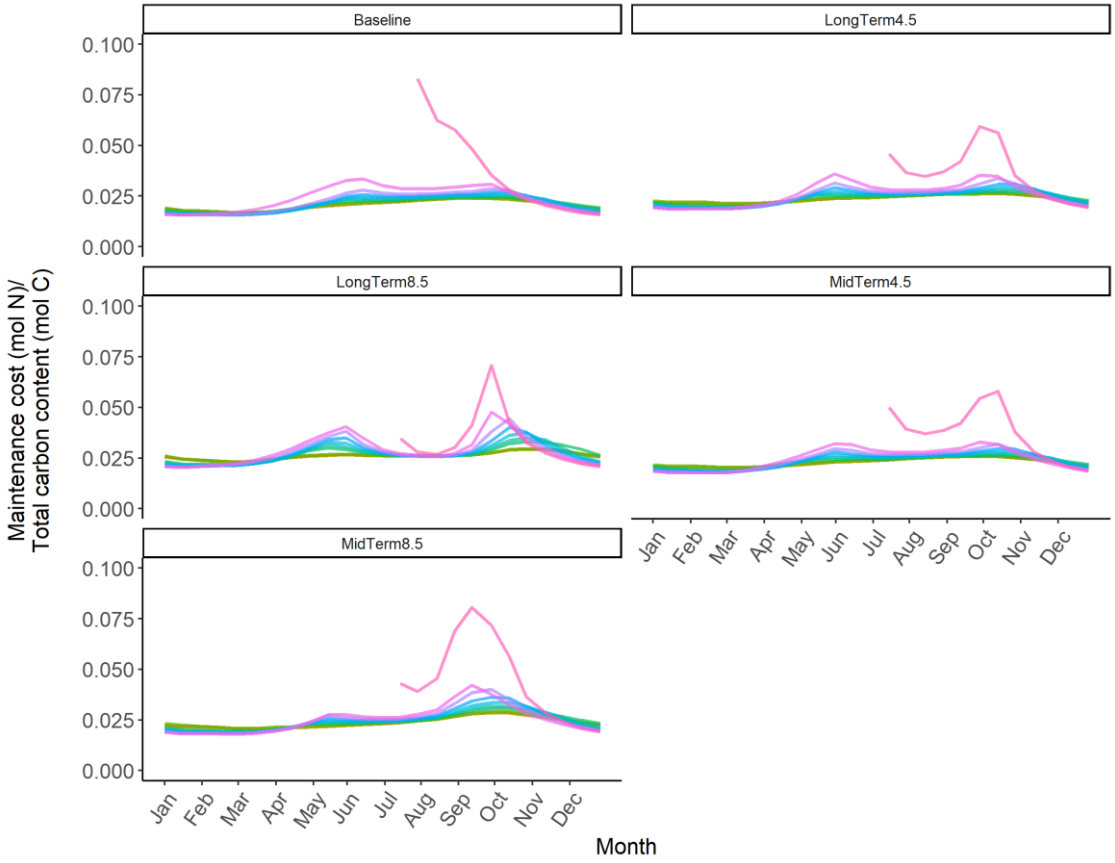

Figure 4.15. Forest model output (b) single annual cycle from years 161 to 162 for maintenance cost (mol N) to total carbon content (mol C). Each cohort is shown in a different colour. The environmental driving data is given by the facet tittle. Using a depth of 3m across all simulations.

4.4 Discussion

The results show the simulated response of *L. hyperborea* individuals both within and outside of a forest scenario to multiple climate change scenarios. In the UK, previous marine ecosystem models have demonstrated the detrimental impacts of environmental changes by using coupled hydrodynamic models that integrate biological processes. These models have revealed effects such as increased metabolic rates, a decline in benthic biomass due to heightened metabolism and reduced food supply, and decreased oxygen concentrations (van der Molen et al., 2013)

In contrast to models in the literature that focus on aquaculture, where each individual develops in relative isolation, the forest model here introduces interactions between individuals within a natural environment. The individual model developed for this thesis provides detailed physiological insights into growth, nutrient assimilation, and energy allocation for *L. hyperborea* without the interference of a canopy. This allows for a clear understanding of its growth in environments where light availability is not constrained by other individuals.

To ease the comparison between responses of the forest and individual models to the different climate change scenarios, data from 9- to 10-year-old individuals were used. These individuals are considered canopy-level, implying they have likely reached their maximum weight during their lifespan, given the environmental conditions they have been subjected to. Individuals in the forest model show a larger variation in sizes-at-age than those in the individual model. This is due to the explicit representation of competition for light in the forest model – a factor which is absent in the individual model. By directly comparing the climate change responses of canopy individuals from both models, this effect can be removed to focus on the impact of climate change, rather than the differences between the models. These methodological differences, which are also important, will be analysed separately.

4.4.1 Weight-Age Dynamics

All simulations consistently display size reductions relative to the mean present-day values under climate scenarios (Figure 4.16). This reduction becomes more pronounced as the environmental conditions deviate further from present-day values. The baseline forest model mean individual weight was 1500g while baseline individual model weight was 1000g. In contrast, the results from the RCP 8.5 long-term scenario individual weight for both model types were under 250g. The range of weights seen for the forest model go from minimum of a few grams, to maximums of 2700g. The high variation seen in the forest model responds to the effects of the individuals belonging to different cohorts having been subjected to different light limitations.

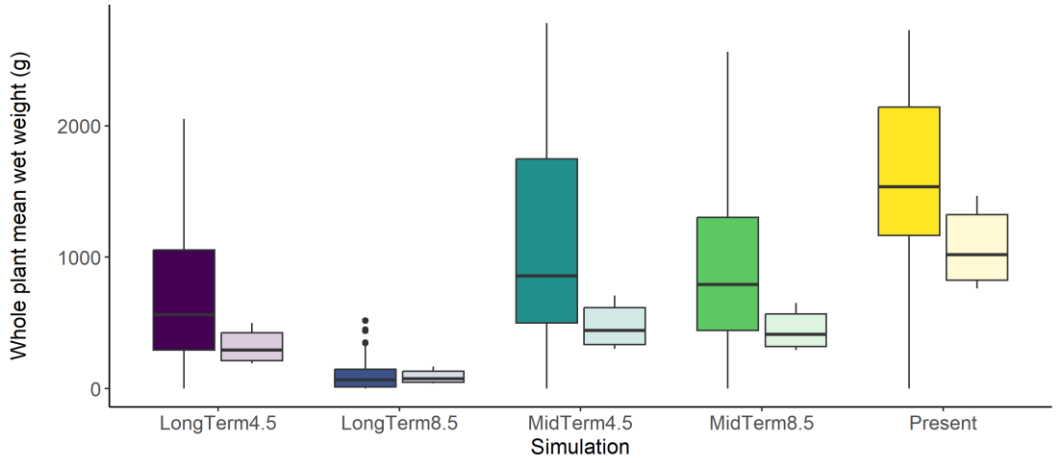

Figure 4.16. Model output for canopy individuals (9-10 years) mean wet weight (g) of the whole plant across different climate change scenarios. The forest model's results are in a darker shade, while the individual model's outcomes are the lighter shade. Forest model data encompasses observations from multiple cohorts of the same age 9 to 10 years, as opposed to a single individual.

In the forest model data includes observations from different groups of plants aged 9 to 10 years in the simulation, rather than just one individual. Overall, the wet weight of the canopy individuals across all future climate scenarios for both model types failed to reach the same size that was seen in the present-day simulations. The effect is clearly seen in the RCP 8.5 long-term (2070–2099) scenario. The pattern of weight reduction is expected since temperature significantly shapes the ecophysiology and spatial arrangement of kelp species (Eggert, 2012). In the model results, the total wet weight of the simulated plants in the warmer regimes that are expected under climate change scenarios, is less than ~50% of the current weight that individuals can achieve under the current environmental conditions. In field studies, populations situated within a warm climatic regime exhibited a 68% reduction in carbon storage (Pessarrodona et al., 2018). However, the trends in nitrate concentration and light intensity in the climate projections must also contribute to the model results. The declining nitrate concentrations will also cause plant weight at age to also decline.

In the individual model, *L. hyperborea* grows without competition. Since there are no other individuals present to interfere with light availability, the plant consistently receives sufficient light, maintaining a high photosynthesis rate throughout the growing season. Biomass accumulation follows a predictable, pattern driven by seasonal fluctuations in light and temperature. The growth rate is closely tied to the availability of key nutrients like nitrogen and carbon, which are regulated by external environmental conditions. The lower sizes seen when compared to the forest model respond to the effects to the different parametrization than the forest model, the different uptake rates will lead to differences. The individual model, when using the same parameters as the forest model, does not adequately match the empirical data, indicating that it is not properly calibrated to the observed measurements.

In contrast, the forest model presents a more complex picture of growth, shaped by the vertical structure and interactions between individuals. In this model, lower-canopy individuals face significant light limitation due to shading by heavier plants, which restricts their ability to photosynthesize at their maximum capacity. Those at the top of the canopy continue to receive abundant light, while individuals beneath them experience stunted growth, resulting in a variable biomass accumulation process for the forest and more variations in individuals' weight at the same age during different times in the forest growth. This dynamic creates a stratified population, with younger and shaded individuals growing more slowly than their canopy-dominating counterparts.

The individual model, seasonal growth dynamics follow a predictable pattern. Without any competition or shading effects, the individual is free to grow with less competition, experiencing a smooth cycle of weight increase that directly correlates with the external environment, particularly the availability of light and nutrients. The forest model, while displaying similar seasonal growth patterns, introduces significant variations due to the effects of canopy shading. Individuals in the lower canopy receive less light, causing a delayed and reduced growth response during the spring and summer. This delay results in a slower onset of the growth phase for shaded individuals, as well as a shortened period of biomass accumulation compared to their counterparts in the upper canopy.

Comparing the two models highlights the stark contrast between individual potential and the reality of population-level interactions. While the individual model reflects optimal growth conditions without competition, the forest model underscores the critical role of canopy interactions. Shading from larger individuals creates a bottleneck in light availability, causing younger individuals to grow more slowly, emphasizing how competition within a forest context can limit growth and biomass accumulation.

4.4.2 Biochemical Fluxes

4.4.2.1 State Variables Dynamics

The forest model individuals exhibit carbon reserves one order of magnitude lower (Figure 4.10, c), than those observed in the individual model (Figure 4.3, c), where a single individual grows without competition for light. Empirical research shows that *L. hyperborea* growing under warmer conditions stored 68% less carbon than the colder regime populations, with a simultaneous significant reduction in size (Pessarrodona et al., 2018). In the individual model reserve carbon, the RCP 8.5 long-term scenario results show a decrease of 75% carbon content when compared to the baseline simulation, while the forest model showed an 83% decrease. The decrease in carbon reserves for individuals as a consequence of warmer climate conditions is due to increased metabolic costs. Additionally, while incoming irradiance shows a slight increase in the climate projection conditions this is not sufficient to offset the higher maintenance costs.

As climate conditions move further from the baseline conditions with each scenario and time period modelled, all of the model state variable show declines (Figure 4.17), in line with the decrease in individual weights. In the scenarios with the most adverse conditions (long-term RCP 8.5), there is a closer alignment between the outputs of individual-based models and forest models in terms of nitrogen content.

The nitrogen (Figure 4.17, b) and carbon reserves (Figure 4.17, c) exhibit a similar pattern to that observed for structural nitrogen (Figure 4.17, a). The maximum structural nitrogen reached in the forest exceeds that reached in nitrogen reserves. Specifically, in the individual model, only under present-day conditions is a higher maximum reserve observed compared to structural nitrogen (structural nitrogen < 0.1 and reserves > 0.15). Additionally, the mean reserves in the forest under present conditions are six times larger than the mean for the RCP 8.5 long-term scenario.

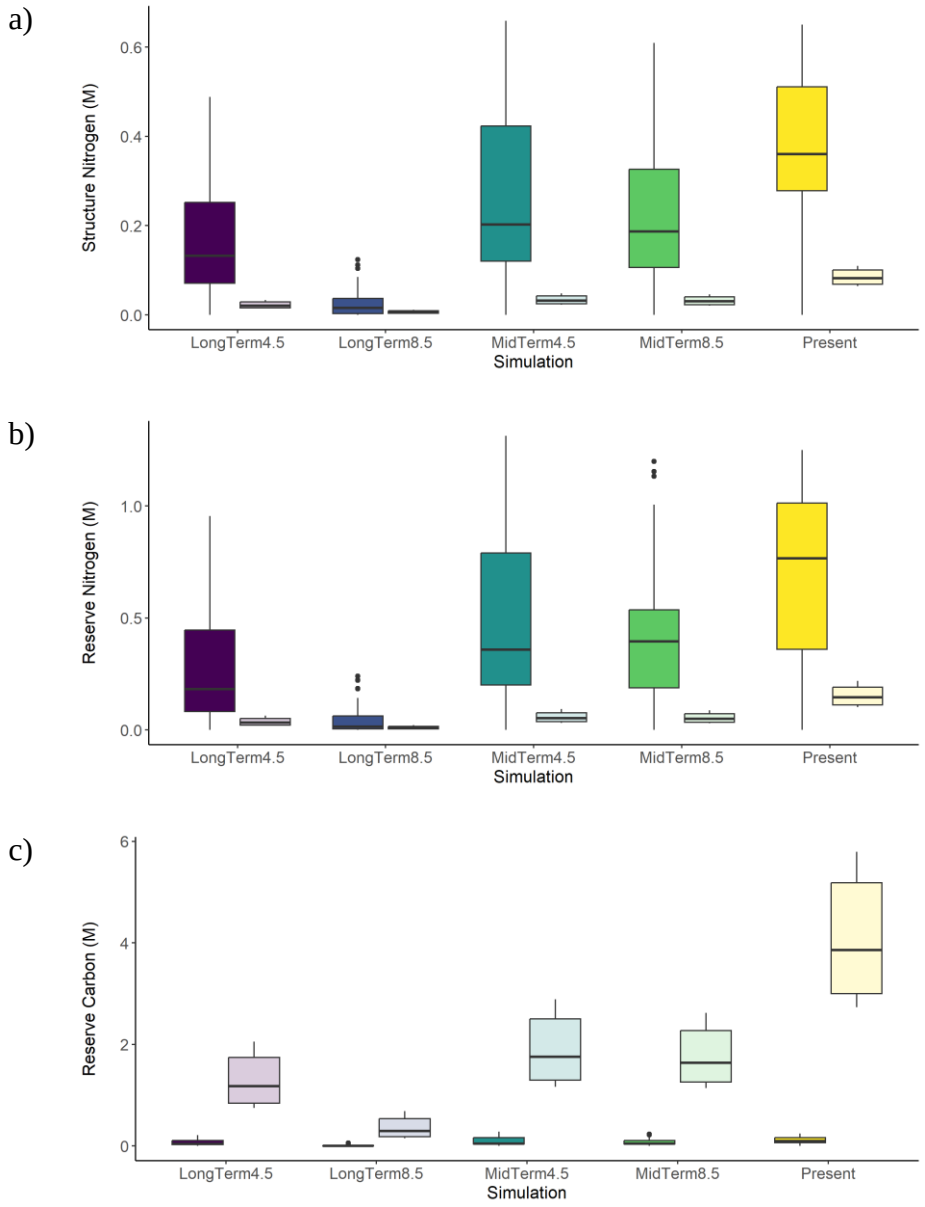

Figure 4.17. Model output for canopy individuals (9-10 years) for structure nitrogen (a), reserve nitrogen (b) and reserve carbon (c) across different climate change scenarios. The forest model's results are in a darker shade, while the individual model's outcomes are the lighter shade. Forest model data encompasses observations from multiple cohorts of the same age 9 to 10 years, as opposed to a single individual.

4.4.2.2 Carbon Dynamics

Simulations for present-day conditions indicate comparable carbon uptake rates for the model types (Figure 4.11). However, the forest model displays a broader range of results, which can be attributed to the variation in plant sizes within the forest model.

A critical distinction between the models is the behaviour of carbon exudation. In the forest model, carbon exudation is virtually non-existent, while the individual model shows more noticeable carbon exudation. This difference arises from the light limitations in the forest model, which reduce the degree of nitrogen exudation and contribute to carbon limitations. The lack of carbon exudation in the forest model underscores how varying light availability affects carbon dynamics and highlights the impact of competitive light conditions on carbon storage and mobilization in natural kelp forests.

The presence of carbon exudation in the individual simulations indicates a surplus of carbon, which is not present in the forest simulations (Figure 4.11). This shows that light is not limiting in any simulated scenario for the individual model simulations, but it is when considering the effect of the canopy. The amount of carbon exuded decreases as the climate conditions move away from the current baseline. The release of DOC, can account for as much as a quarter of the total carbon absorbed and subsequently discharged by *L. hyperborea* (Abdullah and Fredriksen, 2004). In the simulation for the RCP 4.5 mid-term scenario carbon exudation was around 20% of the carbon uptake (with higher values in the RCP 8.5 mid-term scenario), approximating the results seen by Abdullah and Fredriksen (2004).

4.4.2.3 Nitrogen Dynamics

The nitrogen content in both individual-based and forest models is quite similar, mainly because both models show reduced environmental nitrogen alongside increased metabolic costs as temperatures rise (Figure 7.38). This similarity indicates that both approaches react in a comparable way to changes in nitrogen levels and temperature. This convergence occurs because the reduction in environmental nitrogen occurs simultaneously with heightened metabolic costs due to rising temperatures. In the individual model nitrogen exudation (Figure 4.5), pointing to nitrogen as a limiting nutrient.

In the forest model, nitrogen uptake for canopy individuals is approaching the upper limits seen in the other forest layers (Figure 4.12). When these larger canopy individuals die, it leads to noticeable changes in the forest dynamics. This indicates a size-dependent competition, as nitrogen uptake is size-dependent, and the increase in light allowing for higher growth rates through more carbon uptake. The difference observed in the timing of the peak of nitrogen uptake respond to the shading effects, the intraspecies competition, observed in the forest model. To test this the individual model was run with the forest model parameters and initial conditions and the peak remained at the same time.

Overall, the similarity in nitrogen content between the models reflects a shared response to temperature and nitrogen availability. The lack of nitrogen exudation and the changes in nitrogen uptake among different forest layers show how size and light availability influence nitrogen dynamics in kelp forests.

It is vital to understand the nitrogen dynamics of the model as these processes can play an unforeseen role in adaptations to climate change, that is not specifically included in this model formulation. The effect of nitrogen on heat tolerance has been seen for other Laminariales. In *S. latissima* heat tolerance was shown to relate to nitrogen reserves, and also by habitat-specific differences and nutrient status. Heat-tolerant individuals with high nitrogen supply showed enhanced photosynthetic capacity. Under combined N limitation and heat stress, they utilize their nitrogen reserves to fuel metabolic processes, maintaining high rates of carbon fixation and the integrity of the photosynthetic apparatus. (Gerard, 1997). *M. pyrifera* growing in moderate NO_{3-} availability conditions exhibited greater thermal resistance than those in NO_{3-} limited populations, underscoring how nitrogen availability enhances resistance to rising water temperatures (Fernández et al., 2020).

4.4.2.4 C: N Dynamics

The lowest C:N ratios occur under the most severe climate conditions (long-term RCP 8.5 scenario) and among the smallest individuals. The difference in C:N ratios between the models is primarily driven by carbon behaviour. This is expected, given that light limitation in the forest model affects carbon dynamics by affecting photosynthetic rates. There is no distinct canopy effect or layering observed in the C:N ratios in the forest model overall population dynamics, except slightly for individuals in their first seasonal cycle.

In the RCP 8.5 mid-term scenario, the individual model (Figure 4.6) displays some timing differences, with canopy individuals from the forest model (Figure 4.14) (depicted in orange) showing a later peak in C:N ratios. In contrast, younger individuals have higher and earlier peaks, as shown by the pink lines (Figure 4.14), which starts in June and peaks in August. These younger individuals in the forest model take longer to reach their full potential due to the reduced light conditions they experience.

The C:N ratio of the organism is a good indicator of the interactions between the previously seen dynamics. The reduction in the maximum C: N value (Figure 4.6) seen is a clear indicator of the independent fluctuations of the reserves, seen as the climate conditions move away from the current baseline. A reduction in their reserves will decrease their resilience to any unexpected climatic events, which are predicted to increase for future projections and are also forecasted to affect the abundance and distribution of kelp species (Araújo et al., 2016). This would make populations more vulnerable, increasing the chances of local populations going extinct.

Studies have demonstrated that when examining the resilience and biochemical response of *L. digitata* (as no specific studies on *L. hyperborea* where found) to predicted future North Atlantic Ocean temperature conditions and varying light levels, chlorophyll content is temperature-sensitive, whereas fatty acid content exhibits greater sensitivity to light (Schmid et al., 2021). Highlighting the need for a model that is capable of demonstrating the varying responses of different physical components. Other research have also shown the intensified effects of the RCP 8.5 long term effects when compared to other climatic conditions for north Atlantic kelp (Assis et al., 2018).

4.4.3 Maintenance Cost

Maintenance cost increases with temperature, in the model formulation, but the specific rate is also dependant on the individual size. Across season, the effects of changing climate conditions are clear. Both models display similar overall behaviour (Figure 4.18, a, b). The individual model shows a peak in maintenance costs relative to total nitrogen content between September and October (Figure 4.7, a). In contrast, the forest model (Figure 4.7, b) shows a curve with two distinct peaks when comparing maintenance carbon to total carbon: one in September and a smaller peak in May or June. These seasonal variations reflect how climate conditions influence nitrogen dynamics over time in both models.

Given the large variations in individual weights, the effect of size must be accounted for before interpreting the effect of temperature on the maintenance. When taking into consideration the differences in individuals' weights (Figure 4.18, c), the patterns in nitrogen dynamics remain consistent, suggesting that temperature alone does not explain the observed variations. All simulations display similar trends, indicating that the changes are not just a result of temperature but also involve other factors. In these models, maintenance exudation occurs before mobilization, which is then followed by structural allocation.

Examining nitrogen processes in isolation (Figure 4.18, d) reveals an increase in costs, as shown by the maintenance rate, with changing climate conditions. This is consistent with expectations given the rise in temperatures and decrease in nitrogen availability. Elevated temperatures lead to higher metabolic costs, while reduced nitrogen availability adds to the difficulty of paying maintenance cost. This trend underscores how climate change intensifies the challenges associated with nitrogen management, with both temperature and nutrient limitations significantly impacting overall costs in both models.

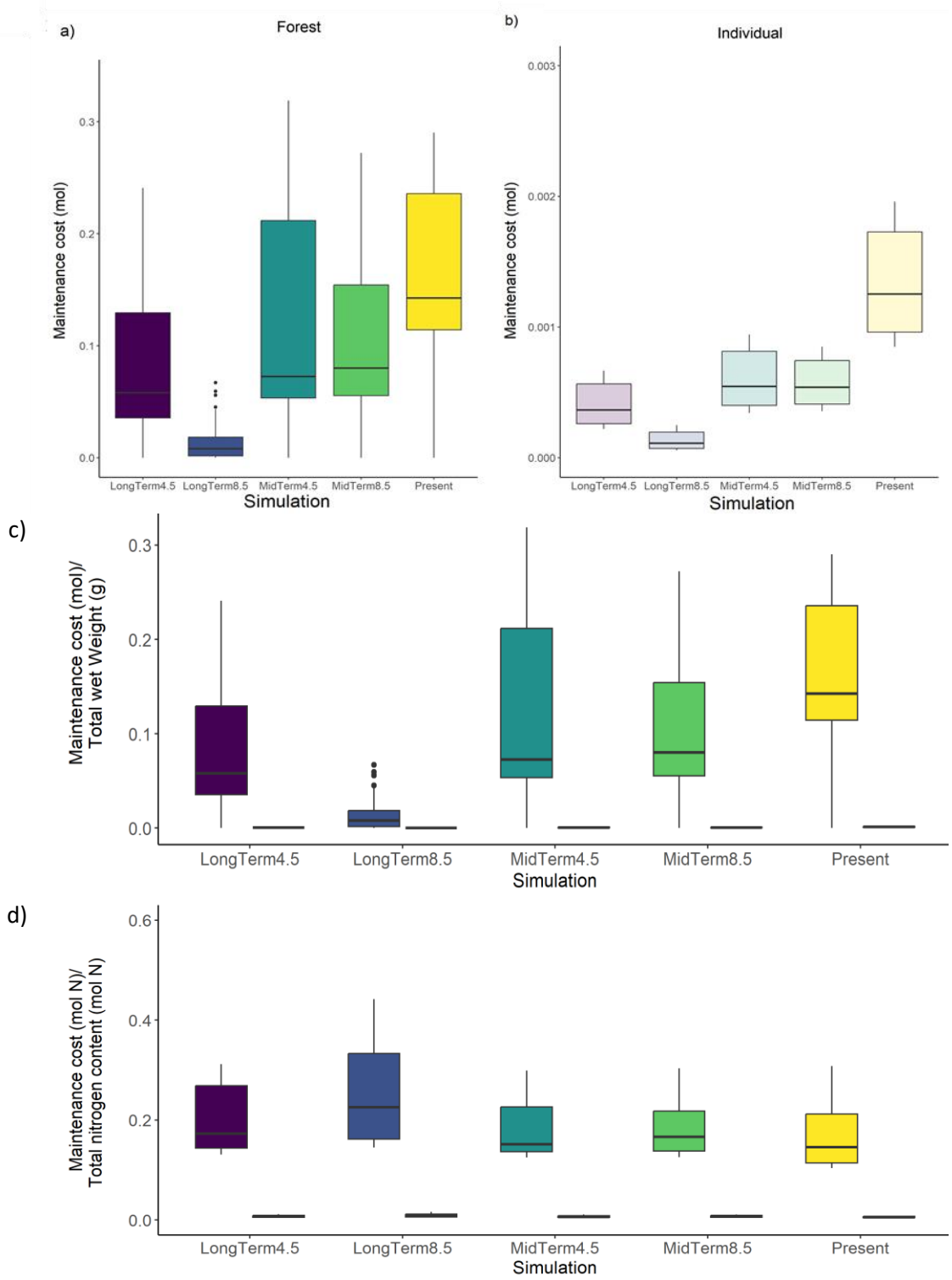

Figure 4.18. Model output for canopy individuals (9-10 years) maintenance cost for the forest model (a) and for the individual model (b), with the maintenance cost (mol N) to total wet weight (g) ratio(c) and the maintenance cost (mol N) to total nitrogen content (mol N) (d) across different climate change scenarios. The forest model's results are in a darker shade, while the individual model's outcomes are the lighter shade. Forest model data encompasses observations from multiple cohorts of the same age 9 to 10 years, as opposed to a single individual.

4.4.4 Modelling choices effects in interpreting climate change effects

The individual model focuses on how a single *L. hyperborea* responds physiologically to climate change, such as rising temperatures or nutrient shifts, but ignores population complexities like shading. This may lead to overestimations of growth, offering an incomplete foundation for understanding future scenarios.

In contrast, the forest model incorporates light competition and kelp forest dynamics, providing a more realistic picture of population responses and ecosystem impacts. The forest model, by including canopy shading and intra-population competition, presents a more realistic and ecologically relevant framework for understanding the future of *L. hyperborea* forests in a warming world. This makes the forest model indispensable for predicting how climate change could reshape these ecosystems, with implications for species dominance, forest structure, and long-term survival.

4.4.5 Limitations

The effect of temperature on nitrogen (N) dynamics was considered only in relation to maintenance costs, despite evidence showing that heat-tolerant individuals with high nitrogen supply exhibit enhanced photosynthetic capacity (Gerard, 1997). This enhancement is attributed to the accumulation and maintenance of high N reserves, which are crucial for increased heat tolerance. Under combined N limitation and heat stress, heat-tolerant specimens utilize their N reserves to sustain metabolic processes, maintain high carbon fixation rates, and preserve the integrity of the photosynthetic apparatus (Gerard, 1997). Hence a possible path that increases resilience to climate change effects is not included.

Additionally, changes in water turbidity mediated by waves play a significant role in shaping ecological outcomes (Smale et al., 2016). Waves not only alter water turbidity but also influence plant morphology, with implications for drag properties and mortality rates. Morphological adaptations to wave-induced stresses can result in more robust plants in turbulent areas, affecting plant weight and tissue composition (Larkum, 1972; Pedersen et al., 2012; Sjøtun et al., 1998; Sjøtun and Fredriksen, 1995; Smale et al., 2016). This effect is not included in the model and limits the information provided.

While these environmental factors are critical, the impacts of climate change introduce unprecedented stress patterns and combinations, exacerbating variability among population structures across sites (Smale et al., 2016). How seaweeds will respond to simultaneous changes in the averages and variability of multiple stressors is highly complex, requiring a mechanistic understanding of both sublethal and lethal stress impacts (Harley et al., 2012).

4.5 Conclusion

This chapter has provided valuable insights into the potential impacts of climate change on the ecophysiology and dynamics of *L. hyperborea* in Scotland. The simulations conducted under various climate change scenarios, including the RCP 4.5 and RCP 8.5 projections, have highlighted the complex interplay between temperature, nutrient dynamics, and individual responses.

The model's results have emphasized a consistent pattern of size reduction and environmental conditions deviate from the present-day baseline. The model results consistently demonstrate that as environmental conditions deviate from the present-day baseline, there is a clear trend of reduced plant size. This reduction is evident across various scenarios and both individual-based and forest models. Specifically, as temperatures rise and climate conditions worsen, plants exhibit a noticeable decrease in size. The forest model's size reduction is compounded by light competition among individuals, while the individual model, without such competition, still shows a decrease in size due to direct climate impacts. This consistent pattern underscores the significant effect of climate change on plant growth, revealing that more extreme environmental conditions lead to smaller plants in both modelled scenarios.

This reduction is particularly pronounced under the more severe long-term RCP 8.5 scenario, indicating a significant challenge for this species' growth and overall health in the face of ongoing emissions for Scotland. The study's findings align with empirical evidence of reduced carbon assimilation and growth under warmer conditions, emphasizing the critical role of temperature in shaping the performance of kelp populations in Scotland.

Additionally, the analysis of nitrogen dynamics and carbon-nitrogen ratios has unveiled nuanced responses to changing climate conditions. These responses carry implications for the resilience and adaptability of *L. hyperborea* in the face of increased stressors. Maintenance costs have revealed a clear association with temperature variations, underlining the role of temperature in driving physiological processes.

Overall, the mechanistic model employed in this study has shed light on the intricate mechanisms that underlie *L. hyperborea* responses to climate change scenarios, with the forest model adding an additional level of detail. Showing that higher model complexity is required to understand these processes. The research underscores the urgency of addressing climate change impacts on marine ecosystems. The findings presented in this chapter contribute to the growing body of knowledge that informs conservation efforts and ecosystem management strategies in the face of a changing climate. As we strive to comprehend the intricacies of species responses to climate change, this study serves as a tool towards a deeper understanding of the complex interactions that shape marine ecosystems in an evolving world.

5 Discussion

5.1 Key Findings

The main finding of this research is that for a coherent model of *L. hyperborea* growth the individual cannot be modelled as growing in isolation. The forest population dynamics enforce drastic changes in the light regime that the individuals are subjected to (Kain, 1971a; Sjøtun et al., 2006; Steen et al., 2016) and this in turn affects their growth rates though their life. The methodological approach developed here has been specially developed to represent *L. hyperborea* ability to endure nutrient limited periods, as seen in winter conditions in northern latitudes, given that a vital element of its physiology is dealing with periods of reduced nutrient and light availability (Lüning, 1971). Modelling the effects of competition for a limited resource among individuals becomes essential under this baseline challenging light conditions, which is critical for accurately portraying an *L. hyperborea* forest.

The mechanistic individual-based forest growth model for *Laminaria hyperborea* that I have developed effectively captures the internal biochemical dynamics of individual plants while also illustrating how forest population dynamics respond to a changing environment. This model integrates two interconnected levels: internal physiological processes and population-level interactions, both of which adjust to their constantly changing environment. It not only tracks individual growth in response to these environmental changes but also highlights how individuals compete with one another. This level of detail reveals how the forest's historical conditions influence the current state of its individuals—such as their biomass, reserve levels, and surface area—ultimately shaping their resilience to future environmental changes. The model developed in this thesis consistently demonstrated size reductions in the warm end of their tolerance range with increasing temperatures, a trend that aligns with empirical research (Rinde and Sjøtun, 2005; Smale et al., 2020; Smale and Moore, 2017). Showing its suitability for applications to study the effects of climate change.

The conditions for growth at different levels of the canopy (at canopy level, in the middle or at the seabed) have strong lifelong effects on the internal biochemical processes of an individual and this is clearly reflected by their weights at different ages. The main point to be emphasized is that understanding the history of the forest is crucial for interpreting the final weights of individuals, as field samples represent only a moment in time and cannot be fully analysed without knowledge of their historical context. The DEB model here considers both carbon and nitrogen, as has been previously done in other seaweed models (Broch and Slagstad, 2012a; Venolia et al., 2020). Applying DEB theory allows the model to distinguish between structural components and reserves, reflecting *L. hyperborea* adaptations to its highly seasonal habitat by modelling how reserves fuel growth during periods of limited photosynthesis.

The model shows shifts in weight distribution, responses to changes in total forest biomass, and the nuanced growth dynamics arising from shading interactions between successive cohorts of plants. Cohorts settling beneath a dense canopy experience diminished growth rates until light availability improved through canopy plant mortality events. All the previously mentioned dynamics lead to significantly different weight distributions and population structures depending on the time of sampling, which highlights the critical importance of long-term studies and the need to consider historical forest conditions when interpreting short-term findings. This should be considered of special importance in cases of anthropogenic clearances of forest sites, as the dynamics of re-colonisation would lead to different growth rates than those seen within a stable forest.

This thesis aimed to address the principal gaps in the literature, which included the absence of a biochemically explicit individual growth model for *L. hyperborea* and an integrated individual forest growth model. Additionally, previous models developed for *Saccharina latissima* are focused on aquaculture rather than natural forests. This makes my model the first DEB model for kelp that emphasizes population-level processes and can be applied to studying natural populations, rather than solely seasonal growth in an aquaculture setting. While a forest model for this species does exist, it was not developed to account for the effects of environmental changes on individual growth, nor the impact of individual size on shading and the forest's light conditions. The models developed stem from previous kelp models (Aldridge et al., 2012; Broch and Slagstad, 2012a; Rinde, 2007) and puts them into context with more traditional bioenergetic models (Broekhuizen et al., 1994; Kooijman, 2000; Nisbet et al., 2012). The integration of the model developed in this thesis with previous kelp modelling work can be seen in Figure 5.1, clearly showing the link between population models and individual growth models that was previously lacking. The placement between population and individual model is in response to this thesis methodology being based on an IBM, hence the information at an individual level is always available. This thesis underscores that modelling the intricacies of kelp population dynamics is a complex yet indispensable undertaking for safeguarding these vital marine ecosystems.

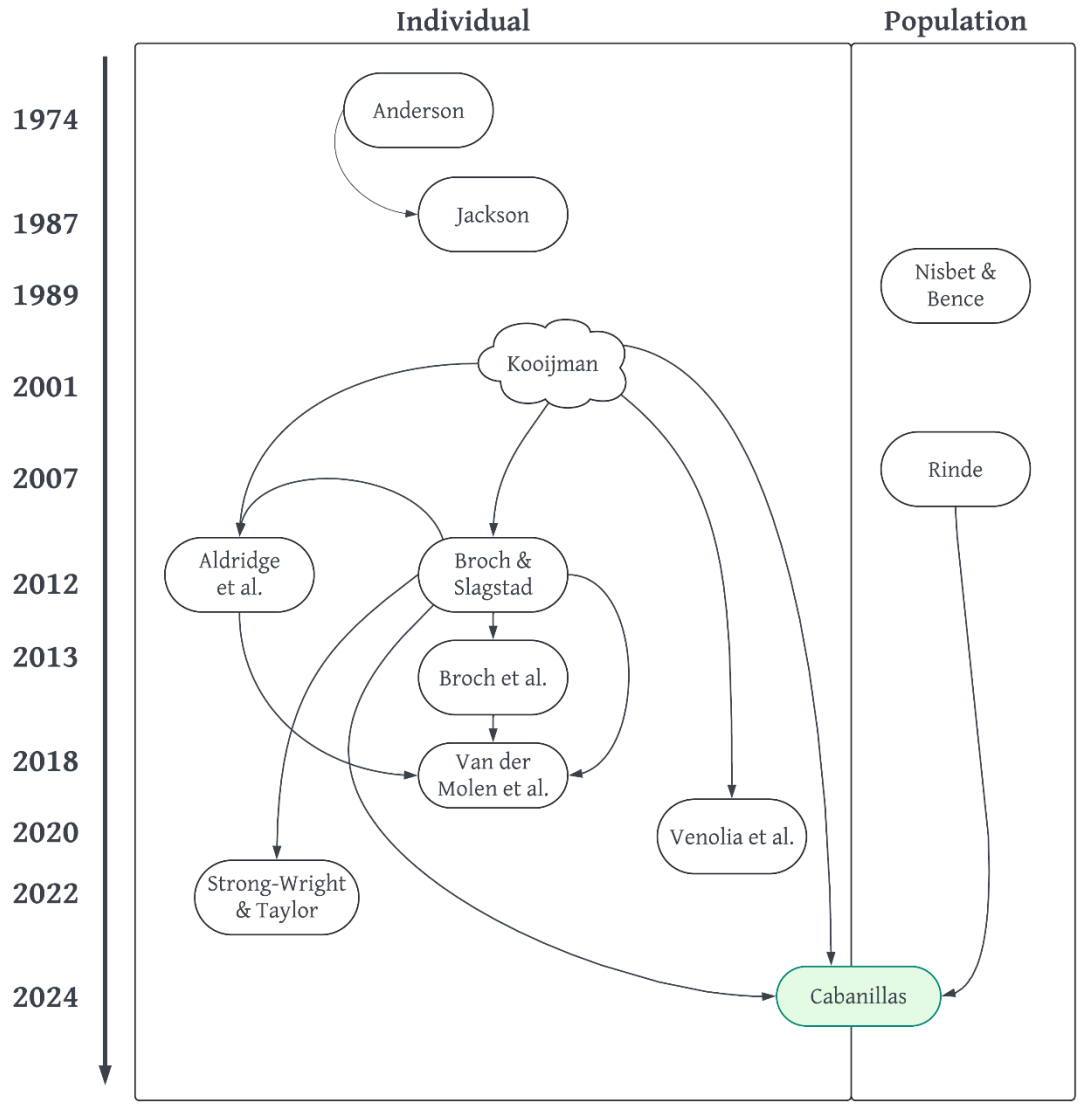

Figure 5.1. A schematic representation illustrating the interconnected methodological choices and concepts among the process-based models for kelp, presented at both the individual and population levels. The circles represent kelp models while the cloud shaped represents a specific theoretical framework. The green circle represents the connection of the work presented in this thesis and its connection to previous models.

5.2 Connecting Biochemical Processes to Forest Dynamics

Traditional theoretical models of kelp forests have often separated individual growth processes from broader population dynamics, resulting in a gap in explicitly linking how internal biochemical processes, such as nutrient uptake and photosynthesis, scale up to influence population-level dynamics. Existing models typically simplify individual physiology or focus narrowly on aquaculture settings, which do not capture the complexity of natural ecosystems and the interplay between individual and population-level processes. The forest model developed (see Chapter 3) addresses this critical gap by integrating the detailed individual growth dynamics of *L. hyperborea* with broader population-level processes, including light competition, recruitment, and mortality. This physiologically explicit IBM simulates a forest of independently growing individuals, providing insights into how environmental factors—like light, temperature, and nutrient availability—affect both individual growth and forest structure.

The model explicitly represents canopy and understory interactions, taking into account light shading effects and competitive interactions that are crucial for accurately depicting natural kelp forest dynamics. This integrated approach not only advances our understanding of kelp forest ecosystems but also serves as a valuable tool for predicting responses to future environmental changes (as applied in Ch4), offering insights critical for conservation and management efforts. By bridging the gap between individual growth processes and population-level dynamics, this comprehensive model enhances our ability to predict how kelp forests respond to varying environmental conditions, making it a significant step forward in forest ecosystem modelling.

5.3 Species-Specific Modelling

Currently, there is no physiologically explicit individual-based model (IBM) for *L. hyperborea* that focuses on internal budgeting using DEB theory. The model developed in this thesis addresses this gap by specifically targeting *L. hyperborea* and its unique physiological and ecological traits, which are not well represented in models that primarily focus on other species like *S. latissima.*

The current geographical distribution of *L. hyperborea* shows that the species has evolved through the development of strategies that allow it to deal with the fluctuating environment and lack of nutrients.

This leads to *L. hyperborea* growth being heavily reliant on effective reserve management. This model explicitly incorporates both carbon and nitrogen dynamics, including uptake, internal processing, and exudation—key processes for *L. hyperborea* growth that are not comprehensively covered in models designed for other species.

5.4 Light Limitation and Competition

Early models apply a simplified treatment of light competition and density dependence, which can have unforeseen consequences**.** Individual growth models often account only for self-shading, while forest population models consider broader impacts of canopy and understory interactions. A unified approach that incorporates both self-shading and inter-species competition for light is developed here, including shading effects from heavier plants on smaller individuals, thereby simulating how the canopy alters light availability for individuals below.

By linking light limitation and competition with growth dynamics, the model illustrates how these factors influence individual growth rates and forest biomass. It shows that reduced light availability can lead to slower growth and lower biomass, while improved light conditions can enhance growth rates. This detailed approach allows for a more accurate comparison of not only growth rates but also the internal composition of individuals, such as responses to nitrogen limitations. Comparing the individual growth model and the forest growth model show that neglecting the effects of the forest canopy leads to an overestimation of individual sizes in the middle canopy layers. This light limitation by the canopy is vital to consider as empirical studies show that light levels often fall below saturation points and significantly affect metabolic processes in kelp forests (Kain, 1976; Lüning, 1971).

5.5 Mortality

Some models emphasize life expectancy over mortality rates, with mortality explicitly included only in certain forest population models (Nisbet and Bence, 1989; Rinde, 2007) and a few individual growth models (Anderson, 1974; Jackson, 1987; van der Molen et al., 2018). The forest model developed here addresses this by explicitly incorporating mortality rates and tuning it against empirical data to ensure realistic representation of mortality dynamics. Additionally, the model allows for flexible adjustment of mortality rates over the number of individuals within a cohort, enabling it to represent different forest conditions.

5.6 Reproduction

The model developed in this thesis establishes a solid foundation for the straightforward integration of reproductive processes into kelp modelling. While the current model does not explicitly incorporate reproductive dynamics due to their complexity and data requirements, it is designed to accommodate these processes in future work. The DEB theory framework underpinning the model offers a modular approach that allows for the addition of new processes, such as reproduction, without fundamentally altering the existing structure. By providing a detailed representation of energy and nutrient dynamics, it will support the future integration of reproductive processes, clarifying how resources are allocated between growth, maintenance, and reproduction.

5.7 Limitations

5.7.1 Environmental Data

The simulations rely on environmental data to drive the model, as the conditions in which these individuals develop dictate their growth, limitations, and survival. For robust modelling parametrization access to frequent measurements of all environmental variables —such as irradiance at different depths, nitrate concentration, and temperature—on a daily or weekly basis for the duration of the individuals life-span would be preferred. A data set on this resolution for a period in excess of 10 years for the same location than the empirical data originates from was not found. A detailed survey of environmental conditions for a single in the west coast of Scotland was available (Berx et al., 2015; Heath, 1991, 1995b; Rees et al., 1995), as was used as a proxy to set up a virtual experimental setting. For model applications in other locations remotely sourced data was also considered. This presented a limited temporal and spatial resolution, as it was not as finely resolved as the manually obtained local data.

Additionally, for either source of data, irradiance was measured at the surface level. As the model was used to simulate multiple depths, surface irradiance had to be attenuated to the appropriate depth. This required the use of a light extinction or attenuation coefficient, which is influenced by water transparency. This makes it a highly sensitive parameter, subject to fluctuations caused by factors like river discharge, storms, sedimentation, and plankton suspension (Smale and Moore, 2017). Finding attenuation data that could meet the temporal requirements proved to be a major challenge. Given that the light data already exhibited a seasonal cycle, I opted for a simplified approach, using a constant value for the attenuation coefficient adjustment. However, it's important to acknowledge that this simplification has limitations, especially concerning the yearly fluctuations.

5.7.2 Biological Data

Acquiring detailed field data on kelp populations presented the main challenge. Repeated non-destructive measurements of individual weight and chemical content data in order to track growth trajectories, simultaneously with their internal composition, is not possible. Even if such frequent measurements were feasible, the logistical and economic constraints of conducting regular scuba diving expeditions in stormy, deep waters, especially during winter, renders this approach unrealistic. As a result, detailed data on seasonal fluctuations in tissue composition and weight are scarce in the literature. Laboratory experiments face their own limitations. Even if multiple individuals were sampled, running a long-term laboratory experiment on such a scale for the complete life-span (> 8 years) of several individuals to be represented, would be challenging.

The multitude of variables involved, both biological and environmental, introduces variations that are intrinsic to the system. An example of this are the uncertainties around age determination, as the yearly growth lines that appear in the cross section of the stipe which are used for determining age are not clearly marked in the first years of life. The age at which an individual can be considered "one year old" is a matter of some debate, as growth lines become distinctly defined only after a certain stage. Values range between 2 years (Kain, 1963), 3 years (Whittick, 1969), or 4 years (Lüning, 1969a). Adding to the complexity, older datasets, which date back more than 60 years (Kain, 1963), were collected using different methods to what is currently available, and the environmental conditions have since changed due to climate change. Additionally, not all research papers provide complete enough information on their methods, making cross-publication comparisons challenging. Due to this the model can only be parametrised on data from one location and study at the time. Given these limitations, the models cannot be formally fitted or expected to be a perfect representation. The constraints dictate that the models are based on assumptions and approximations, reflecting the reality of working with the available data.

5.7.3 Methodological considerations

Defining the area that the forest model occupies was done using the available data and adjusted to what seemed representative. The shaded area was used to define the approximate area of the forest model simulation, as it aligns with the key aspect of interest in the forest model. However, certain aspects, such as the number of recruits in this area and the individual characteristics, could not be precisely determined, especially for younger individuals. Consequently, the results are normalized to the area defined where homogeneous competition for light occurs, i.e., within a specific patch rather than across the entire forest.

The timing of kelp recruitment is a relevant aspect of this research, but poses considerable challenges. While the timing of spore release can be approximately pinpointed from the literature, the life cycle of these plants is far more complex (Kain, 1975, 1964). Kelp individuals in the model do not start as spores; but develop from them, due to the limited exact knowledge of spore growth timing and rates, settlement and mortality rates. This complexity extends to defining when an individual can be considered "one year old" because growth lines in the stipe are not clearly defined before a certain stage. Disagreements persist regarding the specific age at which this transition occurs, with estimates ranging from 2 to 4 years (Kain, 1963; Lüning, 1969; Whittick, 1969). While digging into the intricacies of kelp population dynamics, it's crucial to recognize these challenges. While aiming for accuracy, a balance must be achieved between scientific rigor and practicality, ensuring that models remain useful without becoming overly complex.

5.8 Applications

Future research can explore how the model can contribute to the development of effective harvesting regime strategies, addressing concerns raised by Steen et al. (2016). Integration of the individual model into a forest simulation was a necessary step to examine more intricate interactions and gain deeper insights into the underlying processes driving kelp forest population dynamics.

A detailed model of a long-lived complex species allows for the realization of virtual experiments that would not be feasible in a laboratory or empirical set up, such as the study of forest population cycles under changing environmental conditions and human interventions. This approach can be considered within the Blue Economy and the United Nations Ocean Decade (Franke et al., 2023). Seaweeds, hold significant promise for creating jobs, from aquaculture operations to processing facilities and the broader industry (Angus, 2017; MacLeod et al., 2014). Beyond their economic value, kelp forests also serve as crucial biodiversity hotspots and nursery grounds, playing a pivotal role in maintaining ecosystem health (Christie et al., 1998; Lorentsen et al., 2010). To be able to adequately plan for this economic development in a sustainable manner, the knowledge of how kelp will respond to future conditions is vital. Furthermore, kelp contributes to the concept of "blue carbon," by playing a more substantial role in carbon sequestration than previously thought, yet calculating their precise contributions remains challenging (Burrows et al., 2014; Tanaka et al., 2023). Quantifying the carbon sequestration potential of kelp ecosystems poses complex challenges that require further investigation

My research has implications for policy and management decisions, especially concerning kelp harvesting practices. Studies in Norway have shown that kelp recuperation is a complex process, and existing state guidelines may not fully account for the intricacies involved (Gouraguine et al., 2021; Lorentsen et al., 2010; Steen et al., 2016). It's crucial to ensure that our actions do not harm valuable resources like the Scottish kelp forests, which are already under pressure from climate change (Harley et al., 2012; Smale, 2020). My research, alongside contributions from other studies, highlights the need for comprehensive assessments of kelp forest health and sustainable harvesting practices.

Considering the changing ranges of *L. hyperborea* populations (Diehl et al., 2024; Smale et al., 2015) it becomes evident that proactive policies are necessary to protect and preserve these ecosystems. My findings, as well as those from other researchers, underscore the urgency of addressing climate-related impacts on kelp species. These policies should not only focus on immediate conservation efforts but also consider long-term strategies to ensure the resilience and sustainability of these critical marine habitats.

5.9 Future Research

A possible avenue for future research is the integration of storm damage into the models, accounting for tissue loss and mortality events triggered by extreme weather conditions.

This would involve establishing a size-related mortality rate linked to storm damage and considering background tissue loss due to erosion. By simulating the impact of storms on kelp populations, gaining valuable insights into their resilience and adaptability in the face of increasingly unpredictable climate events (Kain, 1971b, 1963; Kregting et al., 2013; Pedersen et al., 2012).

Another area of potential research involves a deeper examination of reproduction within kelp populations. Although reproduction is already a component of my models, further investigation can refine and parameterize reproduction rates. Data on the proportion of frond cover occupied by sporophytes and minimum age to reach reproductive maturity (Kain, 1975), as influenced by factors like size and forest growing conditions, can be integrated.

To enhance the realism of my models, future research could focus on making shading competition spatially explicit. This would involve modelling multiple patches within a kelp forest and incorporating interactions based on factors like distance from the forest edge or the effects of waves and currents during storms. By exploring how different patches within the forest compete for light and resources, a more nuanced understanding of population structure dynamics can be achieved. However, it's important to note that acquiring the necessary biological data to validate this approach may pose challenges.

Adding the depth of the ocean floor to a spatially explicit models is another avenue worth exploring. By considering the depth of individual plants within the forest, variations in light availability based on their positions within the forest can be simulated. Additionally, including turbidity, especially in areas near river mouths or ports, can further refine growth rate predictions. Detailed examination of the effects of water turbidity, particularly as mediated by waves, is warranted. Waves can influence plant morphology, impacting the drag properties of individual plants and subsequently affecting mortality rates. Variations in morphology can further manifest in differences in weight and tissue composition, with sturdier plants being more prevalent in rougher waters, as noted in previous research (Larkum, 1972; Pedersen et al., 2012; Sjøtun et al., 1998; Sjøtun and Fredriksen, 1995; Smale et al., 2016).

While my analysis has focused on a kelp forest growing at a 3-meter depth with irradiance conditions typical of Scotland, it is essential to recognize the significant influence of depth and local environmental factors. To gain a more comprehensive understanding of *L. hyperborea* populations, future research should explore the model's performance across further depths and locations. The impact of waves and storms, as highlighted in previous studies (Kain, 1971b, 1963; Kregting et al., 2013; Pedersen et al., 2012), should also be considered to improve the model's accuracy in replicating mortality processes observed in natural forests.

The current model does not account for the effects of grazing, which can significantly impact plant density and a forest's resilience to disturbance events. Existing research underscores the importance of grazing in kelp forest dynamics (Harrold and Reed, 1985; Kain, 1971b; Sjøtun et al., 2006). Future research endeavours should investigate the role of grazing in kelp ecosystems to enhance our understanding of these intricate dynamics.

5.10 Conclusion

This model provides a biochemically explicit individual based kelp forest model, which allows the study of both the population level dynamics simultaneously with the internal individual physiological process. Allowing the model to both look “outside” and “inside” the individuals. The interaction between the forest structure and individuals’ growth highlights how individual growth cannot be considered in isolation; rather, it is fundamentally influenced by forest population dynamics. The model effectively captures how changes in the light regime, driven by the interactions between individuals, impact growth rates over time, with a level of detail that allows for the study of seasonal biochemical composition changes. Modelling individual plants and extrapolating their responses by the total plant count overlooks the influential impact of the canopy and the population structure.

This research presents a new approach to modelling kelp forest dynamics by integrating internal nitrogen and carbon content within a natural population framework. It captures the intricate interactions and competitive dynamics among individuals in a changing environment. This framework fills critical gaps in existing literature and has important implications for the conservation and management of these vital marine ecosystems, providing valuable insights into how individual physiological processes and population-level interactions can inform future research and ecological management strategies.

6 Bibliography

Aamot, I.A., 2011. How photosynthesis in *Laminaria digitata* and *Saccharina latissima* is affected by water temperature (Masters Thesis). Institutt for biologi, Bergen, Norway.

Abdullah, M.I., Fredriksen, S., 2014. The exudation of nitrate by the kelp *Laminaria hyperborea*, an observation during in situ incubation experiments. Marine Biology Research 10, 725–730. https://doi.org/10.1080/17451000.2013.850514

Abdullah, M.I., Fredriksen, S., 2004. Production, respiration and exudation of dissolved organic matter by the kelp *Laminaria hyperborea* along the west coast of Norway. Journal of the Marine Biological Association of the United Kingdom 84, 887–894. https://doi.org/10.1017/S002531540401015Xh

Aldridge, J., van der Molen, J., Forster, R., 2012. Wider ecological implications of Macroalgae cultivation. The Crown Estate 95.

Anderson, N., 1974. A mathematical model for the growth of giant kelp. Simulation 22, 97–105. https://doi.org/10.1177/003754977402200404

Angus, S., 2017. Modern Seaweed Harvesting and Gathering in Scotland: The Legal and Ecological Context. Scottish Geographical Journal 133, 101–114. https://doi.org/10.1080/14702541.2017.1293839

Araújo, R.M., Assis, J., Aguillar, R., Airoldi, L., Bárbara, I., Bartsch, I., Bekkby, T., Christie, H., Davoult, D., Derrien-Courtel, S., Fernandez, C., Fredriksen, S., Gevaert, F., Gundersen, H., Le Gal, A., Lévêque, L., Mieszkowska, N., Norderhaug, K.M., Oliveira, P., Puente, A., Rico, J.M., Rinde, E., Schubert, H., Strain, E.M., Valero, M., Viard, F., Sousa-Pinto, I., 2016. Status, trends and drivers of kelp forests in Europe: an expert assessment. Biodiversity Conservation 25, 1319–1348. https://doi.org/10.1007/s10531-016-1141-7

Arnell, N.W., Brown, S., Gosling, S.N., Gottschalk, P., Hinkel, J., Huntingford, C., Lloyd-Hughes, B., Lowe, J.A., Nicholls, R.J., Osborn, T.J., Osborne, T.M., Rose, G.A., Smith, P., Wheeler, T.R., Zelazowski, P., 2016. The impacts of climate change across the globe: A multi-sectoral assessment. Climatic Change 134, 457–474. https://doi.org/10.1007/s10584-014-1281-2

Arrhenius, S., 1889. Über die Dissociationswärme und den Einfluss der Temperatur auf den Dissociationsgrad der Elektrolyte. Zeitschrift für Physikalische Chemie 4U, 96–116. https://doi.org/10.1515/zpch-1889-0408

Assis, J., Araújo, M.B., Serrão, E.A., 2018. Projected climate changes threaten ancient refugia of kelp forests in the North Atlantic. Global Change Biology 24, e55–e66. https://doi.org/10.1111/gcb.13818

Assis, J., Lucas, A.V., Bárbara, I., Serrão, E.Á., 2016. Future climate change is predicted to shift long-term persistence zones in the cold-temperate kelp *Laminaria hyperborea*. Marine Environmental Research 113, 174–182. https://doi.org/10.1016/j.marenvres.2015.11.005

Beer, 1852. Bestimmung der Absorption des rothen Lichts in farbigen Flüssigkeiten. Annalen der Physik 162, 78–88.

Bekkby, T., Rinde, E., Erikstad, L., Bakkestuen, V., 2009. Spatial predictive distribution modelling of the kelp species *Laminaria hyperborea*. ICES Journal of Marine Science 66, 2106–2115. https://doi.org/10.1093/icesjms/fsp195

Bengtsson, M.M., Sjøtun, K., Storesund, J.E., Øvreås, L., 2011. Utilization of kelp-derived carbon sources by kelp surface-associated bacteria. Aquatic Microbial Ecology 62, 191–199. https://doi.org/10.3354/ame01477

Berx, B., Gallego, A., Heath, M., The MASTS Community, 2015. Loch Linnhe and Firth of Lorne. MASTS Case Study Workshop Report (No. 16(1)). Scottish Marine and Freshwater Science. https://doi.org/10.7489/1539-1

Bixler, H.J., Porse, H., 2011. A decade of change in the seaweed hydrocolloids industry. Journal of Applied Phycology. 23, 321–335. https://doi.org/10.1007/s10811-010-9529-3

Black, W.A.P., 1950. The seasonal variation in weight and chemical composition of the common British Laminariaceae. Journal of the Marine Biological Association of the United Kingdom 29, 45–72. https://doi.org/10.1017/S0025315400056186

Bodycomb, R., Pomeroy, A.W.M., Morris, R.L., 2023. Kelp Aquaculture as a Nature-Based Solution for Coastal Protection: Wave Attenuation by Suspended Canopies. Journal of Marine Science and Engineering 11, 1822. https://doi.org/10.3390/jmse11091822

Briggs, G. E., & Haldane, J. B. S. (1925). A note on the kinetics of enzyme action. Biochemical journal, 19(2), 338. https://doi.org/10.1042/bj0190338

Broch, O., Ellingsen, I., Forbord, S., Wang, X., Volent, Z., Alver, M., Handå, A., Andresen, K., Slagstad, D., Reitan, K., Olsen, Y., Skjermo, J., 2013. Modelling the cultivation and bioremediation potential of the kelp *Saccharina latissim*a in close proximity to an exposed salmon farm in Norway. Aquaculture Environment Interactions. 4, 187–206. https://doi.org/10.3354/aei00080

Broch, O.J., Slagstad, D., 2012. Modelling seasonal growth and composition of the kelp *Saccharina latissima*. Journal of Applied Phycology 24, 759–776. https://doi.org/10.1007/s10811-011-9695-y

Broekhuizen, N., Gurney, W.S.C., Jones, A., Bryant, A.D., 1994. Modelling Compensatory Growth. Functional Ecology 8, 770–782. https://doi.org/10.2307/2390237

Brown, J.H., Gillooly, J.F., Allen, A.P., Savage, V.M., West, G.B., 2004. Toward a Metabolic Theory of Ecology. Ecology 85, 1771–1789. https://doi.org/10.1890/03-9000

Burdett, H.L., Wright, H., Smale, D.A., 2019. Photophysiological Responses of Canopy-Forming Kelp Species to Short-Term Acute Warming. Frontiers in Marine Science 6. https://doi.org/10.3389/fmars.2019.00516

Burrows, M.T., Kamenos, N.A., Hughes, D.J., Stahl, H., Howe, J.A., Tett, P., 2014. Assessment of carbon budgets and potential blue carbon stores in Scotland's coastal and marine environment [WWW Document]. URL http://www.snh.org.uk/pdfs/publications/commissioned_reports/761.pdf (accessed 2.22.21).

Chapman, A.R.O., Craigie, J.S., 1977. Seasonal growth in *Laminaria longicruris*: Relations with dissolved inorganic nutrients and internal reserves of nitrogen. Marine Biology 40, 197–205. https://doi.org/10.1007/BF00390875

Chapman, A.R.O., Lindley, J.E., 1980. Seasonal growth of *Laminaria solidungula* in the Canadian High Arctic in relation to irradiance and dissolved nutrient concentrations. Marine Biology. 57, 1–5. https://doi.org/10.1007/BF00420961

Chi, S., Qian, H., Li, T., Wang, X., Liu, C., Ren, L., Tang, X., Liu, T., 2014. Phylogeny of genera *Laminaria* and *Saccharina* (Laminariales, Phaeophyceae) based on three molecular markers. Acta Oceanol. Sin. 33, 139–151. https://doi.org/10.1007/s13131-014-0525-3

Christie, H., Fredriksen, S., Rinde, E., 1998. Regrowth of kelp and colonization of epiphyte and fauna community after kelp trawling at the coast of Norway. Hydrobiologia 375, 49–58. https://doi.org/10.1023/A:1017021325189

Christie, H., Jørgensen, N.M., Norderhaug, K.M., Waage-Nielsen, E., 2003. Species distribution and habitat exploitation of fauna associated with kelp (*Laminaria hyperborea*) along the Norwegian Coast. Journal of the Marine Biological Association of the United Kingdom 83, 687–699. doi:10.1017/S0025315403007653h

Creed, J.C., Kain (Jones), J.M., Norton, T.A., 1998. An Experimental Evaluation of Density and Plant Size in Two Large Brown Seaweeds. Journal of Phycology 34, 39–52. https://doi.org/10.1046/j.1529-8817.1998.340039.x

Darwin, C., 1882. A Naturalist's Voyage: Journal of Researches Into the Natural History and Geology of the Countries Visited During the Voyage of HMS Beagle: with Maps and Illustrations. Murray, London.

Davison, I.R., Stewart, W.D.P., 1983. Occurrence and significance of nitrogen transport in the brown alga *Laminaria digitata*. Marine Biology. 77, 107–112. https://doi.org/10.1007/BF00396307

de la Hoz, C.F., Ramos, E., Acevedo, A., Puente, A., Losada, Í.J., Juanes, J.A., 2018. OCLE: A European open access database on climate change effects on littoral and oceanic ecosystems. Progress in Oceanography 168, 222–231. https://doi.org/10.1016/j.pocean.2018.09.021

Diehl, N., Laeseke, P., Bartsch, I., Bligh, M., Buck-Wiese, H., Hehemann, J.-H., Niedzwiedz, S., Plag, N., Karsten, U., Shan, T., Bischof, K., 2024. Photoperiod and temperature interactions drive the latitudinal distribution of *Laminaria hyperborea* (Laminariales, Phaeophyceae) under climate change. Journal of Phycology. https://doi.org/10.1111/jpy.13497

Drew, E.A., 1983. Physiology of *Laminaria*. Marine Ecology 4, 227–250. https://doi.org/10.1111/j.1439-0485.1983.tb00298.x

Drew, E.A., Jupp, B.P., Robertson, W.A.A., 1976. Photosynthesis and Growth of *Laminaria hyperborea* in British Waters, in: Drew, E.A., Lythgoe, J.N., Woods, J.D. (Eds.), Underwater Research. Academic Press, pp. 369–379. https://doi.org/10.1016/B978-0-12-221950-4.50025-4

Droop, M.R., Mickelson, M.J., Scott, J.M., Turner, M.F., 1982. Light and nutrient status of algal cells. Journal of the Marine Biological Association of the United Kingdom 62, 403–434. https://doi.org/10.1017/S0025315400057362

Dunn, J., Hall, C.D., Heath, M.R., Mitchell, R.B., Ritchie, B.J., 1993. ARIES—a system for concurrent physical, biological and chemical sampling at sea. Deep Sea Research Part I: Oceanographic Research Papers 40, 867–878. https://doi.org/10.1016/0967-0637(93)90076-F

Dunton, K., Schell, D., 1986. Seasonal carbon budget and growth of *Laminaria solidungula* in the Alaskan High Arctic. Marine Ecology Progress Series. 31, 57–66. https://doi.org/10.3354/meps031057

Edwards, A., Sharples, F., 1986. Scottish Sea Lochs: A Catalogue, SAMS Internal Reports. Scottish Association for Marine Science.

Eger, A.M., Marzinelli, E.M., Beas-Luna, R., Blain, C.O., Blamey, L.K., Byrnes, J.E.K., Carnell, P.E., Choi, C.G., Hessing-Lewis, M., Kim, K.Y., Kumagai, N.H., Lorda, J., Moore, P., Nakamura, Y., Pérez-Matus, A., Pontier, O., Smale, D., Steinberg, P.D., Vergés, A., 2023. The value of ecosystem services in global marine kelp forests. Nature Communications. 14, 1894. https://doi.org/10.1038/s41467-023-37385-0

Eggert, A., 2012. Seaweed responses to temperature. In 'Seaweed Biology'.(Eds C Wienke and K Bischof.) pp. 47–66. Springer-Verlag. https://doi.org/10.1007/978-3-642-28451-9_3

Elsmore, K., Nickols, K.J., Miller, L.P., Ford, T., Denny, M.W., Gaylord, B., 2024. Wave damping by giant kelp, *Macrocystis pyrifera*. Annals of Botany 133, 29–40. https://doi.org/10.1093/aob/mcad094

Fernández, P.A., Gaitán-Espitia, J.D., Leal, P.P., Schmid, M., Revill, A.T., Hurd, C.L., 2020. Nitrogen sufficiency enhances thermal tolerance in habitat-forming kelp: implications for acclimation under thermal stress. Scientific Reports 10, 3186. https://doi.org/10.1038/s41598-020-60104-4

Fogg, G.E., 1983. The Ecological Significance of Extracellular Products of Phytoplankton Photosynthesis 26, 3–14. https://doi.org/10.1515/botm.1983.26.1.3

Franco, J.N., Tuya, F., Bertocci, I., Rodríguez, L., Martínez, B., Sousa-Pinto, I., Arenas, F., 2018. The 'golden kelp' *Laminaria ochroleuca* under global change: Integrating multiple eco-physiological responses with species distribution models. Journal of Ecology 106, 47–58. https://doi.org/10.1111/1365-2745.12810

Franke, A., Peters, K., Hinkel, J., Hornidge, A.-K., Schlüter, A., Zielinski, O., Wiltshire, K.H., Jacob, U., Krause, G., Hillebrand, H., 2023. Making the UN Ocean Decade work? The potential for, and challenges of, transdisciplinary research and real-world laboratories for building towards ocean solutions. People and Nature 5, 21–33. https://doi.org/10.1002/pan3.10412

Fredriksen, S., Sjøtun, K., Lein, T.E., Rueness, J., 1995. Spore dispersal in *Laminaria hyperborea* (laminariales, phaeophyceae). Sarsia 80, 47–53. https://doi.org/10.1080/00364827.1995.10413579

Gagné, J.A., Mann, K.H., Chapman, A.R.O., 1982. Seasonal patterns of growth and storage in *Laminaria longicruris* in relation to differing patterns of availability of nitrogen in the water. Marine Biology 69, 91–101. https://doi.org/10.1007/BF00396965

Gattuso, J.-P., Magnan, A., Billé, R., Cheung, W.W.L., Howes, E.L., Joos, F., Allemand, D., Bopp, L., Cooley, S.R., Eakin, C.M., Hoegh-Guldberg, O., Kelly, R.P., Pörtner, H.-O., Rogers, A.D., Baxter, J.M., Laffoley, D., Osborn, D., Rankovic, A., Rochette, J., Sumaila, U.R., Treyer, S., Turley, C., 2015. Contrasting futures for ocean and society from different anthropogenic CO2 emissions scenarios. Science 349, aac4722. https://doi.org/10.1126/science.aac4722

Gerard, V.A., 1997. The Role of Nitrogen Nutrition in High-Temperature Tolerance of the Kelp, *Laminaria Saccharina* (chromophyta)1. Journal of Phycology 33, 800–810. https://doi.org/10.1111/j.0022-3646.1997.00800.x

Gevaert, F., Davoult, D., Creach, A., Kling, R., Janquin, M.-A., Seuront, L., Lemoine, Y., 2001. Carbon and nitrogen content of *Laminaria saccharina* in the eastern English Channel: biometrics and seasonal variations. Journal of the Marine Biological Association of the United Kingdom 81, 727–734. https://doi.org/10.1017/S0025315401004532

Gevaert, F., Janquin, M.-A., Davoult, D., 2008. Biometrics in *Laminaria digitata*: A useful tool to assess biomass, carbon and nitrogen contents. Journal of Sea Research 60, 215–219. https://doi.org/10.1016/j.seares.2008.06.006

Giordano, M., Raven, J.A., 2014. Nitrogen and sulphur assimilation in plants and algae. Aquatic Botany, SPECIAL ISSUE: In Honour of George Bowes: Linking Terrestrial and Aquatic Botany 118, 45–61. https://doi.org/10.1016/j.aquabot.2014.06.012

Gorman, D., Bajjouk, T., Populus, J., Vasquez, M., Ehrhold, A., 2013. Modeling kelp forest distribution and biomass along temperate rocky coastlines. Marine Biology 160, 309–325. https://doi.org/10.1007/s00227-012-2089-0

Gouraguine, A., Moore, P., Burrows, M.T., Velasco, E., Ariz, L., Figueroa-Fábrega, L., Muñoz-Cordovez, R., Fernandez-Cisternas, I., Smale, D., Pérez-Matus, A., 2021. The intensity of kelp harvesting shapes the population structure of the foundation species *Lessonia trabeculata* along the Chilean coastline. Marine Biology 168, 66. https://doi.org/10.1007/s00227-021-03870-7

Hargrave, M.S., Foggo, A., Pessarrodona, A., Smale, D.A., 2017. The effects of warming on the ecophysiology of two co-existing kelp species with contrasting distributions. Oecologia 183, 531–543. https://doi.org/10.1007/s00442-016-3776-1

Harley, C.D.G., Anderson, K.M., Demes, K.W., Jorve, J.P., Kordas, R.L., Coyle, T.A., Graham, M.H., 2012. Effects of Climate Change on Global Seaweed Communities. Journal of Phycology 48, 1064–1078. https://doi.org/10.1111/j.1529-8817.2012.01224.x

Harrold, C., Reed, D.C., 1985. Food Availability, Sea Urchin Grazing, and Kelp Forest Community Structure. Ecology 66, 1160–1169. https://doi.org/10.2307/1939168

Heath, M., 1996. The consequences of spawning time and dispersal patterns of larvae for spatial and temporal variability in survival to recruitment. Survival Strategies in Early Life Stages of Marine Resources.

Heath, M., 1991. An ecosystem research programme in Loch Linnhe. Ocean Challenge 2, 8–9. https://doi.org/10.7489/1539-1

Heath, M.R., 1995a. Size spectrum dynamics and the planktonic ecosystem of Loch Linnhe. ICES Journal of Marine Science 52, 627–642. https://doi.org/10.1016/1054-3139(95)80077-8

Heath, M.R., 1995b. Size spectrum dynamics and the planktonic ecosystem of Loch Linnhe. ICES Journal of Marine Science 52, 627–642. https://doi.org/10.1016/1054-3139(95)80077-8

Henley, W.J., Dunton, K.H., 1995. A Seasonal Comparison of Carbon, Nitrogen, and Pigment Content in *Laminaria solidungula* and *L. saccharina* (Phaeophyta) in the Alaskan Arctic 1. Journal of Phycology 31, 325–331. https://doi.org/10.1111/j.0022-3646.1995.00325.x

IPCC, 2014. Climate Change 2014: Synthesis Report. Contribution of Working Groups I, II and III to the Fifth Assessment Report of the Intergovernmental Panel on Climate Change. Geneva, Switzerland.

Ito, E., Ikemoto, Y., Yoshioka, T., 2015. Thermodynamic implications of high Q10 of thermo-TRP channels in living cells. Biophysics (Nagoya-shi) 11, 33–38. https://doi.org/10.2142/biophysics.11.33

Jackson, G.A., 1987. Modelling the growth and harvest yield of the giant kelp *Macrocystis pyrifera*. Marine Biology. 95, 611–624. https://doi.org/10.1007/BF00393105

Jayathilake, D.R.M., Costello, M.J., 2020. A modelled global distribution of the kelp biome. Biological Conservation 252, 108815. https://doi.org/10.1016/j.biocon.2020.108815

Johnston, C.S., Jones, R.G., Hunt, R.D., 1977. A seasonal carbon budget for a *laminarian* population in a Scottish sea-loch. Helgoländer Wissenschaftliche Meeresuntersuchungen 30, 527–545. https://doi.org/10.1007/BF02207859

Jupp, B. P. (1972). Studies on the growth and physiology of attached marine algae. University of St. Andrews (United Kingdom). https://hdl.handle.net/10023/14281

Jusup, M., Sousa, T., Domingos, T., Labinac, V., Marn, N., Wang, Z., Klanjšček, T., 2017. Physics of metabolic organization. Physics of Life Reviews 20, 1–39. https://doi.org/10.1016/j.plrev.2016.09.001

Kain, 1975. The biology of *Laminaria hyperborea* VII. Reproduction of the sporophyte. Journal of the Marine Biological Association of the United Kingdom 55, 567–582. https://doi.org/10.1017/S0025315400017264

Kain, J.M., 1979. A view of the genus *Laminaria*. Oceanogr. Marine Biology Annual Review.17, 101–161.

Kain, J.M., 1977. The biology of *Laminaria hyperborea* X. The effect of depth on some populations. Journal of the Marine Biological Association of the United Kingdom 57, 587–607. https://doi.org/10.1017/S0025315400025054

Kain, J.M., 1976. The biology of *Laminaria hyperborea*. VIII. Growth on Cleared Areas. Journal of the Marine Biological Association of the United Kingdom 56, 267–290. https://doi.org/10.1017/S0025315400018907

Kain, J.M., 1971a. Synopsis of biological data on *Laminaria hyperborea*. FAO Fisheries Synopsis 87:68 pp.

Kain, J.M., 1971b. The biology of *Laminaria hyperborea*. VI. Some Norwegian populations. Journal of the Marine Biological Association of the United Kingdom 51, 387–408. https://doi.org/10.1017/S0025315400031866

Kain, J.M., 1971c. Continuous recording of underwater light in relation to *Laminaria* distribution, in: Proceedings of the 4th European Marine Biology Symposium. Cambridge University Cambridge, pp. 335–346.

Kain, J.M., 1969. The Biology of *Laminaria hyperborea*. V. Comparison with early stages of competitors. Journal of the Marine Biological Association of the United Kingdom 49, 455–473. https://doi.org/10.1017/S0025315400036031

Kain, J.M., 1967. Populations of *Laminaria hyperborea* at various latitudes. Helgoländer Wissenschaftliche Meeresuntersuchungen 15. https://doi.org/10.1007/BF01618645

Kain, J.M., 1964. Aspects of the Biology of *Laminaria hyperborea* III. Survival and Growth of Gametophytes. Journal of the Marine Biological Association of the United Kingdom 44, 415–433. https://doi.org/10.1017/S0025315400024929

Kain, J.M., 1963. Aspects of the Biology of *Laminaria hyperborea*: II. Age, Weight and Length. Journal of the Marine Biological Association of the United Kingdom 43, 129–151. https://doi.org/10.1017/S0025315400005312

Kitching, J.A., 1941. Studies in sublittoral ecology : iii. *Laminaria* forest on the west coast of scotland; a study of zonation in relation to wave action and illumination. The Biological Bulletin 80, 324–337. https://doi.org/10.2307/1537719

Kleiber, M., 1932. Body size and metabolism. Hilgardia 6, 315–353. https://doi.org/10.3733/hilg.v06n11p315.

Kooijman, S.A.L.M., 2020. The standard dynamic energy budget model has no plausible alternatives. Ecological Modelling 428, 109106. https://doi.org/10.1016/j.ecolmodel.2020.109106

Kooijman, S.A.L.M., 2009. Dynamic Energy Budget Theory for Metabolic Organisation. Cambridge ; New York. https://doi.org/10.1017/CBO9780511805400

Kooijman, S.A.L.M., 2001. Quantitative aspects of metabolic organization: a discussion of concepts. Philosophical Transactions of the Royal Society of London. Series B: Biological Sciences 356, 331–349. https://doi.org/10.1098/rstb.2000.0771

Kooijman, S.A.L.M., 2000. Dynamic Energy and Mass Budgets in Biological Systems, 2nd ed. Cambridge University Press. https://doi.org/10.1017/CBO9780511565403

Kooijman, S.A.L.M., 1986. Population dynamics on basis of budgets. The dynamics of physiologically structured population 266–297.

Krause-Jensen, D., Duarte, C.M., 2016. Substantial role of macroalgae in marine carbon sequestration. Nature Geoscience. 9, 737–742. https://doi.org/10.1038/ngeo2790

Kregting, L., Blight, A., Elsäßer, B., Savidge, G., 2013. The influence of water motion on the growth rate of the kelp *Laminaria hyperborea*. Journal of Experimental Marine Biology and Ecology 448, 337–345. https://doi.org/10.1016/j.jembe.2013.07.017

Kremer, B.P., 1984. Carbohydrate Reserve and Dark Carbon Fixation in the Brown Macroalga, *Laminaria hyperborea*. Journal of Plant Physiology 117, 233–242. https://doi.org/10.1016/S0176-1617(84)80005-X

Lamouroux, J.V., 1813. Essai sur les genres de la famille des thalassiophytes non articulées. Dufour.

Lane, C.E., Mayes, C., Druehl, L.D., Saunders, G.W., 2006. A Multi-Gene Molecular Investigation of the Kelp (laminariales, Phaeophyceae) Supports Substantial Taxonomic Re-Organization1. Journal of Phycology 42, 493–512. https://doi.org/10.1111/j.1529-8817.2006.00204.x

Larkum, A.W.D., 1972. Frond Structure and Growth in *Laminaria hyperborea*. Journal of the Marine Biological Association of the United Kingdom 52, 405–418. https://doi.org/10.1017/S0025315400018762

Lavaud, R., Filgueira, R., Nadeau, A., Steeves, L., Guyondet, T., 2020. A Dynamic Energy Budget model for the macroalga *Ulva lactuca*. Ecological Modelling 418, 108922. https://doi.org/10.1016/j.ecolmodel.2019.108922

Le Roy, N., Jackson, D.J., Marie, B., Ramos-Silva, P., Marin, F., 2016. Carbonic anhydrase and metazoan biocalcification: a focus on molluscs. Key Engineering Materials 672, 151–157. https://doi.org/10.4028/www.scientific.net/KEM.672.151

Ledder, G., 2014. The Basic Dynamic Energy Budget Model and Some Implications. Letters in Biomathematics 1, 221–233. https://doi.org/10.1080/23737867.2014.11414482

Lika, K., Nisbet, R.M., 2000. A Dynamic Energy Budget model based on partitioning of net production. Journal of Mathematical Biology. 41, 361–386. https://doi.org/10.1007/s002850000049

Lobell, D.B., Asseng, S., 2017. Comparing estimates of climate change impacts from process-based and statistical crop models. Environmental Research Letters. 12, 015001. https://doi.org/10.1088/1748-9326/aa518a

Lorena, A., Marques, G.M., Kooijman, S.A.L.M., Sousa, T., 2010. Stylized facts in microalgal growth: interpretation in a dynamic energy budget context. Philosophical Transactions of the Royal Society B: Biological Sciences 365, 3509–3521. https://doi.org/10.1098/rstb.2010.0101

Lorentsen, S.-H., Sjøtun, K., Grémillet, D., 2010. Multi-trophic consequences of kelp harvest. Biological Conservation 143, 2054–2062. https://doi.org/10.1016/j.biocon.2010.05.013

Lüning, K., 1980. Critical levels of light and temperature regulating the gametogenesis of three *Laminaria* species (Phaeophyceae) 1. Journal of Phycology 16, 1–15. https://doi.org/10.1111/j.1529-8817.1980.tb02992.x

Lüning, K., 1971. Seasonal growth of *Laminaria hyperborea* under recorded underwater light conditions near Helgoland, in: Fourth European Marine Biology Symposium. University Press Cambridge, pp. 347–361.

Lüning, K., 1970a. Cultivation of *Laminaria hyperborea* in situ and in continuous darkness under laboratory conditions. Helgoländer wissenschaftliche Meeresuntersuchungen 20, 79–88. https://doi.org/10.1007/BF01609889

Lüning, K., 1970b. Tauchuntersuchungen zur Vertikalverteilung der sublitoralen Helgoländer Algenvegetation. Helgolander Wiss. Meeresunters 21, 271–291. https://doi.org/10.1007/BF01609062

Lüning, K., 1969a. Growth of amputated and dark-exposed individuals of the brown alga *Laminaria hyperborea.* Marine Biology. 2, 218–223. https://doi.org/10.1007/BF00351143

Lüning, K., 1969b. Standing crop and leaf area index of the sublittoral *Laminaria* species near Helgoland. Marine Biology 3, 282–286. https://doi.org/10.1007/BF00360961

Lüning, K., Müller, D.G., 1978. Chemical interaction in sexual reproduction of several Laminariales (Phaeophyceae): release and attraction of spermatozoids. Zeitschrift für Pflanzenphysiologie 89, 333–341. https://doi.org/10.1016/S0044-328X(78)80006-3

Lüning, K., Schmitz, K., Willenbrink, J., 1973. CO2 fixation and translocation in benthic marine algae. III. Rates and ecological significance of translocation in *Laminaria hyperborea* and *L. saccharina.* Marine Biology 23, 275–281. https://doi.org/10.1007/BF00389334

MacLeod, A., Orr, K., Greenhill, L., Burrows, M., 2014. Understanding the Potential Effects of Wave Energy Devices on Kelp Biotopes. (No. 783). Scottish Natural Heritage.

Macreadie, P.I., Anton, A., Raven, J.A., Beaumont, N., Connolly, R.M., Friess, D.A., Kelleway, J.J., Kennedy, H., Kuwae, T., Lavery, P.S., Lovelock, C.E., Smale, D.A., Apostolaki, E.T., Atwood, T.B., Baldock, J., Bianchi, T.S., Chmura, G.L., Eyre, B.D., Fourqurean, J.W., Hall-Spencer, J.M., Huxham, M., Hendriks, I.E., Krause-Jensen, D., Laffoley, D., Luisetti, T., Marbà, N., Masque, P., McGlathery, K.J., Megonigal, J.P., Murdiyarso, D., Russell, B.D., Santos, R., Serrano, O., Silliman, B.R., Watanabe, K., Duarte, C.M., 2019. The future of Blue Carbon science. Nature Communications 10, 3998. https://doi.org/10.1038/s41467-019-11693-w

Marques, G.M., Mateus, M., Domingos, T., 2014. Can we reach consensus between marine ecological models and DEB theory? A look at primary producers. Journal of Sea Research, Dynamic Energy Budget theory: applications in marine sciences and fishery biology 94, 92–104. https://doi.org/10.1016/j.seares.2014.09.007

McHugh, D.J., 2003. A guide to the seaweed industry. Food and Agriculture Organization of the United Nations Rome.

Mcleod, E., Chmura, G.L., Bouillon, S., Salm, R., Björk, M., Duarte, C.M., Lovelock, C.E., Schlesinger, W.H., Silliman, B.R., 2011. A blueprint for blue carbon: toward an improved understanding of the role of vegetated coastal habitats in sequestering CO2. Frontiers in Ecology and the Environment 9, 552–560. https://doi.org/10.1890/110004

Michaelis, L., Menten, M.L., 1913. Die kinetik der invertinwirkung. Biochemistry. 49, 352. https://doi.org/10.1021/bi201284u

Michaelis, L., Menten, M.M.L., 2013. The kinetics of invertin action. FEBS Letters 587, 2712–2720. https://doi.org/10.1016/j.febslet.2013.07.015

Miehle, P., Battaglia, M., Sands, P.J., Forrester, D.I., Feikema, P.M., Livesley, S.J., Morris, J.D., Arndt, S.K., 2009. A comparison of four process-based models and a statistical regression model to predict growth of *Eucalyptus globulus* plantations. Ecological Modelling 220, 734–746. https://doi.org/10.1016/j.ecolmodel.2008.12.010

Mork, M., 1996. The effect of kelp in wave damping. Sarsia 80, 323–327. https://doi.org/10.1080/00364827.1996.10413607

Naylor, R.L., Hardy, R.W., Buschmann, A.H., Bush, S.R., Cao, L., Klinger, D.H., Little, D.C., Lubchenco, J., Shumway, S.E., Troell, M., 2021. A 20-year retrospective review of global aquaculture. Nature 591, 551–563. https://doi.org/10.1038/s41586-021-03308-6

Nisbet, R.M., Bence, J.R., 1989. Alternative Dynamic Regimes for Canopy-Forming Kelp: A Variant on Density-Vague Population Regulation. The American Naturalist 134, 377–408. https://doi.org/10.1086/284987

Nisbet, R.M., Jusup, M., Klanjscek, T., Pecquerie, L., 2012. Integrating dynamic energy budget (DEB) theory with traditional bioenergetic models. Journal of Experimental Biology 215, 892–902. https://doi.org/10.1242/jeb.059675

Nisbet, R.M., Muller, E.B., Lika, K., Kooijman, S.A.L.M., 2000. From Molecules to Ecosystems through Dynamic Energy Budget Models. Journal of Animal Ecology 69, 913–926. https://doi.org/10.1111/j.1365-2656.2000.00448.x

Norderhaug, K.M., Christie, H., Andersen, G.S., Bekkby, T., 2012. Does the diversity of kelp forest macrofauna increase with wave exposure? Journal of Sea Research 69, 36–42. https://doi.org/10.1016/j.seares.2012.01.004

Norton, T.A., 1992. Dispersal by macroalgae. British Phycological Journal 27, 293–301. https://doi.org/10.1080/00071619200650271

Norton, T.A., Hiscock, K., Kitching, J.A., 1977. The Ecology of Lough Ine: XX. The *Laminaria* Forest at Carrigathorna. Journal of Ecology 65, 919–941. https://doi.org/10.2307/2259386

Paine, E.R., Schmid, M., Boyd, P.W., Diaz-Pulido, G., Hurd, C.L., 2021. Rate and fate of dissolved organic carbon release by seaweeds: A missing link in the coastal ocean carbon cycle. Journal of Phycology 57, 1375–1391. https://doi.org/10.1111/jpy.13198

Pedersen, M., Nejrup, L., Fredriksen, S., Christie, H., Norderhaug, K., 2012. Effects of wave exposure on population structure, demography, biomass and productivity of the kelp *Laminaria hyperborea*. Marine Ecology Progress Series. 451, 45–60. https://doi.org/10.3354/meps09594

Pessarrodona, A., Foggo, A., Smale, D.A., 2019. Can ecosystem functioning be maintained despite climate-driven shifts in species composition? Insights from novel marine forests. Journal of Ecology 107, 91–104. https://doi.org/10.1111/1365-2745.13053

Pessarrodona, A., Moore, P.J., Sayer, M.D.J., Smale, D.A., 2018. Carbon assimilation and transfer through kelp forests in the NE Atlantic is diminished under a warmer ocean climate. Global Change Biology 24, 4386–4398. https://doi.org/10.1111/gcb.14303

Pueschel, C.M., Korb, R.E., 2001. Storage of nitrogen in the form of protein bodies in the kelp *Laminaria solidungula.* Marine Ecology Progress Series 218, 107–114. https://doi.org/10.3354/meps218107

Raybaud, V., Beaugrand, G., Goberville, E., Delebecq, G., Destombe, C., Valero, M., Davoult, D., Morin, P., Gevaert, F., 2013. Decline in Kelp in West Europe and Climate. PLOS ONE 8, e66044. https://doi.org/10.1371/journal.pone.0066044

Rees, A.P., Owens, N.J.P., Heath, M.R., Plummer, D.H., Bellerby, R.S., 1995. Seasonal nitrogen assimilation and carbon fixation in a fjordic sea loch. Journal of Plankton Research 17, 1307–1324. https://doi.org/10.1093/plankt/17.6.1307

Rinde, E., 2007. Studies of processes in *Laminaria hyperborea* kelp forest ecosystems, contribution to a scientifically based resource management. (Doctoral dissertation, University of Oslo). Faculty of Mathematics and Natural Sciences, University of Oslo, Norway.

Rinde, E., Sjøtun, K., 2005. Demographic variation in the kelp *Laminaria hyperborea* along a latitudinal gradient. Marine Biology 146, 1051–1062. https://doi.org/10.1007/s00227-004-1513-5

Roughgarden, J., Iwasa, Y., Baxter, C., 1985. Demographic Theory for an Open Marine Population with Space-Limited Recruitment. Ecology 66, 54–67. https://doi.org/10.2307/1941306

Schiener, P., Black, K.D., Stanley, M.S., Green, D.H., 2015. The seasonal variation in the chemical composition of the kelp species *Laminaria digitata*, *Laminaria hyperborea*, *Saccharina latissima* and *Alaria esculenta.* Journal of Applied Phycology 27, 363–373. https://doi.org/10.1007/s10811-014-0327-1

Schmid, M., Guihéneuf, F., Nitschke, U., Stengel, D.B., 2021. Acclimation potential and biochemical response of four temperate macroalgae to light and future seasonal temperature scenarios. Algal Research 54, 102190. https://doi.org/10.1016/j.algal.2021.102190

Sharma, S., Neves, L., Funderud, J., Mydland, L.T., Øverland, M., Horn, S.J., 2018. Seasonal and depth variations in the chemical composition of cultivated *Saccharina latissima*. Algal Research 32, 107–112. https://doi.org/10.1016/j.algal.2018.03.012

Sheppard, C. R. C., Jupp, B. P., Sheppard, A. L. S. and Bellamy, D. J.. "Studies on the Growth of *Laminaria hyperborea* (Gunn.) Fosl. and *Laminaria ochroleuca* De La Pylaie on the French Channel Coast" Botanica Marina, vol. 21, no. 2, 1978, pp. 109-116. https://doi.org/10.1515/botm.1978.21.2.109

Sieburth, J.McN., 1969. Studies on algal substances in the sea. III. The production of extracellular organic matter by littoral marine algae. Journal of Experimental Marine Biology and Ecology 3, 290–309. https://doi.org/10.1016/0022-0981(69)90052-5

Sjøtun, K., 1993. Seasonal Lamina Growth in two Age Groups of *Laminaria saccharina* (L.) Lamour. in Western Norway 36, 433–442. https://doi.org/10.1515/botm.1993.36.5.433

Sjøtun, K., Christie, H., Helge Fosså, J., 2006. The combined effect of canopy shading and sea urchin grazing on recruitment in kelp forest (*Laminaria hyperborea*). Marine Biology Research 2, 24–32. https://doi.org/10.1080/17451000500537418

Sjøtun, K., Fredriksen, S., 1995. Growth allocation in *Laminaria hyperborea* (Laminariales, Phaeophyceae) in relation to age and wave exposure. Marine Ecology Progress Series 126, 213–222. https://doi.org/10.3354/meps126213

Sjøtun, K., Fredriksen, S., Rueness, J., 1998. Effect of canopy biomass and wave exposure on growth in *Laminaria hyperborea* (Laminariaceae: Phaeophyta). European Journal of Phycology 33, 337–343. https://doi.org/10.1080/09670269810001736833

Sjøtun, K., Fredriksen, S., Rueness, J., 1996. Seasonal growth and carbon and nitrogen content in canopy and first-year plants of *Laminaria hyperborea* (Laminariales, Phaeophyceae). Phycologia 35, 1–8. https://doi.org/10.2216/i0031-8884-35-1-1.1

Slangen, A.B.A., Carson, M., Katsman, C.A., van de Wal, R.S.W., Köhl, A., Vermeersen, L.L.A., Stammer, D., 2014. Projecting twenty-first century regional sea-level changes. Climatic Change 124, 317–332. https://doi.org/10.1007/s10584-014-1080-9

Slesser, G., Turrell, B., 2013. Annual cycles of physical, chemical and biological parameters in Scottish waters (2013 update). https://doi.org/10.13140/RG.2.1.2381.4649

Slesser, G., & Turrell, W. R. (1999). Annual Cycles of physical chemical and biological parameters in Scottish Waters (1999 Update). Marine Laboratory, Aberdeen Report No 1, 99.

Smale, D.A., 2020. Impacts of ocean warming on kelp forest ecosystems. New Phytologist 225, 1447–1454. https://doi.org/10.1111/nph.16107

Smale, D.A., Burrows, M.T., Evans, A.J., King, N., Sayer, M.D.J., Yunnie, A.L.E., Moore, P.J., 2016. Linking environmental variables with regional-scale variability in ecological structure and standing stock of carbon within UK kelp forests. Marine Ecology Progress Series 542, 79–95. https://doi.org/10.3354/meps11544

Smale, D.A., Burrows, M.T., Moore, P., O'Connor, N., Hawkins, S.J., 2013. Threats and knowledge gaps for ecosystem services provided by kelp forests: a northeast Atlantic perspective. Ecology and evolution 3, 4016–4038. https://doi.org/10.1002/ece3.774

Smale, D.A., Moore, P.J., 2017. Variability in kelp forest structure along a latitudinal gradient in ocean temperature. Journal of Experimental Marine Biology and Ecology 486, 255–264. https://doi.org/10.1016/j.jembe.2016.10.023

Smale, D.A., Pessarrodona, A., King, N., Burrows, M.T., Yunnie, A., Vance, T., Moore, P., 2020. Environmental factors influencing primary productivity of the forest-forming kelp *Laminaria hyperborea* in the northeast Atlantic. Scientific Reports. 10, 12161. https://doi.org/10.1038/s41598-020-69238-x

Smale, D.A., Wernberg, T., Yunnie, A.L.E., Vance, T., 2015. The rise of *Laminaria ochroleuca* in the Western English Channel (UK) and comparisons with its competitor and assemblage dominant *Laminaria hyperborea*. Marine Ecology 36, 1033–1044. https://doi.org/10.1111/maec.12199

Smith, K.E., Moore, P.J., King, N.G., Smale, D.A., 2022. Examining the influence of regional-scale variability in temperature and light availability on the depth distribution of subtidal kelp forests. Limnology and Oceanography 67, 314–328. https://doi.org/10.1002/lno.11994

Sousa, T., Domingos, T., Kooijman, S.A.L.M., 2008. From empirical patterns to theory: a formal metabolic theory of life. Philosophical Transactions of the Royal Society B: Biological Sciences 363, 2453–2464. https://doi.org/10.1098/rstb.2007.2230

Sousa, T., Domingos, T., Poggiale, J.C., Kooijman, S.A.L.M., 2010. Introduction: Dynamic energy budget theory restores coherence in biology. Philosophical Transactions: Biological Sciences 365, 3413–3428.

Srinivasan, B., 2022. A guide to the Michaelis–Menten equation: steady state and beyond. The FEBS Journal 289, 6086–6098. https://doi.org/10.1111/febs.16124

Starko, S., Soto Gomez, M., Darby, H., Demes, K.W., Kawai, H., Yotsukura, N., Lindstrom, S.C., Keeling, P.J., Graham, S.W., Martone, P.T., 2019. A comprehensive kelp phylogeny sheds light on the evolution of an ecosystem. Molecular Phylogenetics and Evolution 136, 138–150. https://doi.org/10.1016/j.ympev.2019.04.012

Steen, H., Moy, F.E., Bodvin, T., Husa, V., 2016. Regrowth after kelp harvesting in Nord-Trøndelag, Norway. ICES Journal of Marine Science. 73, 2708–2720. https://doi.org/10.1093/icesjms/fsw130

Steneck, R.S., Graham, M.H., Bourque, B.J., Corbett, D., Erlandson, J.M., Estes, J.A., Tegner, M.J., 2002. Kelp forest ecosystems: biodiversity, stability, resilience and future. Environmental Conservation 29, 436–459. https://doi.org/10.1017/S0376892902000322

Strong-Wright, J., & Taylor, J. R. (2022). Modeling the growth potential of the kelp *Saccharina latissima* in the North Atlantic. Frontiers in Marine Science, 8, 793977. https://doi.org/10.3389/fmars.2021.793977

Tanaka, H., Huang, M.C., Watanabe, A., 2023. The Environmental and Economic Potential of Kelp as Blue Carbon: Case of Hakodate, Japan, in: Wu, H.-H., Liu, W.-Y., Huang, M.C. (Eds.), Moving Toward Net-Zero Carbon Society: Challenges and Opportunities. Springer International Publishing, Cham, pp. 107–117. https://doi.org/10.1007/978-3-031-24545-9_7

Taylor, K.E., Stouffer, R.J., Meehl, G.A., 2012. An overview of CMIP5 and the experiment design. Bulletin of the American meteorological Society 93, 485–498. https://doi.org/10.1175/BAMS-D-11-00094.1

Teagle, H., Hawkins, S.J., Moore, P.J., Smale, D.A., 2017. The role of kelp species as biogenic habitat formers in coastal marine ecosystems. Journal of Experimental Marine Biology and Ecology, Ecological responses to environmental change in marine systems 492, 81–98. https://doi.org/10.1016/j.jembe.2017.01.017

Tsiamis, K., Salomidi, M., Gerakaris, V., Mogg, A.O.M., Porter, E.S., Sayer, M.D.J., Küpper, F.C., 2020. Macroalgal vegetation on a north European artificial reef (Loch Linnhe, Scotland): biodiversity, community types and role of abiotic factors. Journal of Applied Phycology 32, 1353–1363. https://doi.org/10.1007/s10811-019-01918-2

Umbarger, H.E., 1956. Evidence for a Negative-Feedback Mechanism in the Biosynthesis of Isoleucine. Science 123, 848–848. https://doi.org/10.1126/science.123.3202.848.a

van der Meer, J., 2006. Metabolic theories in ecology. Trends in Ecology & Evolution 21, 136–140. https://doi.org/10.1016/j.tree.2005.11.004

van der Molen, J., Aldridge, J.N., Coughlan, C., Parker, E.R., Stephens, D., Ruardij, P., 2013. Modelling marine ecosystem response to climate change and trawling in the North Sea. Biogeochemistry 113, 213–236. https://doi.org/10.1007/s10533-012-9763-7

van der Molen, J., Ruardij, P., Mooney, K., Kerrison, P., O'Connor, N.E., Gorman, E., Timmermans, K., Wright, S., Kelly, M., Hughes, A.D., Capuzzo, E., 2018. Modelling potential production of macroalgae farms in UK and Dutch coastal waters. Biogeosciences 15, 1123–1147. https://doi.org/10.5194/bg-15-1123-2018

Venolia, C.T., Lavaud, R., Green-Gavrielidis, L.A., Thornber, C., Humphries, A.T., 2020. Modeling the Growth of Sugar Kelp (*Saccharina latissima*) in Aquaculture Systems using Dynamic Energy Budget Theory. Ecological Modelling 430, 109151. https://doi.org/10.1016/j.ecolmodel.2020.109151

Von Bertalanffy, L., 1957. Quantitative laws in metabolism and growth. The quarterly review of biology 32, 217–231. https://doi.org/10.1086/401873

von Liebig, J.F., Playfair, L.P.B., 1843. Chemistry in its application to agriculture and physiology. JM Campbell & Company. https://doi.org/10.5962/bhl.title.45143

Wei, N., Quarterman, J., Jin, Y.-S., 2013. Marine macroalgae: an untapped resource for producing fuels and chemicals. Trends in Biotechnology 31, 70–77. https://doi.org/10.1016/j.tibtech.2012.10.009

Weigel, B.L., Pfister, C.A., 2021. The dynamics and stoichiometry of dissolved organic carbon release by kelp. Ecology 102, e03221. https://doi.org/10.1002/ecy.3221

Wernberg, T., Krumhansl, K., Filbee-Dexter, K., Pedersen, M.F., 2019. Status and Trends for the World's Kelp Forests, in: World Seas: An Environmental Evaluation. Elsevier, pp. 57–78. https://doi.org/10.1016/B978-0-12-805052-1.00003-6

Whittick, A., 1969. The kelp forest ecosystem at Petticoe Wick Bay lat 55 55'N. Long 2 09'W: an ecological study (Masters). Durham University, England.

Zhu, L., Huguenard, K., Zou, Q.-P., Fredriksson, D.W., Xie, D., 2020. Aquaculture farms as nature-based coastal protection: Random wave attenuation by suspended and submerged canopies. Coastal Engineering 160, 103737. https://doi.org/10.1016/j.coastaleng.2020.103737

Zonneveld, C., Kooijman, S., 1993. Comparative kinetics of embryo development. Bulletin of Mathematical Biology 55, 609–635.

7 Supplementary material

7.1 Scotland West Coast environmental data

7.1.1 Description of the study area

Loch Linnhe is a significant fjord located on Scotland's west coast, characterized by a sequence of long, narrow basins connected by shallow sills (Edwards and Sharples, 1986). The system's primary basins are known as the Inner (landward) and Outer (seaward) basins (Figure 7.1). The Inner basin measures 10 km by 2 km with a maximum depth of 155 m, and is separated from the Outer basin, which is 30 km by 5 km with a maximum depth of 200 m, by the Corran Narrows sill (0.27 km wide and 10 m deep). Additional smaller basins are connected to both the Inner and Outer basins, also via shallow sills. The area is largely remote, with the exception of the town of Fort William situated at the head of the Inner basin, where most of the freshwater input from the area's only major river enters the system. The watershed experiences high rainfall (>2000 mm/year), resulting in pronounced thermohaline stratification throughout the year. The Outer basin extends to the continental shelf west of Scotland through the Sound of Mull and Firth of Lorne, which are well-mixed coastal sea areas featuring numerous islands and reefs (Figure 7.1). The tidal amplitude in the region is substantial (approximately 3.5 m), leading to significant mixing between basins across the shallow sills.

Planktonic primary production in Loch Linnhe's basins is primarily controlled by turbidity, with nutrients playing a minimal role in limiting phytoplankton production (Rees et al., 1995). The zooplankton community within the loch is mainly composed of small neritic calanoid species, benthic invertebrate larvae, euphausiids, and planktonic decapods. The area provides habitat for large populations of juvenile gadoid and clupeoid fish and is considered an important nursery area. There is some spawning activity by cod and whiting, and adult sprat shoals are commonly observed during the winter (Cooper 1980, De Silva 1973, Gordon 1977).

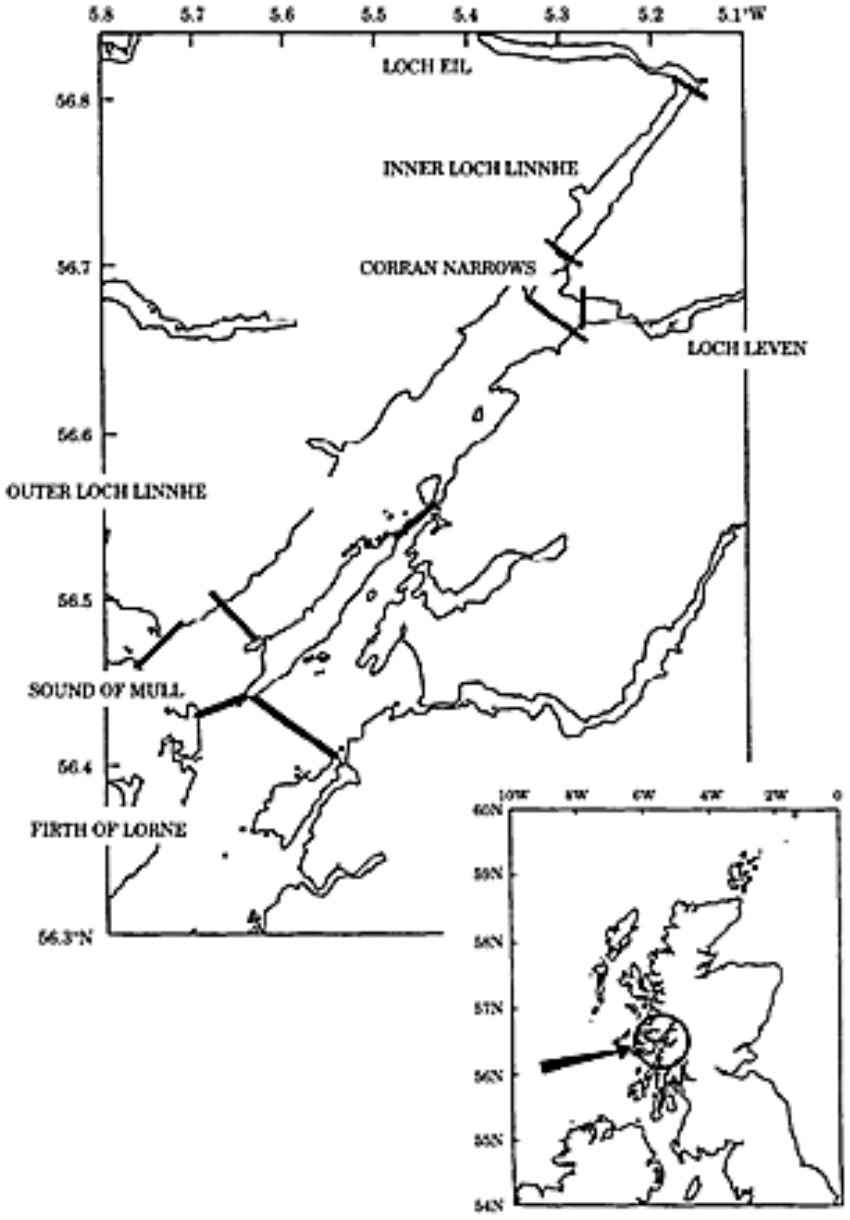

Figure 7.1. Loch Linnhe survey region and the various basins of the system (from Heath, 1995, permission to use given by the author).

Field sampling programme

Sampling in Loch Linnhe was conducted during 12 surveys at roughly 30-day intervals using the vessel "Lough Foyle" in 1991. Each survey included the loch and an adjacent open sea area, employing three main methods:

1. The ARIES system (Dunn et al., 1993) was towed along a vertically undulating track following the loch's axis and extending out to sea (refer to Heath, 1996, 1995a)

2. Instruments were towed at a fixed depth of 4 m alongside the vessel, tracing a horizontally undulating "zig-zag" path across the loch.

3. The vessel also stationed at specific locations in the Inner and Outer basins and the Firth of Lorne, where instruments were vertically deployed and water samples were collected. These samples were used for plankton analysis and live experiments to assess primary production rates, ammonia excretion, feeding rates of zooplankton, and nutrient fluxes in seabed sediments (see Rees et al., 1995).

The focus here is on the vertically undulating and fixed-depth zig-zag surveys.

Additionally, moorings were deployed on each survey and retrieved during the subsequent one. Each mooring was equipped with Recording Current Meters (RCM) and sensors to measure temperature, salinity, nitrate, and chlorophyll fluorescence.

A PAR irradiance sensor, recording hourly averaged data throughout the year, was installed on the roof of the nearby Dunstaffnage Marine Laboratory.

Vertically undulating survey

The ARIES system used for the vertically undulating survey was equipped with several sampling units: (a) a plankton net with a serial sampling coded capable of collecting up to 100 independent samples during a tow, (b) a 60-bottle rosette sampler, (c) a high-resolution oceanographic conductivity-temperature-depth (CTD) instrument (Seabird Electronics), (d) a data logger for sensors measuring fluorescence, PAR irradiance, transparency, and oxygen, (e) an Optical Plankton Counter (OPC) from Focal Technology, and (f) an acoustic transducer that transmitted real-time depth information to the towing vessel. This discussion focuses on data collected from the rosette sampler and CTD.

The system was towed at a speed of 2 m/s, with undulations achieved by adjusting the towing wire length. Each dive reached a maximum depth approximately 7 m above the seabed, subject to safety limits. Ascent and descent rates were maintained at about 0.2 m/s, with undulations averaging a wavelength of roughly 1000 m. The 70 km axial section was completed in five separate tows, each lasting around 100 minutes. The distribution of the water samples can be seen in Figure 7.2. Tows were primarily conducted during daylight hours due to navigational safety requirements.

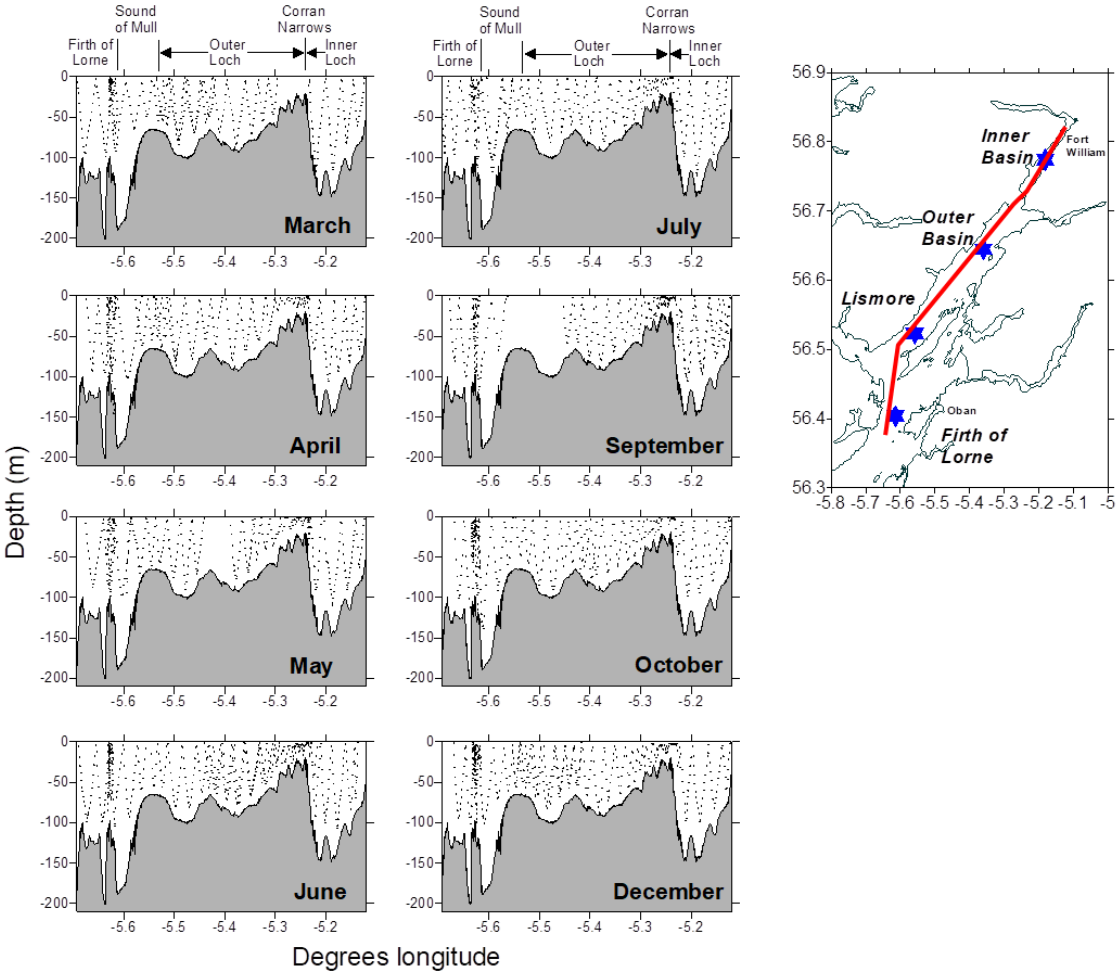

Figure 7.2. Distributions of water samples from ARIES rosette bottles collected along specific vertically undulating tow tracks during each survey are shown. The inset map features blue stars marking the point-station sampling locations, while the red line represents the path of the undulating towed survey track. Figure unpublished by the Prof. Heath and given with permission for this thesis, data gathered during Heath, 1991 sampling

The CTD and data-logging systems on ARIES were synchronized with the ship's GPS navigation system. During each tow, navigational and echo-sounder data were recorded every 60 seconds aboard the vessel. Each sample was then spatially located (latitude, longitude, depth, and altitude above the seabed) by interpolating the recorded times and positions of the vessel to the recorded time of the underwater data (Figure 7.3).

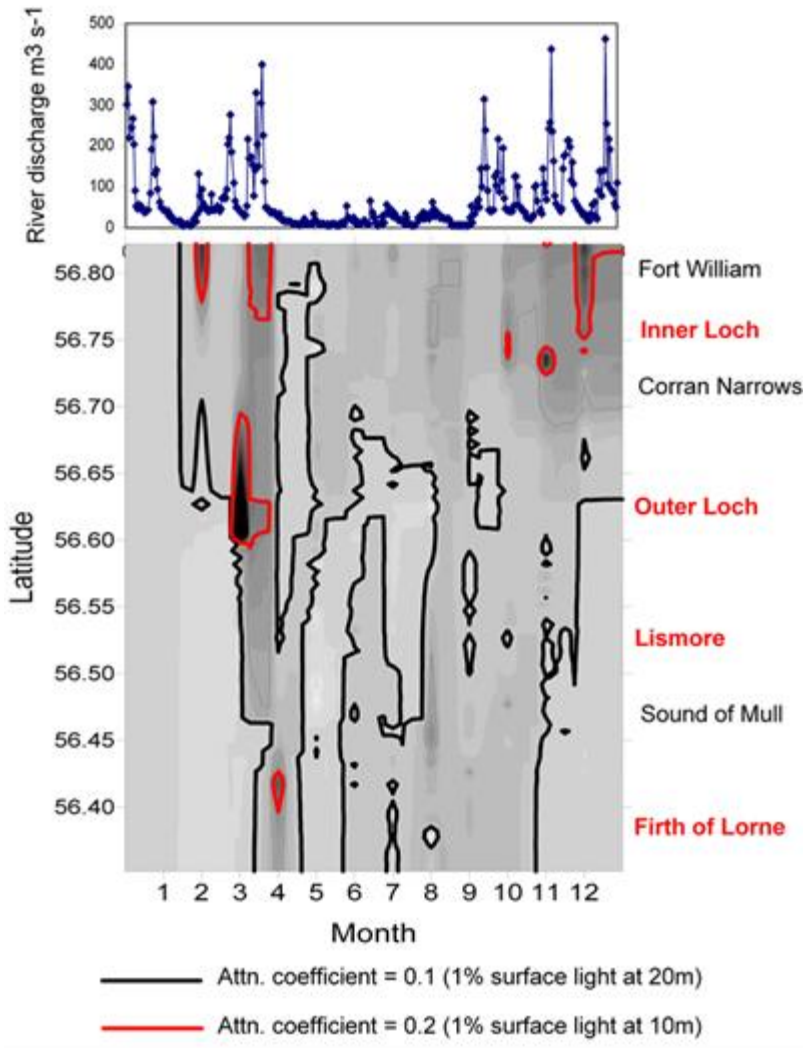

Figure 7.3. Space-time variations in light attenuation coefficients from the vertically undulating tow surveys are depicted. The upper panel displays the flow rate of freshwater from rivers into Loch Linnhe throughout the year. Some peaks in light attenuation align with periods of high river runoff, while others correspond with phytoplankton blooms, as shown in the chlorophyll panel of the zig-zag survey synthesis (Figure unpublished by the Prof. Heath and given with permission for this thesis, data gathered during Heath, 1991 sampling).

The rosette sampler was programmed to collect water samples at 120-second intervals. CTD data were logged at one-second intervals. Water samples were analysed for nitrate and ammonia, with a subset from each tow filtered for chlorophyll analysis or retained for salinity determination to calibrate the CTD (Figure 7.4).

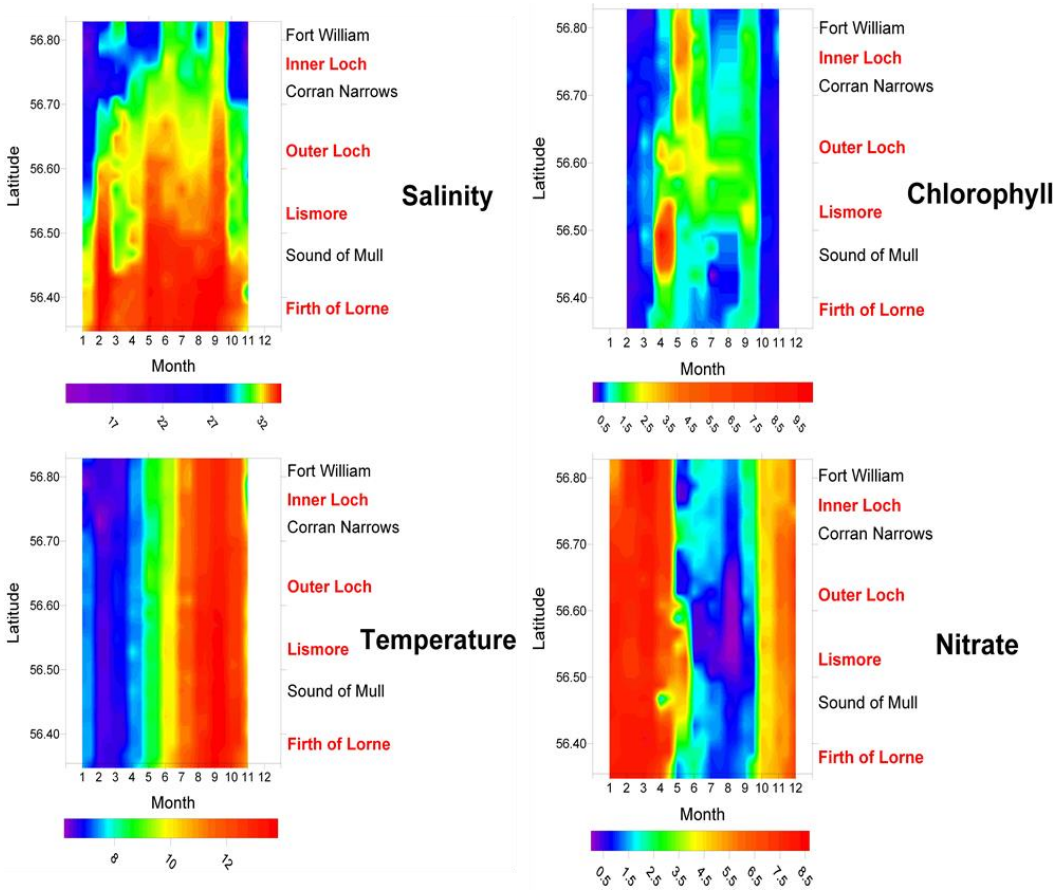

Figure 7.4. Compilation of data from the fixed depth (4m) zig-zag towed surveys Figure unpublished by the Prof. Heath and given with permission for this thesis, data gathered during Heath, 1991 sampling).

Fixed depth zig-zag survey

The fixed depth (4 m) zig-zag surveys were conducted using a re-purposed side-scan sonar tow-fish, deployed from a boom alongside the vessel, with the vessel traveling at speeds of 3–4 m s^{-1}. The tow-fish was equipped with a CTD, along with sensors for measuring chlorophyll fluorescence and transparency. A hose attached to the tow cable continuously pumped water aboard the vessel, feeding into a continuous flow nitrate auto-analyser. The auto-analyser data were electronically digitized at 60-second intervals. Additional point location water samples were taken from the pump flow every 5 minutes for ammonia analysis and for filtering for chlorophyll analysis.

As with the ARIES surveys, navigational data and water depth information from an echo-sounder were continuously recorded and later merged with the environmental data collected from the various instruments. Each survey covered a tow track of approximately 150 km (Figure 7.5).

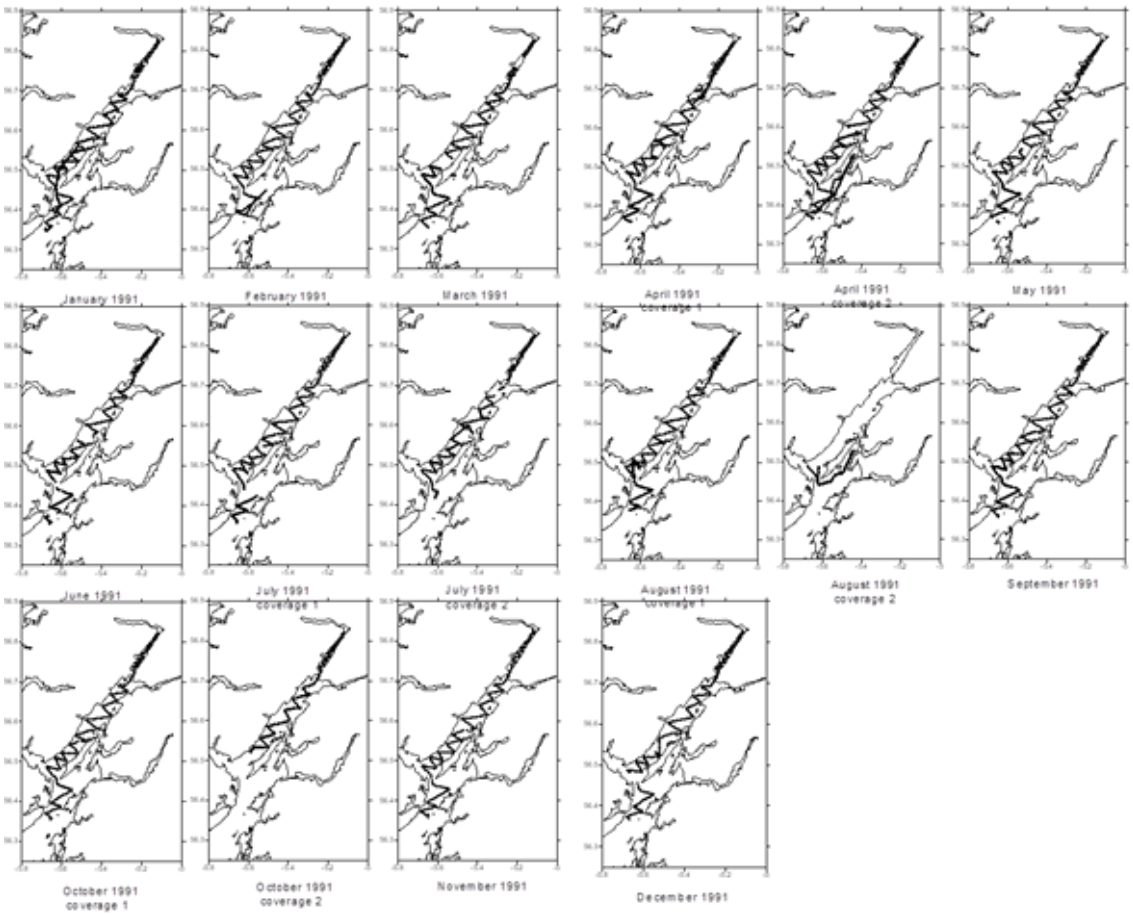

Figure 7.5. Fixed-depth zig-zag survey tracks were used for each survey up until 1991. (Figure unpublished by the Prof. Heath and given with permission for this thesis, data gathered during Heath, 1991 sampling).

7.1.2 Analysis of the relevant data:

Light attenuation:

Each vertically undulating tow was broken down into individual descent and ascent legs, with PAR irradiance measured at 1-second intervals. The vertical attenuation coefficient was determined by performing a linear regression of the natural log-transformed PAR data against depth. The coefficient's location in time and space was referenced to the mean time, latitude, and longitude over the 1-second interval values for each leg.

Incoming surface irradiance:

Hourly averaged PAR data recorded from the roof of the Dunstaffnage Marine Laboratory were integrated over each consecutive day, resulting in a year-long time series of daily irradiance values ($E\ m^{-2}d^{-1}$).

Basin-scale averaging of data:

Attenuation coefficients were obtained from a total of 741 descent and ascent sections of the vertically undulating tows. The combined vertically undulating and horizontal zig-zag sampling methods collected 3023 nitrate measurements and 71,972 temperature measurements. The environmental data were grouped by month and latitude to estimate mean values by depth layer for the Inner Basin, Outer Basin, and Firth of Lorne regions within the survey area.

7.2 Parameter a and b calculation from empirical data

Table 7.1. Data from Kain, (1977) on the frond weight to area and nitrogen content relationship, used to calculate parameters the for coefficient of area to moles structure relationship and power of area scaling with structure.

Frond Wet weight g	Single Side Frond Area cm2	Total Frond Area cm2	Total Dry Weight g	Nitrogen Weight g	Nitrogen moles
10	152.585181	305.170363	6.6	0.17622	0.01258714
50	641.200952	1282.4019	33	0.8811	0.06293571
100	1162.44535	2324.8907	66	1.7622	0.12587143
500	4476.94134	8953.88268	330	8.811	0.62935714

Log (Frond Area cm2)	Log (Nitrogen moles)
2.484542354	-1.900072839
3.108024154	-1.201102834
3.36640254	-0.900072839
3.9520114	-0.201102834

Slope	Intercept
0.86357525	4.13500677

7.3 Constant Environment

In order to gain insights into the growth dynamics of the organism, the model's behaviour was examined under constant conditions. This preliminary analysis aimed to provide a comprehensive understanding of the growth curve that would manifest under such circumstances. By subjecting the model to a controlled environment with consistent environmental conditions, we sought to understand the intricacies of its growth dynamics and uncover the patterns that would emerge over time. This preliminary investigation served as a foundational step, laying the groundwork for subsequent analyses and enabling us to discern the fundamental characteristics and trends that would shape the growth trajectory of the model organism.

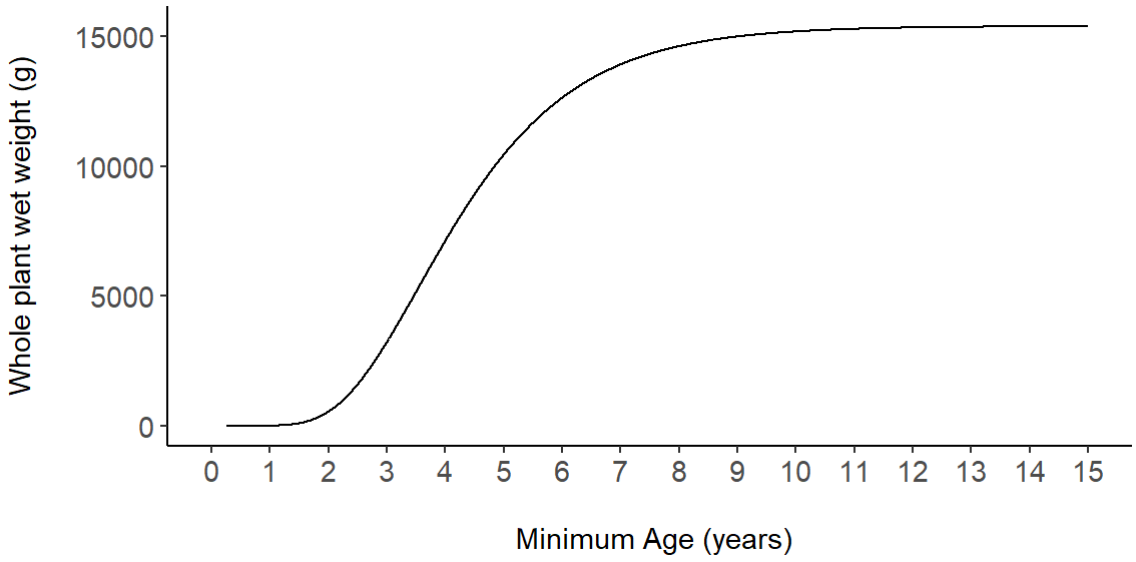

Figure 7.6. Whole plant wet weight growth curve for 15 years. Model output from structure and reserve of nitrogen and carbon moles converted to total plant wet weight.

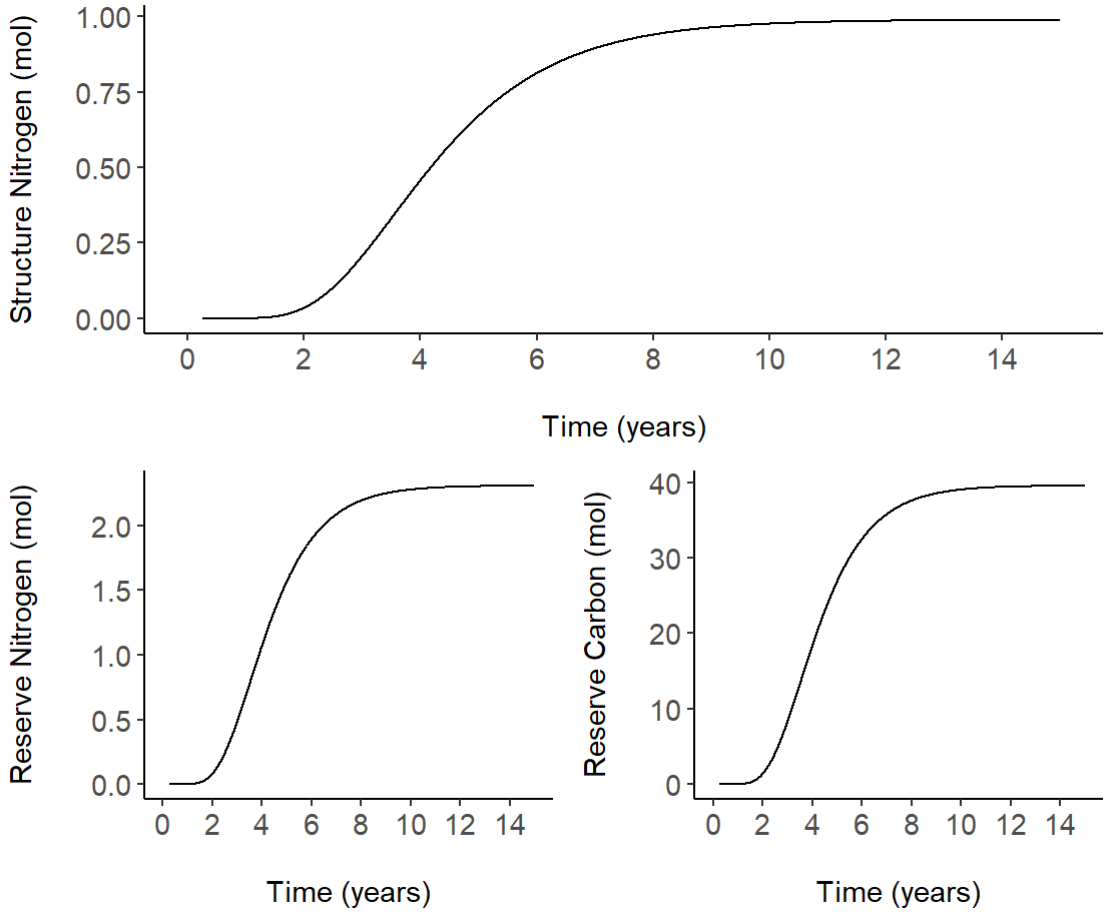

Figure 7.7. Model output, structure and reserve nitrogen, and reserve carbon, growth curves for 15 years simulation. Structure carbon follows a constant ratio from structure nitrogen.

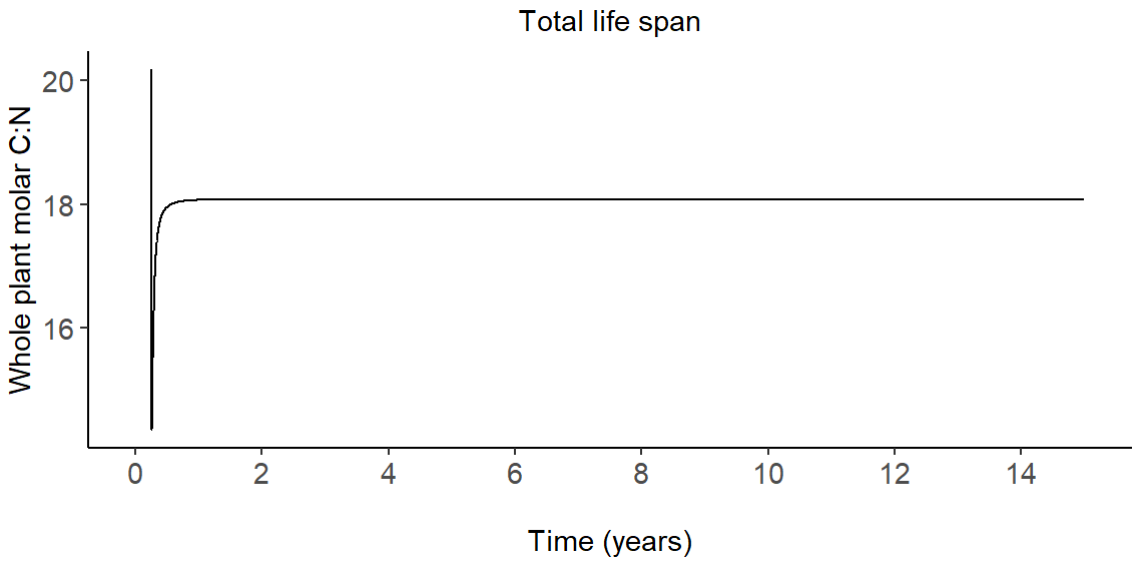

Figure 7.8. Modelled organism internal C:N ratio, considering both reserves and structure biochemical composition and quantity.

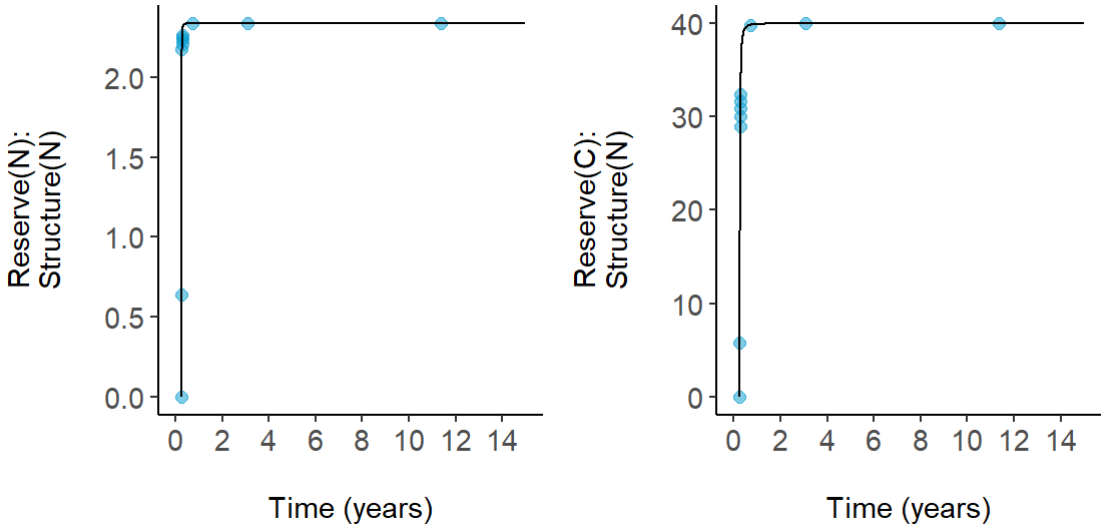

Figure 7.9. Reserves density for carbon and nitrogen based on structure nitrogen. Reflects the feeding conditions of the individual. The blue points show tie points in which the organism was nitrogen limited.

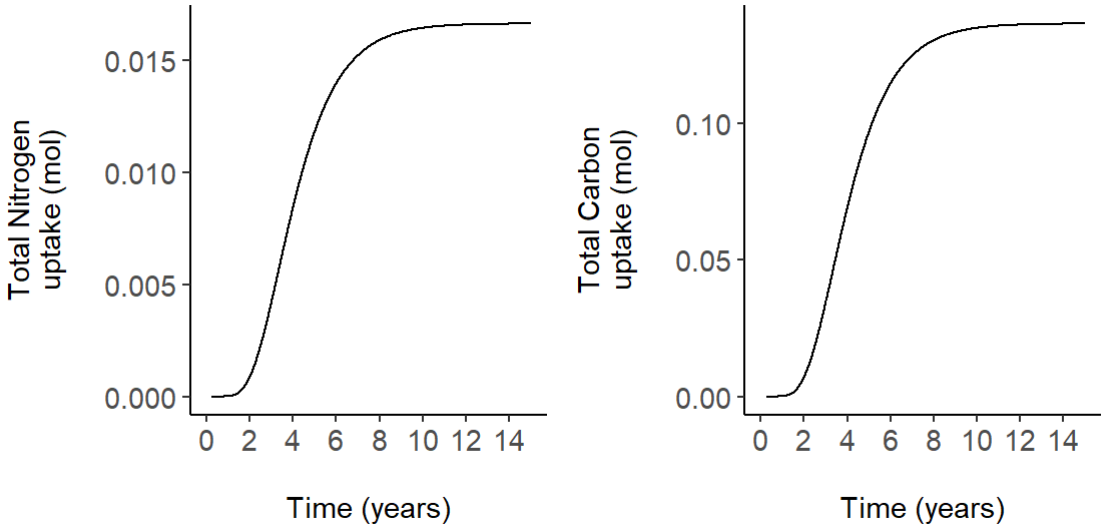

Figure 7.10. Uptake of nitrogen and carbon from the environment through the plants live.

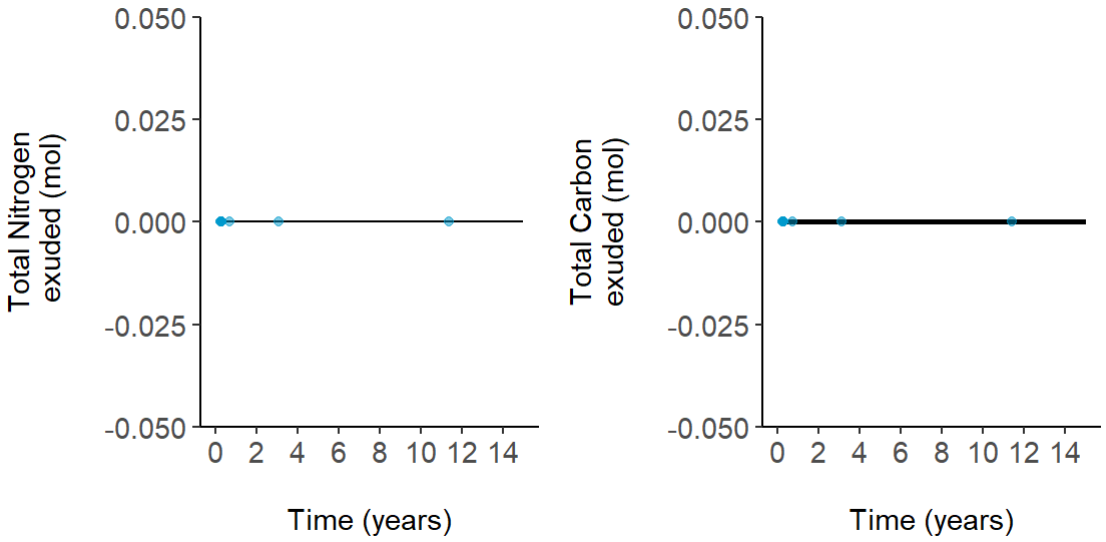

Figure 7.11. Amount of nitrogen and carbon exuded from the organism through its life. The blue points show tie points in which the organism was nitrogen limited.

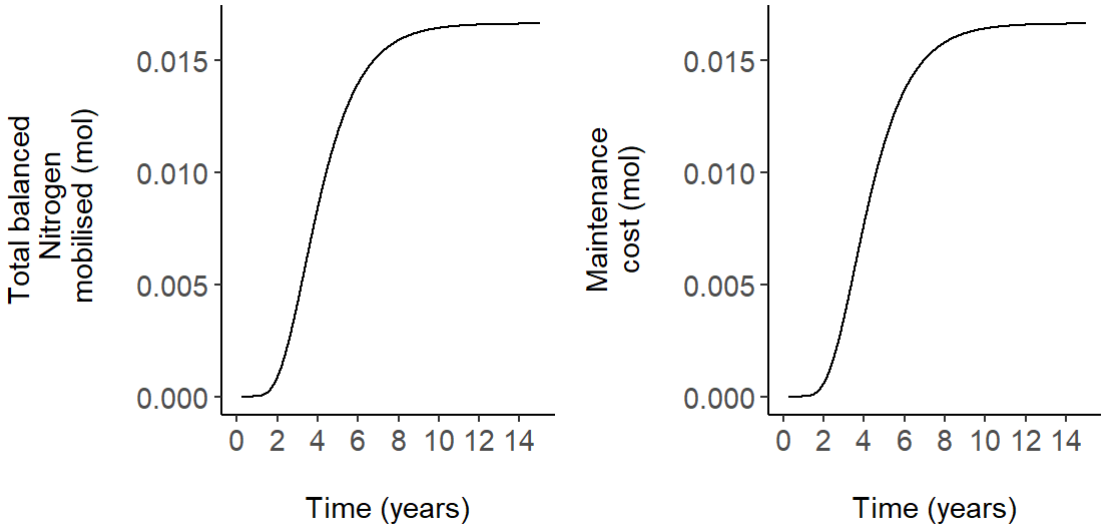

Figure 7.12. Stoichiometrically balanced nitrogen available for growth to the plant on the left. The maintenance cost paid is shown on the right.

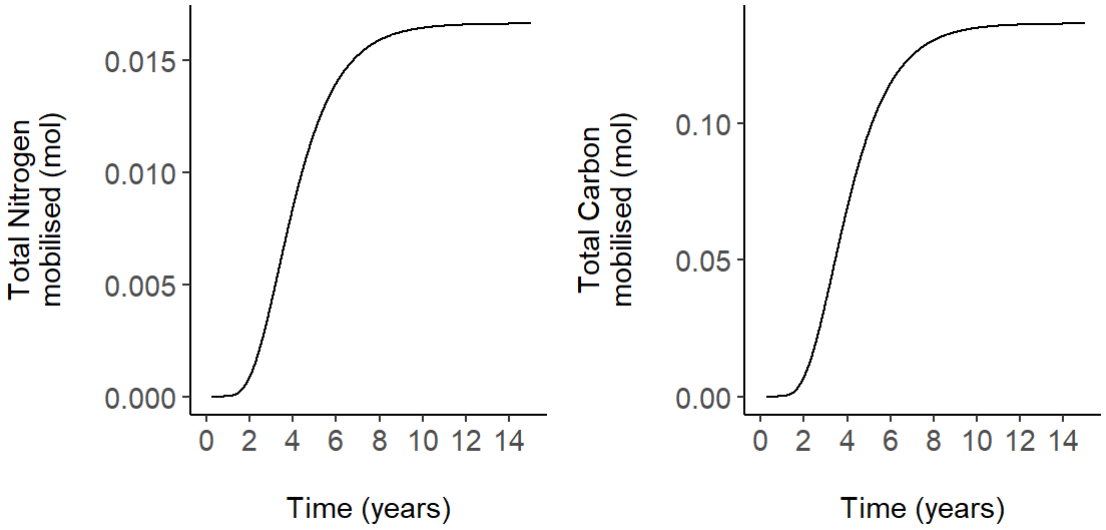

Figure 7.13. the amount of nitrogen and carbon mobilised from reserves, that is then balanced to follow a specific molar ratio before structural growth occurs

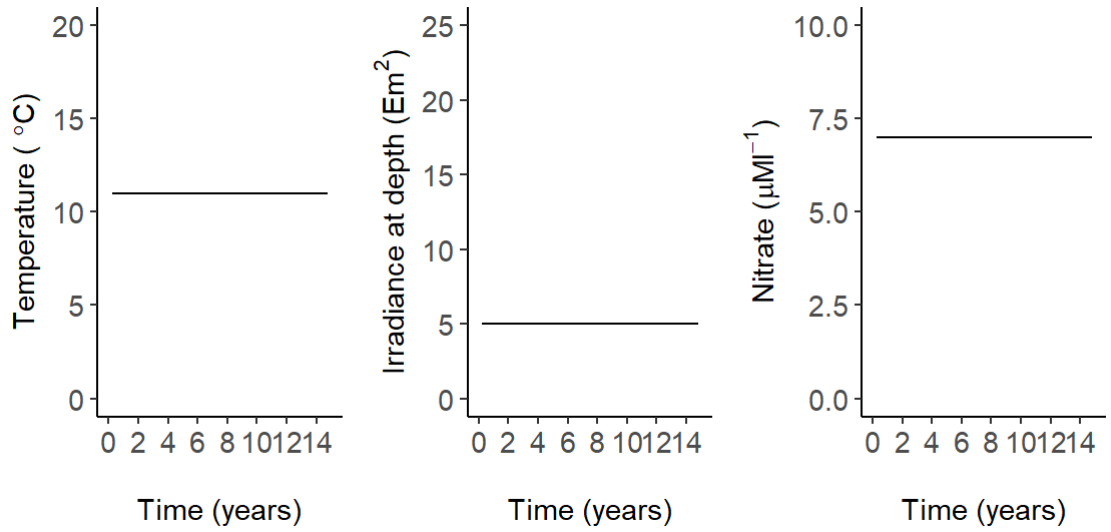

Figure 7.14. Environmental drivers under which the simulation takes place.

7.4 Cycling Environment

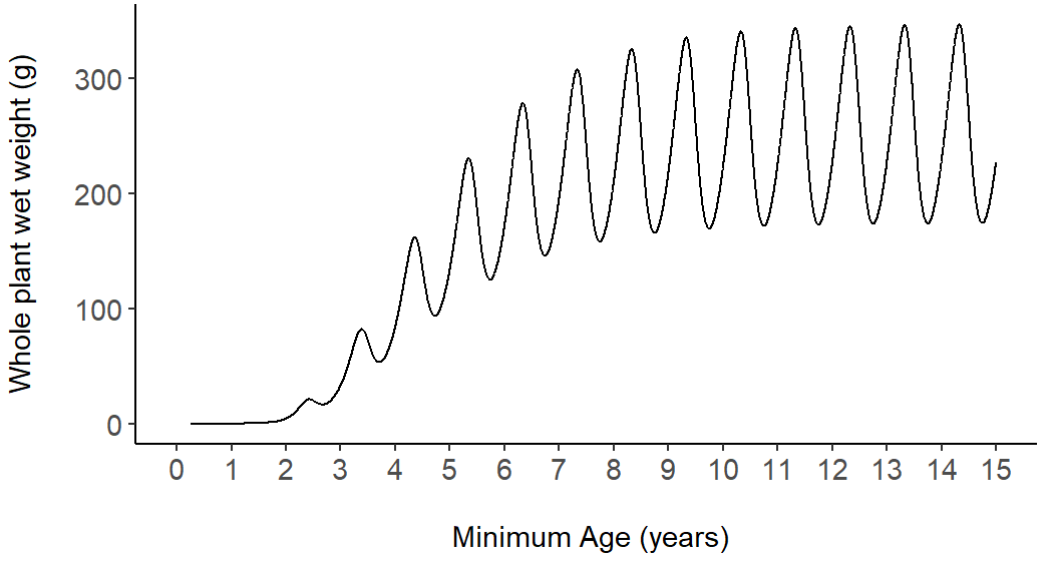

Figure 7.15. Whole plant wet weight growth curve for 15 years. Model output from structure and reserve of nitrogen and carbon moles converted to total plant wet weight.

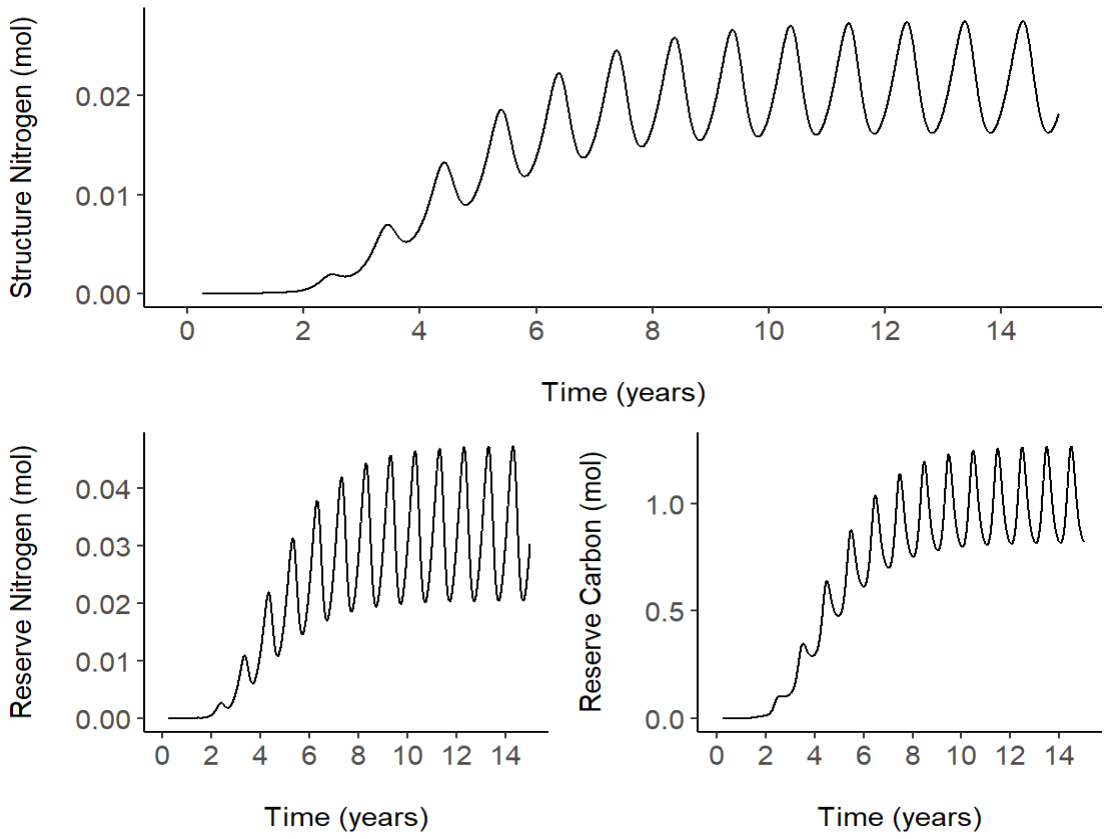

Figure 7.16. Model output, structure and reserve nitrogen, and reserve carbon, growth curves for 15 years simulation. Structure carbon follows a constant ratio from structure nitrogen.

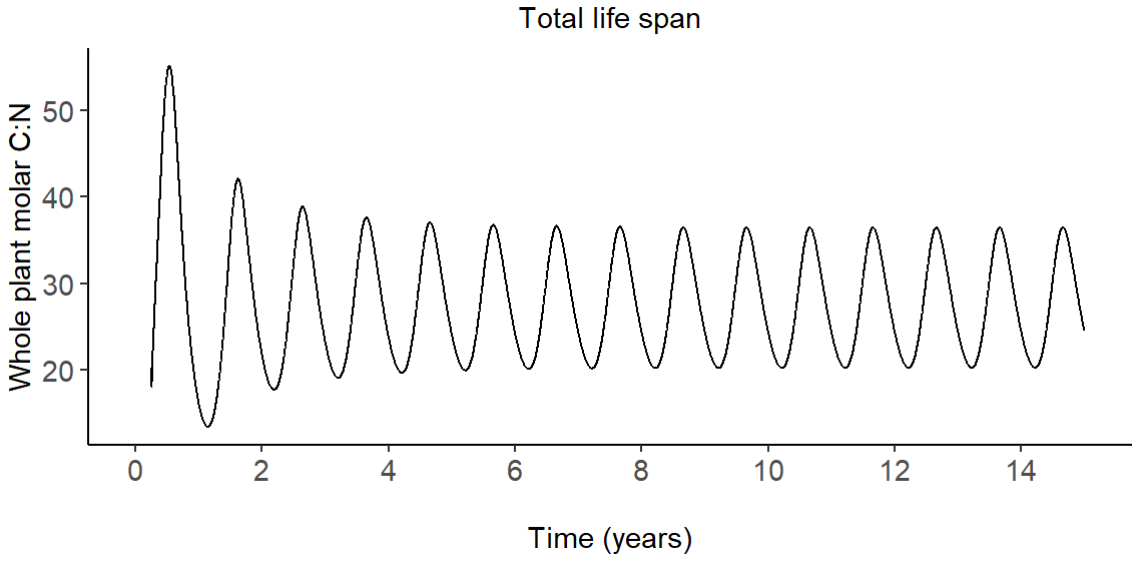

Figure 7.17. Modelled organism internal C:N ratio, considering both reserves and structure biochemical composition and quantity.

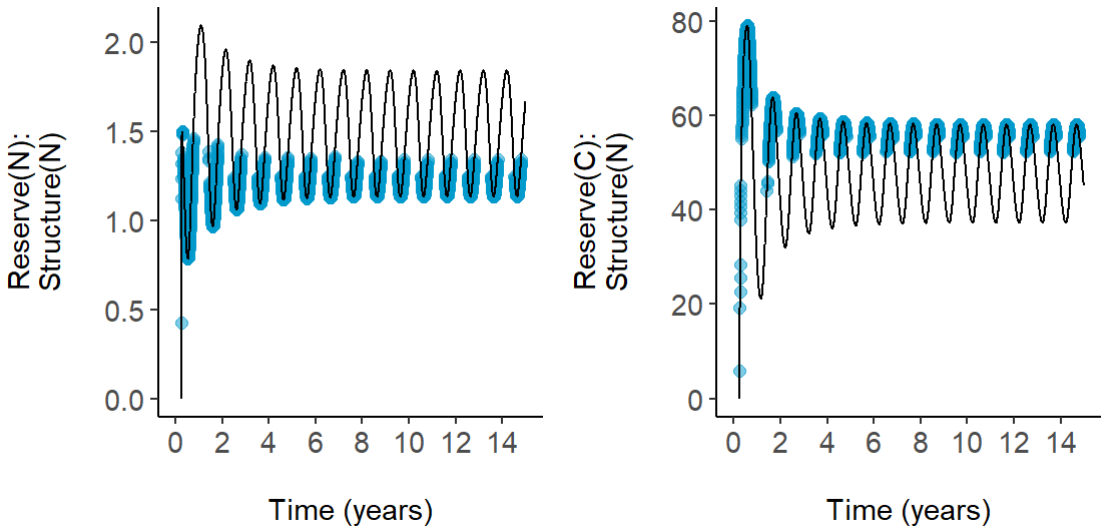

Figure 7.18. Reserves density for carbon and nitrogen based on structure nitrogen. Reflects the feeding conditions of the individual. The blue points show tie points in which the organism was nitrogen limited.

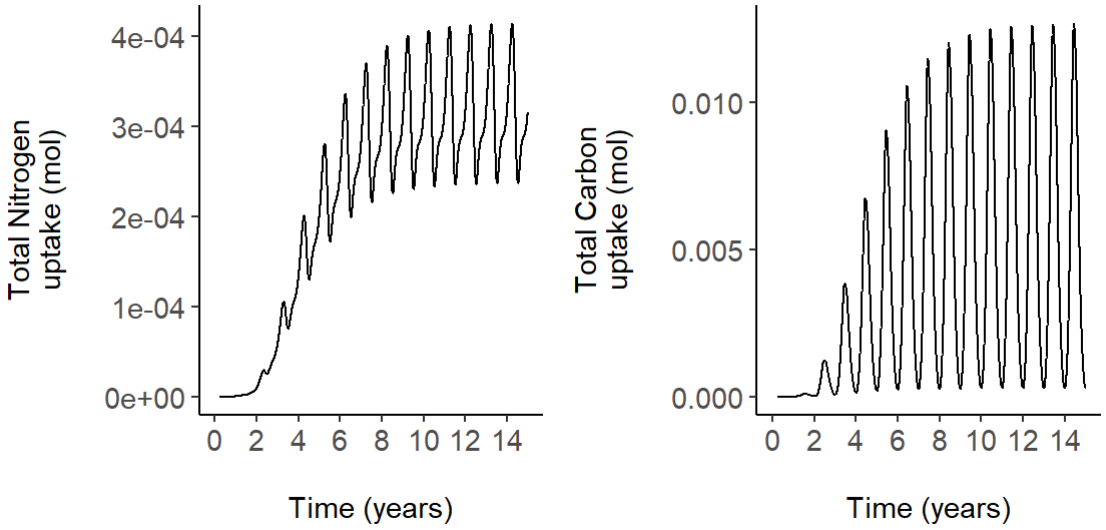

Figure 7.19. Uptake of nitrogen and carbon from the environment through the plants live.

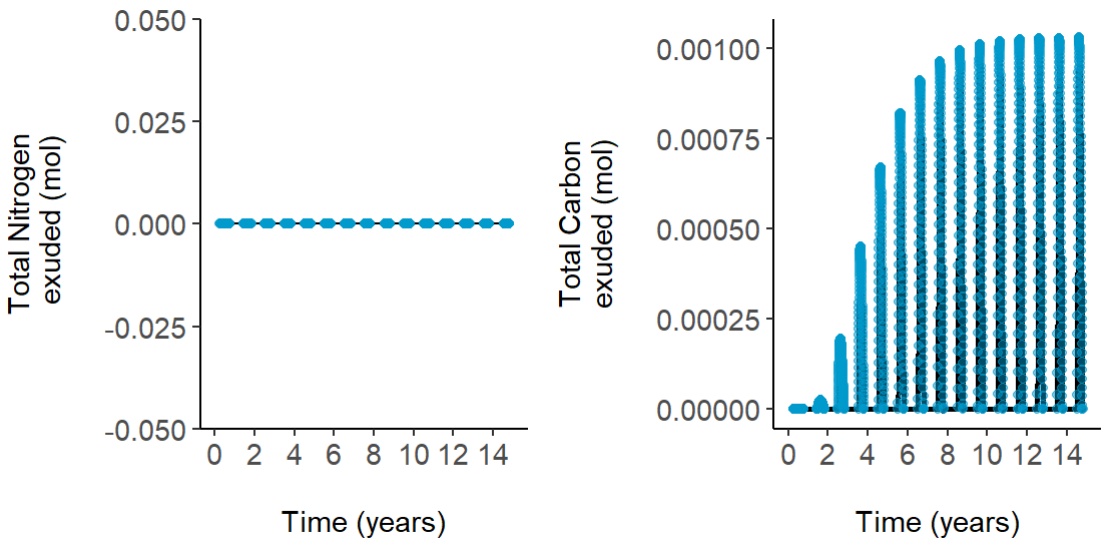

Figure 7.20. Amount of nitrogen and carbon exuded from the organism through its life. The blue points show tie points in which the organism was nitrogen limited.

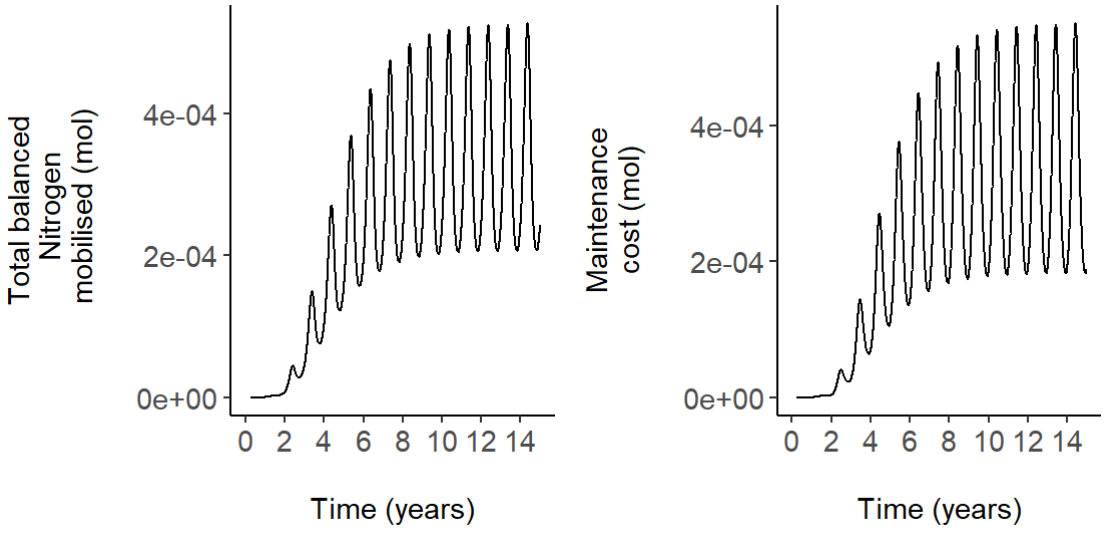

Figure 7.21. Stoichiometrically balanced nitrogen available for growth to the plant on the left. The maintenance cost paid is shown on the right.

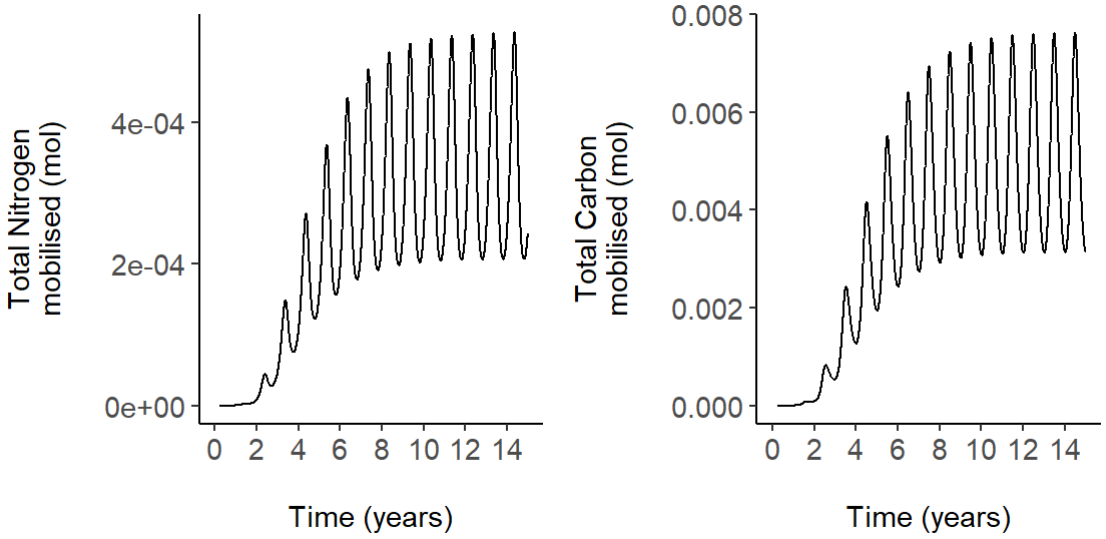

Figure 7.22. The amount of nitrogen and carbon mobilised from reserves, that is then balanced to follow a specific molar ratio before structural growth occurs.

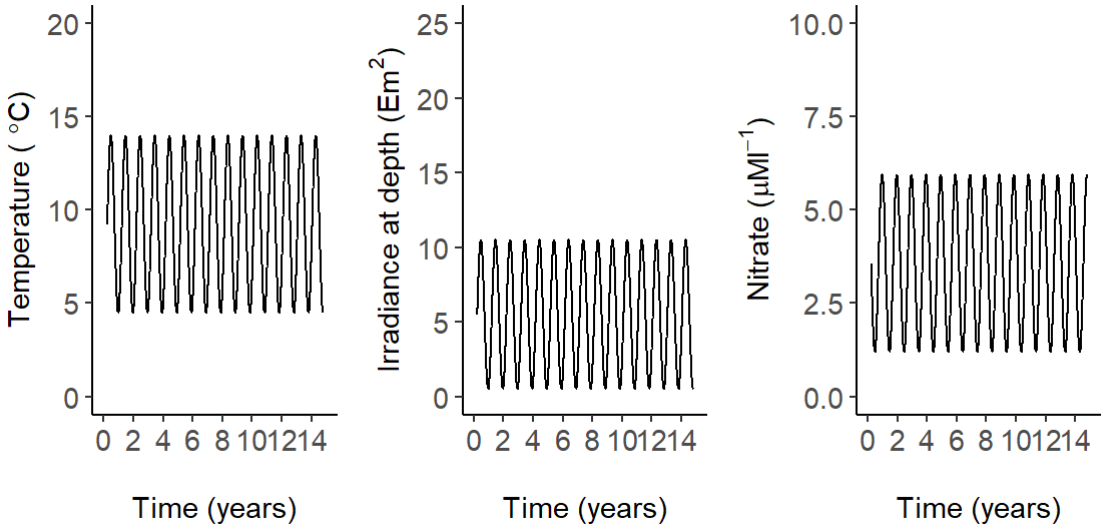

Figure 7.23. Environmental drivers under which the simulation takes place.

7.5 Starvation Experiments

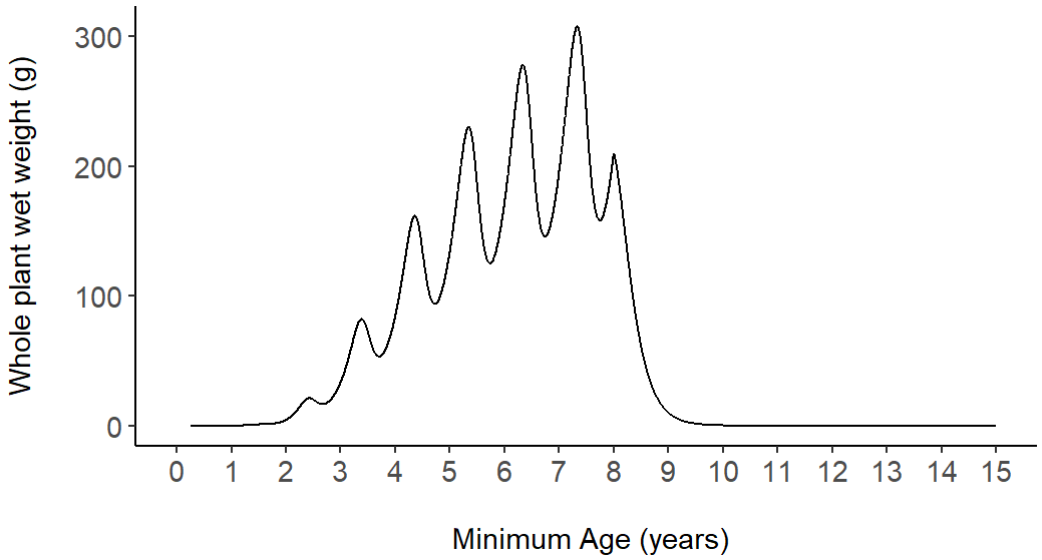

Figure 7.24. Whole plant wet weight growth curve for 15 years. Model output from structure and reserve of nitrogen and carbon moles converted to total plant wet weight.

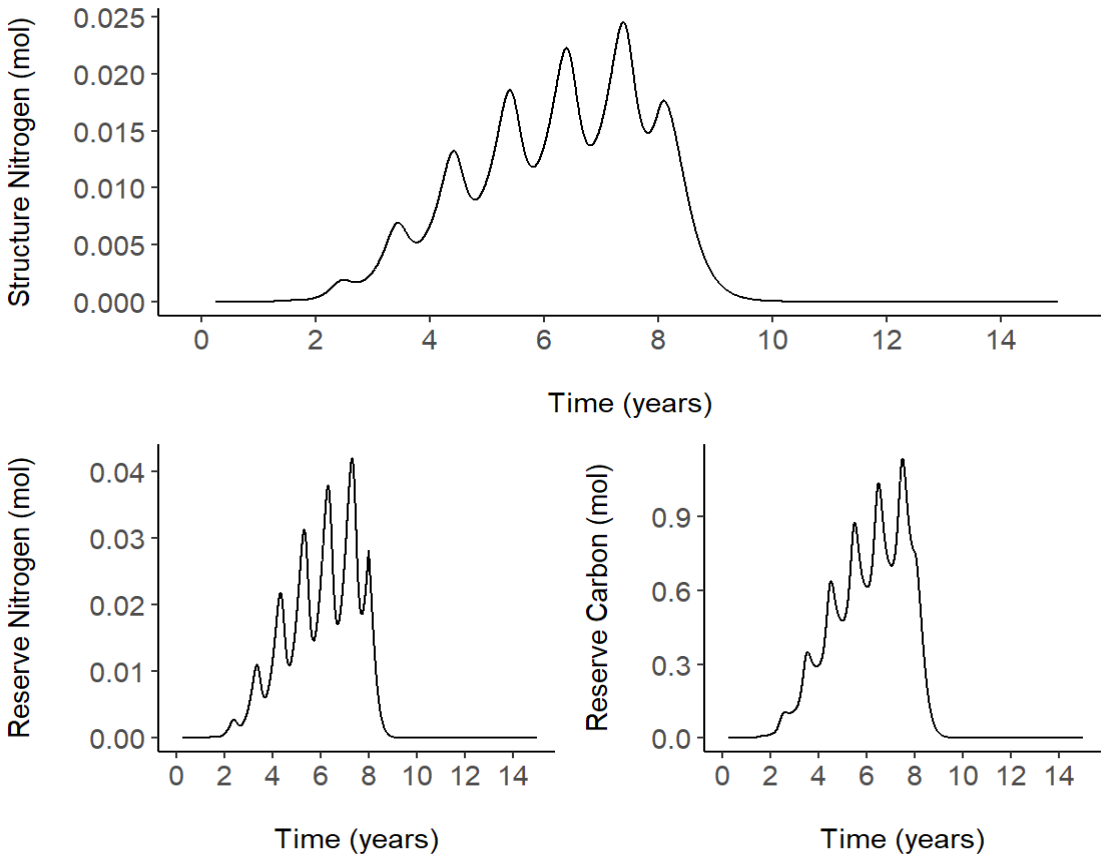

Figure 7.25. Model output, structure and reserve nitrogen, and reserve carbon, growth curves for 15 years simulation. Structure carbon follows a constant ratio from structure nitrogen.

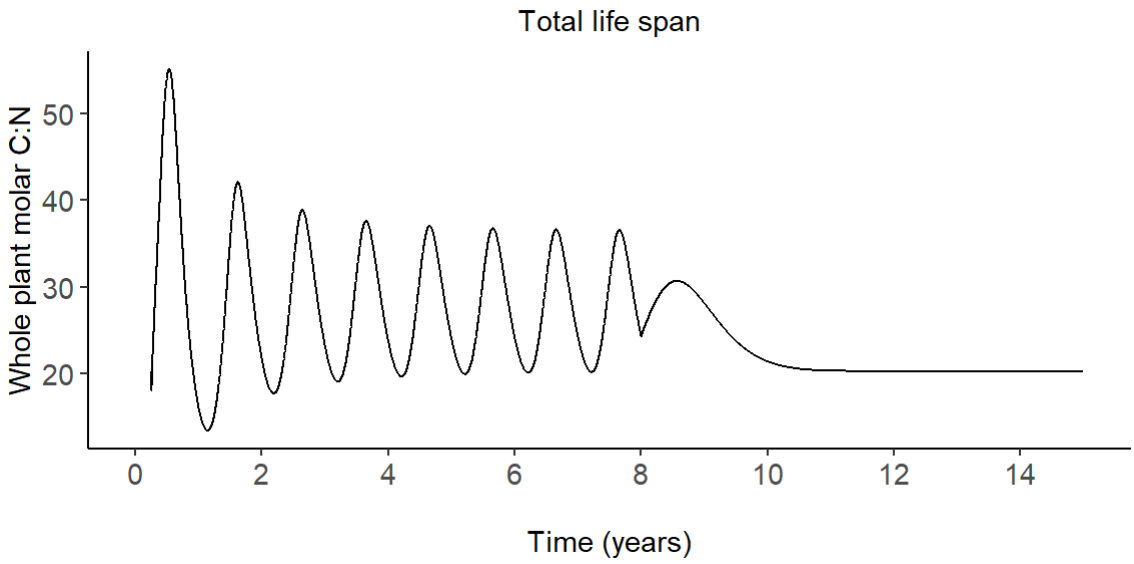

Figure 7.26. Modelled organism internal C:N ratio, considering both reserves and structure biochemical composition and quantity.

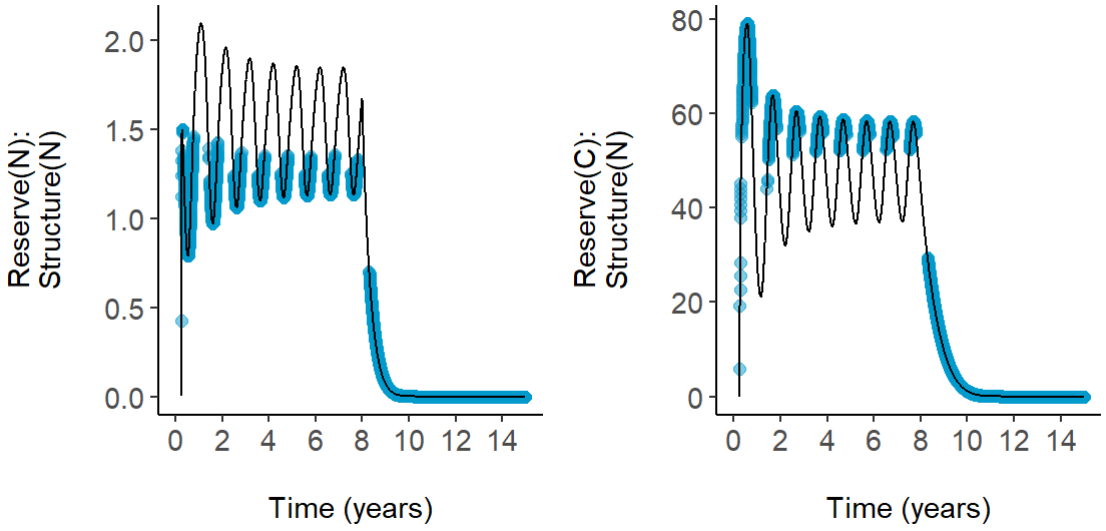

Figure 7.27. Reserves density for carbon and nitrogen based on structure nitrogen. Reflects the feeding conditions of the individual. The blue points show tie points in which the organism was nitrogen limited.

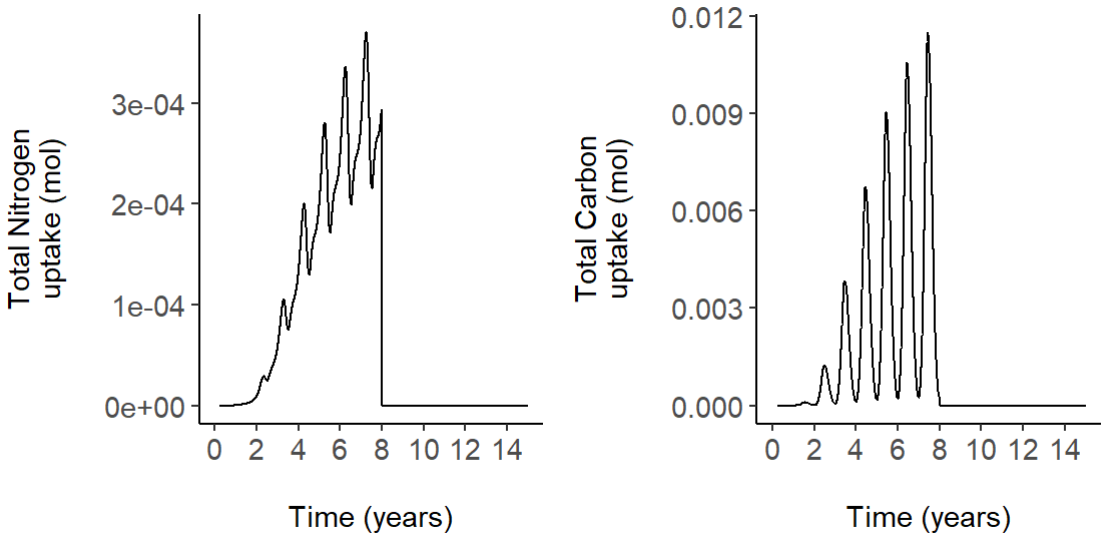

Figure 7.28. Uptake of nitrogen and carbon from the environment through the plants live.

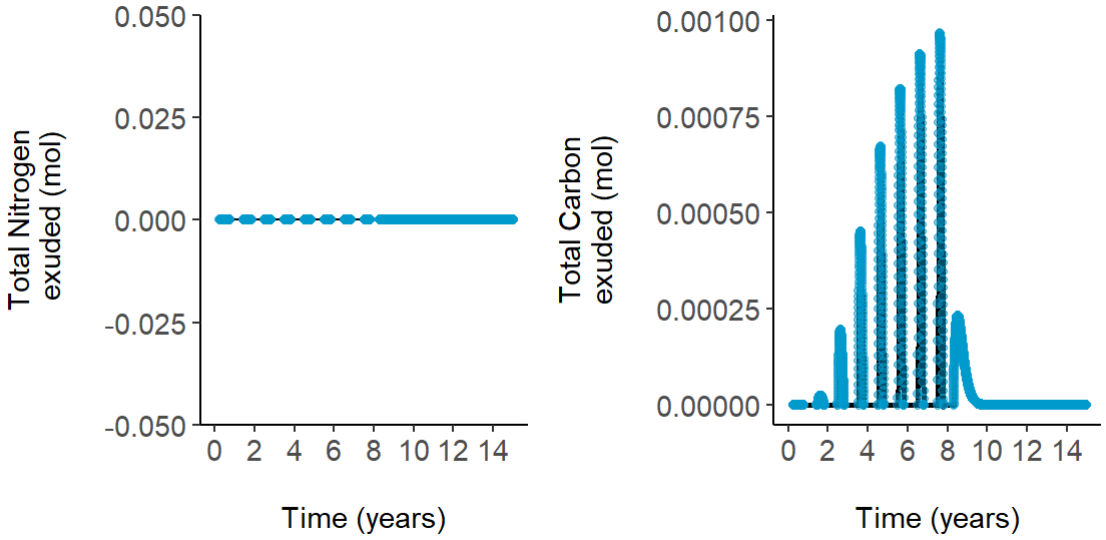

Figure 7.29. Amount of nitrogen and carbon exuded from the organism through its life. The blue points show tie points in which the organism was nitrogen limited.

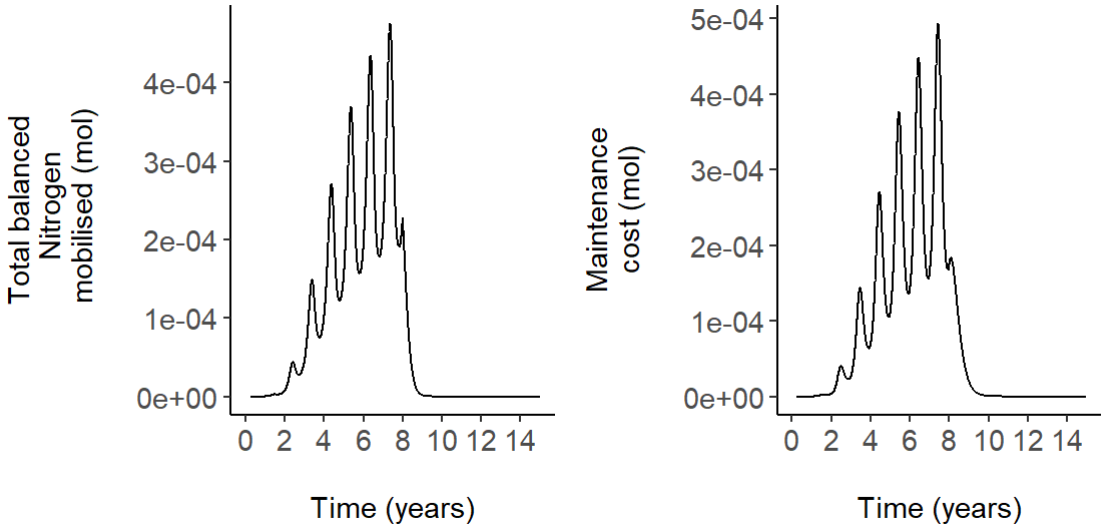

Figure 7.30. Stoichiometrically balanced nitrogen available for growth to the plant on the left. The maintenance cost paid is shown on the right.

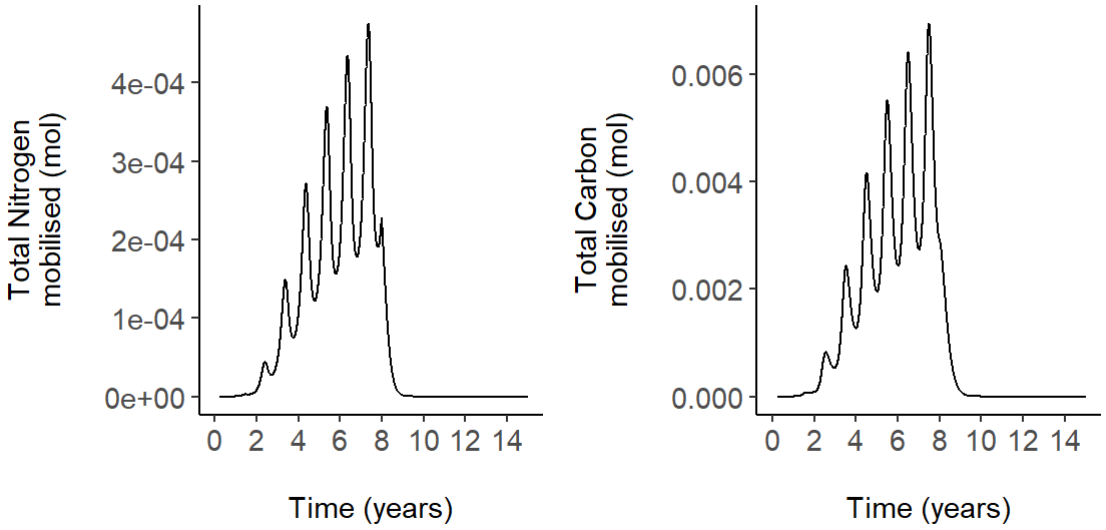

Figure 7.31. The amount of nitrogen and carbon mobilised from reserves, that is then balanced to follow a specific molar ratio before structural growth occurs.

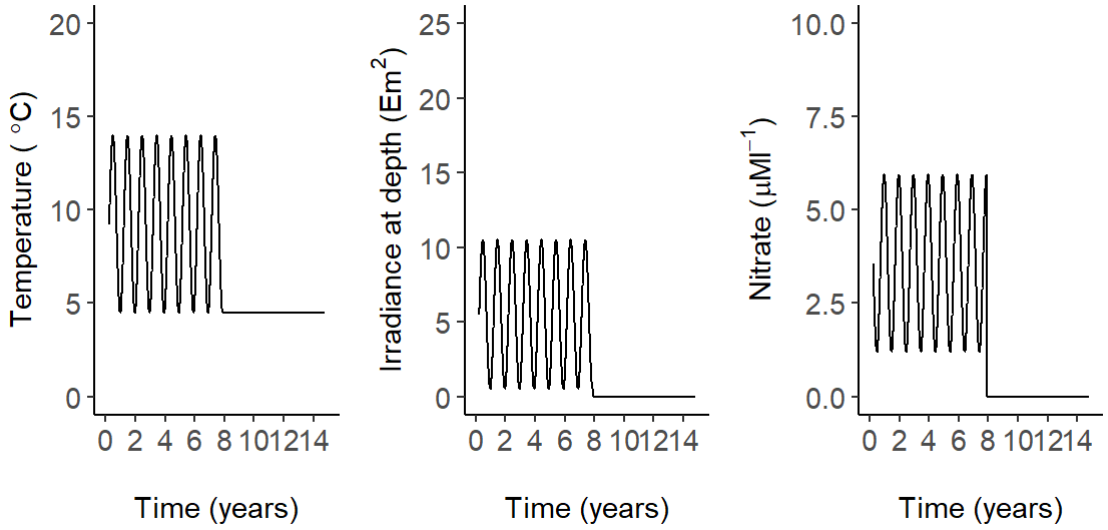

Figure 7.32. Environmental drivers under which the simulation takes place.

7.6 Light Attenuation Experiments

The Jupp (1972) data was gathered by sampling during a 15-month period. A cohort was not tracked, therefore the data we are fitting to is the mean weight of individuals at different ages and not the growth curve of a single individual as the simulation output. Due to this I have to consider that the growing conditions of the older plants sampled are not necessarily the same that those for the younger plants, additionally there is the effect of the older pants themselves are having on the younger ones. For example, the population at 9 m depth is older than that at 3 m.

Here I will be testing a scaling factors for the light attenuation for the first year of life, then removing it and using the raw cycle. This represents a beginning of their life in lower light conditions such as those caused by dense canopy shading.

Value	Parameter	Description
9	Δ	light attenuation coefficient scaling factor

It is important to note that the mean weight presented here represents a hypothetical individual that has had different light conditions during its growth period.

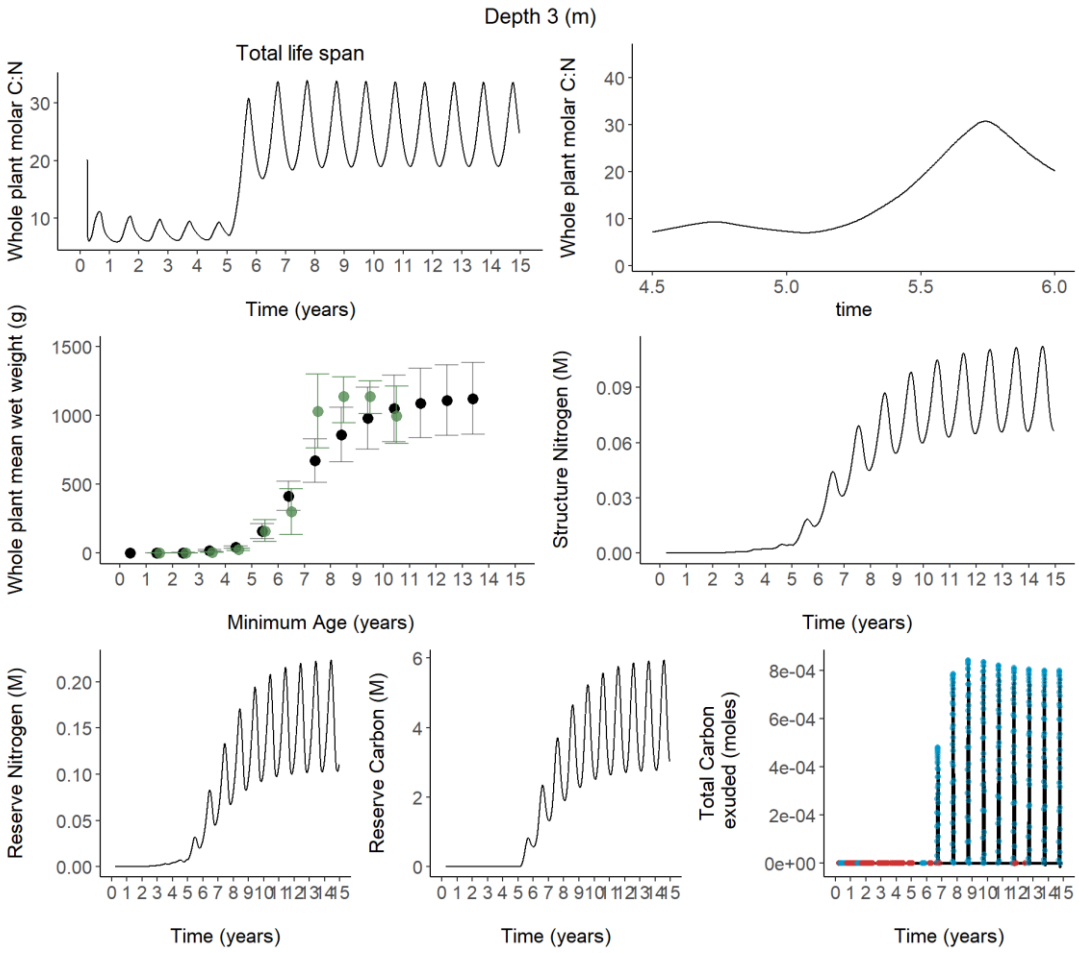

Figure 7.33. Internal composition output from the individual model. The overlayed red points indicate a carbon limitation, while the blue a nitrogen limitation. The model output for whole plant mean weight (g) is shown in black, the green pints indicate the empirical data used for comparison (Jupp, 1972), the bars show the standard deviation for the model data in black and the minimum and maximum values in green for the empirical data.

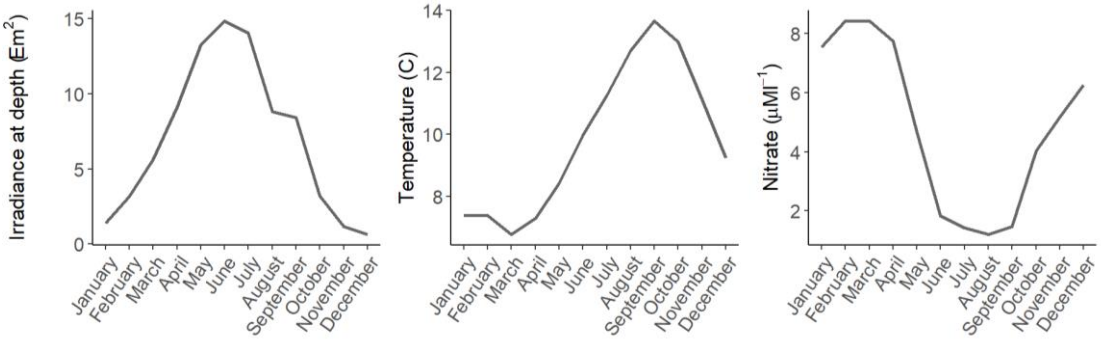

Figure 7.34. Present Day environmental driving data (nitrate concentrations (μ mole N l^{-1}), light intensity ($Em^{-2}day^{-1}$), and temperature ($°C$) data), for the west coast of Scotland (Berx et al., 2015; Heath, 1991, 1995). The environmental conditions

represent the standardised annually repeating cycle that is being used throughout the simulation.

Here we see the younger plants only to have a closer look at the fit.

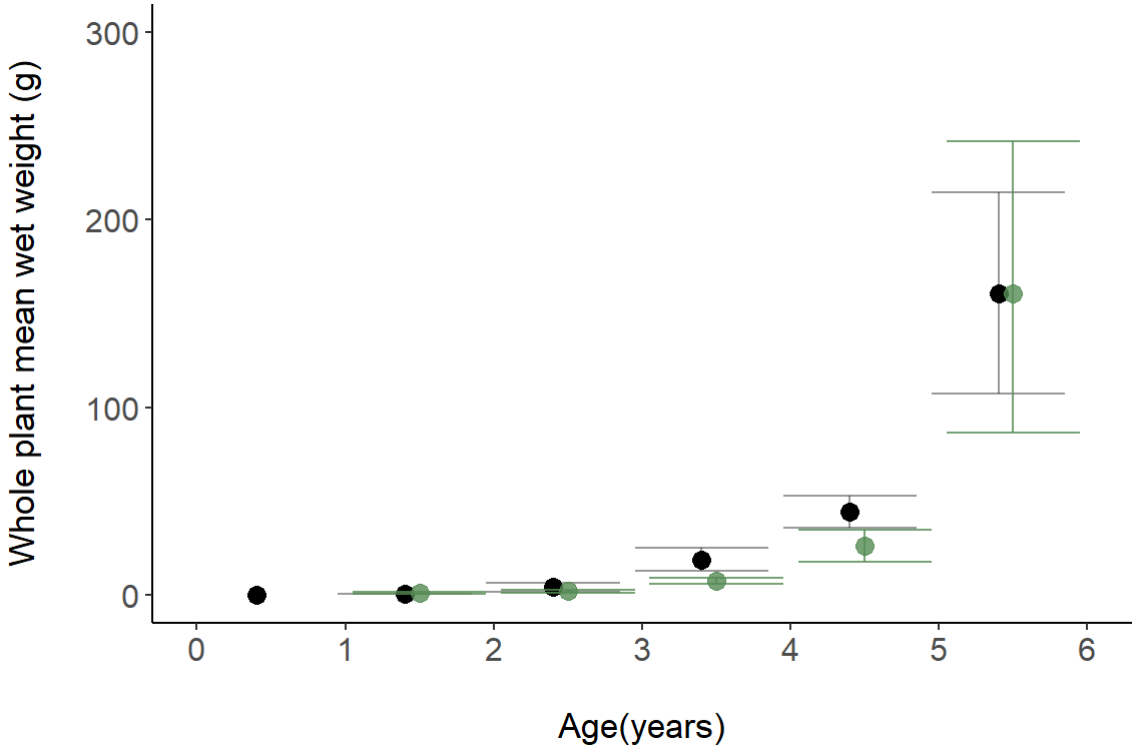

Figure 7.35. Individual whole plant mean wet weight model out for the first 6 years of the simulation. The model output for whole plant mean weight (g) is shown in black, the green pints indicate the empirical data used for comparison (Jupp, 1972), the bars show the standard deviation for the model data in black and the minimum and maximum values in green for the empirical data.

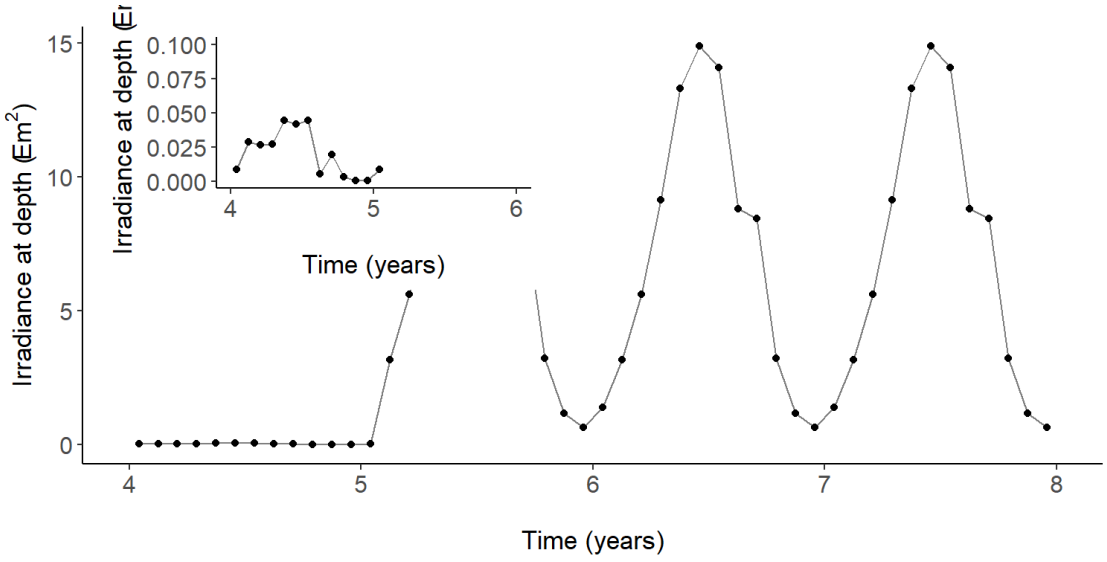

Figure 7.36. Effect of light attenuation scaling factor on the raw data that is fed to the model. Irradiance at depth conditions throughout the model run to show the degree of change from the scaled light attenuation. The inset is a zoomed it version of the first section of the graph, note the different scales.

It is shown how the significant decrease in light reaching the plants have important effects on the plants internal composition and size, but the overall fit to the younger population sample from Jupp (1952) is closer. This highlights the impact on light availability to the modelled individuals. It also highlights that the starting growth conditions can be quickly overcome when the situation improves. Therefore the simulation supports the hypothesis that low light conditions lead to the average lower size of individuals seen in the empirical data.

7.7 Climate Change model comparison

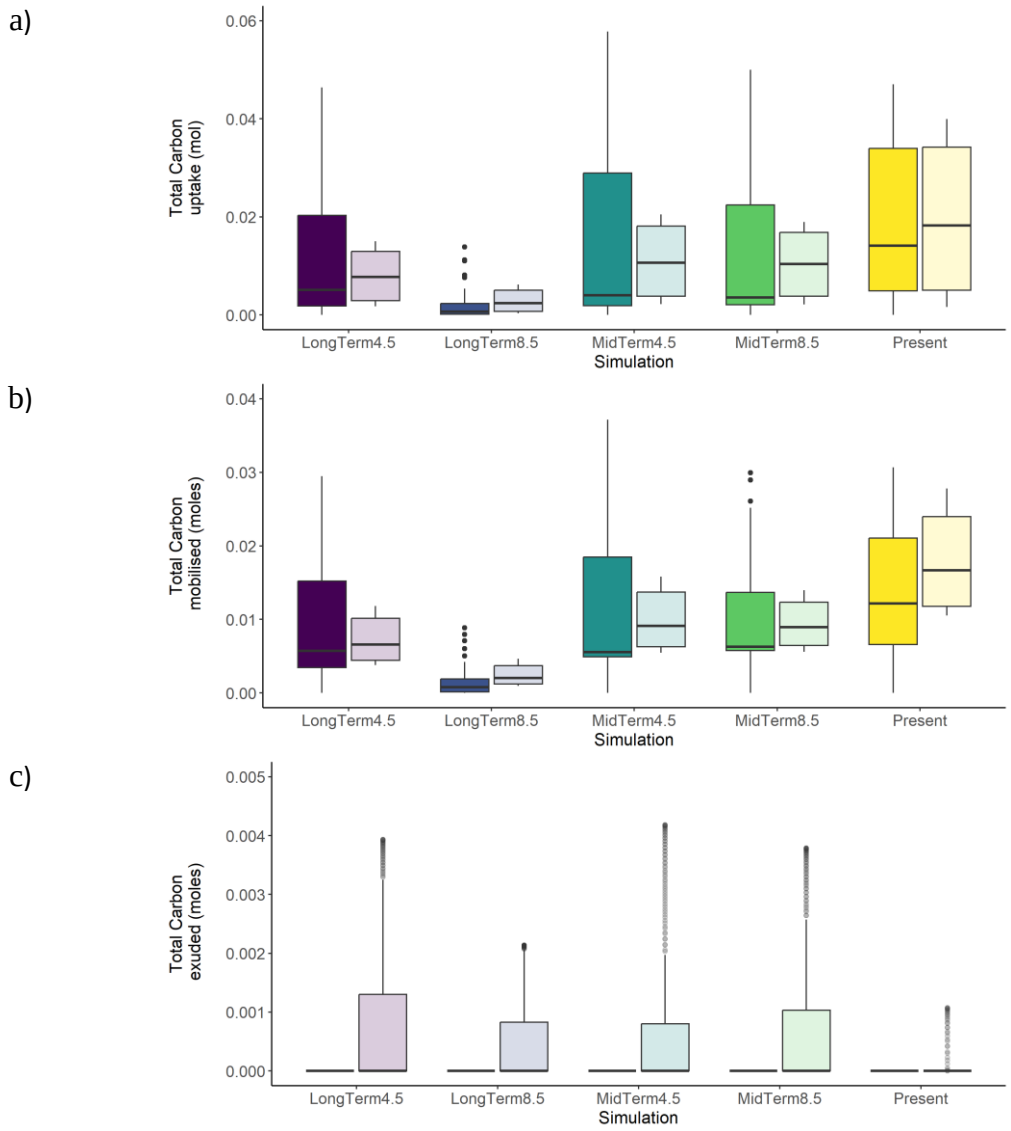

Figure 7.37. Model output for canopy individuals (9-10 years) for their total carbon uptake (a), mobilised (b) and exuded (c) across different climate change scenarios. The forest model's results are in a darker shade, while the individual model's outcomes are the lighter shade. Forest model data encompasses observations from multiple cohorts of the same age 9 to 10 years, as opposed to a single individual.

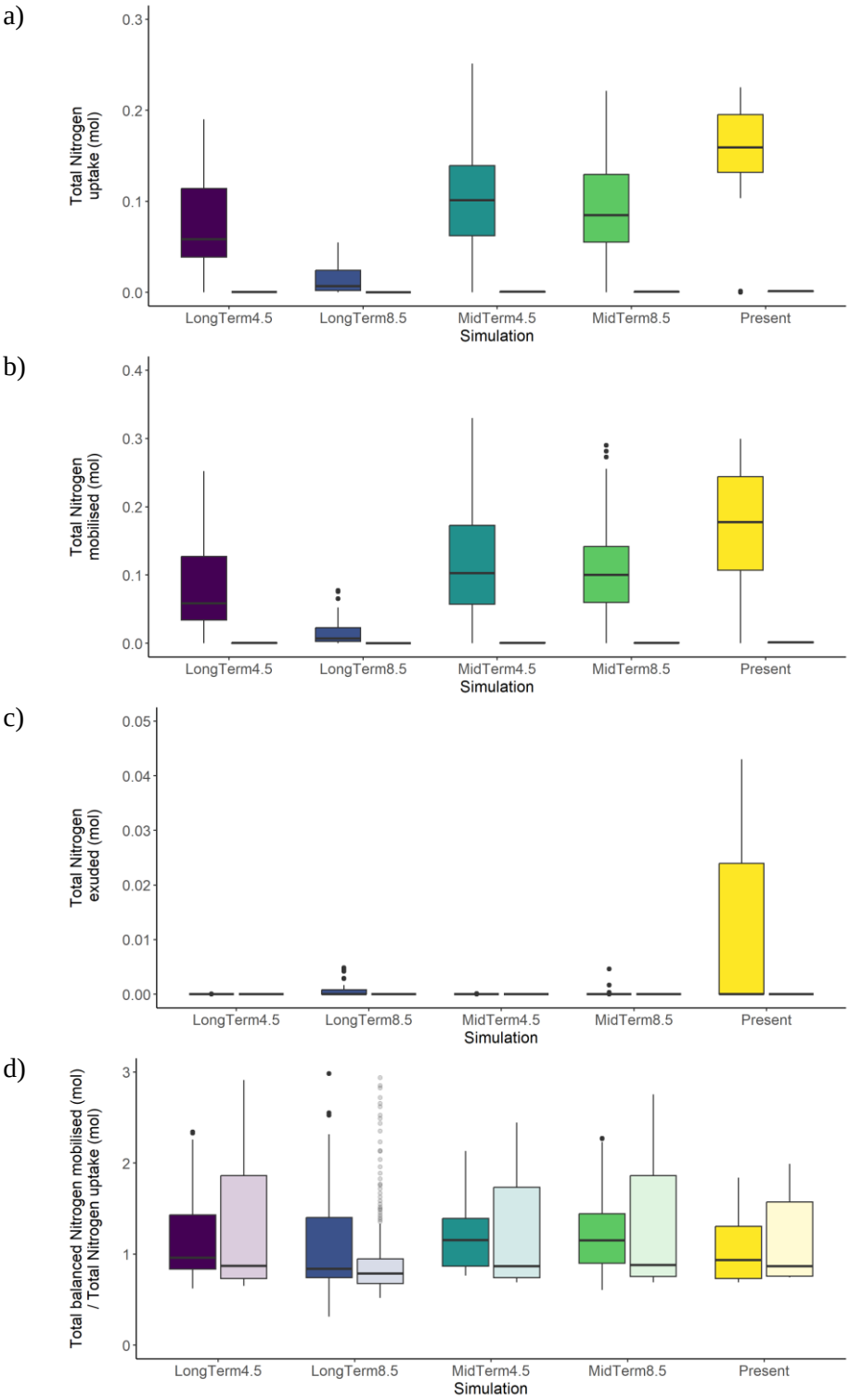

Figure 7.38. Model output for canopy individuals (9-10 years) for their total nitrogen uptake (a) and mobilised (b), exuded (c) and the ratio of the total stoichiometrically balanced nitrogen mobilized to the total nitrogen uptake across different climate change scenarios. The forest model's results are in a darker shade, while the individual model's outcomes are the lighter shade. Forest model data encompasses observations from multiple cohorts of the same age 9 to 10 years, as opposed to a single individual.

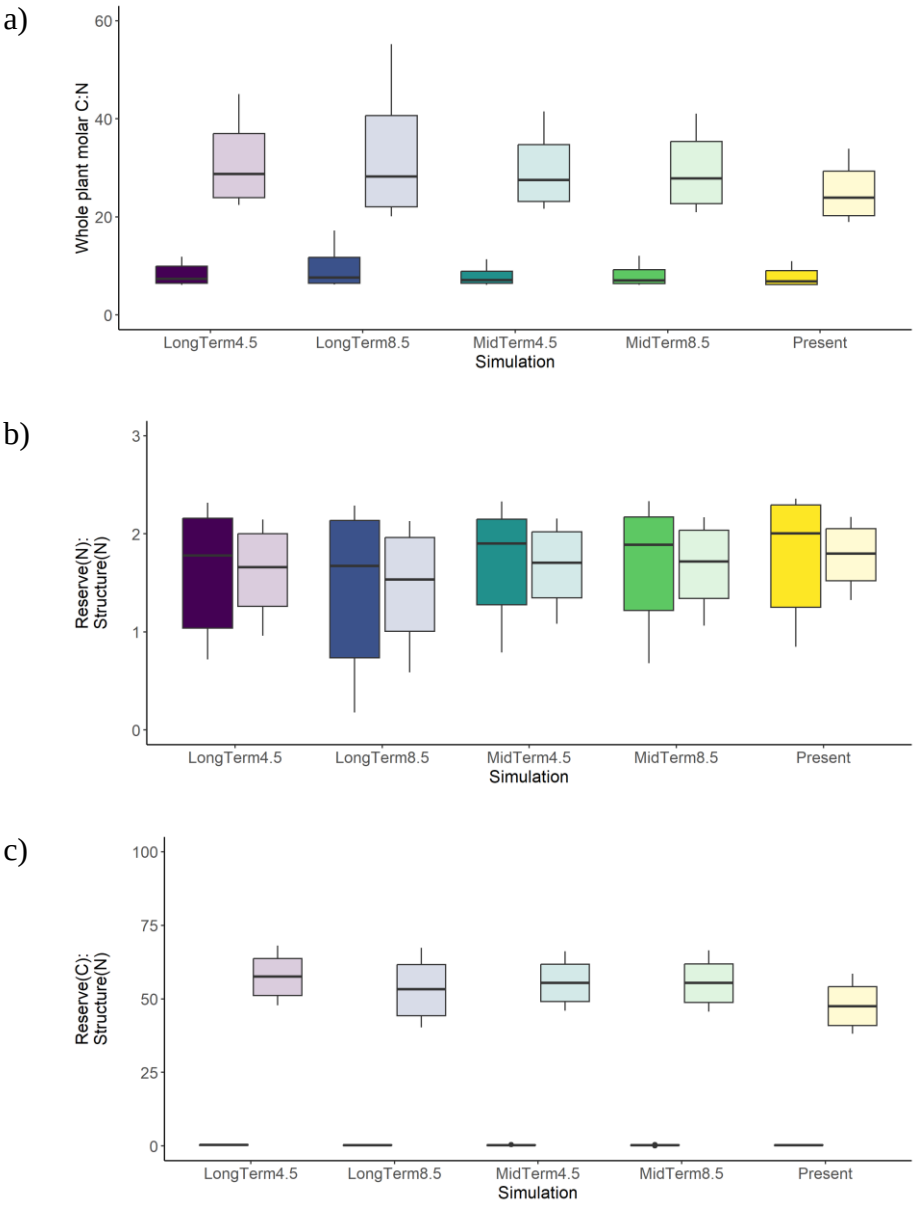

Figure 7.39. Model output for canopy individuals (9-10 years) Whole plant molar C: N (a), Reserve nitrogen to structure nitrogen (b) and reserve carbon to structure nitrogen (c)across different climate change scenarios. The forest model's results are in a darker shade, while the individual model's outcomes are the lighter shade. Forest model data encompasses observations from multiple cohorts of the same age 9 to 10 years, as opposed to a single individual.